**Ionic Liquids: Breakthrough Absorption Technology
for Post-Combustion CO$_2$ Capture**

Final Report
Reporting Period Start Date: 03/01/07
Reporting Period End Date: 09/30/12
Principal Author: Prof. Edward J. Maginn

Report Issued: January 5, 2013
DOE Award Number: DE-FC26-07NT43091

University of Notre Dame
511 Main Building
Notre Dame, IN 46556

# Disclaimer

# Abstract

This is the final report for DE-FC26-07NT43091 "Ionic Liquids: Breakthrough Absorption Technology for Post-Combustion $CO_2$ Capture". A detailed summary is provided of the ionic liquid (IL) discovery process, synthesis and testing results, process / systems modeling, lab-scale operational testing, corrosion testing and commercialization possibilities. The work resulted in the discovery of a new class of ionic liquids (ILs) that efficiently react with $CO_2$ in a 1:1 stoichiometry with no water present and no increase in viscosity. The enthalpy of reaction was tuned to optimize process economics. The IL was found to have excellent corrosion behavior with and without $CO_2$ present. In lab-scale tests, the IL was able to effectively remove $CO_2$ from a simulated flue gas stream, although mass transfer was slower than with aqueous monoethanolamine (MEA) due to higher viscosities. The non-volatile nature of the solvent and its high thermal stability, however, make it an intriguing option. An independent systems analysis indicates that the economics of using the best IL discovered to date (NDIL0157), are at least comparable to – and potentially slightly better than – the Fluor Econamine FG Plus$^{TM}$ process (DOE Case 12). Further work should be directed at improving mass transfer / lowering viscosity and developing commercial synthesis routes to make these ILs at scale in an inexpensive manner. Demonstration of the process at larger scales is also warranted, as is the exploration of other process configurations that leverage the anhydrous nature of the solvent and its extremely low volatility.

This project has resulted in 14 peer reviewed publications, 1 patent application, 55 invited conference presentations and 22 contributed presentations. It also has resulted in the training (partial or full) of 7 postdocs, 18 graduate students and 12 undergraduate students.

## Table of Contents

# Executive Summary

There were six main objectives of this project:

1. Design and synthesize one or more IL absorbents having physical properties tailored for post-combustion $CO_2$ capture.

2. Perform atomistic-level classical and quantum calculations to engineer IL structures that maximize $CO_2$ carrying capacity while minimizing regeneration costs. Properties of candidate ILs in the pure state and in contact with flue gas species will be predicted from parameter-free models.

3. Measure or accurately estimate all physical properties of the absorbent that are essential for detailed engineering and design calculation. These include $CO_2$, $N_2$, $H_2O$, $NO_2$ and $SO_2$ solubility as a function of temperature and pressure, mixed gas solubility, viscosity, heats of absorption, heat capacity, mass transfer coefficients, reaction rates for chemically complexing systems, thermal decomposition temperatures, long term chemical stability and corrosivity.

4. Complete a detailed systems and economic analysis study in accordance with NETL's Carbon Capture and Sequestration (CCS) Systems Analysis Guidelines.

5. Demonstrate the $CO_2$ capture technology with a continuous lab-scale unit.

6. Develop a path forward for commercialization.

As described in this report, all six of these basic objectives were accomplished successfully. A number of new molecular modeling techniques and experimental procedures were developed to design, synthesize and test new ILs with properties specifically tuned for post-combustion $CO_2$ capture. Along the way, strategies to double the $CO_2$ carrying capacity of ILs relative to the best available technology known at the start of the project were developed. The mechanism whereby viscosities were observed to increase when $CO_2$ reacts with an IL were discovered, and an entirely new class of ILs that do not exhibit this viscosity increase were created. Using process modeling, it was learned that there is an optimum $CO_2$ binding energy with ILs that minimizes thermal regeneration duty and overall cost. Molecular modeling procedures were developed by which $CO_2$ binding energies from first principles with no recourse to experimental data

could be accurately predicted. Using this procedure, several new ILs having binding energies in the desired range were developed. Many of these ILs were then synthesized, and subsequent tests validated the computational predictions. A host of physical property measurements on these ILs were taken, and many other properties were computed. Lab-scale demonstration tests were carried out at the University of Notre Dame (Notre Dame) and Babcock and Wilcox (B & W), and these tests demonstrated that ILs can effectively remove $CO_2$ from a simulated flue gas. The efficiency of the IL relative to aqueous MEA is lower due to mass transfer limitations resulting from the relatively high viscosity of the ILs. It was discovered, however, that by diluting the IL with a suitable low viscosity, low volatility fluid the mass transfer performance could be made to approach that of MEA. The IL was found to have excellent corrosion behavior, such that carbon steel materials could probably be used in a process.

Trimeric's systems analysis indicates that the economics of using NDIL0157, the "best" IL identified in this work, are at least comparable to – and potentially slightly better than -– the Fluor Econamine FG Plus$^{TM}$ process (DOE Case 12).

B&W was able to independently evaluate the performance of a non-optimal IL (NDIL0046) in conjunction with lab-scale testing performed at Notre Dame. They concluded that both the quantitative and qualitative results are intriguing and entice more questions regarding application of this novel technology to $CO_2$ scrubbing. This particular class of aprotic heterocylic anion (AHA) IL compounds has several appealing properties akin to solid sorbents. The non-volatile nature is particularly remarkable. An obvious absence of odor, no worry of evaporation and general lack of flammability are attractive characteristics, without the drawbacks of solids handling and transport. The traditional water wash section(s) can likely be eliminated and a lower make-up solvent supply can potentially be realized from the diminished emissions escaping through the exhausting stack. Implications regarding corrosion and materials of construction are also favorable. From a capital investment point of view, it is possible that lower grade and cheaper materials could be employed. Nonetheless, there are still distinct tradeoffs that cannot be neglected. High viscosity, poor mass transfer, limited water miscibility (and hence the need to clean equipment with non-aqueous solvents) and disposal issues remain

of practical concern. More information is crucial pertaining to environmental release, such as toxicological and ecological impacts, energy penalty ramifications, and degradation products in the presence of flue gas contaminants. The balance between pros and cons insinuates that ILs could still be a viable future technology and should not be dismissed without further investigation.

This project provided all or partial support for 7 postdoctoral researchers, 18 graduate students and 12 undergraduate students. A total of 14 peer reviewed papers have been published as a result of this project and one patent has been filed. A total of 55 invited talks and 22 contributed talks describing this work have been given at various technical venues.

## Recommendations

Recommendations for ongoing development needs are identified as follows:

Although the viscosity has been drastically reduced over the course of this program by orders of magnitude, another step-change improvement would significantly enhance mass transfer along with the ability to pump more effectively. Dilution with low volatility, low viscosity solvents is one possibility, as is the exploration of other ILs whose intrinsic viscosity is lower than present liquids.

Exploring IL synthesis techniques to minimize cost and adverse impurities would help to make this solvent a more attractive option.

The regeneration step requires exploration either to identify an inert diluent which can provide sufficient driving force for $CO_2$ desorption and/or a modified process concept to take advantage of the non-aqueous nature of the IL and its low volatility.

A continued collaboration relationship and discussions to seek opportunities for partnership should be maintained. Larger-scale testing, perhaps utilizing slip streams of flue gas, should be pursued to test scale-up efficiency.

# Report Details

## 1. Introduction and Background

This project builds off the successful work performed in a previous NETL-sponsored project "Design and Evaluation of Ionic Liquids as Novel $CO_2$ Absorbents" (DE-FG26-04NT42122) which ran from 7/16/04 to 7/15/07. In that work, Notre Dame researchers explored the feasibility of using ILs, a relatively new class of material, for post-combustion $CO_2$ capture. ILs are pure salts that remain liquid down to low temperatures. When the project was initiated, there was almost no previous work on using ILs for $CO_2$ capture. ILs were identified as a potentially transformational new technology given the fact that they have a number of unique properties, including high intrinsic physical solubility for $CO_2$, essentially no vapor pressure, excellent thermal stability, and they can be used without being heavily diluted by water. Initially, ILs that physically dissolve $CO_2$ were examined, but at the conclusion of DE-FG26-04NT42122 it was apparent that some type of chemical reactivity would need to be added to the ILs in order to get the capacity high enough to make them economically competitive with existing solvent technology.

There were six main objectives of this project:
1. Design and synthesize one or more IL absorbents having physical properties tailored for post-combustion $CO_2$ capture. These properties include: high $CO_2$ carrying capacity; favorable regeneration properties (either thermal swing, pressure swing or both) such that significantly less than 1,400 BTU of energy per pound of $CO_2$ captured is required for regeneration; virtually no volatility, so that solvent losses are negligible; high thermal stability, so decomposition under high temperature service is minimized; low corrosivity; and stability in the presence of typical flue gas components.
2. Perform atomistic-level classical and quantum calculations to engineer IL structures that maximize $CO_2$ carrying capacity while minimizing regeneration costs.

Properties of candidate ILs in the pure state and in contact with flue gas species will be predicted from parameter-free models.

3.  Measure or accurately estimate all physical properties of the absorbent that are essential for detailed engineering and design calculation. These include $CO_2$, $N_2$, $H_2O$, $NO_2$ and $SO_2$ solubility as a function of temperature and pressure, mixed gas solubility, viscosity, heats of absorption, heat capacity, mass transfer coefficients, reaction rates for chemically complexing systems, thermal decomposition temperatures, long term chemical stability and corrosivity.

4.  Complete a detailed systems and economic analysis study in accordance with NETL's CCS Systems Analysis Guidelines. During this process, optimal operating conditions for absorption and regeneration will be identified and used to target one of the absorbents for additional study.

5.  Demonstrate the $CO_2$ capture technology with a continuous lab-scale unit. A lab-scale continuous absorption and regeneration system will be designed, built and operated to demonstrate that the absorbent meets capture, regeneration and stability targets.

6.  Develop a path forward for commercialization. This will include identification of at least one existing power plant where technology can be demonstrated, completion of economic studies to enable cost estimates for the manufacture of the target absorbent, and integration of the systems analysis study (Objective 4) with performance data for use in preparing a competitive proposal for a Phase III field-testing proposal in 2010.

As described below, Objectives 1-5 were successfully accomplished. As for the 6th objective, a commercialization plan was developed and cost studies performed. However, these studies were not completed until 2012, and a specific power plant where testing can be completed has not yet been identified. There is not sufficient data and partners to prepare a field-testing proposal in the coming year.

This report is broken down into four separate sections, based on budget periods. Each budget period had different objectives, and the findings from one budget period were used to help guide the work in subsequent budget periods. For each budget period,

different major tasks or objectives were identified, and results for each of these major tasks are provided.

## 1.1 Note on ionic liquid naming convention

As the ionic liquids in this study were developed, they were given a code name designation in which the initials or name of the organization which made the compound is followed by a number. For ionic liquids made at Notre Dame, the prefix given is "NDIL" for "Notre Dame ionic liquid". In general, the number refers to the sequence in which the ionic liquid was made, although at Notre Dame other ionic liquids made for different projects were also given similar code names. Thus the numerical sequence is not continuous. For example, the first ionic liquid made at Notre Dame was 1-n-hexyl-3-methylimidazolium bis(trifluoromethylulfonyl)imide, which is often called $[C_6mim][NTf_2]$ or $[hmim][Tf_2N]$ in the literature. The code name for this ionic liquid is NDIL0001 in this report. At the end of the report, we provide a listing of the major, non-proprietary ionic liquids studied in this project along with their code names. Some of the ionic liquids developed toward the end of the project are still proprietary and covered under protected data limitations, and so their structures are not reported.

## 2. Budget Period I: 3/1/07-7/21/08

### 2.1 Background

The five major tasks of Budget Period 1 (BP I) were: molecular modeling, synthesis, property measurement, economic and systems analysis, and project management. Notre Dame led the effort, but relied upon partner companies B & W, DTE Energy, Merck/EMD and Trimeric. B & W were expected to provide technical advice on practical aspects associated with equipment and capture conditions. Ultimately, they also carried out corrosion studies and made lab-scale performance measurements. DTE Energy provided practical guidance as to how a $CO_2$ capture system might be integrated with an operating power plant. They mainly provided suggestions during the early stages of the project, and did not play a major role beyond BP1. Merck/EMD is a manufacturer of ILs and was brought on to help supply samples of ILs and provide advice on the kinds of ILs that could be manufactured at scale. Trimeric was retained as a sub-contractor on the

project. Their role was to carry out an independent systems and economic analysis of a $CO_2$ capture process that utilizes an IL.


## 2.2 Molecular Modeling

In order to provide an understanding of the chemistry that occurs when $CO_2$ reacts with an IL, as well as to be able to understand and predict how the composition and structure of an IL governs the resulting properties, molecular modeling was carried out. These activities consisted of two main classes of modeling: 1) classical condensed phase molecular dynamics and Monte Carlo, and 2) quantum chemical calculations. The former simulations are able to determine thermodynamic and transport properties of the bulk IL as well as sorption thermodynamics for $CO_2$ and, to some extent, the solution thermodynamics of the system. Because classical simulations do not treat chemical bonding, they are not capable of examining how $CO_2$ reacts with an IL; to study this process quantum chemical calculations were used.

### 2.2.1 Classical Simulations

To perform classical simulations, one requires an expression for how the energy of the system depends upon the positions of all the atoms. This is typically handled through the use of a "force field" of the following form

$$
\begin{aligned}
\mathcal{V}(\mathbf{r}) \quad = \quad & \sum_{\text{bonds}} k_b (r - r_0)^2 + \sum_{\text{angles}} k_\theta (\theta - \theta_0)^2 \\
& + \sum_{\text{dihedrals}} k_\chi [1 + \cos(n_0 \chi - \delta_0)] \\
& + \sum_{i=1}^{N-1} \sum_{j=i+1}^{N} \left( 4\epsilon_{ij} \left[ (\frac{\sigma_{ij}}{r_{ij}})^{12} - (\frac{\sigma_{ij}}{r_{ij}})^6 \right] + \frac{q_i q_j}{r_{ij}} \right) \quad (2.1)
\end{aligned}
$$

where the potential energy is a function of atomic positions $\mathbf{r}$. The first three terms account for bond stretching, angle bending and dihedral rotation. The fourth term is a Lennard-Jones 12-6 function that accounts for repulsion-dispersion interactions. The final term is a Coulombic term that account for charge-charge interactions. In order for the simulations to be predictive, the parameters in eqn 2.1 need to be developed from first principles. They also need to be generated in a fast manner so that the simulations can be
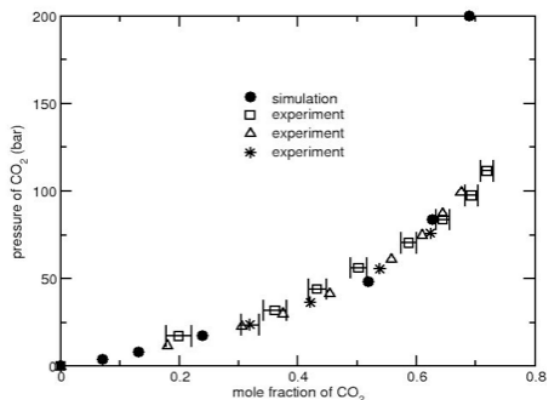
**Figure 1: Simulated and experimental isotherms for $CO_2$ in [hmim][Tf2N] at 333 K. The triangles are the data from [1], the squares are from [2] and the stars are from [3]. The experimental Henry's law constants range from 42.8 to 52.3 bar, while the simulations predict a value of 49.4 bar.**

used to screen a wide range of IL quickly. In this phase of the project, some automated computational tools that enable these parameters to be developed rapidly and reliably were developed. Force fields were generated for a range of ILs, including those that physically dissolve $CO_2$ and those capable of chemical complexation.

The study was begun with the physical solubility of $CO_2$ in an IL by modeling absorption isotherm of $CO_2$ in the IL [hmim][Tf2N]. This IL is also referred to as NDIL0001 and is a widely studied compound. Results are shown in Figure 1. It is extremely difficult to simulate gas solubilities in ILs, so a new simulation method was developed to enable these calculations to be completed [4]. Results of this study were published [5]. The low pressure physical solubility of $SO_2$, $O_2$ and $N_2$ in NDIL0001 was computing by use of the Henry's Law constant. Results are shown in Table 1.

Table 1: Computed Henry's Law constants for $SO_2$, $O_2$ and $N_2$ in NDIL0001.

| Gas | Temperature (K) | Henry's law constant (bar) |
|---|---|---|
| $SO_2$ | 333 | 4.6 |
| $O_2$ | 313 | 430 |
| $N_2$ | 333 | 1261 |

These results are generally consistent with experimental findings, giving confidence that the simulation methods yielded good results. Therefore mixed gas solubilities were studied by computing the sorption behavior of $CO_2$ / $O_2$ and $N_2$ / $SO_2$ mixtures. This is important because mixed gas experiments are quite difficult and time consuming to carry out. A key question to answer was: do gases absorb "ideally" so that pure gas isotherms

can predict selectivity, or are there non-ideal competition effects? The calculations for the mixture of $CO_2$ and $O_2$ binary absorption isotherms show that the selectivity of $CO_2$ over $O_2$ varies between 3 and 20 at 313 K. These results are in agreement with experimental observations from the ND labs. Results of $N_2$ absorption from the mixture of $SO_2$ and $N_2$ suggest that the solubility of $N_2$ is negligibly small compared to that of $SO_2$ in line with the Henry's law constants reported in Table 1. The calculations also show that $SO_2$ and $N_2$ absorb independently. The mixture gas solubility calculations helped in determining the departure of pure gas solubility due to the presence of other gases in the system and allowed the team to more realistically simulate absorption of $CO_2$ from flue gases. Some of these estimates were subsequently used in the process modeling simulations.

Simulations were also conducted on NDIL0016, a candidate IL that contains a reactive group on the cation. A force field was developed for NDIL0016 and the liquid density was computed to be 1.5516 $g/cm^3$ at 298 K. This is in excellent agreement with the experimental liquid density at 298 K measured in the ND labs of 1.5938 $g/cm^3$, a difference of only 2.9%. Then the physical solubility of $CO_2$ was estimated in this IL using molecular dynamics simulations. This is important, because the total amount of $CO_2$ in the liquid is necessary for process modeling, and it is difficult to separate out the physical from chemical solubility in experiments. The results indicated that the Henry's law constant for $CO_2$ in NDIL0016 is greater than that in [hmim][Tf$_2$N], meaning that $CO_2$ has a lower physical solubility in NDIL0016 than in NDIL0001. Given that the experimental liquid density of NDIL0016 is 1.5938 $g/cm^3$ at 298 K, the free molar volume is calculated to be ~265 $cm^3/mol$. In comparison, the free molar volume of IL NDIL0001 is calculated to be ~338 $cm^3/mol$, or nearly 20% larger than NDIL0016. The comparison suggests that a possible explanation for the low solubility of $CO_2$ in NDIL0016 is the lack of free space in which the $CO_2$ molecules can reside. These concepts turned out to be correct, and helped to rank physical solubilities with a relative simple property.

Force field parameters were then developed for the ILs NDIL0017 and NDIL0018. These ILs possess functional groups on cations for $CO_2$ capture. In addition, molecular dynamics simulations were carried out on $[C_{14}C_6C_6C_4P][Tf_2N]$, $[C_{14}C_6C_6C_6P][glycine]$, $[bmim][B(CN)_4]$ and $[emim][B(CN)_4]$.

Calculated results for the liquid density and molar volumes, compared to experimental data where available, are shown in Tables 2-5.

Table 2: Simulated and experimental densities for NDIL0017.

**NDIL0017**

| *Simulation* | | | *Experiment** | |
|---|---|---|---|---|
| **T(K)** | $\rho$ (g/cm$^3$) | $V_{molar}$ (cm$^3$/mol) | $\rho$ (g/cm$^3$) | **%diff** |
| 298.15 | 1.5604 | 269.39 | 1.5920 | -1.99 |
| 308.15 | 1.5561 | 270.14 | 1.5829 | -1.69 |
| 318.15 | 1.5432 | 272.38 | 1.5738 | -1.94 |
| 328.15 | 1.5359 | 273.69 | 1.5647 | -1.84 |
| 333.15 | 1.5309 | 274.59 | 1.5602 | -1.88 |

*$\rho$ = -0.00090932*T(C) +1.614724

Table 3: Simulated and experimental densities for NDIL0018.

**NDIL0018**

| *Simulation* | | | *Experiment** | |
|---|---|---|---|---|
| **T(K)** | $\rho$ (g/cm$^3$) | $V_{molar}$ (cm$^3$/mol) | $\rho$ (g/cm$^3$) | **%diff** |
| 293.15 | 1.5139 | 284.95 | 1.5405 | -1.73 |
| 308.15 | 1.5111 | 285.47 | 1.5269 | -1.04 |
| 323.15 | 1.4940 | 288.73 | 1.5133 | -1.27 |
| 338.15 | 1.4817 | 291.14 | 1.4997 | -1.20 |
| 353.15 | 1.4644 | 294.58 | 1.4861 | -1.46 |
| 363.15 | 1.4585 | 295.77 | 1.4770 | -1.25 |

*$\rho$ = -0.00090764*T(C) +1.558669

Table 4: Simulated and experimental densities for $[emim][B(CN)_4]$.

**$[emim][B(CN)_4]$**

| *Simulation* | | | *Experiment* | |
|---|---|---|---|---|
| **T(K)** | $\rho$ (g/cm$^3$) | $V_{molar}$ (cm$^3$/mol) | $\rho$ (g/cm$^3$) | **%diff** |
| 298.15 | 1.0694 | 211.38 | 1.036 | 3.22 |

Table 5: Simulated and experimental densities for [C$_{14}$C$_6$C$_6$C$_6$P][glycinate].

**[C$_{14}$C$_6$C$_6$C$_6$P][glycinate]**

| _Simulation_ | | | _Experiment_ | |
|---|---|---|---|---|
| **T(K)** | **ρ (g/cm$^3$)** | **V$_{molar}$ (cm$^3$/mol)** | **ρ (g/cm$^3$)** | **%diff** |
| 298.15 | 0.877 | 489.28 | 0.918 | 4.5 |

NDIL0017 and NDIL0018 are of the same family as NDIL0016 and contain reactive groups on the cation. [emim][B(CN)$_4$] was examined because it tends to have a low viscosity, and [C$_{14}$C$_6$C$_6$C$_6$P][glycinate] was studied because its reactive group is on the anion. As shown below, quantum chemical calculations suggested that placing the reactive group on the anion would result in greater uptake of $CO_2$ for a given amount of IL.

In an effort to understand the nature of gas solubility in ILs, it was possible to decompose the energetic interactions between $CO_2$, $SO_2$, $N_2$ and $O_2$ and NDIL0001. Figure 2 shows the energy of interaction of gases (S) with cation (C) and anion (A) of the IL. It is evident from the figure that in the absorption of $CO_2$ and $SO_2$, the interaction of gases with the anion is stronger than that with the cation. In the case of sparingly soluble gases $O_2$ and $N_2$, however, the strength of interaction is slightly stronger with the cation due to larger number of atoms of the cation providing greater van der Waals energy.

Decomposition of total energy into its components reveals that solute-solvent interactions are dominated by van der Waals interaction. Structural analysis indicates that $CO_2$ and $SO_2$ reside closer to the anion. The difference in the interaction of $SO_2$ and $CO_2$ with the anion is primarily due to electrostatic energy.

The absorption mechanism of $SO_2$ is similar to that for $CO_2$ in that both free volume and binding energy between solute and IL contribute to the solubility while in the case of water it is predominantly the binding energy that controls the absorption.
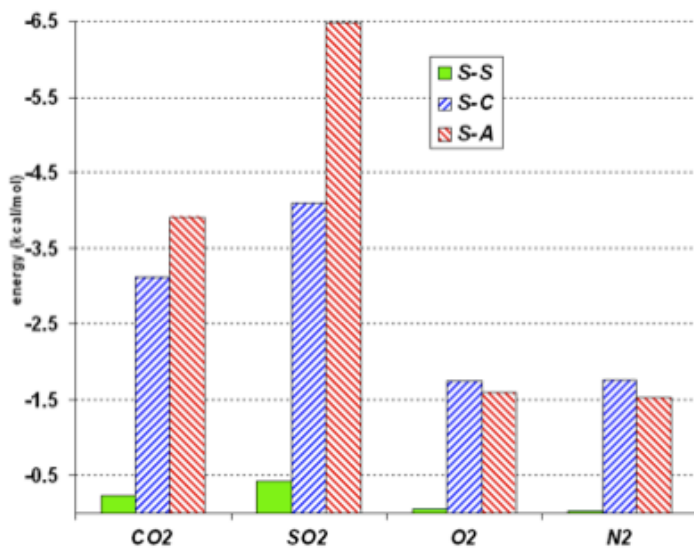
**Figure 2: Interaction energy of gases with cation (C) and anion (A) of NDIL0001**

It had been reported that a simple regular solution theory (RST) model is capable of predicting the physical solubility of gases in ILs. If true, this would provide a rapid screening tool for assessing solubility. The basis of RST can be rigorously tested with simulations, because all the parameters in the model may be computed in addition to the direct isotherm. For highly insoluble gases like $N_2$, it was found that RST predictions are in reasonable agreement with the simulation results, as shown in Figure 3. However, the estimates obtained for other gases differ by 20-60% from experimental and simulation results suggesting that the RST is not applicable for quantitative absorption isotherm determination of these gases.
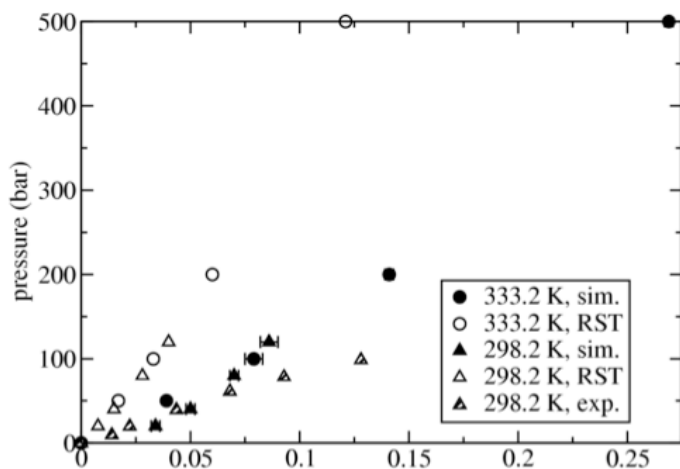
**Figure 3: Simulation and RST predictions of N$_2$ solubility in NDIL0001.**

As discussed below, much of the experimental and practical difficulties associated with the types of ILs studied during BP1 had to do with their relatively high viscosity. It was later learned during BP1 that the viscosity of many of the ILs being investigated showed dramatic increases upon reaction with CO$_2$. The reason for this was unknown, and so it was difficult to determine if new ILs could be developed that did not suffer from this effect. Toward this end, force field parameters were developed for the products that form upon reaction of CO$_2$ with the NDIL0017. These products were denoted as dication (B) and zwitterion (C). The cation of NDIL0017 was referred to as species A.

Molecular dynamics simulations were carried out of various mixture compositions (A:B:C) that represent different extent of reaction from unreacted (all A), to fully reacted (no A and equal parts B and C). The simulations were performed to estimate changes in thermophysical properties as the reaction proceeds and understand the molecular mechanism responsible for the high viscosity of the solution upon complexation with CO$_2$. As water is present in substantial amount in flue gases, the effect of addition of water (3.4 and 6.5 wt %) on dynamical properties was also examined.

The computed density of NDIL0017 was 1.556 g/cm$^3$, in good agreement with the experimental measurement of 1.592 g/cm$^3$. As the reaction proceeds, the computed density increased linearly with mole fraction of CO$_2$ from 1.562 g/cm$^3$ to 1.586 g/cm$^3$.

Upon addition of water, the density was found to decrease as compared to dry counterparts and excess molar volumes are all negative, but small in magnitude indicating that the molar density is only slightly higher than what would be expected of a mixture exhibiting ideal mixing.

In addition to densities and molar volumes, mean square displacements (MSD) and rotational time constants of various species as a function of extent of reaction were also computed. It was observed that there was an order of magnitude drop in MSDs (from 15-20 $A^2$ to 2-3 $A^2$) for species A and the anion for the lowest extent of reaction studied. MSDs for species B and C were even smaller than that for A. The MSDs for B and C were found to be tightly correlated suggesting strong interaction between B and C. The presence of water was found to increase the MSDs for all the species as compared to the corresponding dry systems.

It was observed that rotational time constants increased by a factor of 50 due to the reaction for species A and the anion from 1.5 and 1.0 ns respectively in the unreacted system. The rotational time constants for species B and C were estimated to be even higher, on the order of hundreds of nanoseconds. The addition of water decreased rotational times constants only slightly.

In order to understand the microscopic interactions that lead to sluggish macroscopic dynamical properties described above, a detailed hydrogen bond analysis in the liquid was performed. The analysis showed that the most important interactions occur between the terminal nitrogen donor functionalities on A, B and C and the oxygen acceptor on C (denoted by A---C, B---C and C---C) and anion. As the concentration of reacted $CO_2$ increases, a large number of B---C interactions become occupied relative to A---C and the liquid becomes inundated with persistent, strong hydrogen-bonded networks of (B---C)$_n$ chains or clusters that underlie the slow macroscopic dynamics observed experimentally and computationally.  These hydrogen bonds, when viewed over the course of a typical simulation (several nanoseconds) remain locked in place and persist for very long periods of time.  Thus, the B and C species cease to behave as discrete units,

but act rather as larger polymers or clusters. The translational and rotational motion of these larger units and their interactions with neighboring molecules explains the high experimental viscosities. Introduction of $H_2O$ molecules causes a competition between $H_2O$ and B species for the C terminal sites, although the percentage of B---C interaction still remains high. This study helped answer the question as to why reaction with $CO_2$ causes the viscosity to increase so much, and provided the first clues as to how new ILs could be designed (containing what were later called AHAs) that would not increase in viscosity. This work was published in 2008 [6], and it has already been cited 69 times and opened up a whole new field of investigation by the group and others.

The solubility of water in NDIL0001, and the solubility of oxygen and nitrogen in NDIL0017 were computed. These calculations were performed in lieu of experiments and were used by Trimeric as inputs to preliminary process engineering calculations.

### 2.2.2 Quantum Mechanical Simulations

This aspect of the work was begun with an effort to understand what levels of theory were needed in order to accurately characterize the reaction of $CO_2$ with functionalized ILs. To do this, a study was made of simpler systems for which some literature data are available. The focus was on testing and applying a relatively inexpensive but generally reliable density functional theory (DFT) model for calculating reaction energies of $CO_2$ with several baseline amines as well as a selection of potential alternative functional groups.

Calculations were performed within the generalized gradient approximation (PBE-GGA) as implemented in the Density Functional (ADF) code. Table 6 compares the zero-point corrected PBE-GGA energies calculated here with energies recently reported in the literature for the gas-phase reaction of an amine with $CO_2$:
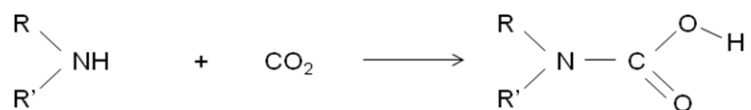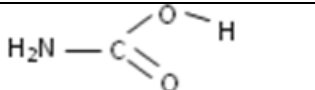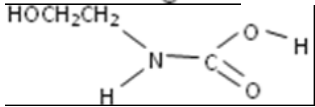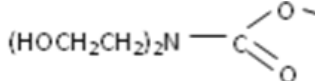
Table 6: Comparison of calculated $CO_2$ adsorption energies by pure DFT and high accuracy wavefunction methods.

| Reactant | Product | Reaction Energy (kJ/mol) | |
| --- | --- | --- | --- |
| | | PBE-GGA | G3MP2B3 |
| Ammonia ($NH_3$) |  | 39 | 55 |
| MEA ($HOCH_2CH_2NH_2$) |  | 23 | 29 |
| DEA (($HOCH_2CH_2)_2NH$) |  | 8 | 22 |

The PBE-GGA captures the general qualitative trends in reaction energy but appears to quantitatively underestimate absolute energies. Therefore the focus was on identifying further calibration points to determine a reliable but affordable method for screening a wider range of functional groups. One interesting observation noted during this initial work was that hydrogen binds to the $CO_2$ fragment in two different conformations that differ by upwards of 20 kJ/mol in stability:
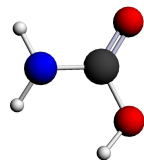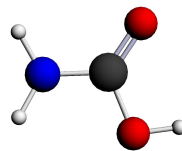


Trans                                    Cis

In subsequent studies, therefore, an exploration was made of how conformational effects might provide an additional variable to exploit in tuning functionalized ILs reactivity.

The process was begun by developing a reactivity scale for various functional groups with $CO_2$, using the PBE-GGA approach to calculate the energies of reaction of $CO_2$ with a wider range of functionalized amines as wells as with hydroxyl (OH), thiol (SH), and phosphine (PH) functionalities. In analogy with the amine chemistry, $CO_2$ was assumed to react by insertion in the heteroatom—H bond. Vibrational spectra for each molecule were calculated and zero-point corrections included in the reaction energies. The results are summarized in Figures 4-7.
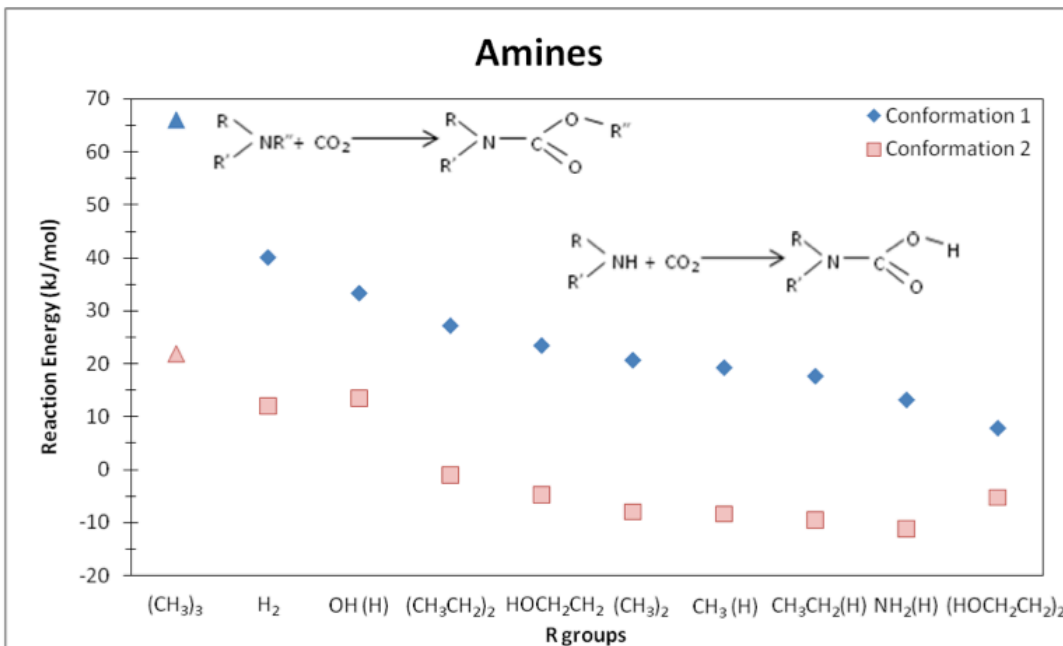
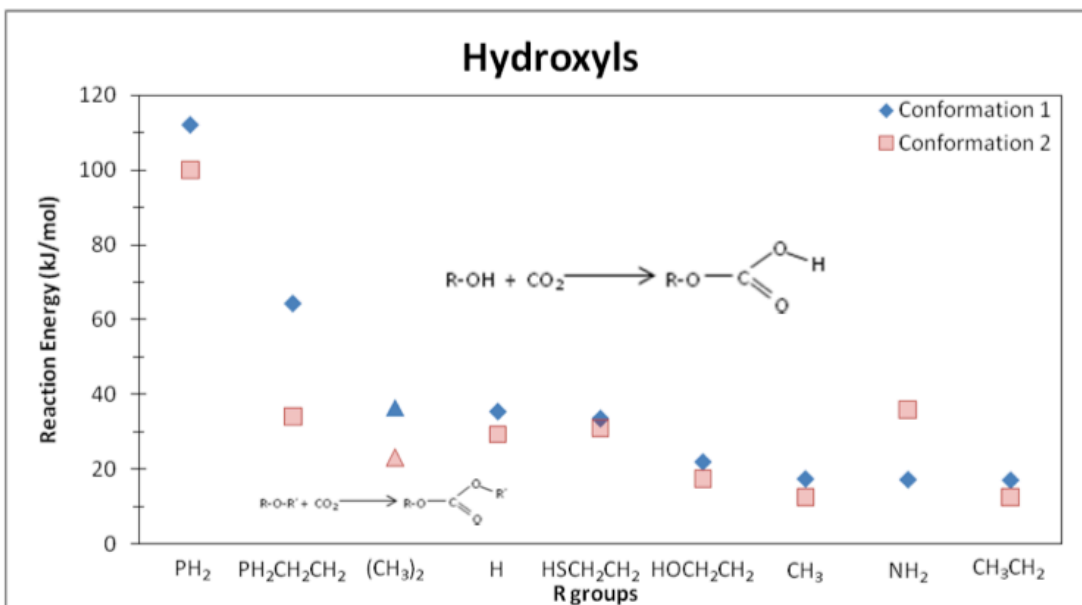**Figure 4: PBE-GGA reaction energies of $CO_2$ with various functionalized amines.**



**Figure 5: PBE-GGA reaction energies of $CO_2$ with hydroxyls.**
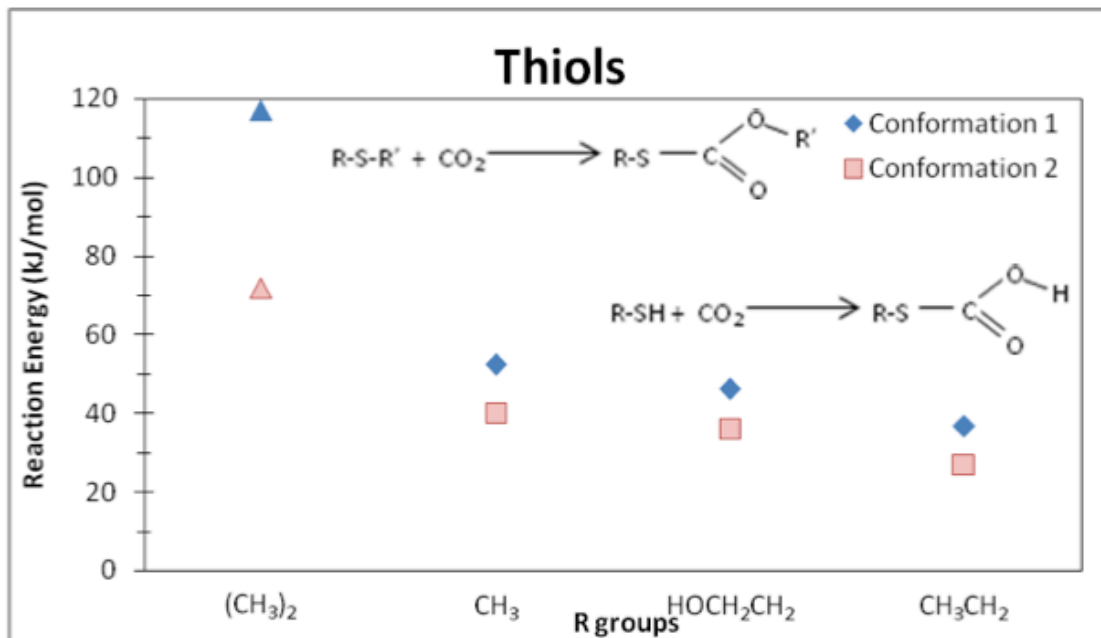
**Figure 6: PBE-GGA reaction energies of $CO_2$ with thiols.**
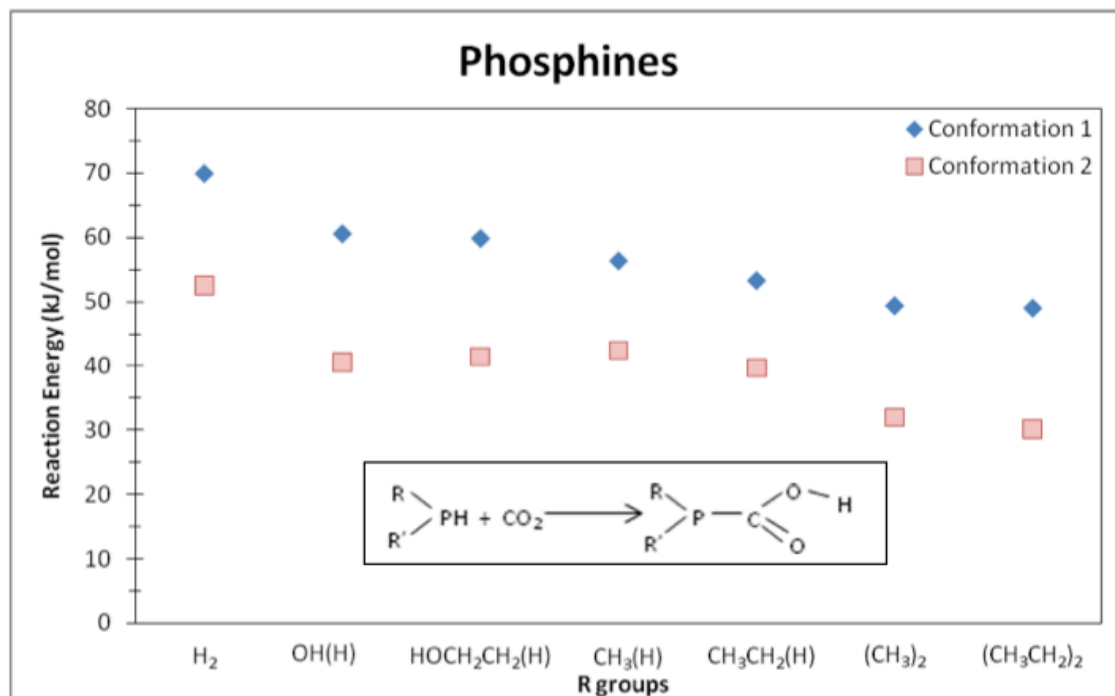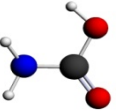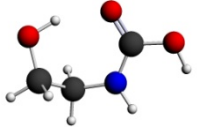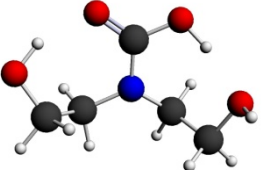


**Figure 7: PBE-GGA reaction energies of $CO_2$ with phosphines.**

Several molecules appear in more than one figure because of the possibility of multiple reaction sites. For instance, the molecule $HOCH_2CH_2SH$ shows up in both Figures 5 and 6 in order to determine the most favorable binding site. It can be seen that $CO_2$ binding with the oxygen is more favorable. The results show that the general order of intrinsic reactivity is amines > hydroxyls > thiols > phosphines. Within each family, intrinsic reactivity can vary by at least 20 kJ/mol.

To further test method, additional calculations were carried out on the reaction of $CO_2$ with simple amines, using B3LYP and MP2 methods both implemented in GAMESS. Table 7 compares the zero-point corrected PBE-GGA, B3LYP and MP2 energies with energies recently reported in the literature for the gas-phase reaction of an amine with $CO_2$:



Table 7: Comparison of calculated $CO_2$ adsorption energies for calculated methods and a high accuracy literature method (Astrad et al.).

| | | Reaction Energies (kJ/mol) | | | |
|---|---|---|---|---|---|
| Reactant | Product | PBE-GGA | B3LYP | MP2 | G3MP2B3[8] |
| Ammonia ($NH_3$) | | 39 | 50 | 60 | 55 |
| MEA ($HOCH_2CH_2NH$) | | 23 | 39 | 46 | 29 |
| DEA (($HOCH_2CH_2$)$_2$N) | | 14 | 21 | 21 | 22 |

All of the methods used capture the overall trends, with B3LYP and MP2 comparing the closest with literature. PBE-GGA is the quickest method to use, while MP2 is the most expensive.

Therefore, it was determined that utilizing either the B3LYP method or a combination of the PBE-GGA and B3LYP methods, should provide inexpensive but reliable energies for subsequent studies.

An expansion was made of the gas phase reaction studies of functionalized amines and then a comparison was made to other functional groups such as hydroxyls (OH), thiols (SH), and phosphines (PH). In analogy with the amine chemistry, $CO_2$ is assumed to react by insertion in the heteroatom—H bond. Vibrational spectra for each molecule were calculated and zero-point corrections included in the reaction energies. All energies reported are for the lowest energy conformations. The results are summarized below in Figure 8.
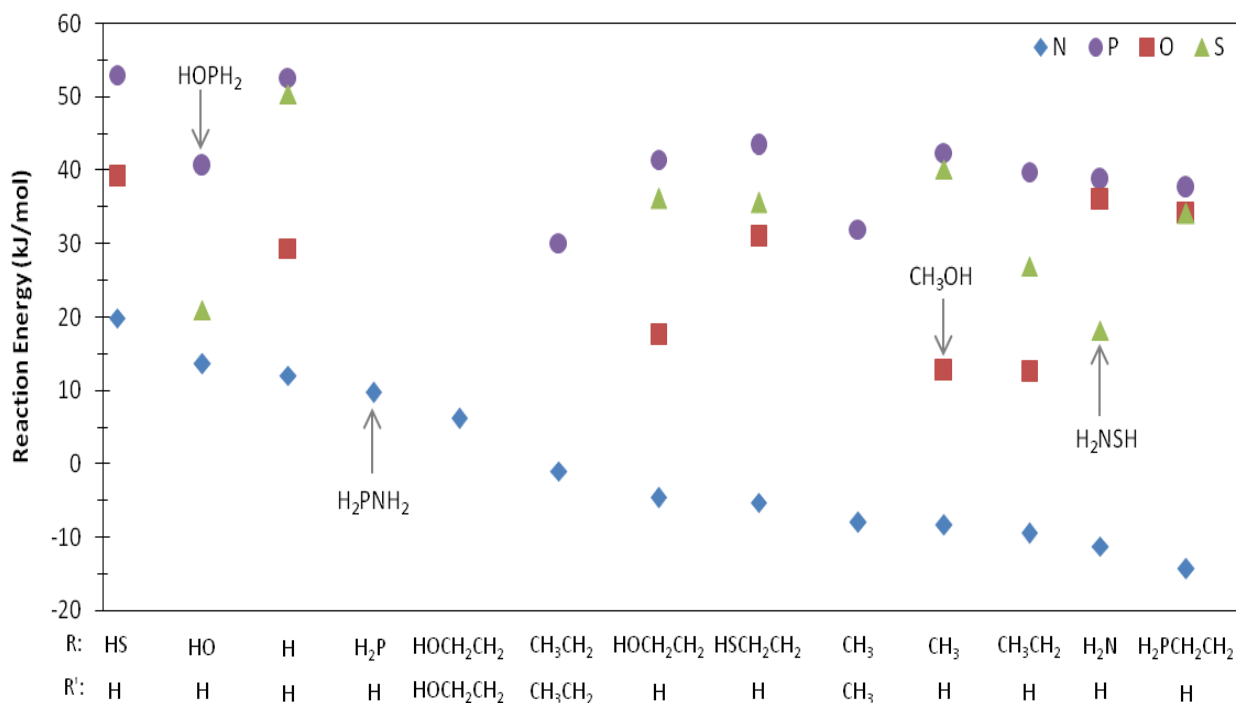


Figure 8: Reaction energies for amine, hydroxyl, thiol, and phosphine functional groups.

Figure 8 shows that functionalized amines have the lowest overall reaction energy with $CO_2$, while phosphines have the highest. It also shows that for the functionalized amines investigated, the reaction energy range is between about -15 and 20 kJ/mol.

Gas phase energies provide useful trends, but are only half the story. Of most interest was the reaction energies in the condensed phase. To account for solvation effects, the conductor-like screening model (COSMO) was used, with water as the solvent, to study the amine reactions. Using the thermodynamic cycle presented in Figure 9, gas phase free energies as well as aqueous free energies were obtained.
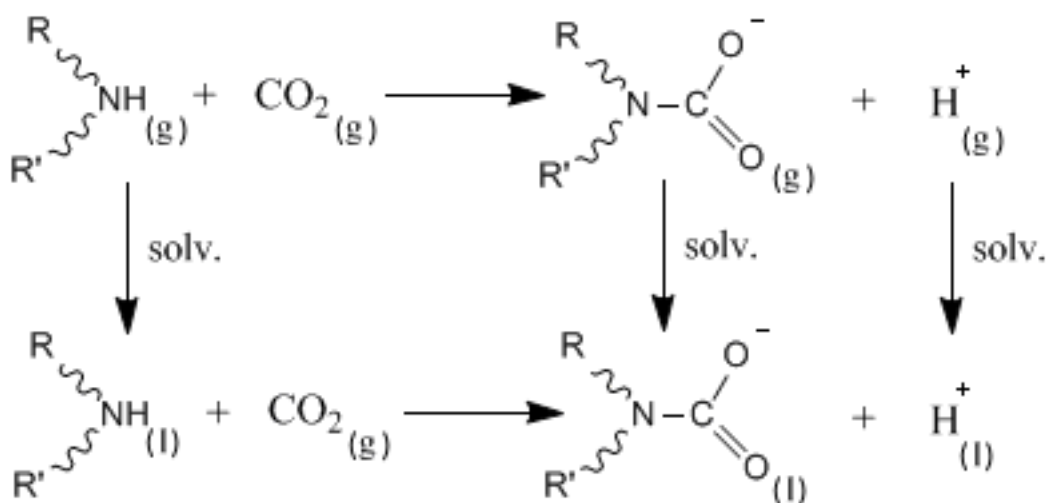


**Figure 9: Thermodynamic cycle used for accounting for solvation effects.**

In Figure 9, the top line corresponds to the gas phase reaction, while the bottom line is the liquid phase to be modeled. By calculating the gas phase free energy and the free energy of solvation for the reaction, it should be possible to obtain the solution phase free energy. The goal is to predict how the binding strength depends on the identity of different functional groups, so that the best functional groups can be tested on IL systems. All calculations were performed with a method and basis set of B3LYP/6-311++G(d,p). To capture the solvation effects, a dielectric continuum model was implemented. This was achieved by using COSMO with water as the solvent.

In Figure 10, the gas phase reaction free energy is plotted versus the free energy of the aqueous reaction for various functional groups.
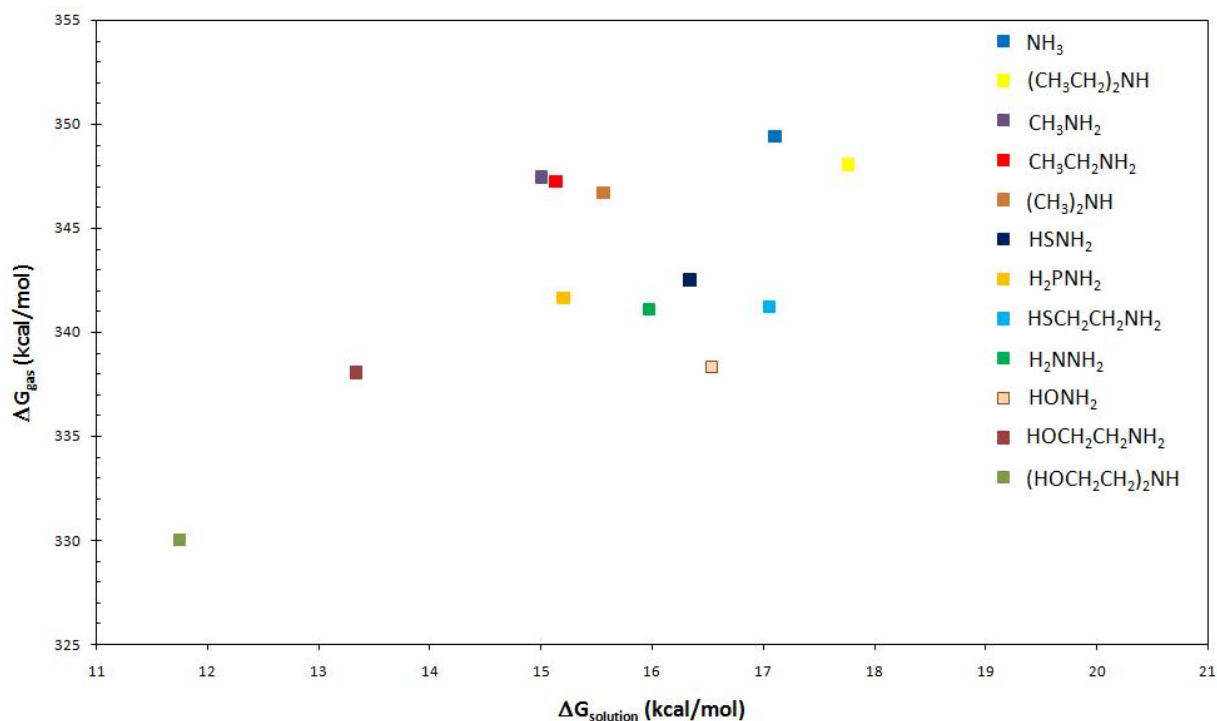


**Figure 10: $\Delta G_{gas}$ vs. $\Delta G_{solution}$ for various functional groups.**

It was observed that there was a correlation between the gas phase free energies and the solution phase free energies, but with some noticeable deviation. It was noted that these initial results were just for solvation in water, which has a dielectric constant of 78.39. ILs tend to have lower dielectric constants, on the order of ~10-15. Using a much lower dielectric constant in the calculations better enable the team to model the real system and give more insight into how the energetics of these reactions would be affected in an IL.

Next, the stoichiometry of the reaction was investigated. There are two reaction pathways that can be taken for $CO_2$ capture. The first pathway is a 1:1 reaction as depicted in Eq. 1, while the second is a 1:2 reaction as shown in Eq. 2



eqn (1)

eqn (2)
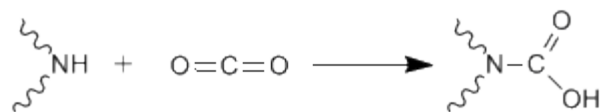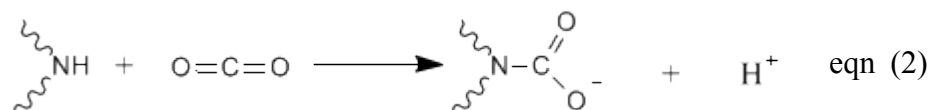
Reaction energies for both pathways were calculated and trends of how different substituent groups attached to the amine effect the reaction energies were established for each pathway. Figure 3 shows the reaction energies for the 1:1 reaction pathway.

In Figure 11, comparing to ammonia, adding an alkyl chain or hydroxyl group to the amine only slightly enhances the bond strength with $CO_2$. Attaching a carbonyl or carboxyl group in the beta position has little to no effect on the reaction energy, while placing either one in the alpha position deactivates the amine. Using a cation as the reactant only slightly deactivates the amine functionality, while using an anion strongly enhances $CO_2$ binding.
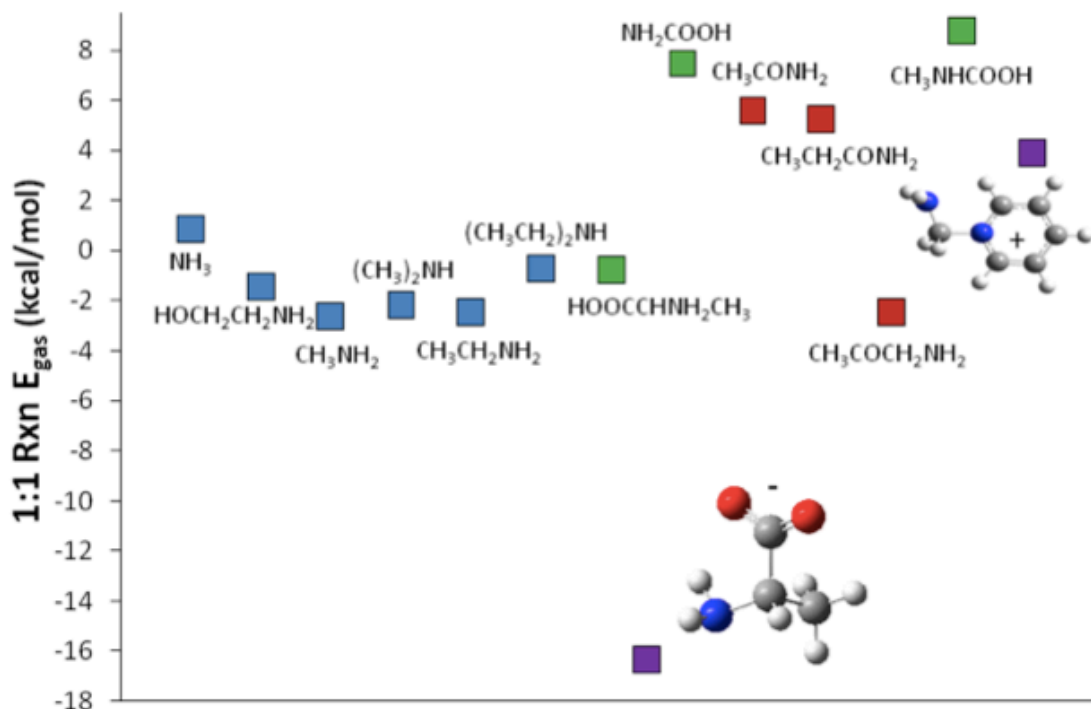


**Figure 11: 1:1 reaction energies of amines reacting with $CO_2$.**
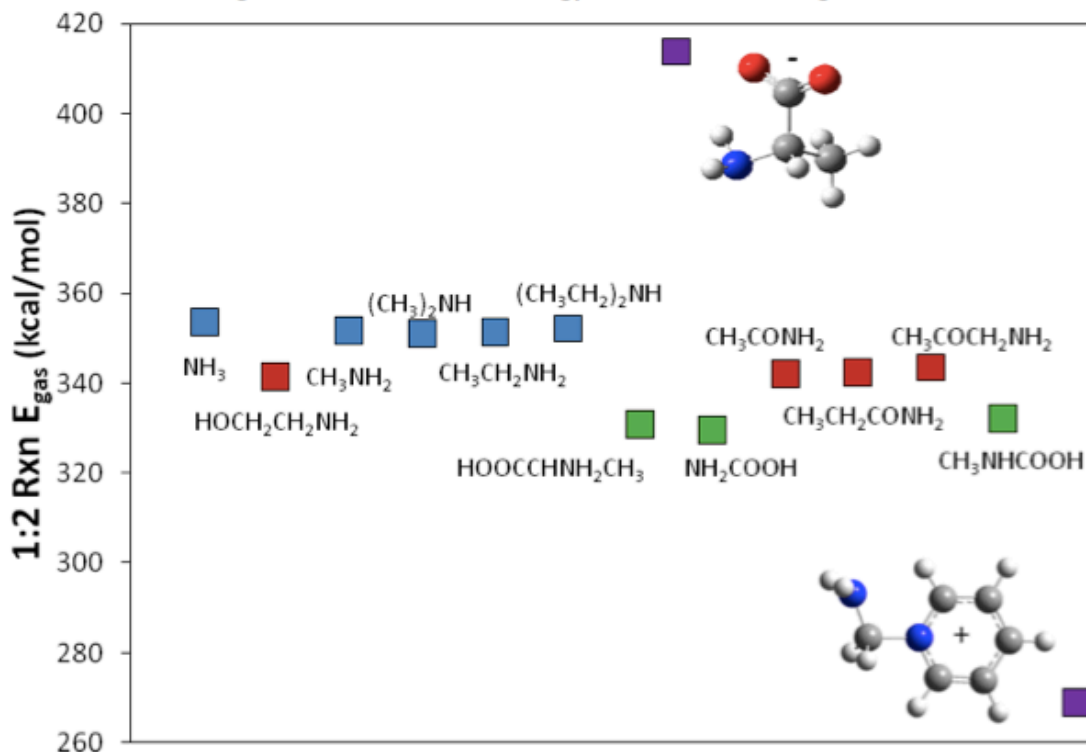
**Figure 12: 1:2 reaction energy of amines with CO₂.**

Figure 12 shows the reaction energy of the 1:2 reaction pathway, and demonstrates that compared to the reaction energy of ammonia, adding alkyl chains has little effect on the reaction energy. Adding a carbonyl or hydroxyl group to the amine enhances the strength of the $CO_2$ binding. Additionally, attaching a carboxyl group strongly promotes the binding of $CO_2$ to the amine.

These results suggest that an amine functionalized cation prefers the 1:2 pathway, while an amino acid anion prefers the 1:1 pathway. The 1:1 pathway is more favorable to have because of the increase in capacity for $CO_2$ over the 1:2 pathway. This was a very important finding, as it suggested that the addition of a functional group on the anion of an IL could double the capacity relative to adding the functional group to the cation (as had been done by everyone up to this point). These calculations were the first time to the knowledge of the team that this effect had been reported.

Additional fundamental studies were carried out to better understand the reaction mechanisms involved. The overall reaction of $CO_2$ was broken down with what were labeled chemically reactive ILs (CRILs) into two parts; carbamate formation and amine basicity. The overall reaction is assumed to be

$$2A + CO_2 \rightarrow Carbamate^- + Ammonium^+$$

The carbamate formation can be described as

$$A + CO_2 \rightarrow Carbamate^- + H^+$$

Amine basicity is defined as:

$$A + H^+ \rightarrow Ammonium^+$$

The method was validated by performing calculations for various molecules and comparing amine basicity with experimental observations reported on the National Institute of Standards and Technology (NIST) WebBook. The comparison is provided in Figure 13. The computed amine basicities are in good agreement with experimental determinations.
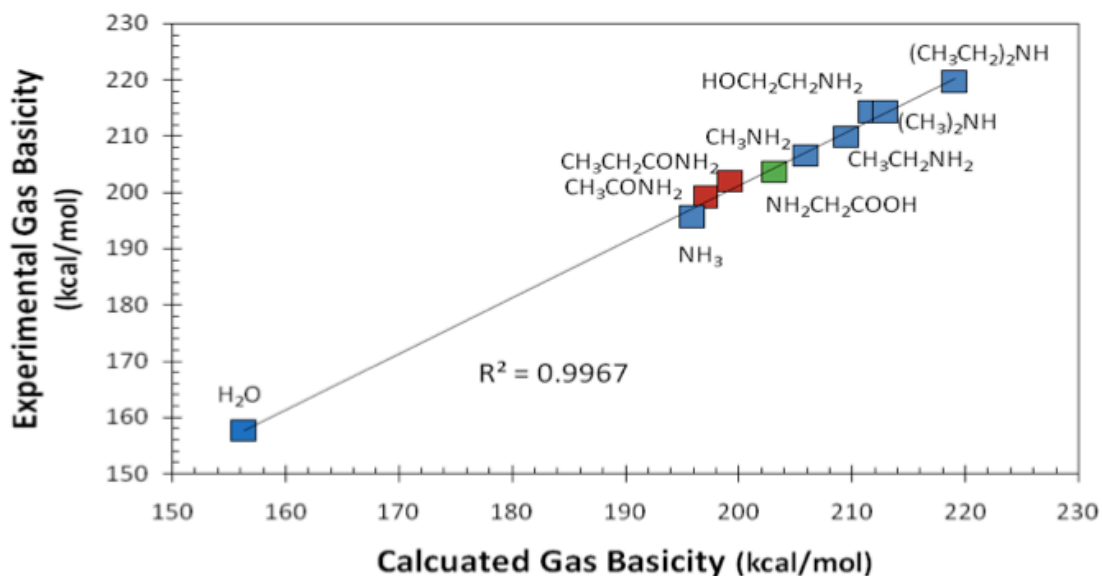


**Figure 13: Comparison of calculated amine basicity with experimental basicity.**

Amine basicity was compared to the carbamate formation reaction as shown in Figure 14 where all energies are plotted with ammonia as reference.
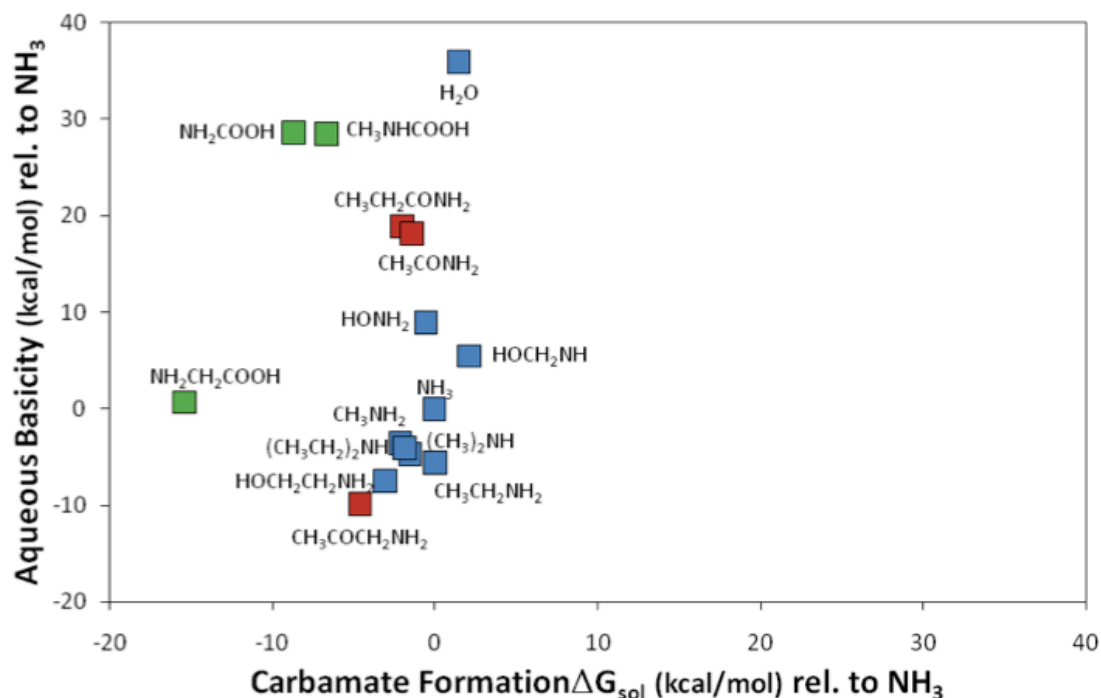


**Figure 14: Amine basicity vs. carbamate formation free energy.**

Figure 14 shows the surprising result that there is no correlation between the two quantities. Therefore, amine basicity and carbamate formation can be tuned independently from each other to obtain the overall best molecule for $CO_2$ capture. This was also a very important finding, as it opened up the range of possible compounds that could be explored.

### 2.3 Synthesis

During BP1, a total of 17 new ILs were synthesized, purified, and characterized. In Q1 NDIL0018, NDIL0027 and NDIL0028 were made. In Q2 NDIL0029, NDIL0030 and NDIL0031 were made. In Q3 NDIL0032-NDIL0038 were made, in Q4 NDIL0024 and NDIL0039 were made, while in Q5 NDIL0041 and NDIL0042 were made. The types of compounds made were guided by the modeling results reported above.

## 2.4 Property Measurement

A wide range of properties were measured on the different ILs synthesized. As an example, Figure 15 shows the temperature dependence of the density of NDIL0018.
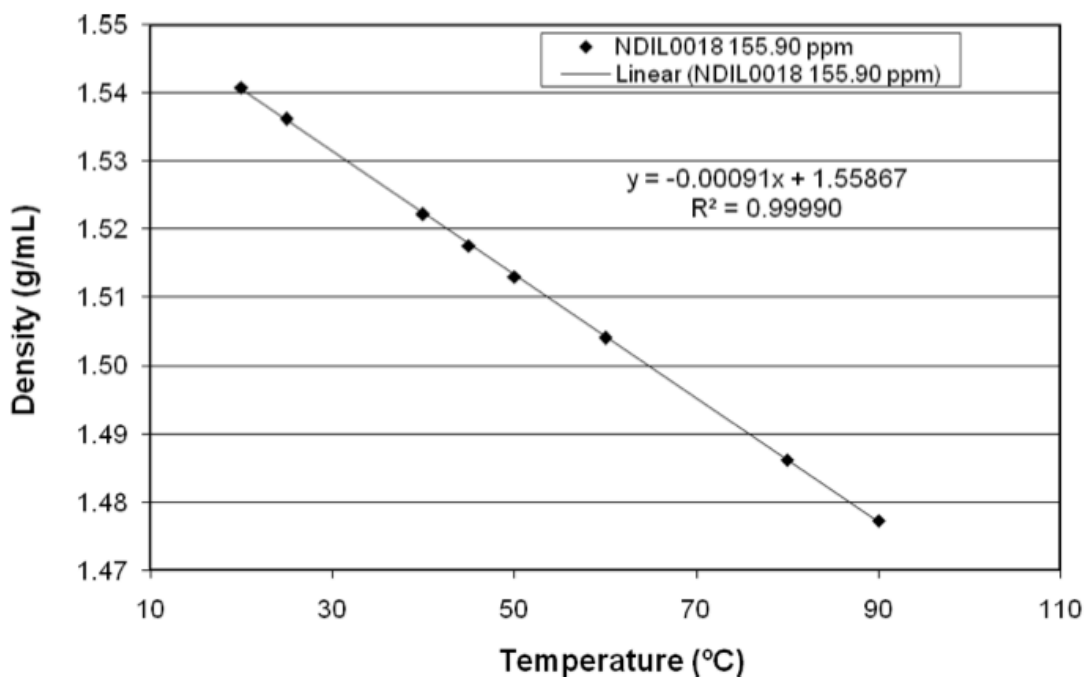


**Figure 15: Density of NDIL0018 as a function of temperature.**

The $CO_2$ solubility in NDIL0018 was measured at 25, 45, 60 and 80 $^oC$. Two different batches of the IL were prepared to determine reproducibility of gas solubility measurements at 45 and 80 $^oC$.

Figure 16 shows the effect of temperature on $CO_2$ solubility at pressures up to 2 bar. Measurements are satisfactory except at 25 $^oC$ where equilibrium was not reached even after 48 hours of $CO_2$ contact with the IL. The data points at 25 $^oC$, however, suggest that the equilibrium solubility of $CO_2$ is at least 0.25 mole fraction. Under the same conditions, the $CO_2$ absorbs in [hmim][Tf$_2$N] with 0.10 mole fraction. The results demonstrated for the first time the successful creation of an IL with enhanced $CO_2$ carrying capacity versus

a physically dissolving IL. It also gave the first indication, although not fully clear at the time, that the viscosity of these ILs increased dramatically upon reaction with $CO_2$, which results in very slow uptake rates.
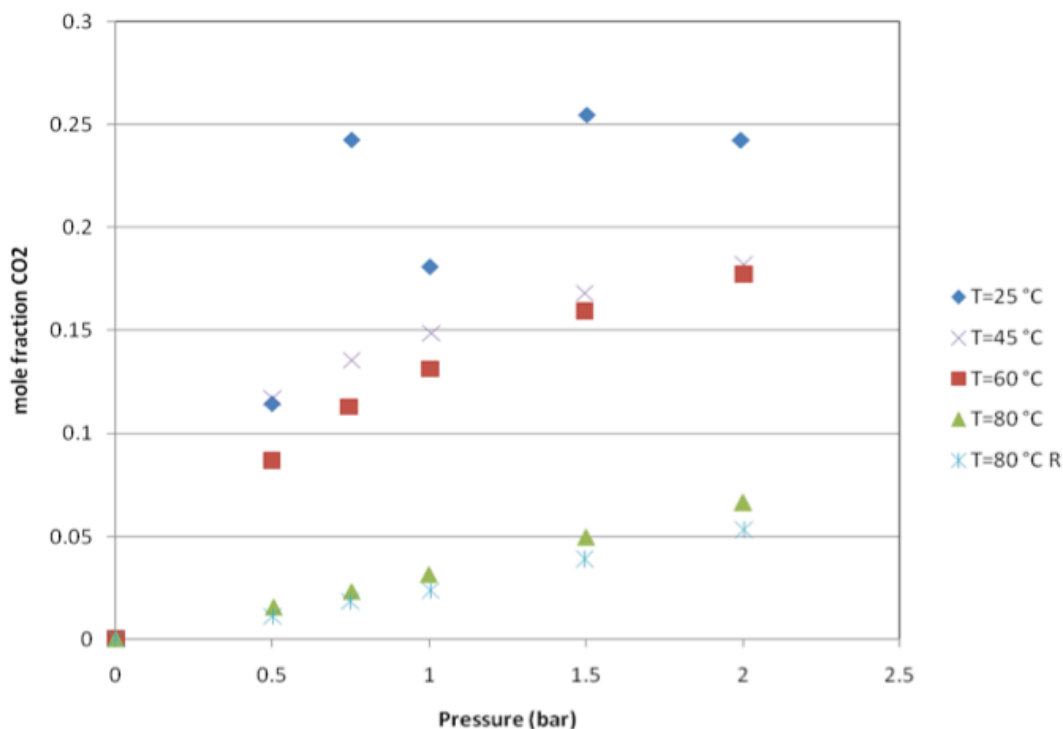


**Figure 16: CO$_2$ solubility in NDIL0018.**

The solubility of $CO_2$ was found to increase with increasing pressures and decrease with increasing temperature, a trend that is consistent with gas solubility in ILs.

Preliminary $CO_2$ absorption experiments in NDIL0017 were also conducted to estimate the contact time required for equilibrium solubility measurements. Two different batches of NDIL0017 were used for this purpose and it was determined that $CO_2$ will have to be contacted for more than 48 hours at 25 $^{\circ}$C to obtain equilibrium solubility data points as a function of pressure. Again, this was an indication that the viscosity was increasing for this class of ILs upon reaction with $CO_2$. It was established that at higher temperature the equilibration is much more rapid requiring only 24 hours at 100 $^{\circ}$C. The solubility of $CO_2$, however, is considerably lower at higher temperature as shown in Figure 16.
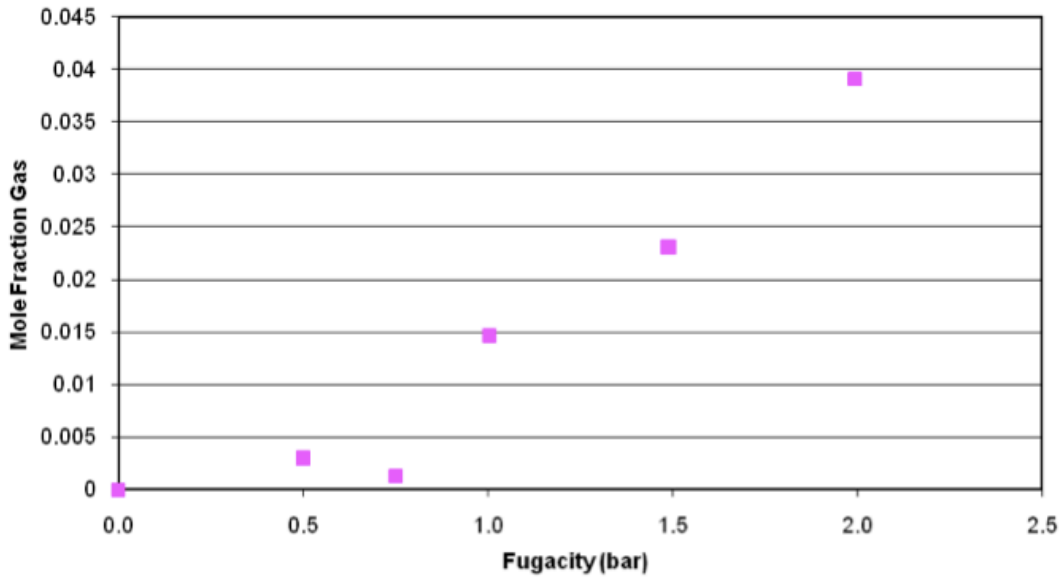
**Figure 17: CO$_2$ solubility in NDIL0017 at 100 $^o$C.**

Then CO$_2$ solubility measurements were performed in a commercially available IL ethylmethylimidazolium tetracyanoborate [emim][B(CN)$_4$]. The results of the measurements at 25 $^o$C are provided in Figure 18.
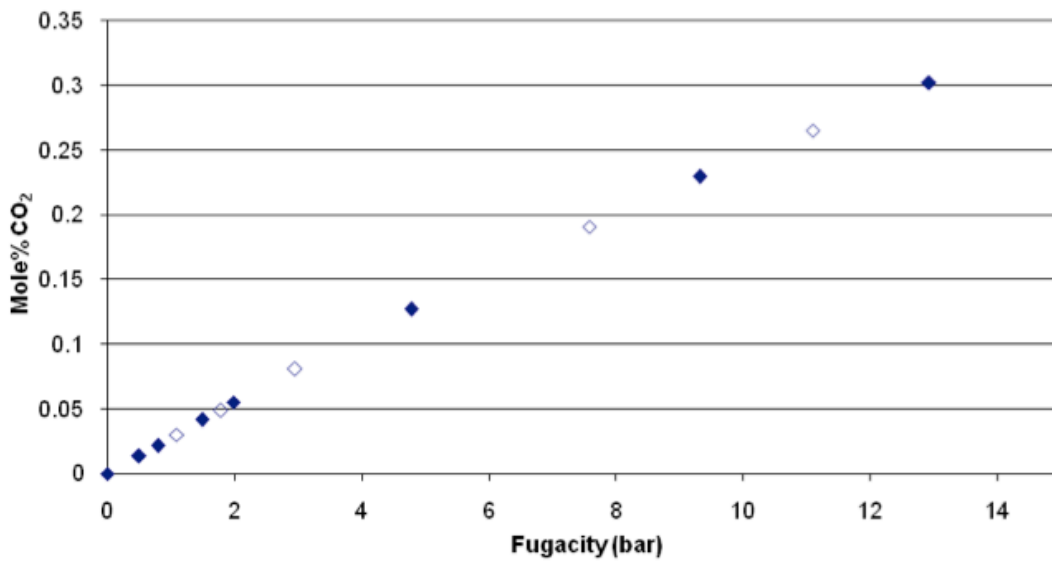


**Figure 18: CO$_2$ solubility in [emim][B(CN)4] at 25 oC.**

As can be seen, $CO_2$ is much less soluble in [emim][B(CN)4] as compared to that observed in ILs NDIL0018 and NDIL0028, but it is simple to measure the solubility at low temperature. Thus the physically dissolving ILs do not have the same mass transfer problems as the CRILs examined up to this point. Other $CO_2$ solubility measurements were performed in physically dissolving ILs to make sure the apparatus was giving reliable results. Figure 19 shows results for $CO_2$ solubility in [hmim][Tf2N] (also known as NDIL0001) at 120 $^o$C and up to pressures of 19 bar. The Henry's Law constant is approximately 125 bar, once again suggesting lower $CO_2$ solubility than the CRILs.
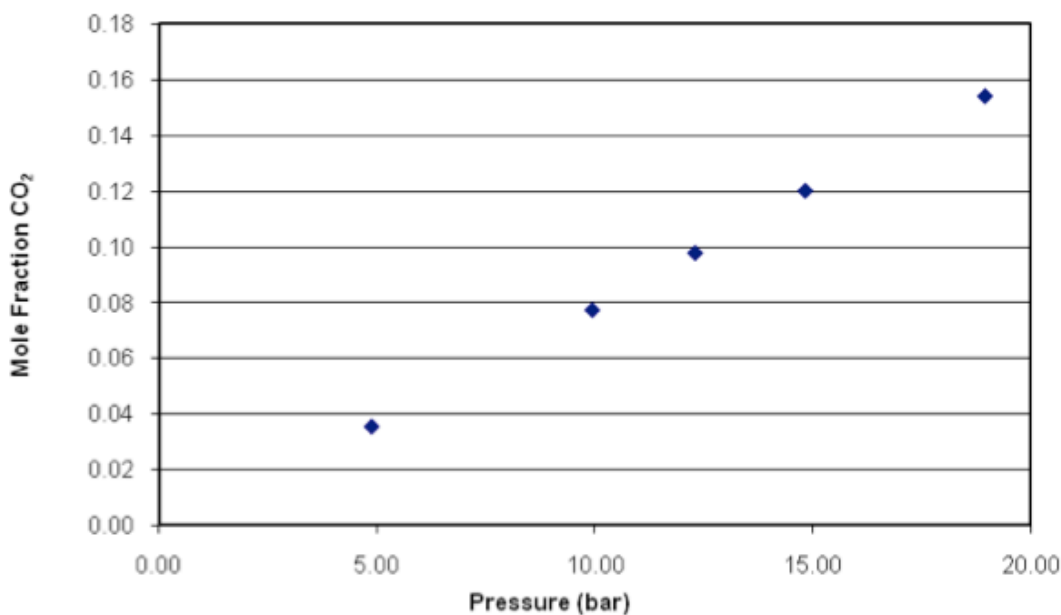


**Figure 19: Solubility of $CO_2$ in [hmim][Tf2N] at 120 $^o$C.**

The unexpectedly slow rates with which $CO_2$ absorbs in the CRILs made determination of uptake in these systems impossible with the conventional gravimetric balances. That is because these balances have no stirring and thus rely on pure diffusion for equilibration. Many more measurements were made for a range of CRILs during BP1, but the results were all unsatisfactory. Therefore gravimetric measurements were discontinued and construction was begun of a new apparatus that had stirring and could measure the uptake rates in these systems. During this period construction was also begun of an apparatus

that could measure mixed gas solubilities instead of just pure gas solubilities. Finally, assembly of a ReactIR system designed to measure reaction rates was begun.

As a first step towards examining the rate of $CO_2$ uptake by ILs, a simple diffusion model was developed to extract rate data from observed $CO_2$ gravimetric uptake rates. Figure 20 illustrates representative fits of data for non-reactive and reactive ILs, respectively. The diffusion constant extracted for the non-reactive IL at room temperature is of the order of $10^{-6}$ cm$^2$/s, consistent with literature results for similar materials. The apparent diffusion constant for the CRIL is approximately 3 orders of magnitude less. This apparent diffusion constant may include contributions both from actual diffusion and from the kinetics of chemical reaction. These rates will be critical for use in developing accurate process models.
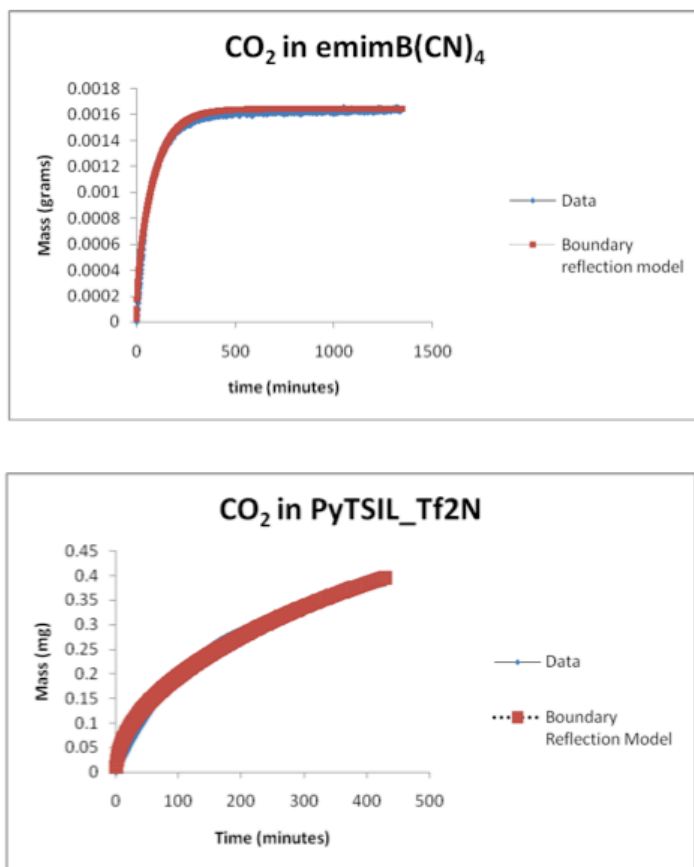




**Figure 20: Uptake rates and fits of diffusion model for a convention IL (top) and a CRIL (bottom).**

Once the ReactIR was assembled, calibration studies were performed for $CO_2$ sorption in NDIL0001 and NDIL0006 at 25 and 50°C. Both ILs are non-complexing; they do not react with $CO_2$ and have known physical solubility, previously measured in the ND laboratory. Preliminary comparisons were made with two CRILs, NDIL0017 and EMD0004. At 25°C, the peak area of the C=O stretching vibration indicates a smaller amount of $CO_2$ is physically absorbed in the CRILs as compared to the physically dissolving ILs at the same pressures, as seen in Tables 8-9. These results are consistent with the molecular simulations that predicted that physical solubility in the CRILs should be lower than in conventional ILs.

Table 8: Comparison of $CO_2$ physical absorption at 4.9 bar and 25°C .

|  | Concentration [μmol $CO_2$/g IL] | Mol ratio [mol $CO_2$/mol IL] |
|---|---|---|
| **NDIL0017** | 0.17 | 0.07 |
| **NDIL0001** | 0.37 | 0.17 |
| **NDIL0006** | 0.34 | 0.16 |

Table 9: Comparison of $CO_2$ physical absorption at 6.0 bar and 25°C.

|  | Concentration [μmol $CO_2$/g IL] | Mol ratio [mol $CO_2$/mol IL] |
|---|---|---|
| **EMD0004** | 0.27 | 0.13 |
| **NDIL0001** | 0.46 | 0.21 |
| **NDIL0006** | 0.42 | 0.20 |

Studies were performed using the ReactIR to see if degradation occurs for the CRILs at higher temperatures. EMD0004 was heated up to 62°C and kept at this temperature for three days at constant $N_2$ pressure then cooled to room temperature in the infrared (IR) cell. No change in the spectra is observed, indicating that no degradation occurs up to 62°C. In order to further address this issue, a repeatability experiment was conducted in one of the gravimetric microbalances with EMD0004 to determine the reliability of previous $CO_2$ absorption measurements. The IL was first evacuated to a pressure of approximately 15 millibar at a temperature of 65˚C until a change in the slope of the mass decrease was observed. Absorption of $CO_2$ was then measured at 60˚C for pressures of 100 and 200 millibar and cycled three times, with equilibration times of approximately 84 hours for each pressure point. For all pressure points where equilibration was reached,

there was no significant change in absorption as the cycle was repeated. The solubility of $CO_2$ at 200 mbar is 0.27 mole fraction $CO_2$. At the time, this IL showed the highest $CO_2$ solubility measurement, and the stability results were encouraging.

Later during BP1, a simple room temperature apparatus (RTA) with stirring was constructed, and the results revealed an increase in viscosity upon $CO_2$ complexation. For EMD0004 and the NDIL0017 at 2% mole fraction $CO_2$ absorbed, viscosities of 410 poise and 38 poise, respectively, were measured. This was the first direct evidence that was obtained of a viscosity increase with $CO_2$ complexation.

Subsequently, an investigation was made to determine if a diluent could be used to lower the viscosity. The ReactIR system was used to obtain a calibration curve for chemically complexing $CO_2$ in the form of concentration versus the peak area by using external barometric measurements of the overall $CO_2$ uptake of CRIL EMD0004 with 25wt% diluent. The CRIL was diluted in order to decrease its viscosity and facilitate a good mixing in the reactor cell. Experiments are performed at 40 and 60°C within the pressure range of 0-2 bar. The absorption-desorption cycle was repeated at 40°C with the same sample and pulling vacuum between the cycles. A calibration curve for physical absorption of $CO_2$ in the diluent was also determined. From this curve and that determined previously for another IL, assuming ideal mixing, the concentration of physically dissolved $CO_2$ was estimated. The remaining uptake of $CO_2$ was then ascribed to the chemical reaction. Relating the chemical uptake of $CO_2$ to the peak area is complicated by overlapping peaks observed in the spectra. Voigt-type curves were fitted, each with 4 coefficients to the peak area of interest. It was estimated that in EMD004+25 wt % diluent, physically dissolved $CO_2$ accounts for only 1 mol % of total uptake.

An absorption experiment at 25°C was performed with NDIL0039. One equilibrium point was collected at 1.9 bar, and the experiment was terminated since no reaction took place. Apparently, $CO_2$ is only physically soluble in NDIL0039 and its capacity is 0.044 mol $CO_2$/mol IL compared to the 0.053 mol $CO_2$/mol IL capacity of NDIL001. It had been expected that this IL to react with $CO_2$, but found that it did not.

Water solubility measurements were carried out in NDIL001 at 25$^o$C from 0 to 25 bar and in NDIL0017 at 60$^o$C for pressures ranging from 0 to 70 mbar. Data for both ILs were compared to previous liquid-liquid equilibria (LLE) measurements and found to extrapolate in good agreement with the LLE data. From the solubility measurements, the solubility of water at saturation was determined to be 4.8 wt % and 13 wt % respectively. This is important information for subsequent process modeling studies, because water will be present in the flue gas. The saturation water solubility in EMD0004 was measured and found to be comparable to that in NDIL0017 and NDIL0018. Also, the water solubilities were determined in NDIL0030, NDIL0031, NDIL0032, NDIL0033 and NDIL0034. All these ILs, except NDIL0030, were found to be water miscible.

The next step was to validate the mixed gas solubility measurement apparatus. $CO_2/O_2$ mixture solubility in NDIL0001 was measured, and the experiments confirmed results from a previous simulation study that there was no enhancement of $O_2$ solubility due to the presence of $CO_2$. Essentially, $CO_2$ and $O_2$ absorb independently of one another, so that pure gas solubilities provide a good estimate of mixed gas solubilities.

$CO_2$ solubility measurements in NDIL0017 were performed at 25$^o$C for two separate batches. The $CO_2$ capacity was found to be different for these batches. It was also noted that the time required to reach the equilibrium solubility was more than 48 hours. Experiments at 100$^o$C were carried out for faster equilibrations. Results, however, showed a decrease in capacity and possible degradation of the IL.

In addition to $CO_2$ solubility measurements, viscosities were also measured. Table 10 provides a summary of the results obtained in BP1.

Table 10: Chemical Absorption of $CO_2$ in ILs using the Stoichiometric Methodology.

| Ionic Liquid (ND Code) | Apparatus | Temperature (ºC) | Pressure (bar) | Absorption % (mol/mol) | Absorption (Mol CO₂/Mol IL) | Viscosity ± 10% at 22 ºC (P) IL | Viscosity ± 10% at 22 ºC (P) CO₂ + IL | Water Content (ppm) |
|---|---|---|---|---|---|---|---|---|
| EMD0004 | RTA | 22 | 0.49 | 41.2 | 0.70 ± 0.03 | 5.1 | 2619.5 | N/A |
| NDIL0017 | RTA | 22 | 1.57 | 16.2 | 0.19 ± 0.01 | 13.7 | 50.0 | N/A |
| NDIL0039 | RTA | 22 | 1.63 | 5.2 | 0.06 ± 0.01 | 56.3 | 16.0 | N/A |
| 0.63[EMD0004] + 0.37[diluent] | RTA | 22 | 1.46 | 26.6 | 0.57 ± 0.01 | N/A | 16.1 | 2403 |
| NDIL0030 | RTA | 22 | 1.21 | 51.5 | 1.06 ± 0.02 | 5.2 | 188.5 | 200 |
| NDIL0033 | RTA | 22 | 1.47 | 41.2 | 0.70 ± 0.02 | 10.7 | 152.6 | 2668 |
| NDIL0033 | ITA | 22 | 1.49 | 38.3 | 0.62 ± 0.07 | N/A | N/A | 3871 |
| NDIL0033 | ITA | 25 | 1.50 | 37.4 | 0.60 ± 0.07 | N/A | N/A | 3871 |
| NDIL0033 | ITA | 40 | 1.58 | 38.2 | 0.62 ± 0.07 | N/A | N/A | 3871 |
| NDIL0038 | RTA | 22 | 1.21 | 54.3 | 1.19 ± 0.03 | N/A | N/A | N/A |
| NDIL0041 | ITA | 20 | 1.36 | 48.0 | 0.92 ± 0.04 | N/A | N/A | N/A |

RTA: Room temperature apparatus
ITA: Isothermal apparatus

## 2.5 Economic and Systems Analysis

Trimeric Corporation (Trimeric) developed an idealized $CO_2$ capture model to document the minimum energy required to perform an ideal separation of $CO_2$ from flue gas and then compress the $CO_2$ to pipeline pressure (2205 psia) as specified in the DOE/NETL Systems Analysis Guidelines (DOE/NETL, 2005). This analysis established an appropriate benchmark and provided context for current post-combustion $CO_2$ capture costs targeted by the DOE. The methodology and results of this idealized model are contained in Appendix I, "An Idealized $CO_2$ Capture Model with Thermodynamic

Analysis of Minimum Energy Requirements". The model shows that, based on thermodynamic constraints, the minimum ideal work required to capture and compress $CO_2$ is in the range of 10-17 kJ/mole of $CO_2$, depending on whether or not water is condensed in the system and at what temperature the flue gas is fed to the capture system. When converted to electrical power for a 500 MW plant, this means a minimum of 26-44 MW of work must be supplied to capture and compress $CO_2$. If this is equal to the plant de-rating, then a new output of 456-474 MW will be expected, with a resulting 5.4-9.6 % increase in the cost of electricity (COE). Note that this is the thermodynamic minimum and does not include any capital cost. With typical thermodynamic efficiencies for separation processes included, the actual COE increase is expected to be 20 % or more. Capital costs for current absorption-based technology has been reported to be about $0.01/kWhr, or roughly another 20 % increase in COE (DOE, 2006). Thus it was concluded that processes that can achieve an increase in COE of less than 40% are probably infeasible.

Work on a commercialization study began with the completion of a technical summary of carbon capture technologies in competition with ILs. The primary competing technologies are the following: oxy-fire combustion as a retrofit to current pulverized coal (PC) power plants, MEA scrubbing utilizing a traditional absorber- stripper configuration, and both MEA and potassium carbonate systems promoted with piperazine (PZ). Other emerging technologies of interest include solid sorbents, membranes, biocatalysis, and metal organic frameworks; however, these technologies are either not yet proven concepts or have not yet gone to the pilot plant stage, so less technical and economic data is currently available than for the primary three candidates.

Trimeric completed a preliminary process model of an IL $CO_2$ capture system using HYSYS. The goal was to use this to conduct baseline simulations on conventional absorber/regenerator configurations with a $CO_2$ compression train. To run the model, data on physical properties and solubilities are required. Notre Dame provided Trimeric with these data for a physically absorbing IL as well as a CRIL at the end of BP1, so results would be generated in BP II.

**2.6 Project Management and Reporting**

The project team held regular meetings and conference calls to stay on track. A kickoff meeting for the project was held in Pittsburgh in conjunction with a CCS meeting. At the end of BP1, a continuation was submitted and efforts were made to add Air Products and Merck / EMD to the project. Air Products was to assist in process development schemes as well as in additional gas solubility measurements. Merck / EMD is a large manufacturer of ILs and was brought on board to help in making larger quantities and also to help guide efforts toward ILs that could be made at scale for relatively low costs.

## 3. Budget Period II: 7/22/08-7/21/09

**3.1 Background**

BP II had five major tasks: 1) molecular modeling; 2) synthesis of generation 2 species; 3) property measurement of generation 2 species; 4) economic, engineering and systems analysis; 5) and project management and reporting. Lab-scale and bench-scale testing were deferred until the following BP due to the need to focus more attention on finding ILs with desirable properties.

Air Products and Merck / EMD were successfully added to the project in BP II and began contributing to the project. The focus was to consolidate some of the findings of BP I, extend the studies of CRILs to focus on capacity and viscosity, and begin developing a knowledge base that would enable the construction and operation of a lab-scale test system.

**3.2 Molecular Modeling**

Air Products participated in this aspect of the project during BP II. They first focused on an atomistic simulation study of the mechanism whereby MEA reacts with $CO_2$. This was done in order to gain experience and validate the simulation tools they were to use. Overall the goal was to use state of the art computational chemistry methods to help

design and develop efficient and cost effective ionic ILs to capture $CO_2$ with high capacity. Their efforts in many ways mirrored those used by Notre Dame in BP I. It was recognized that these methods must be reliable and sufficiently accurate in order to predict properties of materials yet to be made. The methods chosen for this task were quantum mechanical density DFT and ab initio molecular dynamics (AIMD) simulations. Two theoretical models were utilized to describe the $CO_2$ capture mechanisms and to predict thermochemical properties of materials upon interacting with $CO_2$:

1. Implicit model: $CO_2$ interactions with an absorbent are first calculated using DFT in the gas-phase. Subsequently, the interaction pair is studied in an appropriate continuum representing the solvent using the COSMO model. Both the thermochemical energies and reaction barriers are calculated to gain insight into reaction pathways. This is a very similar approach to that taken by Notre Dame in BP I, but the idea was that each group could study different systems and perhaps advance faster than any one group could.

2. Explicit model: AIMD simulations were used to quantitatively simulate $CO_2$ absorption in the selected absorbent in condensed phase. Absorbent, $CO_2$ and solvent molecules were explicitly contained in a selected unit cell with a periodic boundary condition. The potential energies of the unit cell were calculated using DFT with a plane wave basis set and constant canonical ensemble (constant NVT) molecular dynamics simulations are performed in a canonic ensemble with Nose thermostat for temperature control. This is a new technique that had not been used up to this point in the project.

Air Products researchers decided to first benchmark the methods for systems that have been studied experimentally. MEA is such a system and has been widely used in many industrial processes to capture post combustion $CO_2$. It has been found experimentally that 2 MEA molecules in 30% aqueous solution capture 1 $CO_2$ at low partial pressure with a chemisorption energy of -20.4 kcal/mol at $40^{\circ}C$ [8]. The reported liquid density at $15^{\circ}C$ for pure MEA is $1.020 g/cm^3$ and for 30% MEA aqueous solution is $1.015 g/cm^3$.[9]

Air Products therefore performed extensive simulations using the above methods to study $CO_2$ interactions with MEA. The main results are summarized as follows:

1. The calculated liquid densities of pure MEA and 30% MEA aqueous solution were $1.081 g/cm^3$ and $0.947 g/cm^3$. They claimed that this was in reasonable agreement with the experimental values, although it is clear that some aspects of the model is lacking.

2. The room temperature AIMD simulations suggest that the dominant mechanism of $CO_2$ in 30% MEA aqueous solution is $CO_2$ absorption induced proton transfer. The MEA molecules act both as a $CO_2$ acceptor and as a base to accept a proton. Water does not explicitly participate in the capture process.

3. The calculated average chemisorption energy of $CO_2$ in 30% MEA aqueous solution is -22.5 kca/mol, in good agreement with the experimental value.

4. $CO_2$ attachment to MEA in aqueous solution is an exothermic process with an activation barrier of ~3-4 kcal/mol, indicating the process is thermodynamically and kinetically facile at near ambient conditions.

Some of the CRILs synthesized at Notre Dame show strong interactions with $CO_2$ and exhibit 1:1 reactivity. However, some of these materials undergo several irreversible reactions that give rise to byproducts. To help identify these byproducts, Air Products performed quantum mechanical calculations to explore possible side reactions. The IR, Nuclear Magnetic Resonance (NMR) and Ultraviolet/Visible (UV/Vis) spectra were calculated for a range of ionic species that bind with $CO_2$. The calculations were done using DFT with the B3LYP exchange-correlation functional and 6-311+G** basis set. Various conformations of these species were examined. The calculated main spectral features show a strong dependence on structural conformations. They further examined the sensitivity of the calculated spectra with respect to ion pairing effects. The results indicated that the main features of the spectra are indeed sensitive to ion pairing, suggesting that a realistic theoretical model for spectral characterization of ILs should

incorporate both cations and anions in order to compare with experimental spectra. The sensitivity of these spectral features to the intrinsically loose binding structures between cations and anions remains an unanswered question. The results of these studies by Air Products were inconclusive. As discussed later, Air Products dropped out of the project, and so this avenue of investigation was abandoned.

Classical force fields were developed for the Generation 2 ILs using a combination of electronic structure calculations for intramolecular terms and partial charges and the Generalized Amber Force Field (GAFF) database. These force fields were then used to compute a wide range of physical properties for these ILs.

The impact of an additional functional group, fluoro-amines, on $CO_2$ binding was examined.

The overall stoichiometry for an amine reaction is generally accepted to be

$$2 \text{ amines} + CO_2 \longrightarrow \text{carbamate}^- + \text{ammonium}^+$$
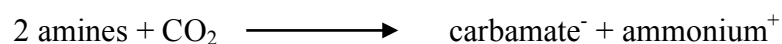
The overall reaction can be broken down into two reactions as follows. The first would be the carbamate formation reaction as follows:

$$\text{amine} + CO_2 \longrightarrow \text{carbamate}^- + H^+$$
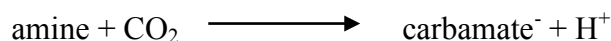
The other reaction would be the protonation or basicity reaction as shown:

$$\text{amines} + H^+ \longrightarrow \text{ammonium}^+$$
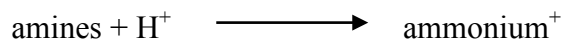
Figure 21 compares the two reactions on the same plot for various functionalized amines. As can be seen, there isn't any correlation between the two reactions. This would suggest that each reaction could be independently tuned to obtain the desired reaction energy. Also, the dashed lines are contours of constant reaction energy in kcal/mol. Using these, which functional groups can be added to obtain the desired reactivity can be determined. One last thing to note is that the basicity reaction plays a more significant role in the

overall energy than the carbamate formation as seen by the larger spread in the energies than in the other reaction. This information builds off the studies shown earlier in Figure 14 and was used to search for new functional groups that could be attached to an IL.

Work was carried out to build an analytical model for $CO_2$ absorption / reaction that could be used in both future process modeling work and to help make sense of simulation results.

In order to achieve this, two equilibrium models were used, one for a 1 amine : 1 $CO_2$ reaction ratio and one for a 2 amine : 1 $CO_2$ reaction ratio, leading to expressions 1 and 2 respectively for equilibrium constants.

$$K_{eq} = \frac{x_{IL\text{-}CO_2}}{P_{CO_2} x_{IL}} \qquad\qquad K_{eq} = \frac{x_{IL-CO_2}}{P_{CO_2} x_{IL}} \qquad\qquad\qquad \text{eqn (3)}$$

$$K_{eq} = \frac{\left(x_{IL\text{-}CO_2}\right)^2}{P_{CO_2} x_{IL}^2} \qquad\qquad K_{eq} = \frac{\left(x_{IL-CO_2}\right)^2}{P_{CO_2} x_{IL}^2} \qquad\qquad\qquad \text{eqn (4)}$$
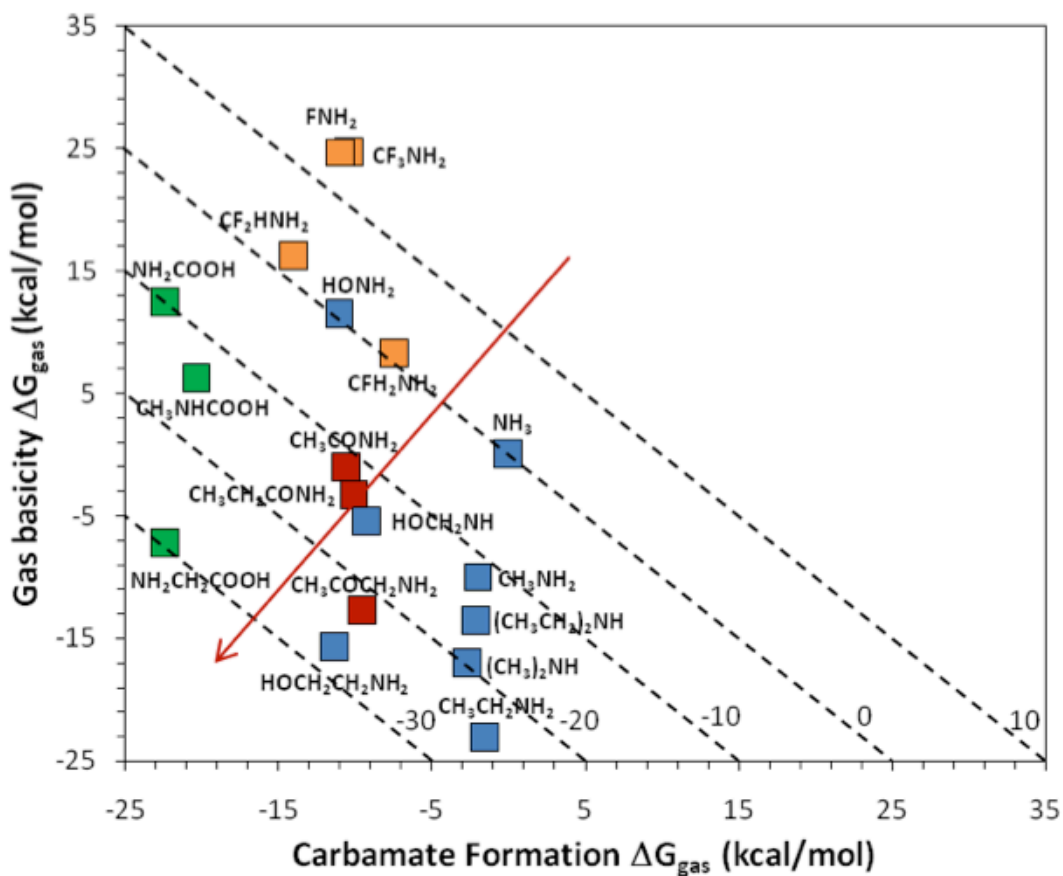
**Figure 21: Protonation vs. carbamate formation free energies.**

Based on simulations performed on NDIL0030, a $\Delta H$ of -62 kJ/mol was used along with a $\Delta S$ of -0.156 kJ/mol-K. Figure 22 shows the experimental $CO_2$ isotherm along with calculated isotherms for 1:1 and 2:1 stoichiometry.
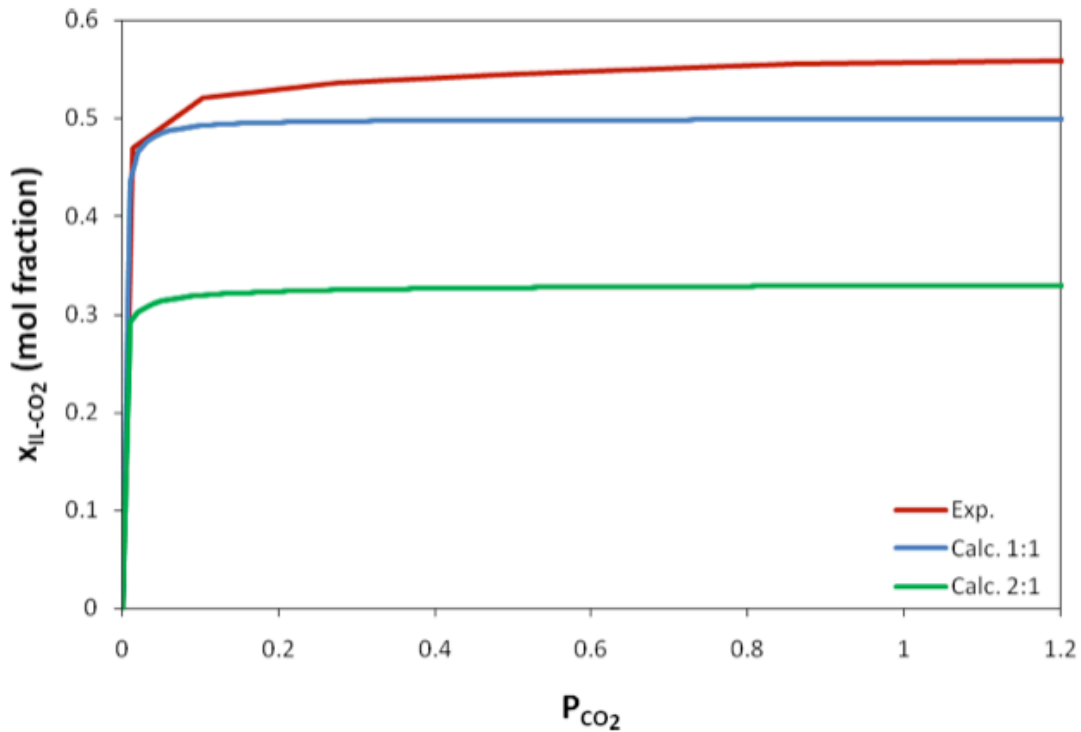
**Figure 22: Experimental CO$_2$ isotherm and isotherms obtained from equilibrium models at 22° C. Pressure is expressed in bar.**

Clearly, the 1:1 reaction stoichiometry better models the experimental results than the 2:1 reaction stoichiometry. It is to be noted that in this particular case, neither model includes physically absorbed CO$_2$, while experimental data contains physically absorbed CO$_2$. Figure22 also shows that the ΔH obtained from simulations agrees reasonably well with experiment.

Since the 1:1 reaction model captures experimental data reasonably well, the ΔH sensitivity was determined just for this reaction model. Three different values of ΔH were explored over three different temperatures. Figures 22, 24 and 25 show the ΔH

sensitivity of ΔH values of -62, -56, and -50 kJ/mol, respectively.
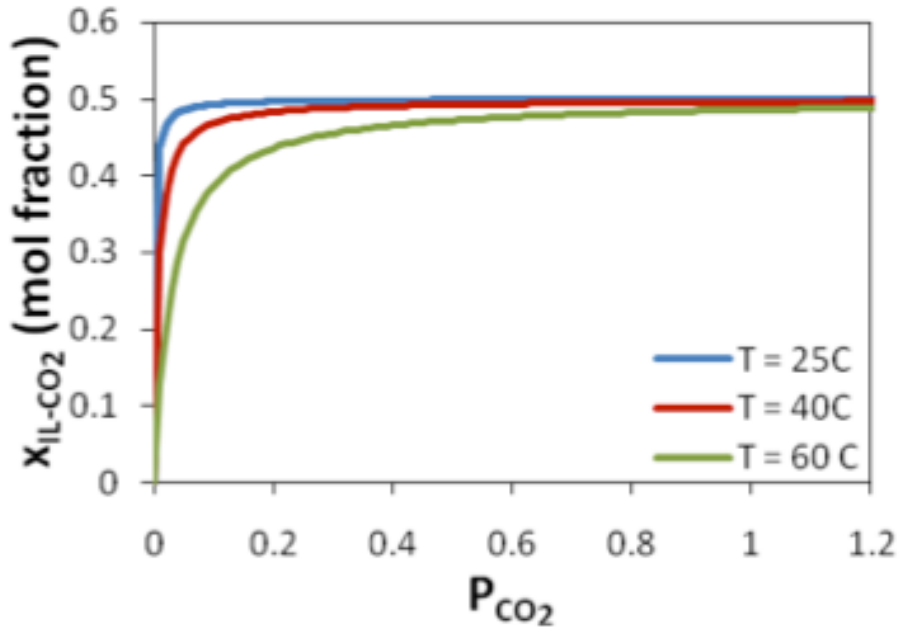


**Figure 23: ΔH = -62 kJ/mol for various temperatures**
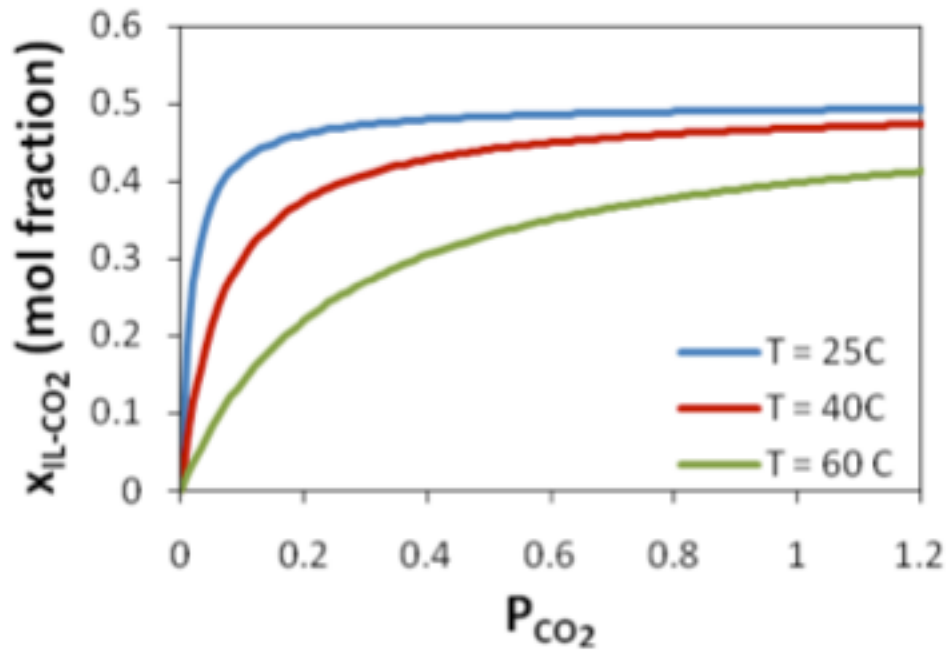


**Figure 24: ΔH = -56 kJ/mol for various temperatures**
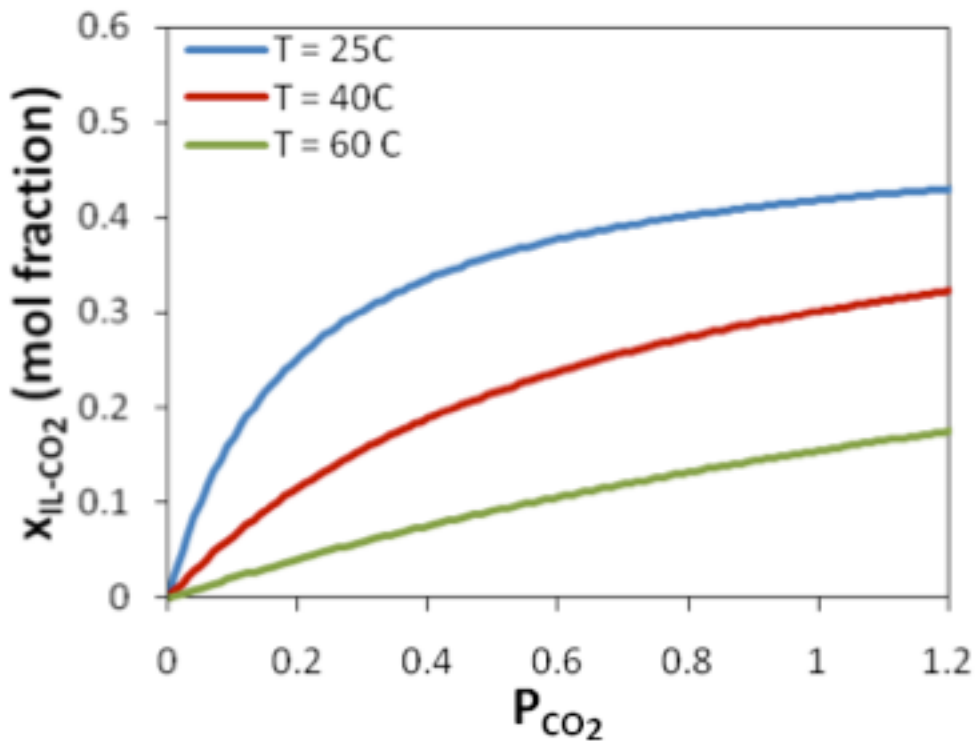
**Figure 25: ΔH = -50 kJ/mol for various temperatures**

These results show just how sensitive the $CO_2$ isotherms are to both changes in ΔH and temperature. Using this information, certain enthalpy ranges were targeted as being most feasible for $CO_2$ capture. Then the equilibrium model was updated to include both the physical solubility as well as the temperature dependence. Applying the equilibrium model for two different conditions (absorber and desorber) and subtracting the difference in the mole ratio for the two conditions, the optimal enthalpy of reaction corresponding to the maximum loading of $CO_2$ was determined. Figure 26 shows the graph of the optimal ΔH versus the change in mole fraction between the two conditions. As shown, the optimal ΔH is around -50 kJ/mol and that corresponds to a change in mole ratio of about 0.4.
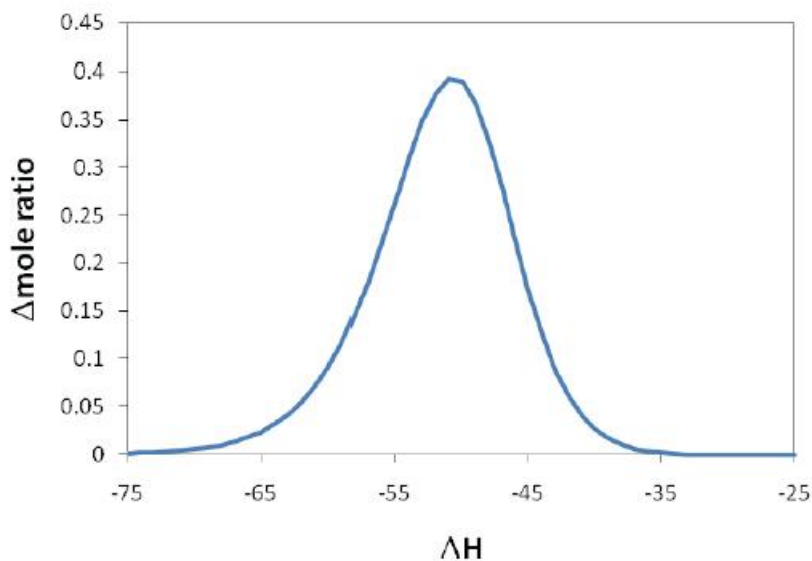
**Figure 26: Plot of the optimal enthalpy of reaction that maxims net loading difference for $CO_2$ between the absorber and the stripper at one set of conditions.**

This result is significant because, even without performing detailed process modeling calculations, it could be predicted that an "optimum" enthalpy of reaction exists and that it should be around -55 kJ/mol. Rochelle and others have argued that, for aqueous amine systems, stronger binding is always better, but for the case of an anhydrous IL solvent, this is not the case. Very strong binding results in efficient removal of $CO_2$ from the flue gas, but a large amount of energy must be expended to regenerate the solvent. On the other hand, weak binding minimizes the regeneration energy, but requires lots of solvent to remove a given amount of $CO_2$. The heuristic shown in Figure 26 predicts that the "best" solvent is the one that maximizes the change in concentration of $CO_2$ in the solvent at a given set of absorber / stripper conditions. As shown later, the enthalpy estimated in this was very similar to the value obtained with the detailed process modeling calculations.

In the last quarter of BP II, these results were searched for candidate ILs that had $CO_2$ binding energies in the target range.
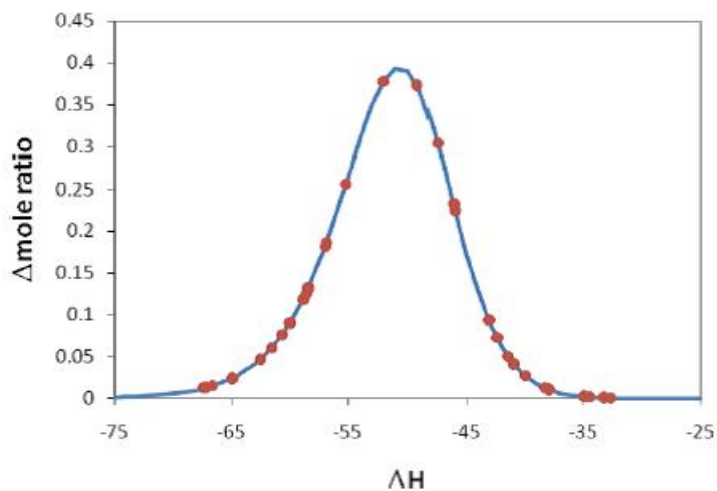
**Figure 27: Same curve as shown in Fig. 26, except now the red symbols represent enthalpies of reaction for different ILs. All results predicted using quantum calculations.**

### 3.3 Synthesis

Seven new ILs were made during BP II. These include NDIL0043, NDIL0044, NDIL0045, NDIL0046, NDIL0047, NDIL0048 and NDIL0049. In addition, kilogram quantities of NDIL 0030 and NDIL0045 were made for larger scale testing at Notre Dame and Air Products. As with all new ILs, these were tested for purity using NMR and ion specific conductivity measurements, and impurities were kept below 1000 ppm.

### 3.4 Property Measurement

$CO_2$ uptake measurements were performed on a new batch of NDIL0030, and there was excellent agreement with the previous batch. Results are summarized in Table 11.

Table 11: Chemical Absorption of $CO_2$ in NDIL0030 IL using the Stoichiometric Methodology.

| Apparatus | Temperature | Pressure | Absorption | | Viscosity ± 10% (Poise) at 295 K | | Water Content | Decomposition |
| | | | | | | | | |
| | (K) | (MPa) | % (mol/mol) | (Mol $CO_2$/Mol IL) | IL | $CO_2$ + IL | (ppm) | Temperature (K) |
|---|---|---|---|---|---|---|---|---|
| RTA | 295 | 0.0031 | 50.4 | 1.02 ± 0.01 | 5 | N/A | 517 | 595 |
| RTA | 295 | 0.0080 | 52.0 | 1.08 ± 0.02 | 5 | N/A | 517 | 595 |
| RTA | 295 | 0.0154 | 52.9 | 1.12 ± 0.01 | 5 | N/A | 517 | 595 |
| RTA | 295 | 0.0273 | 53.7 | 1.16 ± 0.01 | 5 | N/A | 517 | 595 |
| RTA | 295 | 0.0390 | 54.2 | 1.18 ± 0.01 | 5 | N/A | 517 | 595 |
| RTA | 295 | 0.0617 | 55.0 | 1.22 ± 0.01 | 5 | N/A | 517 | 595 |
| RTA | 295 | 0.0897 | 55.7 | 1.26 ± 0.01 | 5 | N/A | 517 | 595 |
| RTA | 295 | 0.1302 | 56.7 | 1.31 ± 0.01 | 5 | 286 | 517 | 595 |
| RTA | 295 | 0.1212 | 51.5 | 1.06 ± 0.02 | 5 | 189 | 200 | 595 |
| ITA | 313 | 0.0033 | 40.0 | 0.67 ± 0.01 | 5 | N/A | 536 | 595 |
| ITA | 313 | 0.0241 | 44.0 | 0.79 ± 0.01 | 5 | N/A | 536 | 595 |
| ITA | 313 | 0.0482 | 45.4 | 0.83 ± 0.01 | 5 | N/A | 536 | 595 |
| ITA | 313 | 0.0794 | 46.5 | 0.87 ± 0.01 | 5 | N/A | 536 | 595 |
| ITA | 313 | 0.1163 | 47.1 | 0.89 ± 0.01 | 5 | N/A | 536 | 595 |
| RTA[1] | 295 | 0.0013 | 47.1 | 0.89 ± 0.01 | N/A | N/A | 1100 | 588 |
| RTA[1] | 295 | 0.0102 | 52.2 | 1.09 ± 0.01 | N/A | N/A | 1100 | 588 |
| RTA[1] | 295 | 0.0276 | 53.7 | 1.16 ± 0.01 | N/A | N/A | 1100 | 588 |
| RTA[1] | 295 | 0.0507 | 54.6 | 1.20 ± 0.01 | N/A | N/A | 1100 | 588 |
| RTA[1] | 295 | 0.0857 | 55.6 | 1.25 ± 0.01 | N/A | N/A | 1100 | 588 |
| RTA[1] | 295 | 0.1277 | 56.0 | 1.27 ± 0.01 | N/A | N/A | 1100 | 588 |

(1) = New batch

Previously, $CO_2$ solubility data were collected in IGA001 and IGA003 for which we have since determined the ILs had not reached equilibrium. Avrami's model was fit to these data to extrapolate to equilibrium values. Table 12 shows the results along with the decomposition temperatures of the ILs.

Table 12: Decomposition temperatures of various ILs.

| IL | Pressure (Mpa) | Temperature (°C) | Mole % $CO_2$ | Fast Decomposition Temperature (K) |
|---|---|---|---|---|
| NDIL0033 | 0.05 | 80 | 38.19 | 589 |
| NDIL0030 | 0.05 | 80 | 41.89 | 595 |
| NDIL0038 | 0.05 | 80 | 32.04 | 546 |
| NDIL0029 | 0.05 | 80 | 49.92 | N/A |
| NDIL0028 | 0.05 | 60 | 33.70 | 461 |

Water solubility measurements were conducted using a gravimetric balance for NDIL0017 and NDIL0030. The conditions measured were at 25°C from 0 to 25 mbar for NDIL0017 and 60°C and 47°C from 0 to 50 mbar for NDIL0030. The data show NDIL0030 to have a much higher affinity for water (infinite dilution activity coefficients of 0.135 and 0.238 for 60°C and 47°C, respectively) than NDIL0017 (infinite dilution activity coefficients of 1.40 and 1.97 for 60°C and 25°C, respectively). This agrees with previous liquid-liquid equilibria data at 25°C which indicates NDIL0017 is saturated with water at 7 w% and NDIL0030 at 77 w%.

Air Products collected pure component $CO_2$ isotherms for MEA and three CRIL, EMD0004, NDIL0017 and NDIL0030. For the purpose of benchmarking, Air Products obtained data for 30 weight percent aqueous MEA and the results were in very good agreement with data from the literature [10] (Fig. 28). The Air Products isotherm obtained at 43 °C differs only slightly from the isotherm reported by Otto, *et al*. at 40 °C, while Air Products isotherms obtained at 20 °C and 60 °C are nearly coincident with the literature isotherms for 25 °C and 60 °C. Data were collected using a volumetric apparatus by monitoring pressure and temperature during absorption and desorption of $CO_2$. The equilibrium vapor pressure of water was determined for each aqueous MEA sample prior to adding $CO_2$, and this pressure was assumed to remain constant. The partial pressure of $CO_2$ was determined by subtracting the equilibrium water vapor

pressure from the total pressure for each data point. The agreement between Air Products experiments and the literature data indicates that the method is quantitative and reliable.
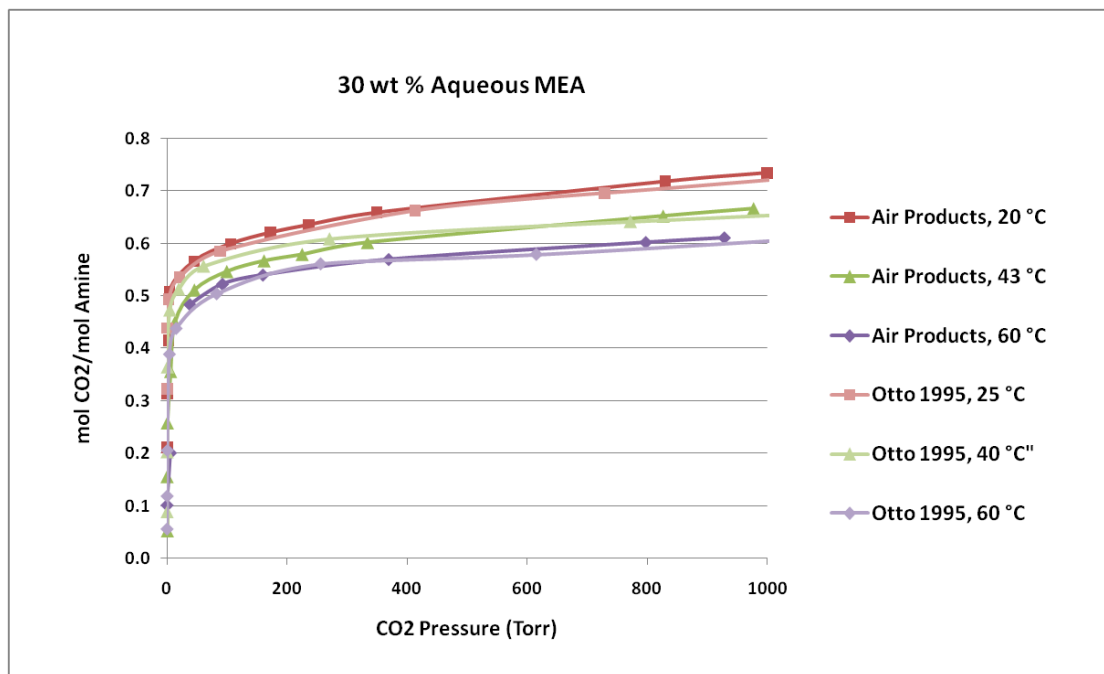


**Figure 28: CO$_2$ isotherms for 30 wt. % aqueous MEA; Air Products results compared to literature data.**[10]

Air Products attempted to collect data for EMD0004 as a neat liquid but, upon addition of moderate pressures of CO$_2$, the liquid became an unmixable gel. Isotherms were obtained at 40 °C, 60 °C and 80 °C for EMD0004 by diluting with another liquid (25 weight percent diluent). Isotherms were also obtained for the solubility of CO$_2$ in the neat diluent at the same temperatures. Isotherms for pure EMD0004 were then estimated by subtracting the CO$_2$ capacity contribution from the diluent (Fig. 29).

Air Products also attempted to collect CO$_2$ isotherms for the CRIL NDIL0017 as a neat liquid, but again a significant increase in viscosity upon addition of CO$_2$ was observed. The IL was diluted (26 weight percent diluent) to overcome the viscosity increase, and the isotherms were estimated for pure NDIL0017 by subtracting the contribution from physical solubility of CO$_2$ in the diluent (Fig. 28). The capacity measured for a diluted sample (0.18 mol CO$_2$/mol IL at 1000 Torr, 40 °C) was within reasonable agreement with

the capacity measured by Notre Dame for the neat IL (0.19 mol $CO_2$/mol IL, 1200 Torr, 22 °C). The difference between the Air Products and ND data could be a result of batch-to-batch variation of the IL, as different samples were used by the two groups.
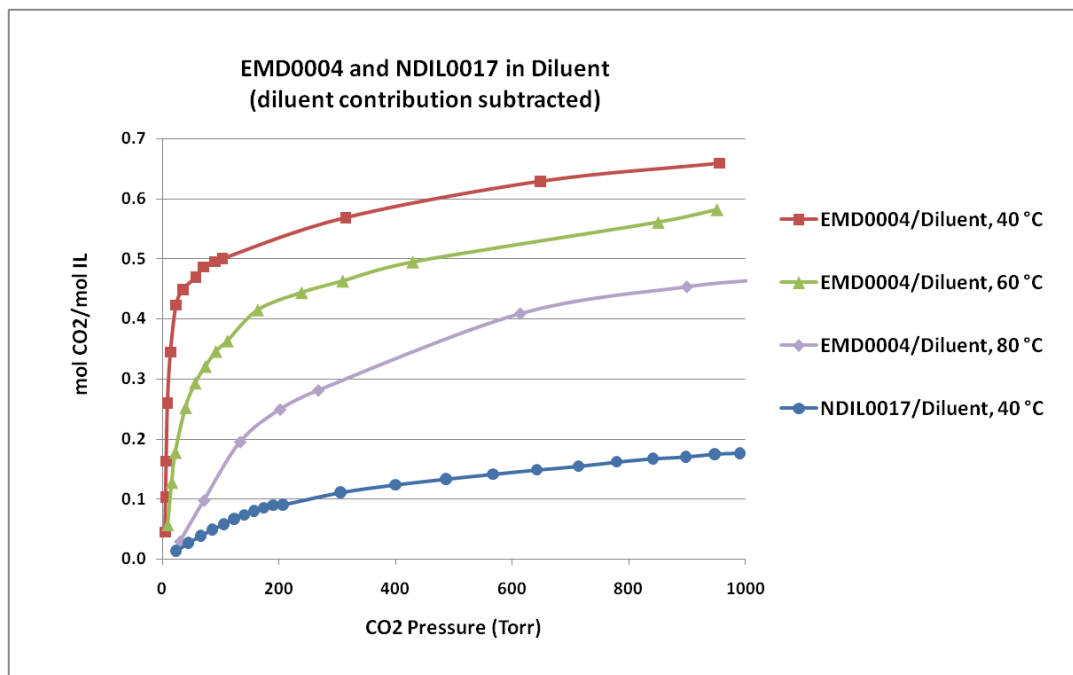


**Figure 29: $CO_2$ isotherms for EMD004 and NDIL0017 (capacity data corrected by subtracting contribution from physical solubility of $CO_2$ in diluent).**

Air Products collected isotherm data for NDIL0030 both as a neat liquid and as a mixture in 50 weight percent diluent. Although the viscosity of neat NDIL0030 does not increase to the same degree as EMD0004 and NDIL0017 upon reaction with $CO_2$, stirring was still inefficient and the time required to reach equilibrium was on the order of days. Results are shown in Figure 30. Upon comparison of Air Products's data for the diluted IL to ND's data for the neat IL, ND noted that the neat IL provides more capacity on the basis of the pure IL (about 12 % more capacity at the lowest temperature). A decrease in capacity was noted for diluted NDIL0030 with repeated absorption/desorption cycles at all temperatures and was more pronounced as the temperature was increased. This behavior may be a result of decomposition, and the data collected at 81.5 °C may be questionable.
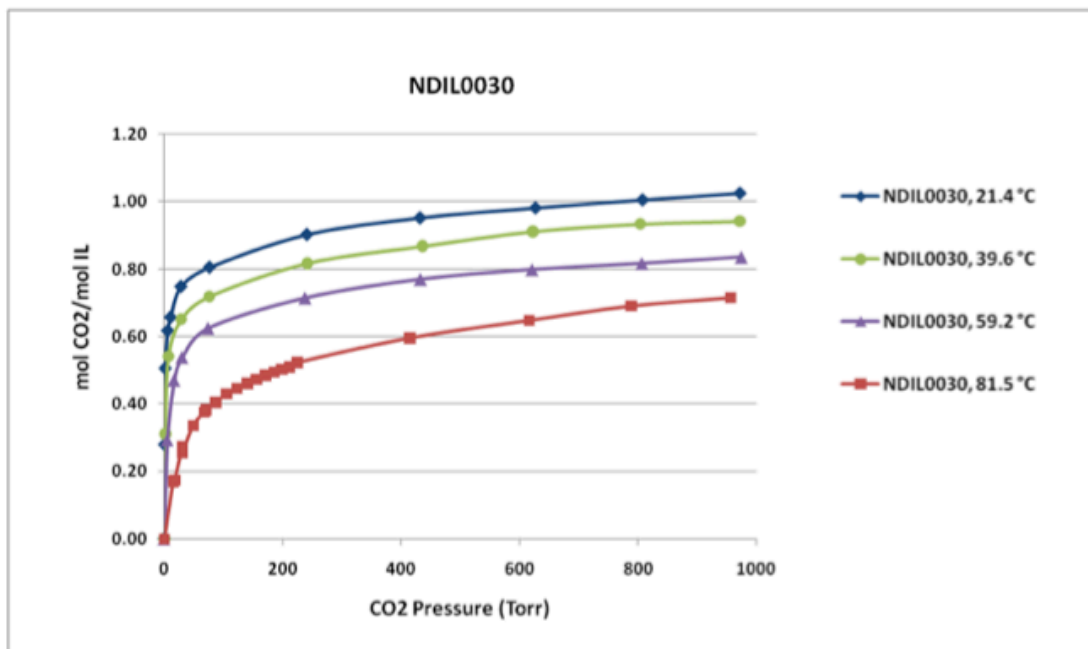
**Figure 30: CO$_2$ isotherms for NDIL0030 (capacity data corrected by subtracting contribution from physical solubility of CO$_2$ in diluent).**

Air Products completed screening experiments for aqueous solutions of NDIL0030 and NDIL0043 using a volumetric isotherm apparatus that does not provide gas phase mixing. Although the gas phase is not mixed during equilibration, trends in the data are likely a good representation of a mixed system. In their initial studies of NDIL0030 at 40 °C (Fig. 31), the data indicated that the presence of water substantially decreases the capacity of the IL. The capacities of roughly 0.5 mol CO$_2$/mol IL for the aqueous solutions suggested that bicarbonate formation between the amine group, water and CO$_2$ (2:1 amine to CO$_2$ ratio) is favored over direct carbamate formation between the IL and CO$_2$ (1:1 amine to CO$_2$ ratio, see isotherm for 'IL in Diluent' in Fig. 31). At every concentration, the IL and water were fully miscible in the absence of CO$_2$; however, each sample exhibited two phases upon introduction of even small quantities of CO$_2$ (the non-ideal isotherms in Fig. 31 are consistent with the observed phase changes). The two phases appeared to be liquids during absorption but, upon complete CO$_2$ desorption, we observed a solid precipitate. The formation of a precipitate could be consistent with decomposition of the reaction mixture to bis(phosphonium) carbonate.
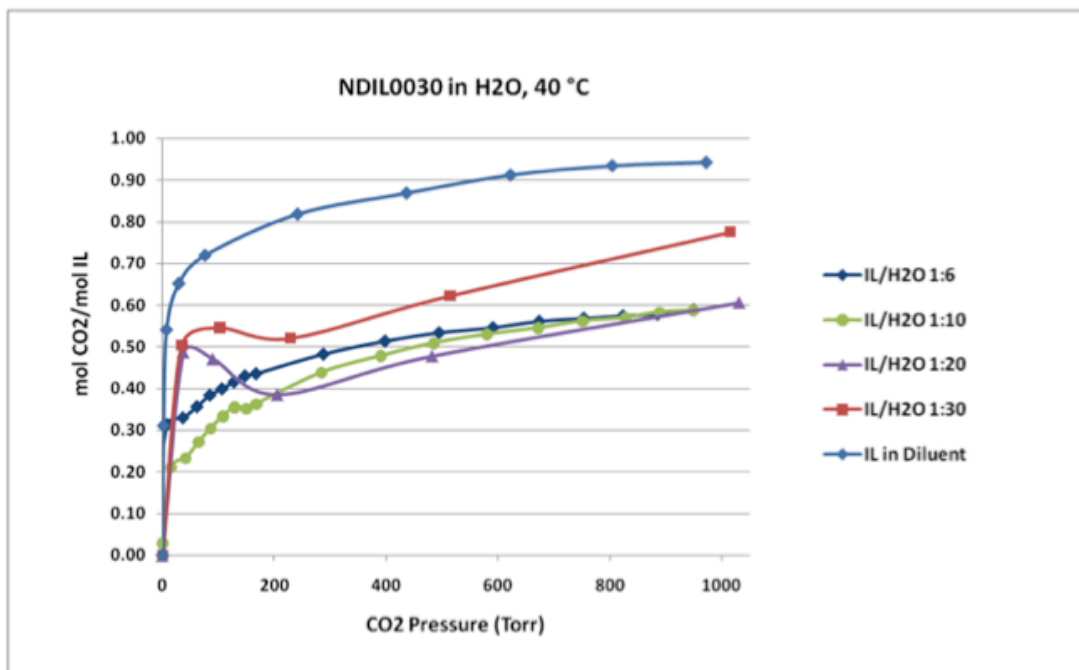
**Figure 31: $CO_2$ isotherms for aqueous solutions of NDIL0030 at 40 °C (IL/H$_2$O = mol ratio). These results were later found to be in error by Air Products.**

Later, Air Products found that their measurements were in error. The corrected data indicate that water has no detrimental effect on the reactivity of NDIL0030 toward $CO_2$ (see Figure 32). The isotherms for the two samples with the most water exhibit the highest capacities; however, the IL is very dilute in these samples, and the capacities likely reflect a large contribution from physical solubility of $CO_2$. This error by Air Products caused several months of delay as we tried to understand and fix the "problem" of water impacting capacity.
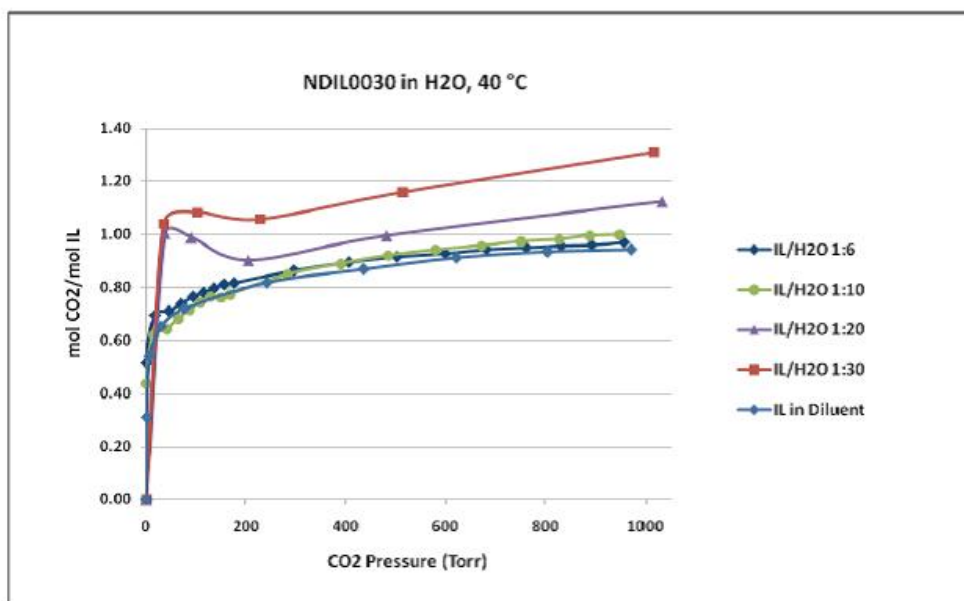
**Figure 32: Corrected $CO_2$ isotherms for aqueous solutions of NDIL0030 at 40 °C (IL/H$_2$O = mol ratio). These results show that water has no detrimental effect on $CO_2$ capacity.**

Air Products attempted to collect data for aqueous NDIL0043, but the IL mixture failed to reach equilibrium with the gas phase upon addition of $CO_2$. Although they observed a pressure minimum during periods of equilibration, the pressure did not level out but rather started to increase slowly with time. One possible explanation for this behavior is that the slow increase in pressure is due to slow equilibration of water between the liquid and vapor phase. In this case, mixing the gas phase should enhance the rate of equilibration. Another explanation could be that the mixture is decomposing to release $CO_2$ or another gas phase species.

Air Products completed construction of a system for measuring mixed gas, multicomponent isotherms. They incorporated a controlled temperature Fourier transform infrared (spectroscopy) (FTIR) cell into a gas mixing loop, which provides efficient mixing and allows for in situ characterization of the gas phase composition for IR-active components. They also have the ability to analyze gas phase components that are not IR-active by gas chromatography. The system was calibrated and experiments using NDIL0043 carried out.

Mixed $CO_2/H_2O$ isotherms were collected for NDIL0045 using Air Products' multicomponent isotherm apparatus. Most of the components of the apparatus are contained within an oven to ensure that a uniform temperature is maintained. The system includes a gas mixing loop that is incorporated into a controlled temperature FTIR cell located just outside of the oven. In this way, efficient mixing is achieved and the technique allows for in situ quantitation of $CO_2$ and $H_2O$ in the gas phase. The concentrations of $CO_2$ and $H_2O$ reacted or dissolved in the IL are determined by keeping account of the total moles of $CO_2$ and $H_2O$ in the system and subtracting the moles of these components in the gas phase.

Data for NDIL0045 were collected by first equilibrating the IL with water at 40 Torr of vapor pressure. A water ballast was heated to about 35 °C to maintain this pressure. The ballast was opened to the sample vessel containing NDIL0045, and the IL was stirred for a period of at least 24 hours. After equilibrating, the system was isolated from the water ballast to maintain the total quantity of water in the system. Isotherm data for $CO_2$ and $H_2O$ were collected simultaneously by metering in $CO_2$ and allowing the system to equilibrate. Each set of data points required a minimum of 24 hours for equilibration. The total quantity of $H_2O$ in the liquid and vapor phase remained constant while the quantity of $CO_2$ was increased during the experiment.

The results collected at 40 °C are shown in Figure 33. The starting concentration of $H_2O$ in the IL was estimated to be 2.2 mol $H_2O$/mol IL (6.2 wt % $H_2O$) by interpolating from a pressure of 40 Torr using previously measured pure $H_2O$ isotherm data for 43 °C. An isotherm for total gas uptake was determined through the standard volumetric means in which $CO_2$ and $H_2O$ are not accounted for separately and all gas uptake is assumed to be $CO_2$ (Fig. 33, mol $CO_2$/mol IL – Apparent). Independent isotherms for $CO_2$ and $H_2O$ were determined by directly measuring the moles of each species in the gas phase and calculating the moles of each species in the liquid phase (Fig. 33, mol $CO_2$/mol IL – Actual and mol $H_2O$/mol IL). Data were not collected beyond a pressure of 325 Torr to minimize the time required to complete the experiment. The isotherms measured in this way exhibited substantially lower capacities for $CO_2$ than the neat IL. In contrast, the

capacities measured for NDIL0045 using Air Products's single component apparatus approach 1 mol $CO_2$/mol IL and show little effect from water, as seen in Figure 34.
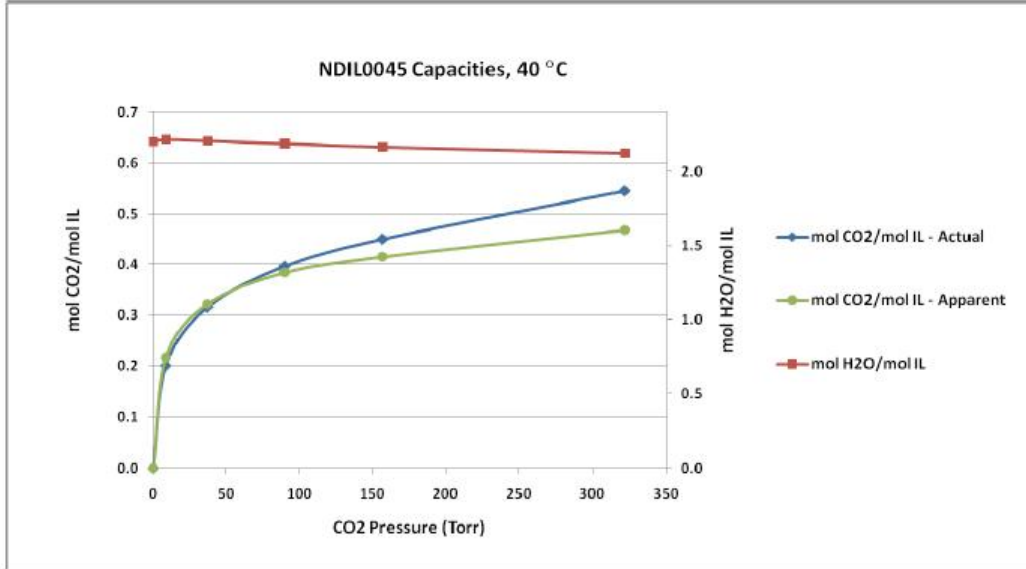


**Figure 33: Results from multi-component isotherm analysis for NDIL0046 equilibrated under 40 Torr of water at 40 $^o$C.**
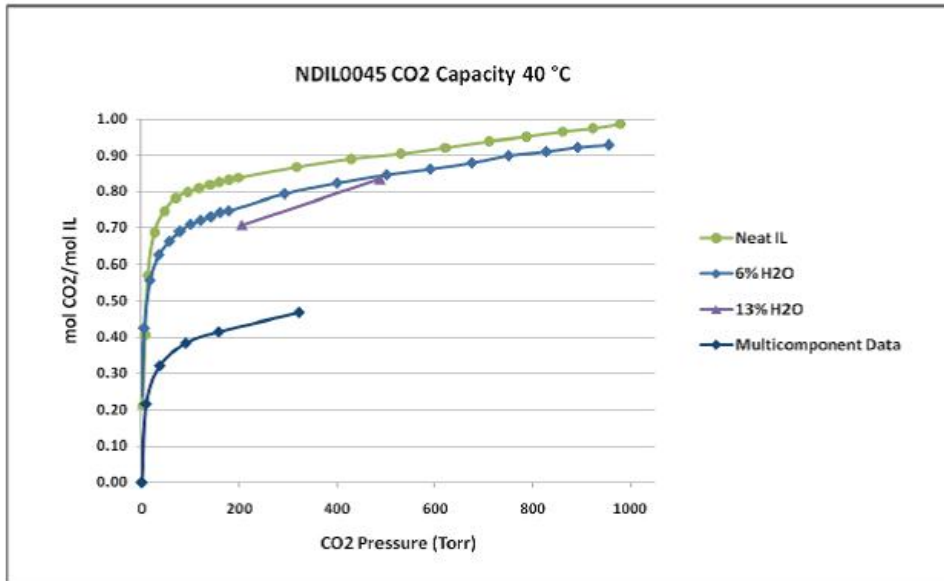


**Figure 34: $CO_2$ isotherms for NDIL0045 at 40 °C.**

The same experiment using the multicomponent apparatus was carried out by Air Products at 60 °C and, again, yielded a lower than expected capacity (see Fig. 35). The procedure and calculation method used to determine the isotherms using the multicomponent apparatus are being examined to understand the unexpectedly low capacities. Regardless of the inconsistent quantitative results, these results suggested that the concentration of water in the IL decreased upon $CO_2$ uptake. One might expect the hydrophilicity (polarity) of the liquid phase to increase with $CO_2$ uptake if the reaction yields carbamate and/or bicarbonate salts. Perhaps the decrease in hydrophilicity indicates that new salt species are not formed. This is consistent with the proposed mechanism for the 1:1 reaction between IL and $CO_2$ in which carbamate formation is disfavored, and provides additional support to the mechanisms proposed.

Notre Dame researchers made extensive measurements of $CO_2$ solubility with and without water on many different ILs. Figure 35 shows the mol of $CO_2$ for mol of IL as a function of the pressure for the system $CO_2$ + NDIL0043. It also presents the data for $CO_2$ uptake in the presence of water. The absorption isotherm of $CO_2$ in NDIL0045 is presented in Figure 36.
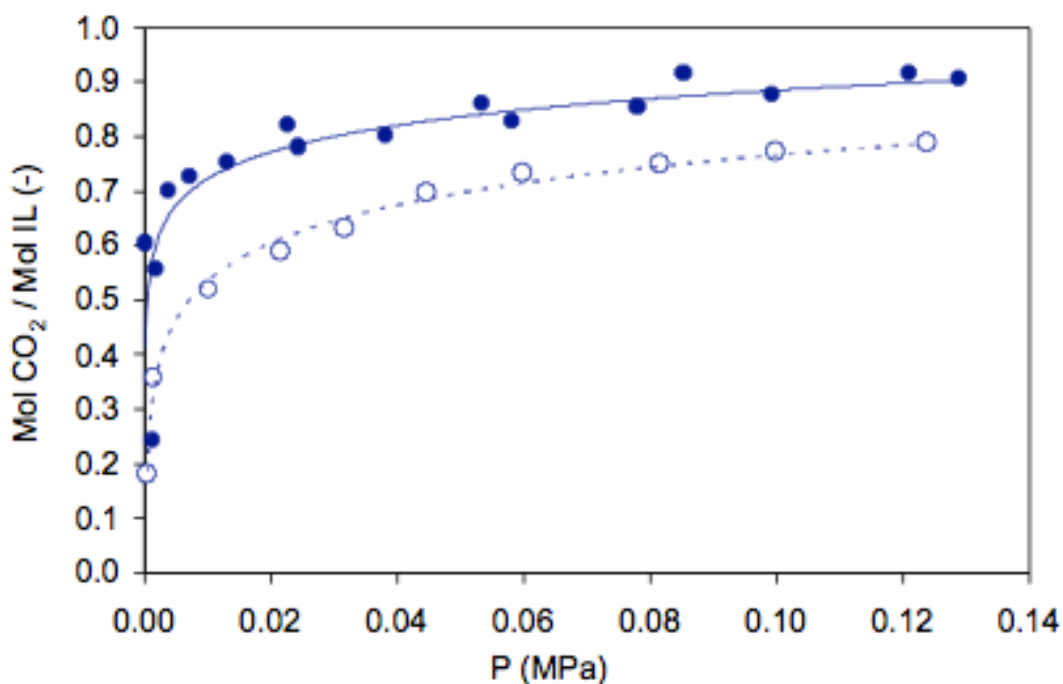
**Figure 35: Absorption isotherm of $CO_2$ in neat NDIL0043 and in presence of water at 295 K. Filled symbols represent data for neat IL while open symbols are for IL+ 14 wt % water.**

It can be seen that the isotherms are very steep for NDIL0045, indicating strong binding of $CO_2$. The binding appears to be weaker for NDIL0043. When NDIL0043 was mixed with 14 wt% water, the absorption at atmospheric pressure was decreased by approximately 0.1 mol $CO_2$ per mol IL. Likewise, NDIL0045 with 4 wt% water showed a decreased capacity, but only slightly, compared to the neat IL, as seen in Figure 37. On the other hand, another IL, NDIL0036, experiences an increase in $CO_2$ capacity in the presence of 2 wt% water. This is likely due to the decrease in viscosity that is observed when the ILs are mixed with water, allowing equilibrium to be reached on the laboratory scale. In Figure 38 the absorption isotherm indicates that the mole ratio of $CO_2$ to IL surpasses 1:1 at pressures lower than 0.01 MPa.
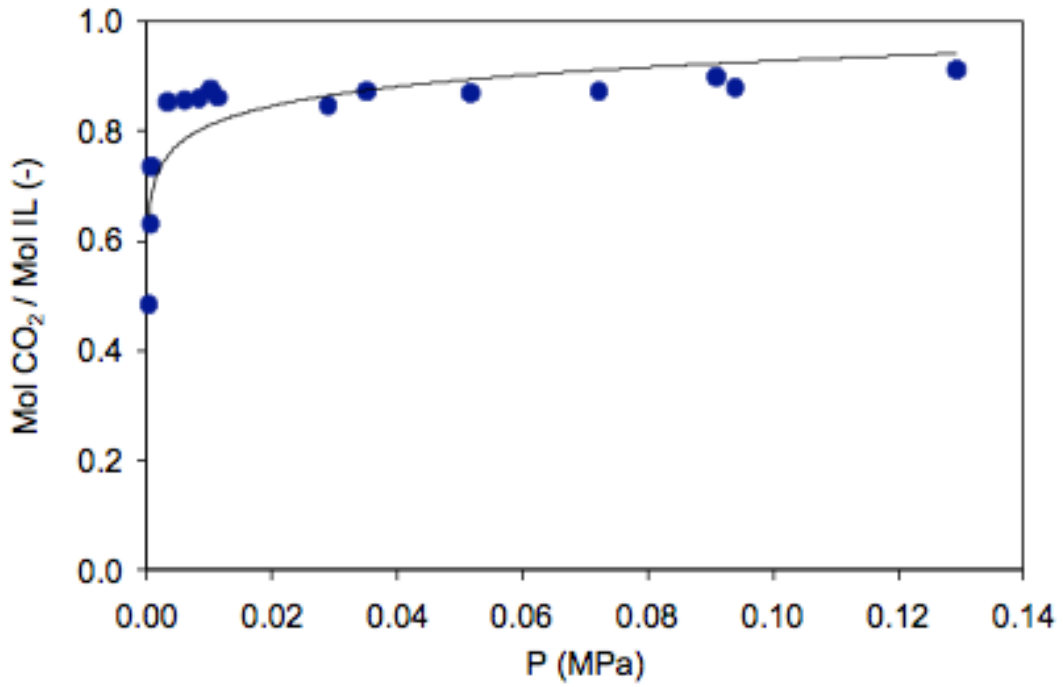
**Figure 36: Absorption isotherm of $CO_2$ in NDIL0045 at 295 K.**
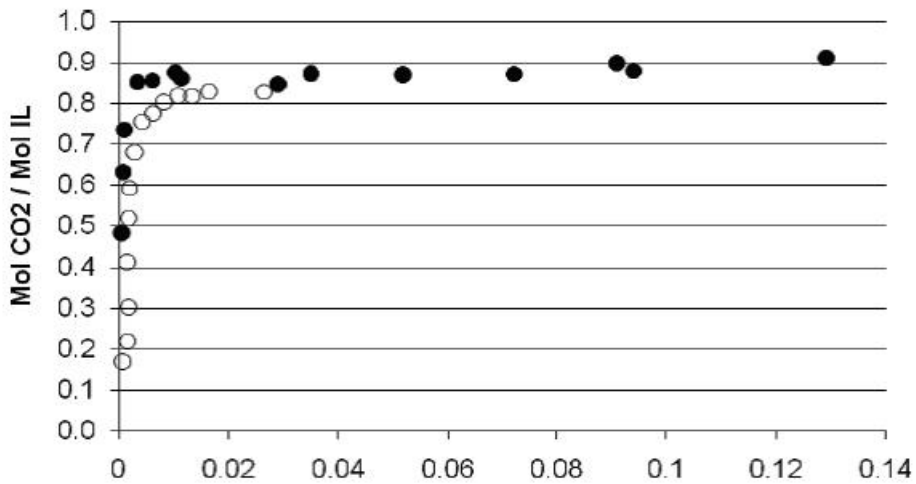


**Figure 37: Absorption isotherm of $CO_2$ in NDIL0045, solid circles, and NDIL0045 with 4% water (by weight), open circles, at 295 K.**
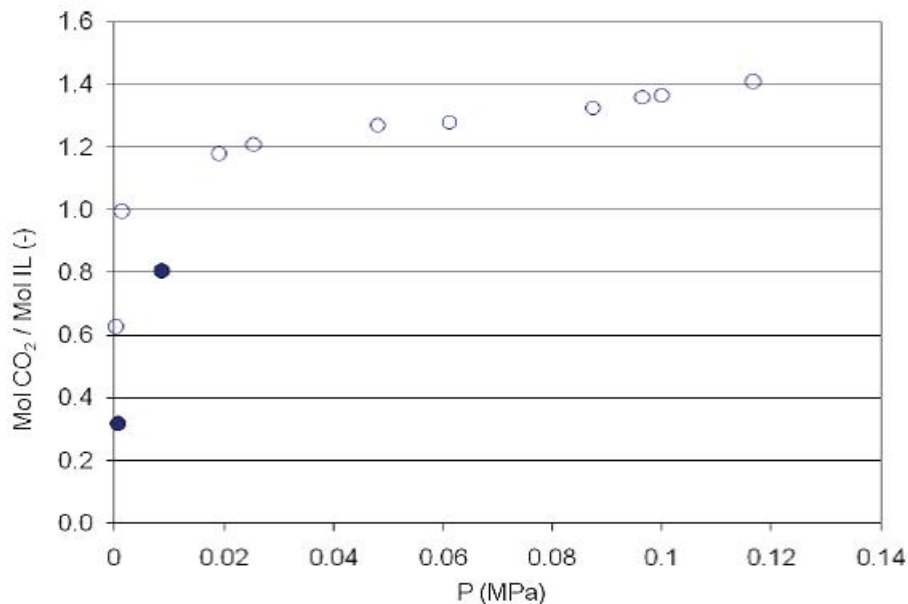
**Figure 38: Absorption isotherm of $CO_2$ in NDIL0036, solid circles, and NDIL0036 with 2 wt% water, open circles, at 295 K.**

The effect of temperature on the absorption equilibrium of carbon dioxide in NDIL0045 was investigated.  As Figure 39 shows, the absorption equilibrium decreased with increasing temperature.  A minor difference was observed between room temperature and 60°C with a difference of 0.025 moles of $CO_2$ per mole of IL.  A measured difference of 0.058 moles of $CO_2$ per mole of  IL was observed between 60°C and 80°C. Absorption of $CO_2$ reduced to the same extent between 80°C and 100°C.
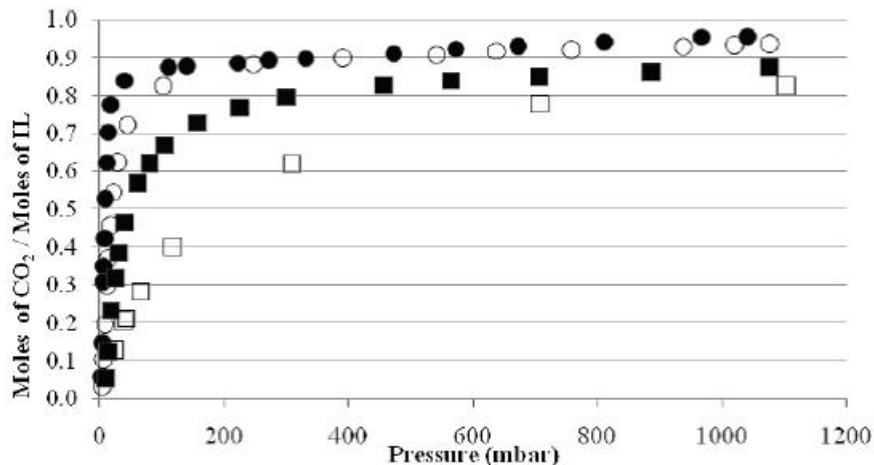


**Figure 39: Absorption isotherm of $CO_2$ in NDIL0045 performed at different temperatures.  Solid circles indicate 22°C, empty circles are 60°C, solid squares are 80°C, and empty squares are 100°C.**

The regenerative properties of the $CO_2$ absorption in NDIL0045 were also examined, as shown in Figure 40. First the absorption isotherm was measured at room temperature. Then vacuum was applied for 2 days at 40°C before reabsorbing $CO_2$ at room temperature. Initial results showed the curve leveling out at 0.5 moles of $CO_2$ per mole of IL, so vacuum was reapplied for 1 week at 60°C, which showed improved regeneration capabilities. Vacuum was then applied at 80°C for 1 day and then $CO_2$ was absorbed at room temperature. Applying vacuum at 80°C was observed to be the best regeneration attempt, but still did not fully regenerate the IL. Since regeneration at significantly higher temperatures in the actual process was anticipated, regeneration at these lower temperatures is not considered a major concern.
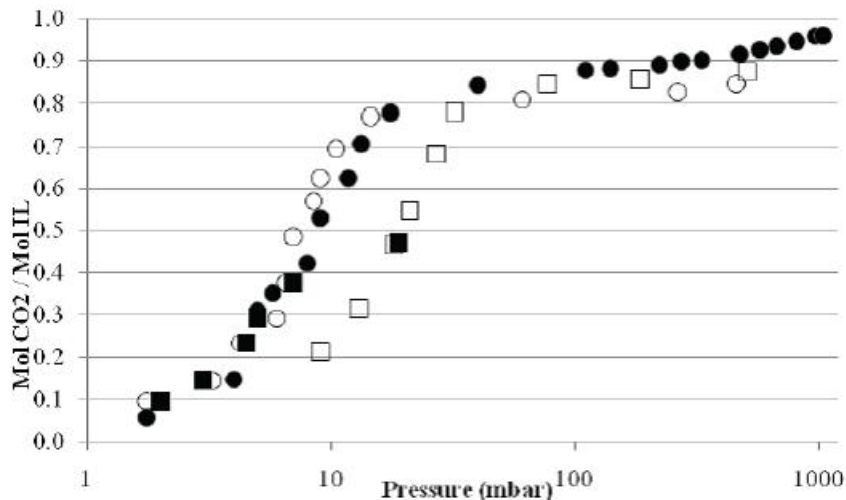


**Figure 40: Absorption isotherm of $CO_2$ in NDIL0045 at 22°C. Note the x-axis is on a log plot. The solid circles indicate the initial run. The solid squares indicate the absorption after the first regeneration attempt (regeneration conditions were apply vacuum at 40°C for 2 days. The empty circles indicate the absorption after the second regeneration attempt (regeneration conditions were applying vacuum at 60°C for 1 week). The empty squares indicate the absorption after the third regeneration attempt (regeneration conditions were applying vacuum at 80°C for 1 day).**

Finally, $CO_2$ isotherms were measured for NDIL0035, NDIL0045 and NDIL0047. NDIL0035 and NDIL0047 both absorbed just under one mole of carbon dioxide per mole of IL. NDIL0045, which was designed to have a significantly lower heat of reaction, absorbed carbon dioxide to a much lower capacity. Results are shown in Figure 41.
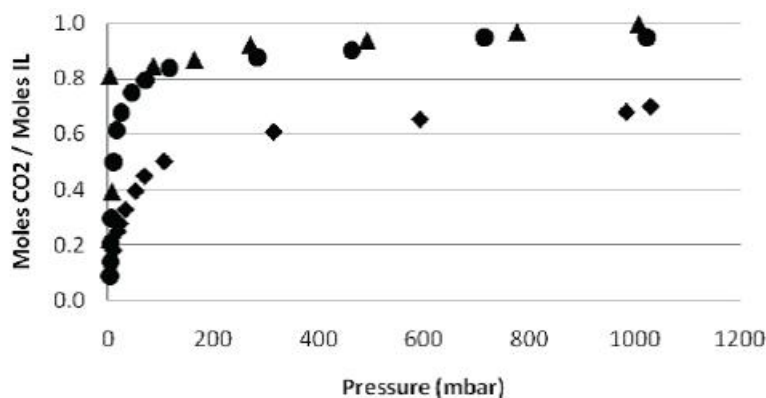
**Figure 41: Absorption isotherm of CO$_2$ in NDIL0035 (black triangles), NDIL0046 (black diamonds), and NDIL0047 (black circles).**

In BP II direct calorimetric measurements of the enthalpy of reaction of CO$_2$ with the ILs were begun. A Setaram MicroDSCIII calorimeter was used (see Figs. 42 and 43). The procedure consists of taking and IL sample, approximately 0.04 grams, and loading it into the sample vessel. As there is no stirring, a small sample size was desired to reduce long equilibration times. The entire system is evacuated overnight at an elevated temperature of 323.15 K. CO$_2$ is introduced in one injection through the opening/closing of a valve, and then allowed to reach equilibrium. The heat (in Joules) is determined from the integration of the heat flow as a function of time. The moles of CO$_2$ in the IL are determined from the IL capacity of CO$_2$, which is measured using a stoichiometric method at room temperature, and the equilibrium pressure of the system. Using this method, the heat of absorption at 298.15 K and 39 psi was measured for two IL + CO$_2$ systems: NDIL0045 and NDIL0046. The average heat of absorption was -77 kJ/mol of CO$_2$ and -56 kJ/mol of CO$_2$, respectively. This trend is consistent with the theoretical heats of reaction calculated using quantum chemical methods. This was a very encouraging result because it confirmed that have sound theoretical methods are in place that can be used to design ILs having the desired complexation strength.
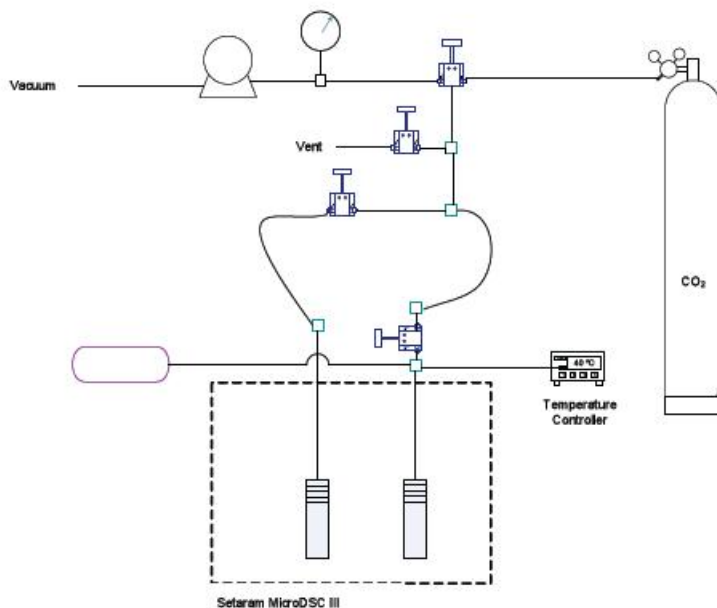
**Figure 42: Experimental setup used to measure enthalpies of reaction.**



**Figure 43: Photograph of experimental calorimeter.**

As has been discussed extensively during the presentation of the absorption experimental results, the viscosity of these ILs is a major concern. While the unreacted viscosity tends to be on the high end, there was a lot of evidence that upon reaction with $CO_2$, the viscosity increased tremendously. The calculations suggested that this was due to the formation of hydrogen bonded "salt bridges". A system was constructed whereby direct measurements could be made of the viscosity with and without the presence of $CO_2$. Some results were shown earlier in Table 11. The effect that temperature and water have

on the viscosity of ILs saturated with carbon dioxide was investigated, since in actual applications there will be water present. The viscosity of NDIL0043 was measured from 283 K to 343K. The values are reported in Figure 44, with viscosity on a logarithmic scale. Also in this figure are the values measured for the viscosity of NDIL0043 (with and without 14 wt% water) after it has been saturated with $CO_2$ at atmospheric pressure in the RTA. It is observed that the neat IL shows a large increase in viscosity upon reaction with $CO_2$. However, when sufficient amounts of water are present, the viscosity drops considerably.

Viscosities were measured for NDIL0045 at varying concentrations of water (from 0.08 wt% to 7.5 wt%) at temperatures between 283 K and 343 K. At 7.5 wt% water the viscosity is approximately one-third the value of the pure IL at all temperatures measured.
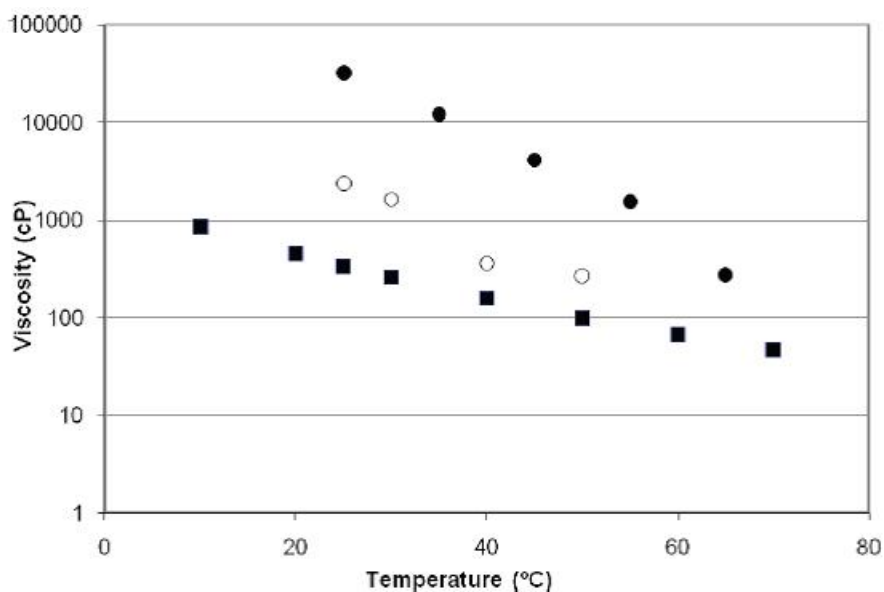


**Figure 44: Viscosity of NDIL0043 at temperatures from 10-70 °C. Note the logarithmic scaling used in the viscosity axis. Solid squares indicate pure NDIL0043, solid circles are NDIL043 with 0.1 MPa $CO_2$. Open circles are NDIL0043 with 14 wt% water and 0.1 MPa $CO_2$.**

The presence of carbon dioxide at room temperature raised the viscosity of NDIL0047 by 750 cP and of NDIL0035 by 147,000 cP. However, at higher temperatures, for example at 60 °C, the viscosity is always much lower, as shown in Figures 45 and 46. As discussed above, simulations suggested that the increase in viscosity is caused by the

formation of a pervasive hydrogen bond network in the system. Therefore, an investigation was begun to discover new ILs that would not form such a network. As shown in Figure 45, NDIL0046 shows very little increase in viscosity upon complexing with an increase upon $CO_2$ absorption of only 65 cP. This was a major breakthrough and led to the discovery of a new class of ILs – those having AHAs. An invention disclosure was filed on this class of ILs, and Notre Dame is working on a patent for these new materials.
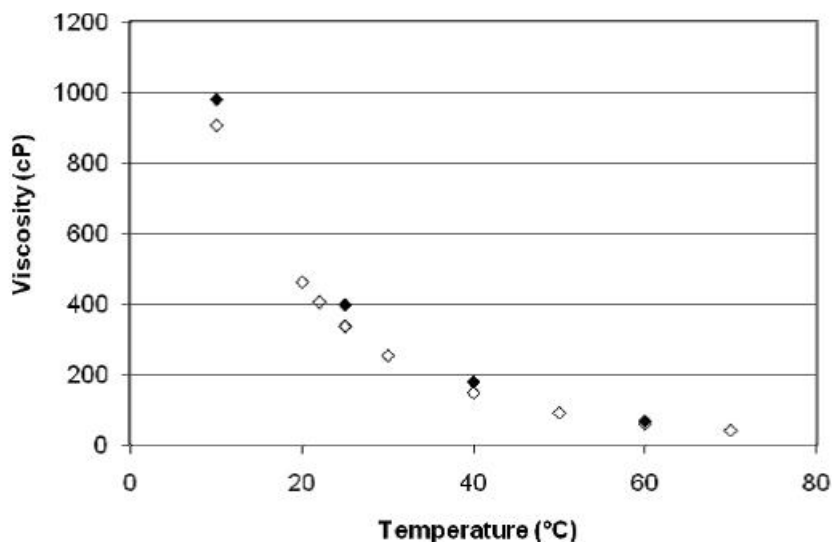


**Figure 45: Effect of $CO_2$ on the viscosity of NDIL0046. The empty diamonds are the viscosity of pure NDIL0046 and the black diamonds are the viscosity of NDIL0046 saturated with $CO_2$ at atmospheric pressure.**
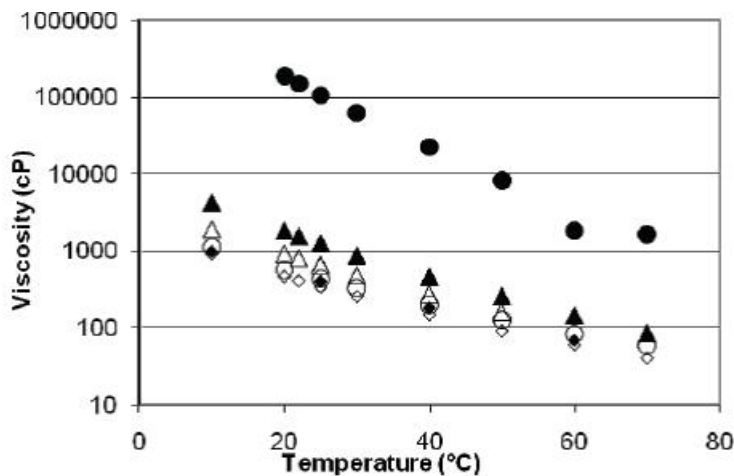
**Figure 46: Effect of $CO_2$ on the viscosity of NDIL0035 (circles), NDIL0046 (diamonds) and NDIL0047 (triangles). The empty markers represent the viscosity of the pure component under 1 atmosphere of nitrogen. The filled markers represent the viscosity of samples saturated with $CO_2$ at atmospheric pressure.**

It is also important to understand the solubility of oxygen and nitrogen in these ILs so that these gases can be accounted for in the process modeling. Therefore, oxygen solubility measurements were performed in the gravimetric microbalance for NDIL0043 at 40˚C and 120˚C and NDIL0045 at 40˚C. At both temperatures, NMR results indicated that the anion of NDIL0043 completely reacted with oxygen. A color and smell change was also observed as further evidence of the reaction. For NDIL0045, however, it was possible to obtain a preliminary estimate of Henry's Law constant of 187 bar. This suggested that some of these reactive ILs might not be stable in air, and led us to investigate this carefully.

Nitrogen solubility measurements were performed in NDIL0045 at 40 °C. Solubility measurements were performed for pressures up to 100 bar. Figure 47 shows the graph of the solubility of $N_2$ in NDIL0045 at 40 °C and pressure up to 100 bar.
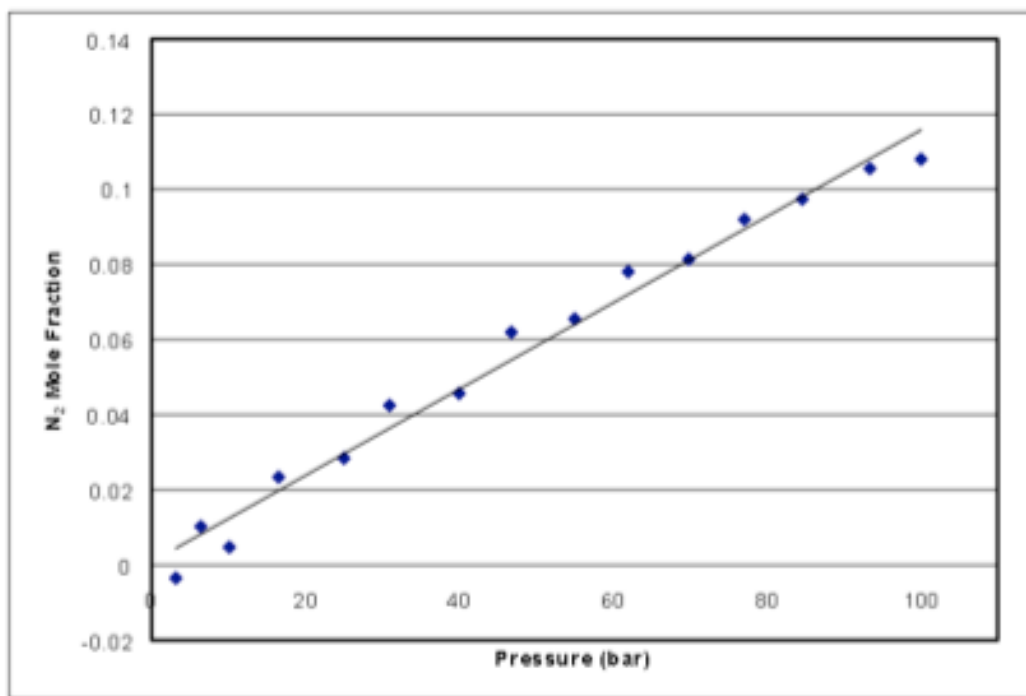
**Figure 47: Solubility measurements of $N_2$ in NDIL0045 at 40 oC.**

It is observed that the solubility follows a linear relationship, typical of sparingly soluble gases. This happens over a very broad pressure range, much broader than what will be observed in a $CO_2$ capture application. Therefore, it will be appropriate to model $N_2$ solubility using a simple Henry's Law.

In addition to measuring $CO_2$ uptake isotherms, it was also desirable to investigate the reaction in more detail and determine reaction rates and mass transfer behavior. The process was initiated by collecting spectroscopic data for EMD0004, with the purpose of making a calibration curve for C=O stretching band of the chemically complexed IL. Careful study of the spectral changes during reaction with $CO_2$ provides information about the structure of the reacted species as well as any intermediates, thereby leading to elucidation of the reaction mechanism. Figure 48 shows that the absorption does not perfectly follow Beer's Law for any of the different fitting procedures using either Gaussian or Voigt shaped peaks.

The spectra for NDIL0030 with 34 w% diluent reacted with $CO_2$ at 25, 40, 60, and 80 ˚C were obtained and the absorbance peaks associated the chemical complex were compared to the $CO_2$ capacity measurements for this IL (at 22 and 40 ˚C). In addition, an estimation of the enthalpy of reaction (-22 kJ/mol) was obtained by conserving the number of moles of $CO_2$ in the reaction cell as the temperature increased and observing the pressure change. This value is quite a bit different from the values obtained calorimetrically. As discussed below, this procedure was subsequently refined, and much better enthalpies of reaction from this apparatus were obtained.
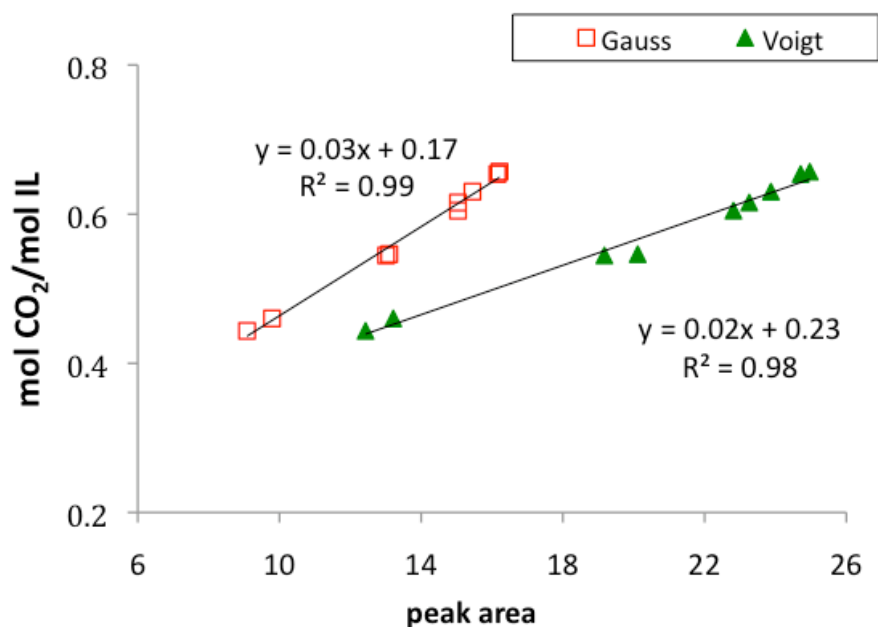


**Figure 48: Concentration of $CO_2$ chemically reacted with EMD0004 versus the fitted peak area of the C=O stretching vibration, fit with Gaussian and Voigt peaks.**

The reaction spectrum of NDIL0030 (with 37w% diluents) and $CO_2$ was then examined. The observed mechanical couplings and overtones shown in the region in Figure 49 suggest that the stable complex that forms over time is due to zwitterion formation. The sample is observed to be dark brown and inhomogeneous in color after reacting with $CO_2$. It is believed this may be due to side reactions that form precipitates.
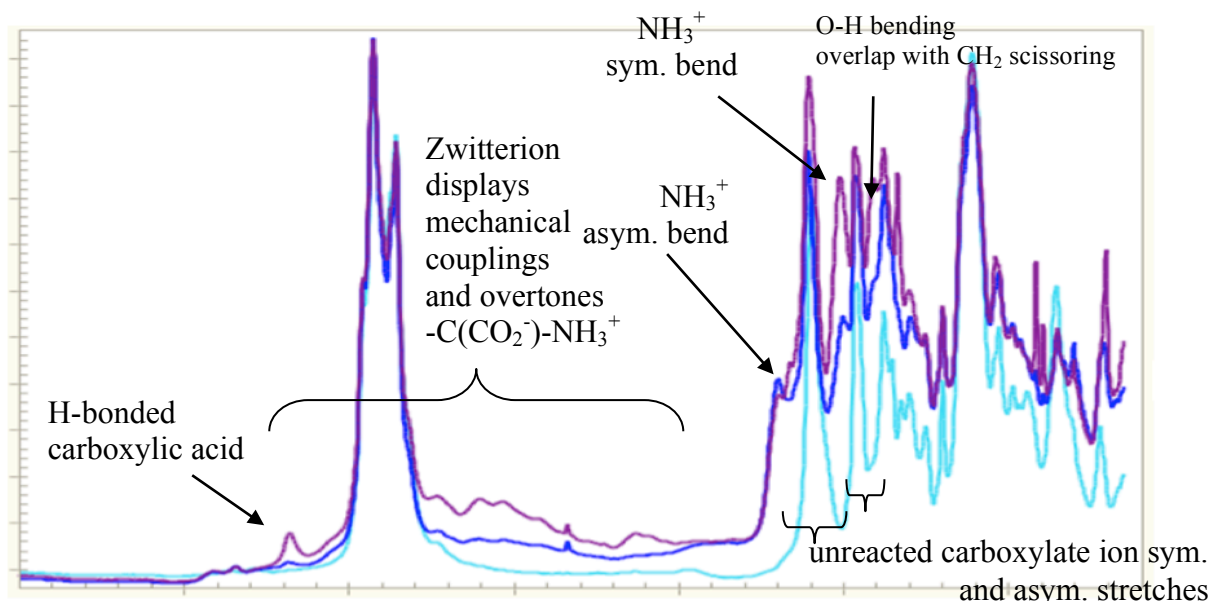
**Figure 49: Absorbance spectrum of NDIL0030 before (torquoise) and after CO₂ (blue-instant reaction, purple-slower reaction)**

The ReactIR apparatus used in these studies was outfitted with a pressure gauge, which enables measurements of $CO_2$ uptake. Measurements were made on NDIL0043 (with 40w% diluent) at 20mbar and 25°C. Temperature was raised to 40, 60 and 80°C and the change in pressure observed. The uptakes at these conditions are presented as in Table 13.

Table 13: Total uptake of $CO_2$ by NDIL0043 in mol fraction percentages at different pressure and temperatures.

| P (bar) | T (°C) | % mol $CO_2$ / mol IL |
|---------|--------|----------------------|
| 0.02 | 25.1 | 67.68 |
| 0.06 | 40.5 | 65.72 |
| 0.18 | 59.9 | 60.20 |
| 0.43 | 80.1 | 49.49 |

To assess the reproducibility of $CO_2$ uptakes of the second batch of NDIL0043 with the first batch and to construct a calibration curve, the experiment is repeated with more data points (Fig. 50).
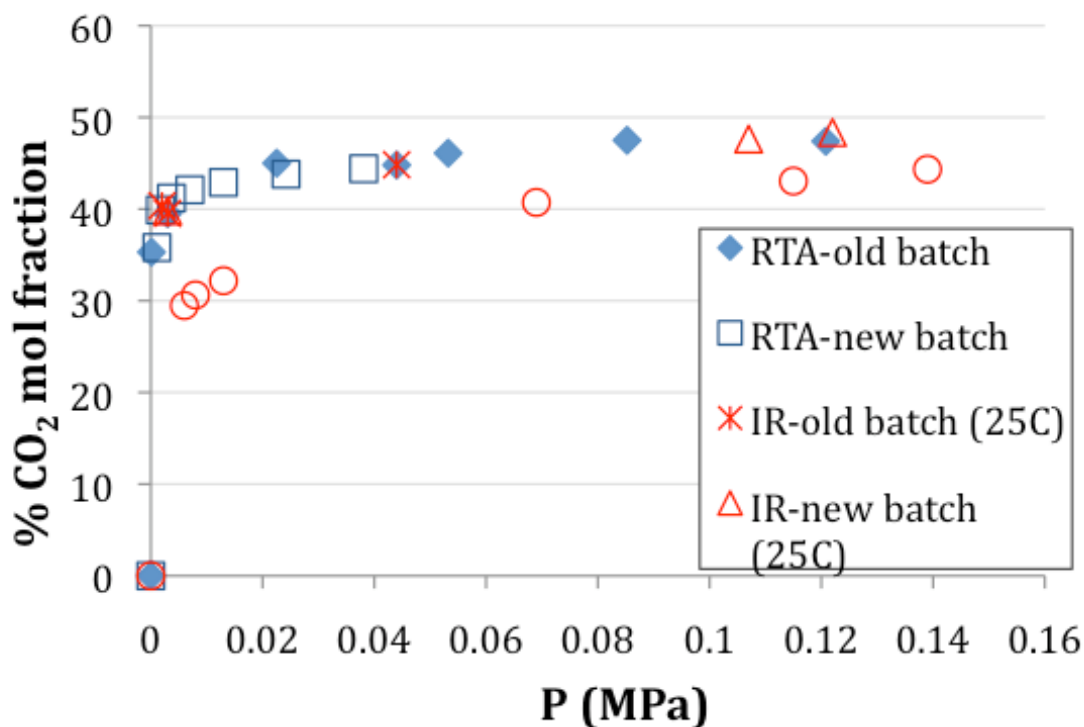
**Figure 50: The CO$_2$ uptake of NDIL0043 old and new batches, compared with RTA. The 60ºC isotherm is obtained by desorbing the saturated TSIL(final point at 25ºC).**

The estimated enthalpy for NDIL0043 using the equilibrium pressures at 25 and 40ºC for the first cycle is -69.9 kJ/mol; using the desorption data at 40, 60 and 80ºC, it is calculated to be -61.4 kJ/mol whereas the entropies are -228.5 and 184.7 J/mol.K, respectively. These results are much more in line with other measurements.

Chemical calibration curve is obtained by performing voigt fits to the spectral region of interest as shown in Figure 51. Total of 4 peaks are fitted that can be attributed to reasonable absorption bands of present groups.
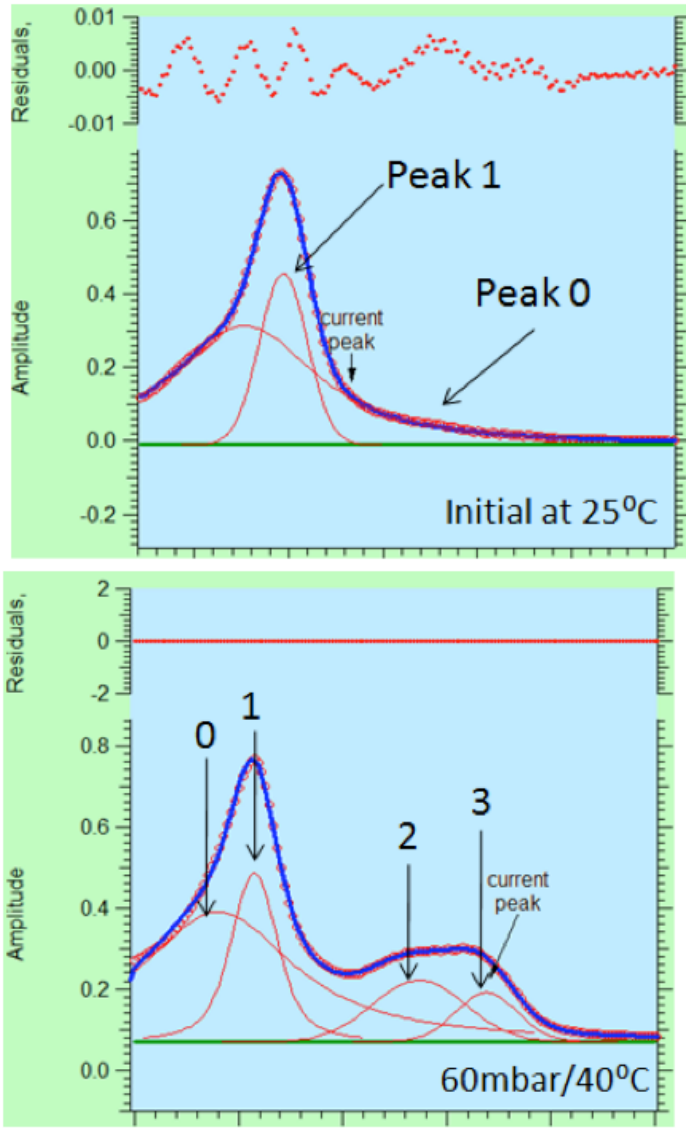
**Figure 51: Example to the fitted spectral region of unreacted (right figure-25⁰C) and reacted (left figure-60mbar/40⁰C) spectrum of NDIL0043. The broad region corresponding to the total absorbance of peaks 2 and 3 is used for calibration.**

The observed trend of these peak areas with respect to time from initial loading of $CO_2$ at time zero until equilibrium (1st absorption point at 25⁰C) is shown in Figure 52.
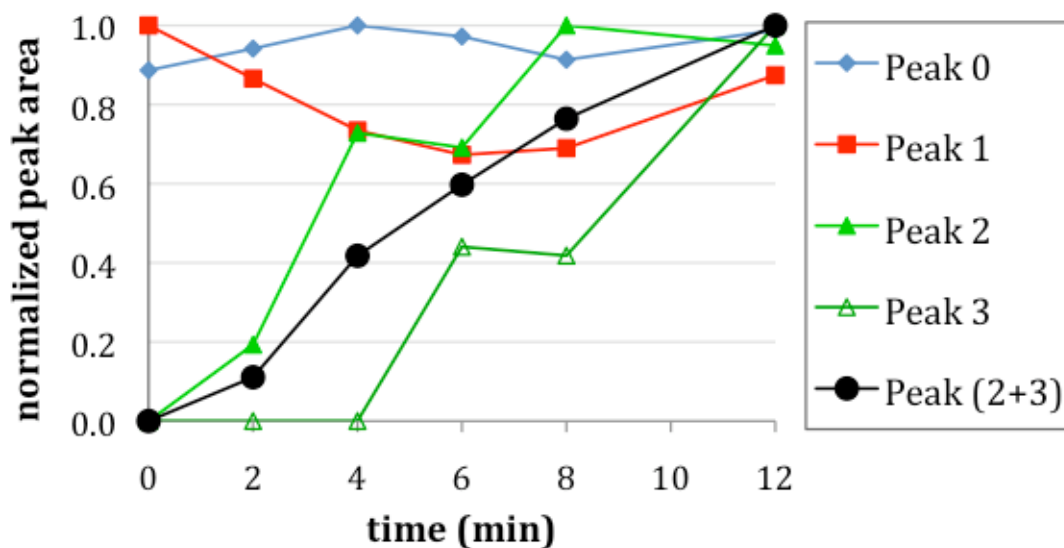
**Figure 52: The change in peak areas as $CO_2$ is absorbed. Peaks 0 and 1 are due to groups that exist initially and do not change during significantly during the reaction. Peaks 2 and 3 are new absorbance bands due to the reaction product.**

It is important to note that Attenuated Total Internal Reflectance-Infrared (ATR-IR) that was used to obtain the spectrum finishes one scan in 60 seconds. Therefore the peak area obtained by ATR-IR is not truly representative of the pressure and, therefore, the absorbed $CO_2$ at a specific time, except at equilibrium.

Pressure and peak areas are recorded with respect to time as the reaction occurs. Using the pressure, temperature and the known volume of the React-IR cell, absorbed moles of $CO_2$ is calculated using NIST values. Hence, the calibration curve is obtained by plotting the peak area with respect to $CO_2$ uptake per gram of the IL as illustrated in Figure 53.
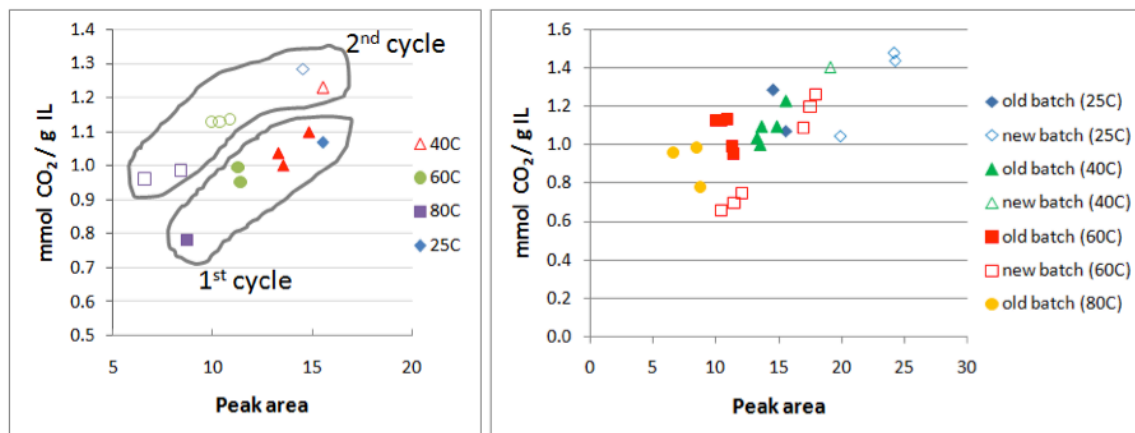
**Figure 53: The peak area of absorbance of reaction product with respect to mmol CO₂ per gram of IL; a) points obtained from 1st and 2nd absorption cycles of old batch of NDIL0043, b) more calibration points obtained with new batch of NDIL0043.**

It is clear from Figure 53 that a single linear calibration curve is not obtained for NDIL0043. Possible reasons can be summarized as: i) inefficiency in the uptake of NDIL0043, ii) instrument instability over a long experiment duration, iii) error in barometric measurements - vapor pressure, iv) error involved in curve fits that treat part of the spectrum isolated from the rest.

In order to investigate the possible mass transfer limitations in the React-IR apparatus, NDIL0043 was initially loaded with $CO_2$ not enough to reach saturation and the rate of the chemical complex peak area was observed. Second, more $CO_2$ was loaded and the rate of same peak area was recorded. These two rates did not match, suggesting slow diffusion, consistent with the high viscosity observed for these and related ILs. NDIL0045 has a viscosity on the low end of these ILs, and similar absorbance trends to that of NDIL0043 were observed.

One powerful feature of the IR system is that the amount of physically dissolved $CO_2$ can be determined, whereas uptake measurements only give the total amount absorbed. Table 14 summarizes the Henry's law constants that were calculated for physically dissolved $CO_2$ in the studied ILs, by using the previously established calibration curve for the physical uptake.

Table 14: Comparison of physical portion of Henry's law constants of TSILs and NDIL0001.

| Ionic liquid | H (bar) | | | | | |
| --- | --- | --- | --- | --- | --- | --- |
| | 10°C | 25°C | 40°C | 50°C | 60°C | 80°C |
| NDIL0001 | 24.2 | 31.6 | | 45.6 | | |
| EMD0004 | | | 109.9 | | 344.9 | |
| NDIL0030 | | 125.9 | | | | |
| NDIL0043 | | 147.1 | | | 256.4 | 333.3 |
| NDIL0045* | | 56.8 | | | | |

* Only 2 points used

**Note** that 40, 60 and 80**°C** calculations are based on 50**°C** calibrations of NDIL0001.

Figure 54 shows the IR spectrum for NDIL0045 in contact with $CO_2$ at 25 $^o$C. This IL does not form the stable zwitterionic complex observed in NDIL0030, and therefore desorption of the carbon dioxide is easily achieved by applying vacuum at 80**°C**.
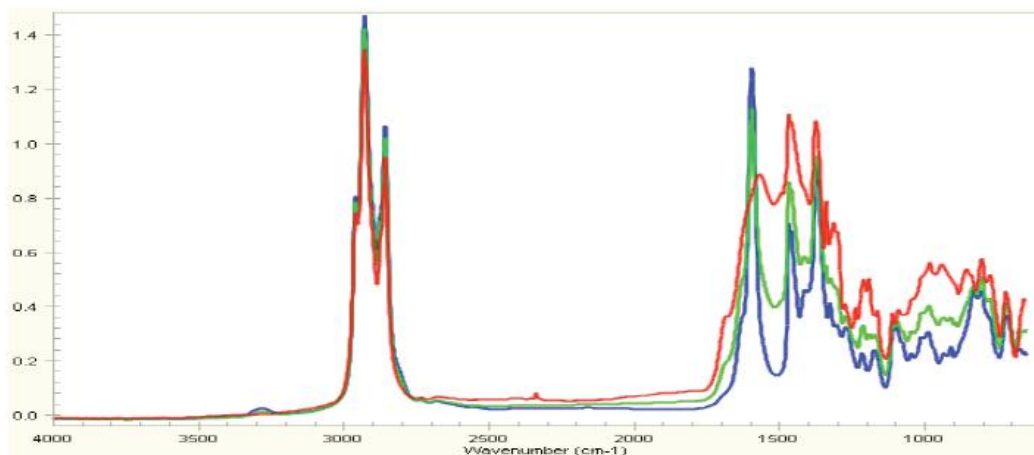


**Figure 54: Reaction spectrum of NDIL0045 with $CO_2$ at 25$^0$C: blue = pure IL before reaction, green = reacted spectrum at low $CO_2$ pressure (25 mbar), red = reacted spectrum at higher $CO_2$ pressure (40 mbar).**

For kinetic calculations, it is necessary to know the mass transfer coefficient for $CO_2$ in a particular IL in the React-IR apparatus. When the mass transfer on the gas side is ignored, the measurement of the liquid side mass transfer coefficient, $k_La$, is straightforward. In

order to observe only the physical absorption rate of $CO_2$, ILs that do not chemically complex with carbon dioxide, NDIL0001, NDIL0006, and NDIL0039, were used for this set of experiments. The rate expression for physically absorbing ILs can be written as: $Ra = k_L a(C^* - C^0)$, where $C^*$ and $C^0$ are the concentrations of $CO_2$ at the interface and in the bulk, respectively. Assuming that $k_L a$ and the volume of the gas and liquid are essentially constant and that the gas is ideal, the following expressions hold:

$$ln\left(\frac{P_0 - P_{eq}}{P - P_{eq}}\right) = k_L a \frac{P_0}{P_{eq}} t \quad \text{and} \quad ln(\alpha) = -k_L a \frac{P_0}{P_{eq}} t \quad \text{where} \quad \alpha = \frac{P - P_{eq}}{P_0 - P_{eq}}$$

$P_0$ is the initial $CO_2$ pressure that is loaded to React-IR cell after applying vacuum to the cell. $P_{eq}$ is the equilibrium pressure. Pressure was recorded every 15 seconds through a serial port connection with the pressure transducer. The slope of $ln(\alpha)$ versus *time* gives the mass transfer coefficient. In the initial experiments, the coefficients appeared to change linearly with stirring speeds.

Due to the complications associated with the viscosity change upon reaction with $CO_2$, estimates of mass transfer coefficients using unreacting $N_2O$ was attempted. The so-called $N_2O$ analogy assumes that since they are similar in size and electronic structure, $CO_2$ and $N_2O$ will diffuse similarly and that the two gases should have the same mass transfer characteristics. Figure 55 shows the results for the mass transfer coefficient of $CO_2$ in NDIL0001 and NDIL0006 as a function of stirring speed. As expected, the mass transfer coefficient increases with increasing stirring speed. Measurements for $N_2O$ in NDIL0006 were not completed in BP II.
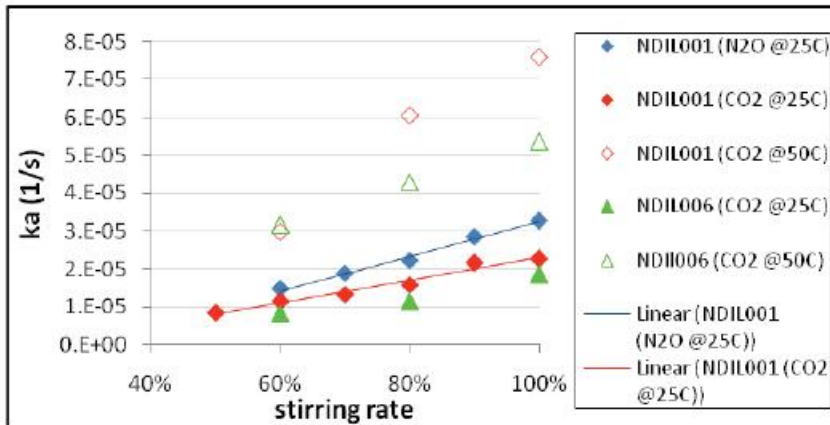
**Figure 55: Mass transfer coefficient, ka for CO$_2$ and N$_2$O in NDIL001 and NDIL006 at 25 and 50°C with respect to stirring rate in ReactIR.**

## 3.5 Economic, Engineering and Systems Analysis

At the start of BP II, Air Products conducted several brainstorming sessions both internally and in combination with Notre Dame. The idea was to see if it was possible to come up with some novel process concept that could exploit the unique properties of ILs. This exercise identified more than 15 different process concepts. Air Products discussed the advantages, disadvantages, benefits and challenges of various process elements, to narrow the choices and identify the key prospects for further evaluation. A description of seven of the most viable concepts that emerged from this exercise, along with their development needs, is provided below.

*Baseline IL absorber regenerator system with post compression*
This is the first generation process concept, which is equivalent to the benchmark MEA system utilizing an absorber and regenerator configuration. It features a chemical IL solvent operating at near atmospheric pressure to recover the CO$_2$ and then post-compression of the captured CO$_2$ to pipeline pressure. At the time of this study, the key drawback identified was the high viscosity of the known solvent systems especially after absorption of CO$_2$. It was suggested that the project endeavor to discover a system that

can operate at no more than about 100 centipoise in both the absorber and the regenerator. As the ILs known at that stage of the project were orders of magnitude away from this target, it was suggested that lower viscosities could be accomplished by adding sufficient diluents to the primary IL solvent. The drawback of course is that this will work against some of the other constraints, such as working capacity. In principle, chemical ILs can be developed with a selectivity of about one mole per mole of $CO_2$ at low $CO_2$ pressures. If the viscosity can be brought down by the addition of one or two moles of diluent per mole of IL, then the ratio of solvent is still only two or three relative to the $CO_2$. This would be much smaller than the 18 moles of MEA plus water per mole of $CO_2$ in the benchmark MEA system. While the overall amount of solvent required in the final system will depend on the difference between absorption and regeneration conditions and the pumping power will depend on the volume of solution that is circulated, such simple molar ratios suggest the potential for finding promising IL candidates. Note that these discussions confirmed that the time and effort devoted toward the discovery of lower viscosity ILs was worthwhile.

The second factor that is important is the temperature at which regeneration needs to take place. The lower this temperature the lower the lost work from the reboiler duty. The third factor that is important is the pressure at which the regenerator can operate. The higher this pressure the lower the power needed to raise the $CO_2$ to pipeline pressure. But raising this pressure will also increase the temperature needed for regeneration. Thus this is a multivariable optimization problem. In summary, what was needed in order to be competitive was a winning combination of as many of the following factors as possible – a chemical IL solvent with or without a suitable diluent which can be maintained at or below 100 centipoise for easy pumpability, operation of the regenerator at an elevated pressure, e.g. 2-5 bar, a regeneration temperature that is lower than that of MEA, a solvent working capacity that is higher than that of the MEA system per unit volume and a heat of absorption/regeneration that is no more than that of the MEA system. The eventual challenge involves finding suitable solvents and measurement of isotherms, physical and transport properties, mass transfer coefficients and column hydraulics.

A preliminary Air Products review of Trimeric's work was provided under subtask 9.0.2 of the October 2008 report. As noted in that report, Trimeric's method of calculating the parasitic power from $CO_2$ capture is useful in comparing various alternatives. Trimeric has shown an approximate value of 129 MW for the parasitic power from a plant that would nominally produce 500 MW (gross) before such parasitic losses for $CO_2$ capture and other utility requirements are accounted for. The parasitic loss includes 73 MW in lost work from the regenerator reboiler duty, 9 MW for pumping the solvents to the absorption and regeneration columns and 47 MW for compressing the $CO_2$ to pipeline pressure from the regeneration column. Trimeric has also noted that a more rigorous calculation from an overall conventional plant analysis utilizing an MEA system would yield parasitic losses of 132 MW. Air Products has evaluated the parasitic loss from a conventional system by considering variations in the number of stages in the absorber and regenerator, the solvent recirculation rate, $CO_2$ loading in the lean solvent and stripper pressure, and found that the parasitic power varies in the range of 105 to 145 MW. Note that this range brackets the values stated by Trimeric.

As also noted in the October 2008 report, the parasitic losses calculated by Trimeric for the equivalent baseline first generation IL system (NDIL0017) amount to 171 MW, which consists of 82 MW in lost work from the regenerator reboiler duty, 42 MW for pumping the solvents to the absorption and regeneration columns and 47 MW for compressing the $CO_2$ to pipeline pressure from the regeneration column. Although this value is not optimized, it is much higher than the range calculated for the MEA system noted above. This is because of the low working capacity of NDIL0017, which increases parasitic losses from the regenerator reboiler duty and the pumping power for circulating the solvents to the two columns. Note that the recirculation rate is about five times higher due to the low working capacity relative to the MEA system. Another drawback of NDIL0017 is its high viscosity - on the order of several Poise - which increases further upon absorption of $CO_2$ and likely affects pumpability.

*IL absorber regenerator system with pre-compression*

The challenges associated with the chemical IL solvent system make one look at a physical solvent system which has a much lower viscosity and in the acceptable range of lower than 100 centipoise. However, the capacity of physical IL solvents is significantly lower at atmospheric conditions. But given the pipeline pressure of about 2200 psi, one can evaluate the possibility of absorption and regeneration at the delivery pressure or some intermediate pressure to raise the working capacity while also reducing the post compression work. As the initial feedstock contains only about 12.5% $CO_2$, the compression of the extra flue gas will require seven times as much energy as post compressing the $CO_2$. Although part of this energy can be recovered by expansion prior to venting, currently available compressors and expanders will lead to a loss of about half this input. Given today's technology, the added power will be 3.5 times the $CO_2$ compression power, namely about 165 MW. This is clearly impractical against the potential saving in lost work from reboiler duty or pumping power from increased capacity. There is the further cost from the added capital equipment for compression and expansion. Thus the concept of using pre-compression with a physically dissolving IL was abandoned.

*Sequential solvents with an intermediate exchange column followed by post compression*

This concept features absorption of the $CO_2$ from the flue gas into a first solvent with high $CO_2$ capacity, transfer of the $CO_2$ in a second liquid-liquid extraction column into a chemical IL which is immiscible with the first solvent and also with a higher affinity for the $CO_2$, regeneration of the $CO_2$ in a third regeneration column followed by post compression to pipeline pressure. While such a system can lower the volume requirements of the IL system, the challenges mentioned above for the baseline system will remain for the back end of the system, e.g. viscosity control. Also this system will be meaningful only if the primary solvent with high $CO_2$ capacity cannot be heated for some reason such as thermal instability at higher regeneration temperatures. It should be noted that if and when promising candidates are identified, the work required to characterize them completely could be as much as two to three times more compared to

the baseline system in terms of isotherms, physical and transport properties, mass transfer coefficients and column hydraulics.

*Adsorption desorption on supported ILs followed by post compression*

This process would feature adsorption and desorption of the $CO_2$ from a chemical IL that is supported on a solid matrix followed by post compression to pipeline pressure. The main advantage of this process is that it avoids the viscosity challenge noted earlier and that there is much prior art available from other applications. The challenges would be finding suitable supports with a high surface area and with sufficient porosity for adsorption and good diffusion characteristics. Even if such materials are available, the support needs to be stable from the repeated expansion from adsorption and contraction from desorption. The eventual challenge involves finding suitable solvents and supports, measurement of isotherms, mass transfer coefficients, column flow limits from fluidization considerations and development of mechanical support systems. It was also noted that the solid matrix will need to be heated and cooled repeatedly, which can be technically challenging and could lead to increased heat duties. However, there is some encouraging prior art in terms of ILs on solid supports used for catalyzing reactions. One study in particular reports the use of ILs supported on silica for $CO_2$ adsorption. The high surface area and porosity of the silica allowed fast and reversible adsorption and desorption kinetics, and the silica support was stable for at least four cycles. Besides silica, there is a whole range of commercially available solid supports comprising sufficient pore sizes to accommodate ILs, high enough surface areas for rapid adsorption and desorption, sufficient stability to the anticipated maximum regeneration temperature of about 140 °C, and the capability to be readily formed into stable pellets suitable for adsorption and desorption. In terms of process options, one can consider pressure swing, vacuum swing or temperature swing. Of these options, pressure swing is not considered to be attractive, as this would require the compression of the entire flue gas stream to a high pressure in order to facilitate adsorption. This excess compression power cannot be effectively recovered as noted in one of the options above, although the pressure in this instance would be much less than the pipeline pressure. Likewise, vacuum swing is also not attractive as the product $CO_2$ must be recovered under vacuum, which will increase

the post compression power in an unacceptable fashion. The best regeneration option is thought to be temperature swing using steam, in which the water can be readily separated from $CO_2$ downstream. The overall challenge in pursuing this option involves finding a suitable solvent and support, measurement of isotherms, mass transfer coefficients, column flow limits from fluidization considerations and development of mechanical support systems. The primary advantage is that this process circumvents the viscosity problem, which, although it can be mitigated, adds to the cost of the adsorption regeneration system. Overall, this option is seen to be a worthy candidate for the next phase of this program.

*Membrane supported IL for pre-concentration*

This process would feature the use of a membrane-supported IL system for pre-concentrating the $CO_2$. An advantage of the membrane system is that it would avoid the expansion contraction issue associated with solid adsorbent pellets as the IL would be present on only one side. However, the low partial pressure of the feed gas would necessitate a deep vacuum on the other side in order to recover the $CO_2$, thereby adding to the cost of the overall system. This would increase the parasitic power from post compression quite significantly, making the overall process unattractive. In addition, the cost of separating the water from $CO_2$ would remain as part of the overall system. For this reason, this option should not be considered further.

*Solid-to-liquid-phase-changing IL system with post compression*

This process features a supported or solid phase IL system that becomes liquid upon absorption of $CO_2$ and then flows through the support and is pumped into another vessel. In the second vessel this material is heated and sprayed to release the $CO_2$ while the IL freezes into particles like snow or onto a support system. The challenge of such as system is finding a suitable material for the $CO_2$ system, but it is encouraging that such phase changing ILs do exist for some other solutes. The assessment made by Air Products at the time was that this option is highly speculative, and even if prospective materials could be found, it would present severe operational control problems. They felt that, even if a successful process were developed, it is very likely that it would be more

expensive than a simple adsorption regeneration cycle using temperature swing with steam. For this reason, they recommended that this option not be considered further.

Note that, several years later, these types of phase changing ILs were discovered serendipitously, and are presently being investigated for $CO_2$ capture by Notre Dame as part of a different DOE-sponsored ARPAe project.

*Liquid-to-solid-phase-changing IL system with post compression*

This process features the reverse of the previous system and would probably be more difficult to control. Air Products also recommended that this process not be followed up on. Note that General Electric researchers are now exploring such a system as part of a DOE –sponsored ARPAe project.

Air Products also did a preliminary review of Trimeric's earlier report. The approximate calculation they performed for the conventional MEA process would yield a parasitic power of 129 MW which is close to the 132 MW calculated earlier using more rigorous methods. The parasitic power for the MEA process includes 73 MW in lost work from the regenerator reboiler duty, 9 MW for pumping the solvents to the absorption and regeneration columns and 47 MW for compressing the $CO_2$ to pipeline pressure from the regeneration column. The equivalent calculation for the baseline IL $CO_2$ capture process shows a total parasitic power of 171 MW and the breakdown into the three main components, roughly 82, 42 and 47 MW respectively.

Trimeric conducted a sensitivity study using the HYSYS process simulation software for a hypothetical IL $CO_2$-capture process. The goal for the sensitivity analysis was to provide guidance to the developers of IL compounds about target properties for $CO_2$ capture. The primary variable of interest for the sensitivity study was the enthalpy of reaction ($\Delta H^o_{rxn}$) between IL and $CO_2$, with water solubility in IL a secondary variable. The performance metric for the sensitivity study was the total equivalent work that must be supplied by the power plant to run the $CO_2$ capture process, which would result in a derating of the power plant electricity output.

Within the range covered by the sensitivity analysis ($\Delta H_{rxn}^{o}$ 40 – 60 kJ/gmole), the minimum equivalent work (87.2 MW) was with an IL having a 50 kJ/gmole heat of reaction with $CO_2$ and partial miscibility with water. A minimum exists because of offsetting effects of $CO_2$ loading and regeneration energy. At $\Delta H_{rxn}^{o}$ less than 50 kJ/gmole, the capacity of the IL is reduced, leading to relatively high energy penalties for sensible heating and pumping of the liquid solvent. At $\Delta H_{rxn}^{o}$ greater than 50 kJ/gmole, the increased regeneration energy becomes the primary penalty.

The total equivalent work was extremely sensitive to changes in the $\Delta H_{rxn}^{o}$ between 40 and 50 kJ/gmole, with the 40 kJ/gmole minimum equivalent work about 70% higher than the 50 kJ/gmole minimum equivalent work. The minimum equivalent work for the 60 kJ/gmole case was only 3% higher than the 50 kJ/gmole minimum equivalent work, but the 60 kJ/gmole minimum occurred at a much higher regeneration temperature and pressure.

The total equivalent work for the 50kJ/gmole cases was not particularly sensitive to regeneration temperature at a given regeneration pressure, and the equivalent work for a wide range of regeneration temperatures and pressures varied only by about 10-15%. The water miscibility had a secondary effect, with fully-miscible systems resulting in slightly higher (3-5%) total equivalent work than partially miscible systems.

The sensitivity analysis evaluated only the power plant derating required for the $CO_2$ capture process, which is just one factor to be considered in a system design. The optimization of a $CO_2$ capture system would need to consider capital and operating cost factors not captured in the sensitivity analysis, including equipment sizing and makeup chemical costs.

Sensitivity Analysis Technical Approach and Results

The input parameters for the sensitivity study were selected by Trimeric and Notre Dame to reflect the ranges of IL properties in which the optimum loading or process efficiency was expected to fall.  The values of the sensitivity variables with proposed ranges for the values are listed in Table 15.

Table 15:  Values of IL $CO_2$ capture process sensitivity parameters.

| Variable | Values for Sensitivity Analysis |
|---|---|
| Enthalpy of reaction, $\Delta H_{rxn}^o$ (kJ/gmole) | 40, 50, and 60 |
| Water solubility in IL | Partially miscible, totally miscible |

Two other variables were included in the preliminary list of proposed sensitivity parameters in the previous progress report:   the $CO_2$ loading in the IL and the stoichiometry of the IL-$CO_2$ reaction.  Preliminary molecular modeling by Notre Dame was used to eliminate both variables from consideration in the sensitivity analysis:

- The entropy of reaction ($\Delta S_{rxn}^o$) could be approximated as a constant, so the equilibrium constant ($K_{eq}$) with corresponding $CO_2$ loading was fixed for a given $\Delta H_{rxn}^o$.  [ $RT \ln K_{eq} = \Delta G_{rxn}^o = \Delta H_{rxn}^o - T\Delta S_{rxn}^o$ ]
- The peak $CO_2$ loading was predicted to be for a 1:1 stoichiometry (IL:$CO_2$), so the 2:1 stoichiometry was not included in the sensitivity analysis.

A standard absorption / stripping process configuration was used to model the IL $CO_2$ capture process in HYSYS (see Fig. 56).  A five-stage compressor train was used to model compression of the recovered $CO_2$ to 13.9 MPa (2000 psig) for transport in a pipeline or injection in a well.  Other key process configuration choices were:

- The absorber and regenerator were modeled as two equilibrium-stage systems;[1]
- The rich/lean heat exchanger $\Delta T$ was assumed to be 5°C (9°F); and
- The height of the rich IL inlet to the regenerator would result in a pressure drop of 414 kPa (60 psi) from the rich/lean heat exchanger.
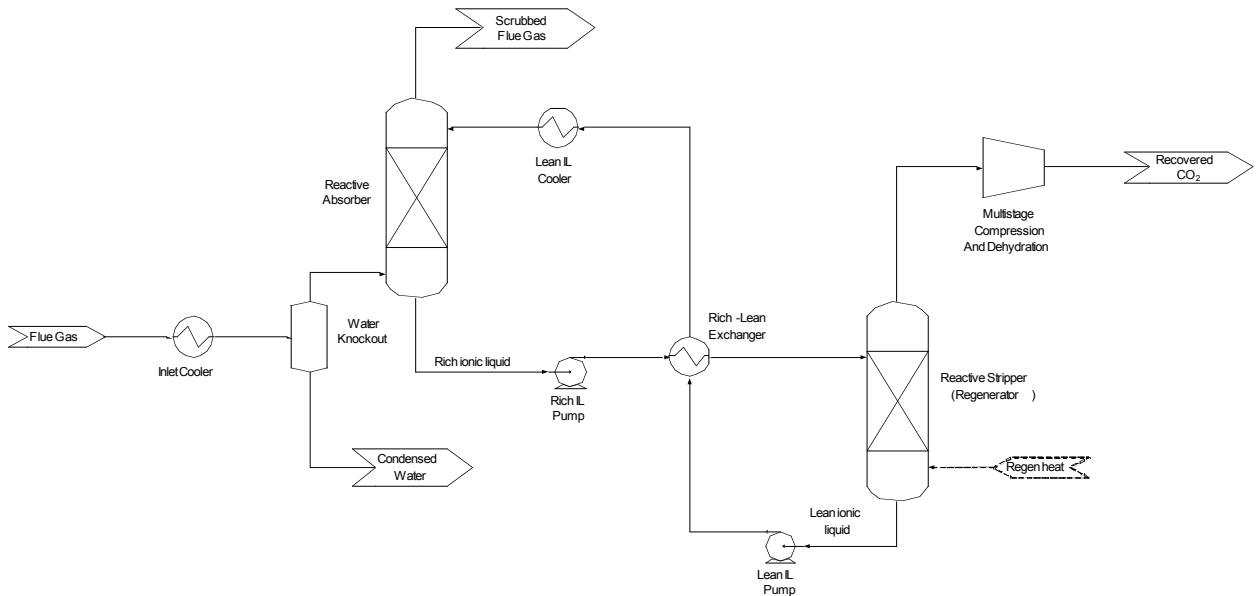


**Figure 56: Basic CO$_2$ capture process flow diagram.**

Equivalent work was used as the metric for comparing cases at different conditions. Total equivalent work was defined for the sensitivity analysis as the sum of power requirements in the capture process that will reduce the net electrical power from the power plant. Pumps (with 65% adiabatic efficiency) and compressors (with 80% polytropic efficiency) were assumed to be electrically-driven, so were accounted for directly in the derating. The heat required for regeneration presumably will be supplied by steam that could otherwise be used to generate electricity. The equivalent electrical work for regeneration heat was calculated using the formula[2]

---

[1] Increasing the number of stages may reduce the total equivalent work but likely would lead to increased equipment cost for taller columns. The economics of the absorber and regenerator designs can be evaluated at a later time, if necessary, when rate and transport property data are available for a particular ionic liquid.
[2] Oyenekan, B.A. and G.T. Rochelle. "Alternative Stripper Configurations for CO$_2$ Capture by Aqueous Amines." Presentation at the 6th Annual Conference on Carbon Capture and Sequestration, Pittsburgh, 7-10 May 2007.

$$Regeneration\,Equivalent\,Work = \left(Q_{regen}\right) \times \left(\varepsilon\right) \times \frac{\left(T_{reboiler} + 10K\right) - T_{reject}}{T_{reboiler} + 10K}$$

where

$Q_{regen}$ = regenerator heat duty (different for each case)

$\varepsilon$ = isentropic efficiency of steam turbine (assumed to be 75%)

$T_{reboiler}$ = reboiler temperature (different for each case)

$T_{reject}$ = ultimate heat reject temperature (assumed to be 313K)

For each combination of $\Delta H_{rxn}$ and water solubility, the procedure for the sensitivity analysis included the following steps:

1. Selected a regeneration pressure.
2. Set the regeneration temperature.
3. Varied the IL circulation rate until $CO_2$ removal was 90% (±0.1%).
4. Repeated Steps 2 and 3 until the temperature was identified at which the minimum total equivalent work occurred for the selected regeneration pressure.
5. Repeated Steps 1 – 4 until the regeneration pressure and temperature were identified at which the minimum equivalent work was located for the chosen combination of $\Delta H_{rxn}^{o}$ and water miscibility.

The primary output from the sensitivity analysis for each combination of $\Delta H_{rxn}^{o}$ and water miscibility was a series of curves of total equivalent work as a function of temperature. The constant-regeneration pressure curves that include the minimum equivalent work point for each combination of $\Delta H_{rxn}^{o}$ and water miscibility are shown Figure 57. For comparison, the total equivalent work for a baseline MEA system was estimated to be 132 MW.[3] The lowest point from all of the cases (87.2 MW) is on the curve for 50 kJ/gmole and partial water miscibility. This result indicates that a $\Delta H_{rxn}^{o}$ of 50 kJ/gmole would be a reasonable target for the development of new IL compounds at a

[3] Fisher, K.S., *et al*. *Advanced Amine Solvent Formulations and Process Integration for Near-Term CO₂ Capture Success*. Final Report to U.S. Department of Energy, National Energy Technology Laboratory. Grant No. DE-FG02-06ER84625, June 2007.

fixed $\Delta S_{rxn}^{o}$. The minimum total equivalent work point may be at a different $\Delta H_{rxn}^{o}$, temperature, and/or pressure if the $\Delta S_{rxn}^{o}$ changes from the value assumed for the sensitivity analysis.

Note that the total equivalent work is not a strong function of temperature for the constant regeneration-pressure curves in Figure 57. The economic optimum operating point may be at a higher or lower temperature when equipment and operating costs are considered along with the power plant derating. Additionally, the total equivalent work values for the fully water-miscible cases were only 3-5% higher than for the partially water-miscible cases, so water solubility in the IL is a secondary consideration to $\Delta H_{rxn}^{o}$ (and $\Delta S_{rxn}^{o}$) for the design of new compounds.

The net $CO_2$ loadings and IL circulation rates for the cases with minimum total equivalent work at each $\Delta H_{rxn}^{o}$ and water partially miscible with IL are shown in Figure 58. Because the $\Delta S_{rxn}^{o}$ is fixed, there is a sharp decline in the $K_{eq}$, and thus in the $CO_2$ loading, as the $\Delta H_{rxn}^{o}$ was reduced from 60 to 40 kJ/gmole. The higher IL circulation rate for the 40 kJ/gmole case compared to the other cases leads to increased pumping power and regenerator thermal requirements that contribute to the significantly higher total equivalent work.
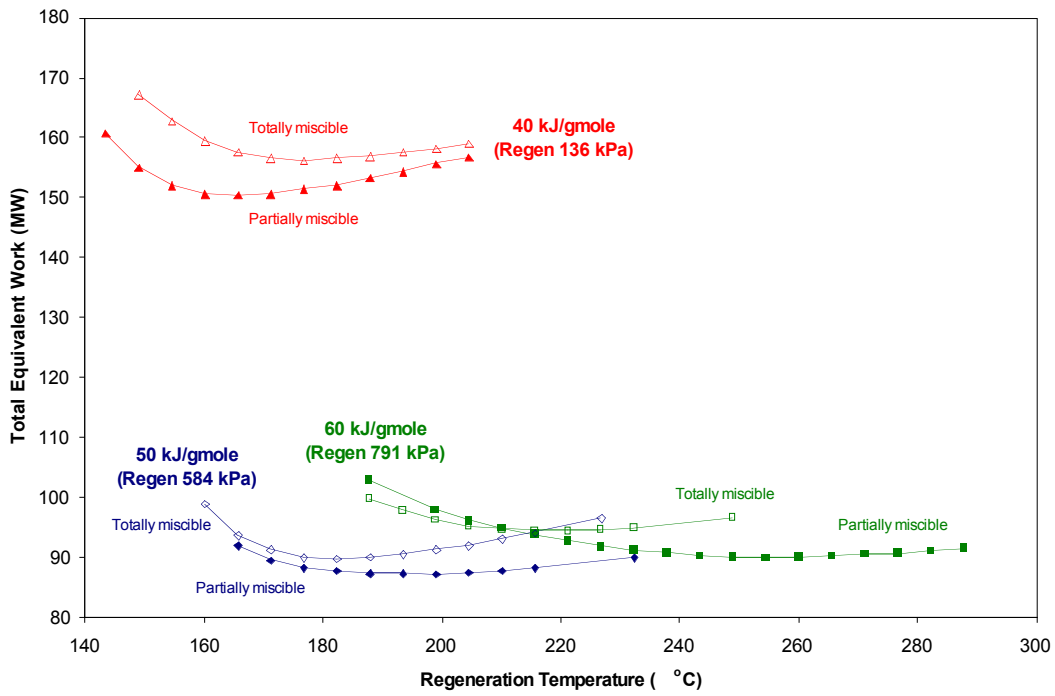
**Figure 57: Curves of lowest equivalent work for each $\Delta H_{rxn}$ and water miscibility.**
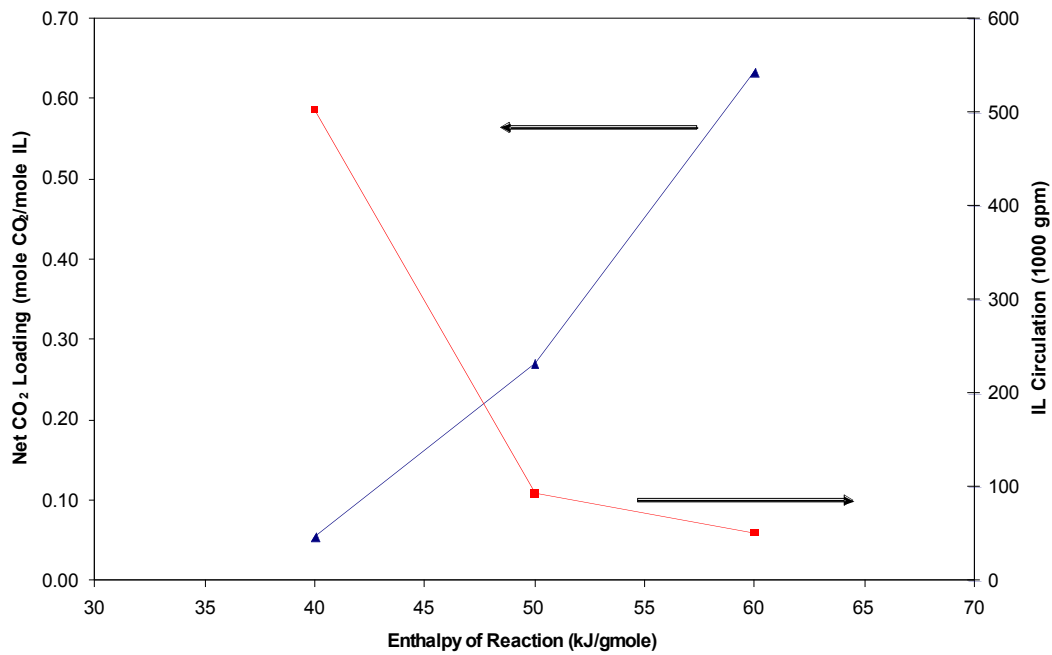


**Figure 58: CO$_2$ loading and IL circulation rate for the lowest equivalent work case at each $\Delta$Hrxn (IL partially miscible with water).**

Following the release of the sensitivity study, Trimeric worked to update the report by including process economics. The study estimated that $CO_2$ capture increased the base COE from 5 ¢/kWh to 10.6 ¢/kWh for MEA and 8.8 to 9.5 ¢/kWh for the hypothetical ILs, properties of which were identified by Notre Dame. Note that the increase in COE *does not include the solvent management costs associated with degradation or other losses*. The corresponding cost per metric tonne $CO_2$ avoided was \$66.8/tonne $CO_2$ and \$44.8 to 52.5 /tonne $CO_2$, respectively. Derated capacities were 339 MWe for MEA and 361 to 368 for the ILs. When compared to the base case, the ILs reduced the reboiler steam requirements by 41 to 48%, reduced derating due to $CO_2$ capture by 13 to 18%, and reduced the cost of $CO_2$ avoided by 21 to 33%.

The complete systems analysis was provided to DOE in a technical report on 20 July, 2009. The results of this study suggested that ILs have a very good chance of being a competitive alternative to MEA for post-combustion capture. The report identified some key unknowns, including the overall thermodynamics and intrinsic properties of the ILs, corrosion behavior, thermal and oxidative stability, mass transfer characteristics and cost. Importantly, it provided a target enthalpy of reaction, which was used in subsequent modeling studies to discover new ILs with optimized reaction thermodynamics.

At the conclusion of BP II, Air Products submitted a Summary Analysis of its process design studies to DOE on 30 July, 2009. This analysis is reproduced below.

Introduction

About fifteen broad process concepts developed through brainstorming sessions at Air Products and Notre Dame were evaluated as part of the initial screening study in terms of the advantages, disadvantages, benefits and challenges of their constituent process elements to narrow the choice to seven process options. Further analysis was used to narrow the choices to two top process options namely, 1) a viscosity modified absorber regenerator process with post compression (VMAS process) and 2) an adsorption/desorption process using a supported IL followed by temperature swing adsorption (TSA process). The second process would use temperature swing

regeneration with low pressure steam. The current report describes the completion of the process analysis as outlined by Subtask 9.0.3 and the summary analysis as outlined by Subtask 9.1.1 for the two chosen options. The analysis is based on the measured and/or calculated properties of NDIL0045 for absorption and desorption of $CO_2$ in the presence of water for the VMAS process and the measured and/or calculated adsorption and desorption properties of NDIL0045 supported on silica for the TSA process.

For the two processes chosen for further investigation and costing, process flow diagrams (PFD) were developed. The VMAS utilizes a diluent (e.g. water) with the IL (e.g. NDIL0045) to lower the overall viscosity below at least 100 Centipoise (cP) anywhere in the system to permit reasonable pumping of the solution. However, the quantity of diluent should be minimized in order to optimize the heat duty needed for regeneration and separation. As noted in the January 2009 report, the goal was a VMAS system developed by solving a multivariable optimization problem with a winning combination that contains as many of the following factors as possible: 1) a viscosity modified chemical IL solvent system which can be maintained at or below 100 cP for ease of pumping, 2) operation of the regenerator at an elevated pressure (e.g. 1.5-5 bar), 3) a regeneration temperature that is lower than that of MEA, 4) a solvent working capacity that is higher than that of the MEA system per unit volume and, 5) a heat of absorption/regeneration that is no more than that of the MEA system. It should be noted that while some of these factors are necessary conditions, others are only desirable; and as shown later, the parasitic power from $CO_2$ capture has been minimized as the objective function in the multivariable optimization problem with due consideration given to as many of the above factors as possible. The overall challenge in pursuing this option involves establishing the final solvent system through measurement of isotherms, physical and transport properties, mass transfer coefficients and column hydraulics.

The TSA process would feature adsorption and desorption of the $CO_2$ from a chemical IL that is supported on a solid matrix followed by post compression to pipeline pressure. The main advantage of this process is that it avoids the challenges associated with processing due to the viscosity of certain IL solutions. As noted in the January 2009

report, the challenge is in finding suitable supports with a high surface area and with sufficient porosity for adsorption and good diffusion characteristics. There is a whole range of commercially available solid supports comprising sufficient pore sizes to accommodate ILs, high enough surface areas for rapid adsorption and desorption, sufficient stability to the anticipated maximum regeneration temperature of about 150°C, and the capability to be readily formed into stable pellets suitable for adsorption and desorption. Silica was selected earlier as a suitable support for the screening phase based on its high surface area and porosity and thermal stability at the expected regeneration temperatures as well as the existence of some prior art results showing its potential suitability for this application. In terms of process options, one can consider pressure swing, vacuum swing or temperature swing. The best regeneration option is thought to be temperature swing using steam, in which the water can be readily separated from $CO_2$ downstream. The overall challenge in pursuing this option involves establishing a suitable solvent and support, measurement of isotherms, mass transfer coefficients, column flow limits from fluidization considerations and development of optimized process cycles.

Results

The VMAS process is similar to the benchmark MEA process with the key difference being the use of diluents to control and maintain the viscosity well below 100 cP in all parts of the process so that the solvent mixtures remain pumpable. The ILs that were available at the time the prior reports were written would have needed special diluents in addition to water to achieve viscosity control. But the invention of NDIL0045 has made it possible to achieve this using only water as the diluent. This is very convenient as water is naturally present in the flue gas, although it lowers the capacity for $CO_2$ and so would have to be optimized to keep the regeneration duty at reasonable levels.

Aspen process modules were developed which utilize thermodynamic models to describe the measured adsorption characteristics of $CO_2$ into NDIL0045 in the presence of water. The thermodynamic models account for both the chemical and physical absorption of the $CO_2$ in the IL as well as the presence of water as a reactive species rather than just as an

inert diluent. As described later under detailed results, the forms of equations were limited to those derived from known theoretical principles with their constants adjusted to obtain as good a fit to the data as possible. As part of the process modeling, a number of variations were tested, including the number of theoretical stages in the absorber and regenerator and the pressure in the regenerator. The results reported here have been simulated using an absorber with four theoretical stages at a pressure of 1.1 bara and a regenerator with eight theoretical stages at a pressure of 2.6 bara. The parasitic power from the VMAS process is about 112 MWe, wherein, due to the presence of sufficient water, the maximum viscosity is only about 50 cP and well below the target of 100 cP. This parasitic power of 112 MWe on a 500 MWe baseline power plant compares favorably with the published value of 132 MWe as the parasitic load from an MEA based absorption regeneration system.

As part of this study the capital and operating costs have been estimated. These are based on the use of packed distillation columns in the absorber and stripper and the use of five parallel trains. The overall capital cost is estimated to be $412 million. It is to be noted that this compares favorably with the published capital costs for the MEA based process in the range of $470 million to $700 million when adjusted for the plant size and conditions of this report. [4]The operating costs are estimated to be $14 million/year which includes maintenance, labor and consumables, but excludes parasitic power. Note that the parasitic load of 112 MWe derating has not been monetized since the basis for this conversion can be highly variable depending on the location and the specifics of the financing and base price for the electricity being generated.

A temperature swing adsorption process was proposed consisting of feed, steam heating, and air cooling steps. It was found to be unattractive compared to the VMAS approach

---

[4] Fisher, K. S., *et al*., "Advanced Amine Solvent Formulations and Process Integration for Near-Term $CO_2$ Capture Success." Final Report, U.S. Dept. of Energy, National Energy Technology Laboratory. Grant No. DE-FG02-06ER84625, June 2007; Xu, B., *et al*., "Future $CO_2$ Capture Technology Options for the Canadian Market." Department for Business Enterprise & Regulatory Reform, Report No. Coal R309 BERR/But URN 07/1251, March 2007; Panesar, R. S., *et al*., "Coal-Fired Advanced Supercritical Retrofit with $CO_2$ Capture." June 2009.

due to both excessive capital costs ($840 million) and operating costs ($24 million/year). The TSA process would also have a parasitic load well in excess of either the VMAS or MEA process. The air cooling step is the bottleneck of the process because gas phase heat transfer is not very efficient. The cooling step requires 80% of the total process cycle time. It also necessitates employment of eight separate beds to cover the time spent on cooling. This leads to the high capital costs via excessively large adsorbent/vessel/valve requirements. The approach also suffers from relatively high regeneration costs. One reason for this is due to the relatively high heat of reaction between $CO_2$ and the supported IL (20 kcal/mol). The TSA approach needs energy to heat up all of the adsorbent to the regeneration temperature as well as the heat of desorption of $CO_2$; however, this energy is not recovered unlike in the case of the VMAS process.

Based on these results, it is evident that the VMAS process is much more economical than the TSA process. It is also competitive with the benchmark MEA based absorption regeneration process, but considerable challenges remain.

A draft commercialization report was submitted to the program manager during BP II. Feedback was given and the report was updated later in the project.

### 3.6 Project Management

Regular conference calls and email communications were held throughout BP II. Air Products sent a team to Notre Dame during the second quarter of BP II for meetings on alternative process designs. Notre Dame made a presentation at the DOE NETL on $CO_2$ capture in March, 2009. Representatives from Babcock & Wilcox and Trimeric Corporation visited the research team at Notre Dame during the 4th quarter of BP II. The meeting involved project updates and discussions and identification of key issues for the design of bench-scale experiments to be performed under Task 12.0 of the next budget period.

## 4. Budget Period III: 7/22/09-7/31/10

### 4.1 Background

Phase III consists of seven tasks: Temperature swing adsorption summary analysis; bench-scale experiments in support of laboratory scale capture system; design of laboratory scale capture system; test plan development; development, synthesis and testing of Generation 3 ILs; systems and economic analyses update; and project management and reporting.

### 4.2 Temperature Swing Adsorption Analysis

Trimeric performed an economic analysis of purchased equipment, capital and operating costs of a temperature swing adsorption (TSA) process for $CO_2$ capture using ILs. The completed economic analysis was utilized to perform a high-level economic comparison alongside two different evaluations of a VMAS process. These VMAS evaluations were carried out by Air Products and Trimeric. The Trimeric TSA analysis was based on an earlier economic analysis of a TSA process conducted by Air Products (***Subtask 9.1.1 Milestone Report: Air Products Summary Analysis***, 21 July 2009), but several enhancements were made. In November 2009, Trimeric submitted to Notre Dame a report containing a detailed process configuration (with PDF), energy and material balances, and economic analysis of the modified TSA process. On December 3, 2009, this report was forwarded to the Department of Energy for review. Based on the highly unfavorable economics of the TSA process, Notre Dame recommended that further work on the TSA process be halted, and that the project focus only on the VMAS process. The program manager (David Lang) concurred with this assessment, and so no further work on the TSA process will be conducted.

### 4.3 Bench-Scale Experiments

The goal of this task was to measure the relative mass transfer coefficient for $CO_2$ absorption by ILs. The benchmark mass transfer coefficient is to be the current industry

standard, $CO_2$ absorption by MEA, in a MEA-water solution. Figure 59 shows a schematic of the design.
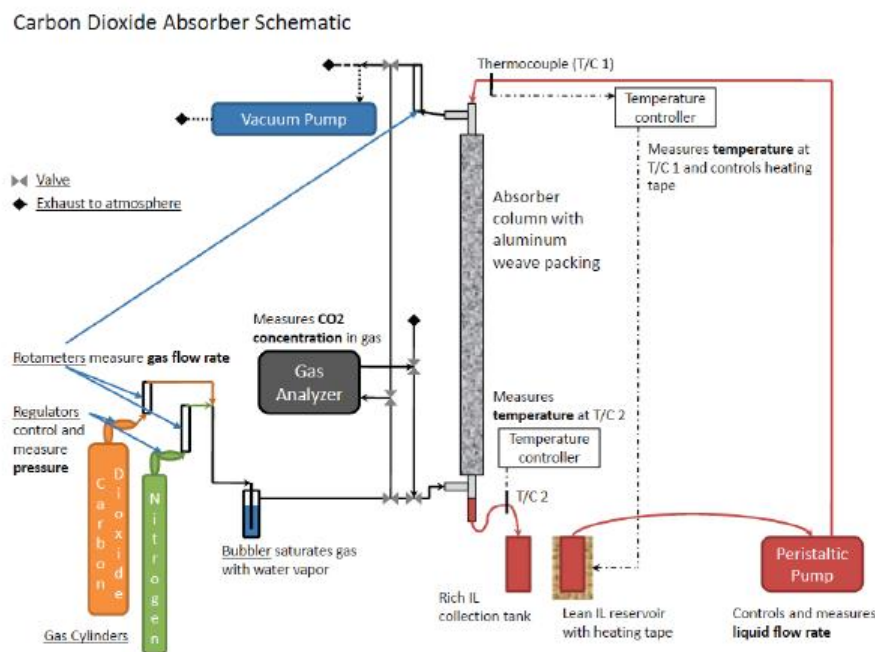


**Figure 59: Design of the bench-scale test system.**

The absorber column is glass, with woven aluminum packing to increase the mass transfer area. It was designed to take a synthetic flue gas stream of 15% carbon dioxide and 85% nitrogen and reduce the $CO_2$ concentration 15% to 5% by volume. A non-dispersive infrared (NDIR) gas analyzer was used to measure the concentration of $CO_2$ in the gas both pre- and post-absorption.



**Figure 60: Photo of bench-scale test system. The glass packed column in on the left, $CO_2$ detector in foreground and associated piping and valves in the background.**

Prior to preliminary testing of the system, liquid pumps and thermocouples were calibrated. In the initial tests, an aqueous solution of 0.25 M NaOH was used as a liquid

absorbent. A number of technical problems were experienced with the unit, including improperly sized rotameters. By the third quarter of BP III, good results were being obtained for aqueous MEA solutions and NaOH modified with glycerin to increase the viscosity. Table 16 shows the conditions of each MEA experiment performed.

Table 16: MEA test conditions used with the bench-scale system.

| Name | Absorbant | Concentration (M) | Solvent | Flow rate (mL/min) | Inlet temp (° C) |
|-------|----------------|------|-------|------|----|
| MEA 2 | monoethanolamine | 4.9 | water | 30.5 | 26 |
| MEA 3 | monoethanolamine | 4.9 | water | 30.5 | 27 |
| MEA 4 | monoethanolamine | 4.9 | water | 30.5 | 26 |
| MEA 5 | monoethanolamine | 4.9 | water | 40.0 | 26 |
| MEA 6 | monoethanolamine | 2.5 | water | 30.5 | 25 |
| MEA 7 | monoethanolamine | 4.9 | water | 30.5 | 40 |

At the end of BP III, all testing was completed and it was time to use an actual IL sample. The laboratory was moved to a new facility, so the unit was disassembled, moved, and reassembled in the new location.

**4.4 Design of Laboratory Scale Capture System**

Notre Dame researchers visited the labs of B&W in Ohio and examined their lab-scale testing facilities. Based on this visit, the Notre Dame team planned to design a system similar to the B&W unit, but with more manual control features to save cost. However, the final design of the system was not completed until after BP III.

**4.5 Test Plan Development**

The test plan development proceeded in parallel with the design of the lab scale unit, and as discussed below, was completed during BP IV.

**4.6 Development, Synthesis and Testing of Generation 3 ILs**

This task involved an integrated set of molecular modeling studies, compound synthesis, and property measurement. The work was driven by the earlier process modeling studies, which helped determine targets for properties such as uptake thermodynamics and viscosity.

**4.6.1 Classical Simulations**

Molecular dynamics calculations were conducted to study the gas-liquid interface of a prototypical IL NDIL0001 and $CO_2$ and also examined $CO_2/H_2O$ mixtures. The process of $CO_2$ absorption on the liquid surface and absorption into the bulk IL was quantified in terms of flux and concentration difference across the interface. The simulations provided an estimate of the interfacial thickness and gave a better fundamental understanding of mass transfer resistance associated with $CO_2$ absorption in the IL. This work was reported in two journal articles [11,12]; reference 11 was featured on the cover of the *Journal of Physical Chemistry B*.

Force field parameters for the chemically complexing IL NDIL0058 were developed. The IL was chosen as it absorbs a large amount of $CO_2$ at low partial pressures of $CO_2$ (see below) but does not increase in viscosity. The density of the IL and mixtures of reactants and $CO_2$-IL products for different extents of reaction were predicted. The calculations were carried out at 100 $^o$C. The simulation predictions are shown in Figure 61. Note that this particular IL is predicted to have a density less than that of water.
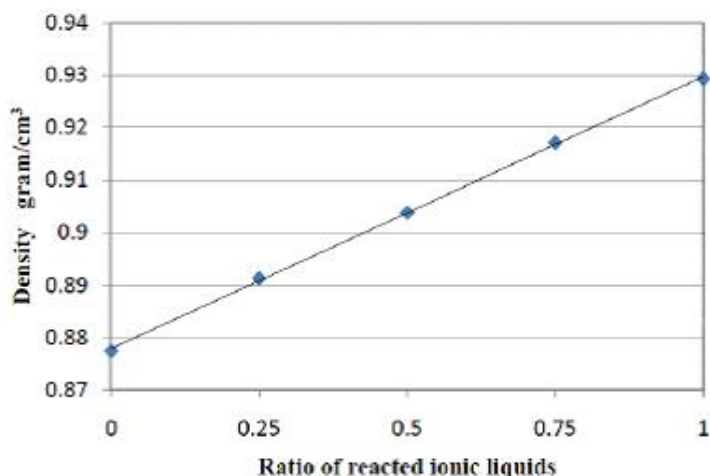


**Figure 61: Densities of the IL mixture containing NDIL0058 and $CO_2$-NDIL0058 complex as a function of extent of reaction. The results are obtained from molecular dynamics simulations at 100 $^o$C.**

This IL was simulated at other temperatures, including 333 K and 413 K, which are typical of the temperatures where absorption and stripping take place. Results are shown in Figures 62-63.
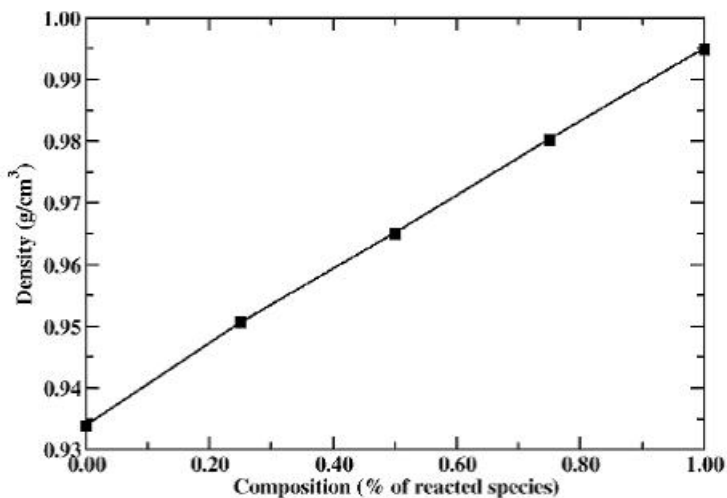


**Figure 62: Density predictions for NDIL0058 vs extent of reaction with $CO_2$ at 333 K.**
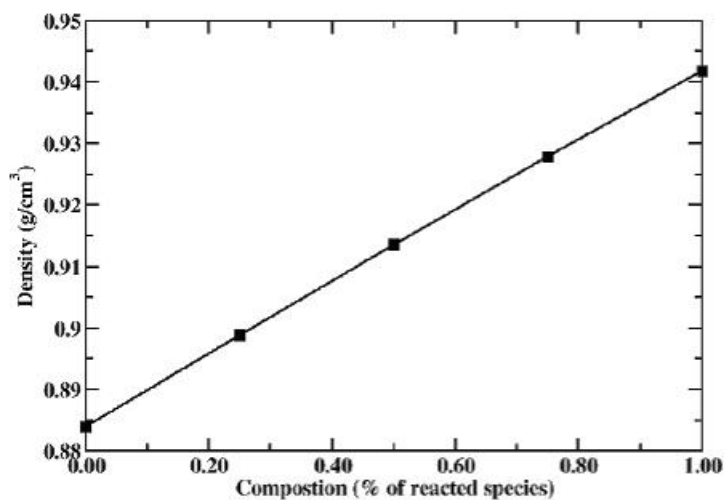


**Figure 63: Density predictions for NDIL0058 vs extent of reaction with $CO_2$ at 413 K.**

The diffusivity and rotational relaxation time constants of the cation and anion, anion-$CO_2$ complex were also determined from the simulations and are reported in Tables 17 and 18 respectively.

Table 17:  Diffusivity ( x $10^{12}$ m$^2$/s) of the cation, anion in NDIL0058. Also reported are the diffusivities of the anion-$CO_2$ complex.

| | | 333 K | | 373 K | | 413 K | |
|---|---|---|---|---|---|---|---|
| | | $D_s$ | ±σ | $D_s$ | ±σ | $D_s$ | ±σ |
| unreacted | Cation | 8.6 | 1.7 | 29.8 | 1.0 | 99.6 | 5.4 |
| | Anion | 13.1 | 3.2 | 49.8 | 4.6 | 150.6 | 18.7 |
| | | | | | | | |
| 25% reacted | Cation | 7.5 | 0.7 | 36.0 | 8.2 | 99.9 | 15.1 |
| | Anion | 10.4 | 0.6 | 44.4 | 14.8 | 152.0 | 8.7 |
| | Anion-$CO_2$ | 10.0 | 1.8 | 44.2 | 12.9 | 128.2 | 38.6 |
| | | | | | | | |
| 50% reacted | Cation | 8.1 | 1.8 | 33.6 | 4.3 | 85.8 | 7.0 |
| | Anion | 10.4 | 3.1 | 46.3 | 4.6 | 138.4 | 18.7 |
| | Anion-$CO_2$ | 13.8 | 6.4 | 41.8 | 8.0 | 127.0 | 26.4 |
| | | | | | | | |
| 75% reacted | Cation | 9.3 | 3.3 | 37.0 | 6.7 | 107.3 | 13.2 |
| | Anion | 12.6 | 3.0 | 39.5 | 0.9 | 119.1 | 18.0 |
| | Anion-$CO_2$ | 12.3 | 3.1 | 45.8 | 3.9 | 134.6 | 5.3 |
| | | | | | | | |
| 100% reacted | Cation | 9.8 | 4.1 | 35.1 | 6.2 | 122.6 | 12.8 |
| | Anion-$CO_2$ | 12.3 | 5.2 | 45.4 | 7.9 | 146.3 | 11.7 |

Table 18:  Rotational relaxation time constants of cation and anion in NDIL0058. Also reported are the time constants for anion-$CO_2$ complex. The time constants are in ns.

| | | | unreacted | | 25%reacted | | 50%reacted | | 75%reacted | | 100%reacted | |
|---|---|---|---|---|---|---|---|---|---|---|---|---|
| | | | τ | ±σ | τ | ±σ | τ | ±σ | τ | ±σ | τ | ±σ |
| 333K | Cation | | 1.36 | 0.11 | 1.74 | 0.26 | 1.66 | 0.43 | 1.55 | 0.42 | 1.73 | 0.27 |
| | Anion | plane | 0.21 | 0.02 | 0.25 | 0.02 | 0.27 | 0.04 | 0.26 | 0.02 | - | - |
| | | normal | 0.52 | 0.06 | 0.72 | 0.12 | 0.74 | 0.22 | 0.62 | 0.21 | - | - |
| | Anion-$CO_2$ | plane | - | - | 0.41 | 0.09 | 0.51 | 0.27 | 0.40 | 0.07 | 0.43 | 0.09 |
| | | normal | - | - | 0.58 | 0.15 | 0.57 | 0.17 | 0.46 | 0.09 | 0.54 | 0.13 |
| | | | | | | | | | | | | |
| 373K | Cation | | 0.364 | 0.006 | 0.376 | 0.054 | 0.358 | 0.021 | 0.396 | 0.022 | 0.385 | 0.047 |
| | Anion | plane | 0.049 | 0.004 | 0.060 | 0.006 | 0.058 | 0.004 | 0.066 | 0.004 | - | - |
| | | normal | 0.128 | 0.010 | 0.143 | 0.017 | 0.144 | 0.009 | 0.158 | 0.003 | - | - |
| | Anion-$CO_2$ | plane | - | - | 0.086 | 0.009 | 0.096 | 0.001 | 0.092 | 0.012 | 0.097 | 0.009 |
| | | normal | - | - | 0.109 | 0.008 | 0.123 | 0.002 | 0.120 | 0.014 | 0.129 | 0.014 |
| | | | | | | | | | | | | |
| 413K | Cation | | 0.128 | 0.008 | 0.130 | 0.004 | 0.142 | 0.006 | 0.136 | 0.005 | 0.137 | 0.008 |
| | Anion | plane | 0.017 | 0.001 | 0.019 | 0.001 | 0.021 | 0.001 | 0.020 | 0.001 | - | - |
| | | normal | 0.045 | 0.002 | 0.049 | 0.001 | 0.055 | 0.004 | 0.052 | 0.003 | - | - |
| | Anion-$CO_2$ | plane | - | - | 0.034 | 0.003 | 0.037 | 0.001 | 0.035 | 0.001 | 0.034 | 0.001 |
| | | normal | - | - | 0.043 | 0.002 | 0.045 | 0.003 | 0.043 | 0.001 | 0.043 | 0.001 |

Data from these tables indicate that the translational and rotational dynamics of ions of NDIL0058 are much faster compared to generation 1 NDIL0017. Significantly faster dynamics in NDIL0058 suggests that the IL and its product with $CO_2$ do not suffer from high viscosity as was observed with NDIL0017. Hydrogen bond analysis in NDIL0058 was carried out and found little evidence of hydrogen bonded-network in the IL, thus confirming the hypothesis that elimination of hydrogen bonded-network leads to lowering of the viscosity of ILs. These calculations thereby helped validate the hypothesis that creating the AHA-type Generation 3 ILs is an effective means for getting rid of the large viscosity increases that had been observed when Generation 2 ILs reacted with $CO_2$.

The heat capacity of the NDIL0058 and its completely reacted analogue was also computed. This information is important for process modeling calculations. The calculated heat capacity of the ILs is provided in Table 19.

Table 19: Calculated heat capacity of NDIL0058 and its reacted analogue (J K$^{-1}$ mol$^{-1}$) obtained from molecular dynamics simulations.

| ILs | $C_p^{IG}$ | $C_p^{Res}$ | $C_p$ |
|---|---|---|---|
| NDIL0058 | 570.6 | 221.9 | 792.5 |
| NDIL0058-$CO_2$ | 617.0 | 231.2 | 848.2 |

$C_p^{IG}$ is the ideal gas heat capacity obtained from ab initio calculations, $C_p^{Res}$ is the residual heat capacity determined from the molecular dynamics simulations while $C_p$ is the total heat capacity as the sum of $C_p^{IG}$ and $C_p^{Res}$.

In addition, thermodynamic integration was used to evaluate the Henry's law constant of various gases in the NDIL0058 as a function of temperature. The data are provided in Tables 20-21 for NDIL0058 and the reacted analogue. These calculations have been performed in lieu of experiments, as the physical solubility of $CO_2$ is difficult to measure in reactive ILs. The calculated Henry's constants will be used by Trimeric for process modeling. It is especially noteworthy that the simulations predict that $CO_2$ is about as soluble in the reacted IL as the unreacted IL, but water appears to be much more soluble

in the reacted IL. These predictions will need to be tested experimentally. Oxygen and nitrogen are sparingly soluble in this IL, which is good from a selectivity standpoint.

Table 20: Henry's constant (bar) of gases in NDIL0058 calculated from thermodynamic integration.

| Temp (K) | $CO_2$ | Nitrogen | Oxygen | Water |
|---|---|---|---|---|
| 333 | 214±46 | 1891±282 | 1137±284 | 0.17±0.08 |
| 373 | 312±58 | 2141±180 | 1112±167 | 0.34±0.15 |
| 413 | 443±57 | 2548±138 | 1167±161 | 0.78±0.21 |

Table 21: Henry's constant (bar) of gases in the fully reacted analogue of NDIL0058 obtained from free energy calculations.

| Temp (K) | $CO_2$ | Nitrogen | Oxygen | Water |
|---|---|---|---|---|
| 333 | 225±49 | - | 744±141 | 0.014±0.012 |

**4.6.2 Quantum Simulations**

The reaction energies of several reactions containing anions and carbon dioxide was calculated using the density functional based tight-binding method (DFTB). These results were then compared to previously calculated B3LYP reaction energies. The DFTB method allows for calculations on very large systems such as ILs. The previous B3LYP results were determined from gas phase reactions, while ILs will be interacting in a bulk liquid phase. The goal was to verify whether this method can reproduce the reaction energies found in the gas phase, with the hope that calculations on larger, bulk systems can produce the same agreement.

Table 22: Reaction energy comparisons of selected anions in which functional group attached to the anion is varied

| | DFTB (kJ/mol) | B3LYP (kJ/mol) |
|---|---|---|
| Compound 1 | -78.05 | -71.00 |
| Compound 2 | -65.55 | -58.41 |
| Compound 3 | -48.35 | -38.37 |

Table 22 shows the comparison of reaction energies involving select anions with different functional groups. The product, a complex of the reactant with $CO_2$, and the reactants

were optimized using the DFTB method. Reaction energies were calculated and compared to those previously reported using B3LYP. These energies show good agreement between the two approaches. Later during BP III, however, it was found that for some complexes of reactant and $CO_2$ the DFTB overestimates the bond length between the anion and $CO_2$ as compared to the B3LYP results. This also causes the reaction energy to be more exothermic than is predicted by B3LYP. Therefore, care needs to be taken about interpreting results from these different methods.

Molecular orbital diagrams were produced for the reaction of the anion in NDIL0046 with $CO_2$ to form a complex. Additionally, the same anion combines were studied with a proton to observe how they form a neutral molecule. It was observed, based on the molecular orbital diagrams, that the reaction with a proton is more strongly favored as the combined molecular orbitals are significantly lower in energy. This gave greater insight into the mechanistic details of the reaction of these species with $CO_2$.

The basic isotherm model was updated to include temperature dependence. This was accomplished by including the heat capacity in both the $\Delta H$ and $\Delta S$ terms. If temperature dependence is not included, then the optimal $\Delta H$ occurs around -60 kJ/mol. If temperature dependence is included, then the optimal $\Delta H$ occurs around -57 kJ/mol. Later in BP III, the isotherm model was updated to account for a situation in which it is possible for the IL to take up 2 $CO_2$ molecules for every 1 molecule of IL. Ideas were generated (computationally) for ILs that might do this. For this model, there is an enthalpy associated with the uptake of the first $CO_2$ ($\Delta H_1$) and an enthalpy associated with the uptake of the second $CO_2$ ($\Delta H_2$). Figure 64 shows how changing both $\Delta H_1$ and $\Delta H_2$ affect the change in mole ratio between the absorber and desorber.
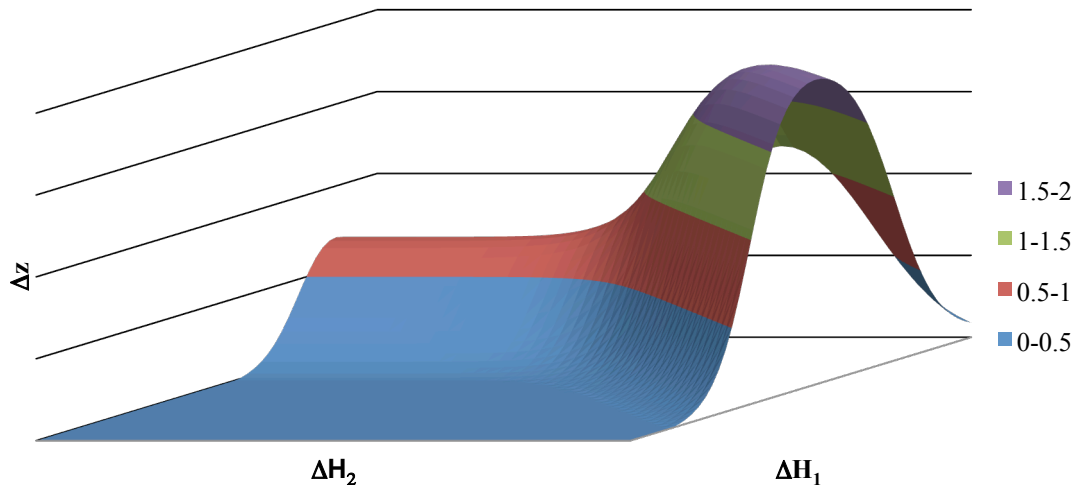
**Figure 64: 3-D plot of $\Delta H_1$ and $\Delta H_2$ versus change in mole ratio.**

The contour plot of Figure 64 is shown below in Figure 65.
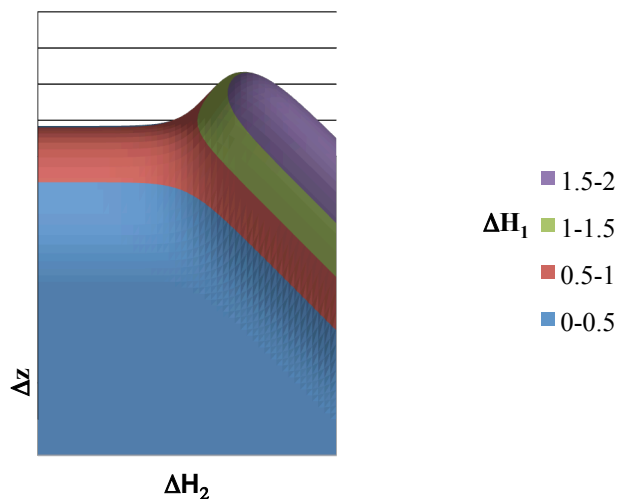


**Figure 65: Contour plot of the 3-D plot of $\Delta H_1$ and delta $\Delta H_2$ versus the change in mole ratio.**

Finally, attention was given to determine the impact of a solvent environment on the reaction energetics and how the solvent effects would differ from the gas phase. Up to this point, all the quantum calculations for $CO_2$ reacting with an IL were for "gas phase"

reactions. In reality, the reaction occurs in the liquid phase, and the energetics could differ because of the condensed phase environment. The effect of the solvent environment on the reaction energies was estimated by using both explicit and implicit models. Explicit calculations were performed using a single cation of NDIL0058. The reaction of the anion of NDIL0058 with the counterion was studied. The enthalpy of reaction of the anion with $CO_2$ in the presence of the counterion is only different from the gas-phase energy by 5 kJ mol$^{-1}$.

For the implicit model, the polarized conductor-like medium (PCM) continuum solvation model as implemented in Gaussian 03 was used. Since the dielectric constants of ILs are not well known, the effects of three different solvent models corresponding to aniline, isoquinoline, and acetonitrile was compared, with dielectric constants of 6.8882, 11.00, and 20.493, respectively. Table 23 shows the reaction free energies for the anion of NDIL0058 (A) and two anions (B & C) derived from this anion in the three solvents.

Table 23: Free energies of reaction for the reactions of NDI0058 ("A"), and two other hypothetical ILs with similar structures ("B" and "C") with $CO_2$ in the gas-phase, aniline, isoquinoline, and acetone.

| | $\Delta G_{gas}$ (kJ mol$^{-1}$) | $\Delta G$ Aniline (kJ mol$^{-1}$) | $\Delta G$ IsoQuinoline (kJ mol$^{-1}$) | $\Delta G$ Acetone (kJ mol$^{-1}$) |
|---|---|---|---|---|
| C + $CO_2$ → C-$CO_2^-$ | -53.53 | -47.84 | -47.55 | -47.63 |
| B + $CO_2$ → B-$CO_2^-$ | 9.23 | 3.08 | 2.46 | 1.07 |
| A + $CO_2$ → A-$CO_2^-$ | -14.25 | -11.49 | -11.41 | -11.91 |

Table 23 shows that using the three different solvents only changes the reaction free energies compared to the gas-phase by around 5 to 8 kJ mol$^{-1}$. This is consistent with the explicit solvation calculation and shows that adding a solvent does not change the reaction energies from the gas-phase energies much at all. This suggests that the gas-phase energies are sufficient enough to use, especially when determining relative energies. This was very good news, as it meant that the (faster) gas phase calculations could continue to be used with confidence.

### 4.6.3 Synthesis

22 new ILs were synthesized during this BP (NDIL0051, NDIL0052, NDIL0054-NDIL0059, NDIL0063-NDIL0066, NDIL0068-76 and NDIL0079). The synthesis of about a dozen other ILs was started at the end of this BP. NDIL0046 was identified as being a good candidate for future studies, so larger quantities of this IL were prepared and a battery of tests run to determine all the properties needed for a process simulation study by Trimeric. Note that the synthetic procedures necessary for producing high quality samples needed to be refined during this process. For example, batch-to-batch variation was observed in some of the properties of NDIL0046 early on. Subsequent work led to a solution for this problem such that reproducible results were obtained, although as noted in BP IV, differences in properties between Notre Dame samples of NDIL0046 and those provided by Koei were experienced. Thus quality control of the samples during synthesis is an important consideration.

### 4.6.4 Property Measurement

Figure 66 shows $CO_2$ uptake isotherms for NDIL0051 and NDIL0049. NDIL0051 absorbed about 0.9 moles of carbon dioxide per mole of IL at 1 bar and reached a molar ratio of 1 at about 2.4 bars. NDIL0049, which was designed computationally to have a significantly lower heat of reaction, absorbed carbon dioxide to a much lower capacity. This result is an impressive confirmation of the capability the team developed to design ILs with "tuned" $CO_2$ uptake characteristics. It was first predicted that NDIL0051 would bind $CO_2$ more strongly than NDIL0049, and this was confirmed experimentally in Figure 66. In addition, it was determined that NDIL0051 would bind one $CO_2$ molecule for every one IL molecule of IL. Again, this prediction was reflected in the experimental data.
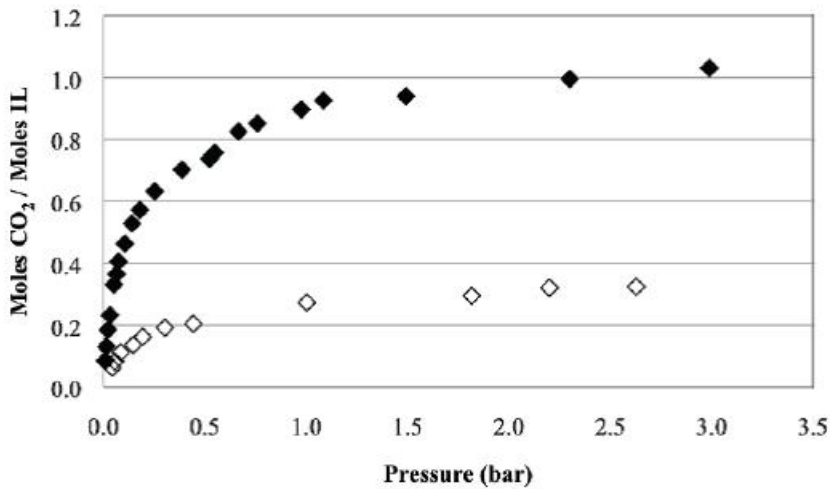
**Figure 66: Absorption isotherm of $CO_2$ at 22°C in NDIL0051 (black diamonds) and NDIL0049 (empty diamonds).**

Previously, absorption isotherms of carbon dioxide into NDIL0045 was measured at 22, 60, 80 and 100°C. The equipment was modified during BP III to add the capability to measure absorption isotherms at temperatures below room temperature. As shown in Figure 67, the absorption isotherm at 10°C agrees with the previously reported trend of increased absorption at lower temperatures.
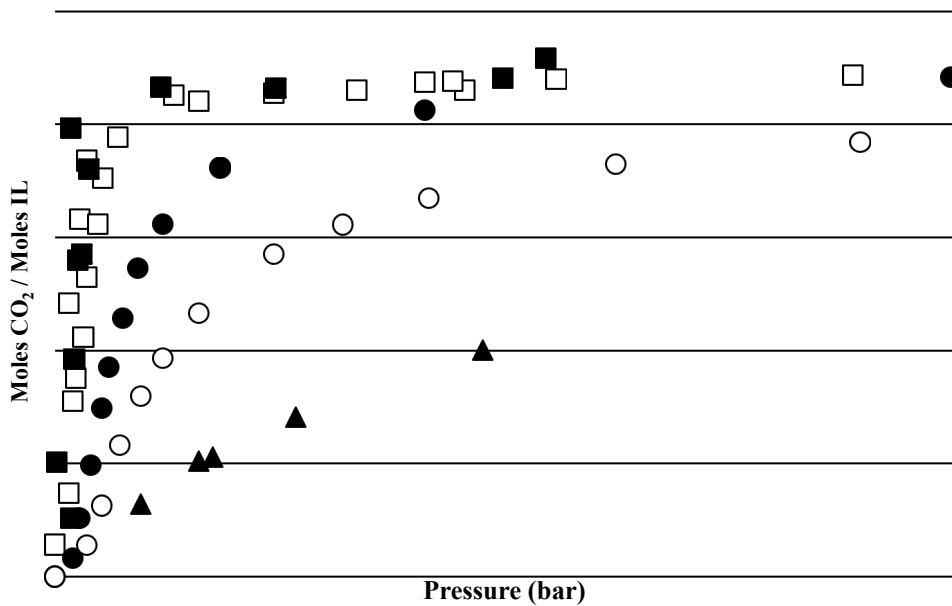


**Figure 67. Absorption isotherm of $CO_2$ in NDIL0045 performed at different temperatures. Solid squares represent 10°C, empty squares represent 22°C, solid circles represent 60°C, empty circles represent 80°C, and solid triangles represent 100°C.**

111

Of interest was the fraction of $CO_2$ in the ILs that is chemically reacted and that which is physically dissolved. This information is important for model development and also for the process simulation studies. An estimation was made of the amount of $CO_2$ physically dissolved using simulations, but independent experimental route to this information was desired. Toward that end, the physical solubility was estimated using FTIR spectroscopy and a calibration based on NDIL0001, but this is not a perfect solution. Therefore,work was continued, this using the 'N$_2$O analogy' to estimate $CO_2$ solubility. This analogy is based on the observation that the solubility of $N_2O$ and $CO_2$ is quite similar in many conventional solvents. Therefore, experiments were conducted in the IGA gravimetric microbalances with $N_2O$ and the ILs NDIL0001 and NDIL0053 in order to establish a correlation between the physical solubility of $N_2O$ and that of $CO_2$. The goal was to use this correlation in order to estimate the $CO_2$ physical solubility in the task-specific ILs. For NDIL0001, experiments were conducted at 25˚C and 50˚C and for NDIL0053 isotherms were measured temperatures of 25˚C, 50˚C, and 80˚C. In both cases the pressure range was from 0.25 to 14 bar. The results show that the physical solubilities of both $N_2O$ and $CO_2$ are virtually the same in both ILs within the uncertainty of the balance. Figures 68-69 show the results for these two ILs. As can be seen, the two species have almost identical solubilities, therefore confirming that the "analogy" may be accurate (at least for these two ILs).
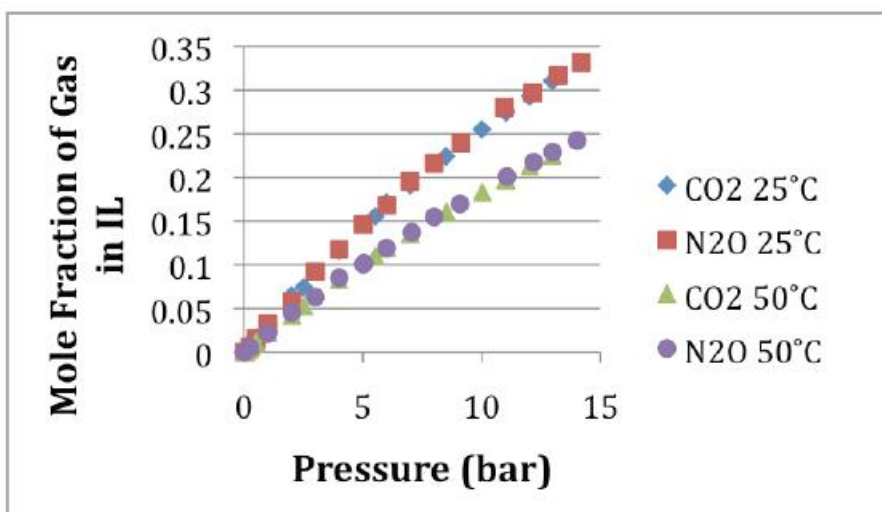
**Figure 68: Comparison of physical solubility of $N_2O$ and $CO_2$ in NDIL0001 at 25 °C and 50 °C.**
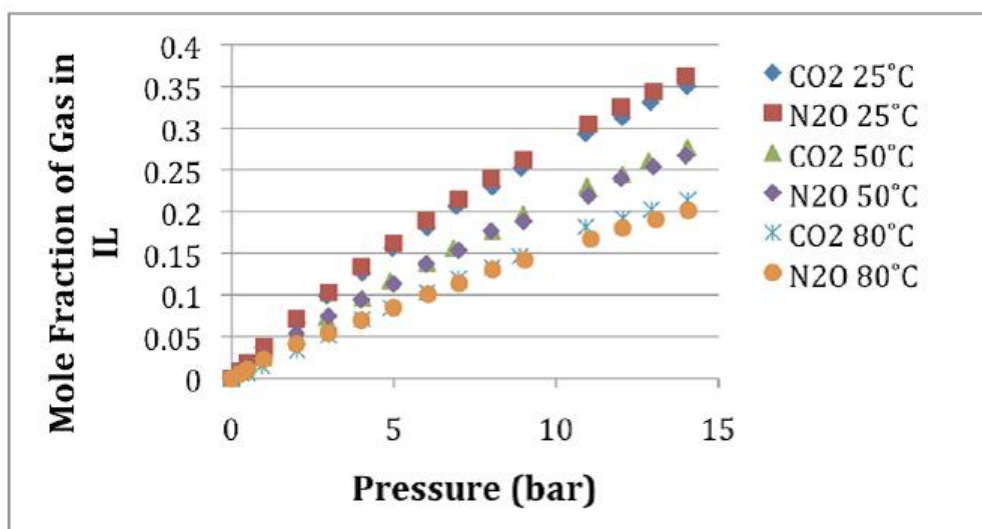


**Figure 69: Comparison of physical solubility of $N_2O$ and $CO_2$ in NDIL0053 at 25, 50 and 80 °C.**

Because the isotherms are essentially linear, a Henry's law constant can easily be extracted. Table 24 compares the Henry's constants for the two gases.

Table 24: Comparison of Henry's Law Constants for $CO_2$ and $N_2O$ in NDIL0001 and NDIL0053 in units of bar, as measured by the IGA gravimetric microbalance.

| | NDIL0001 | | NDIL0053 | |
|---|---|---|---|---|
| | $CO_2$ | $N_2O$ | $CO_2$ | $N_2O$ |
| 25˚C | 31.25 | 31.55 | 29.07 | 27.86 |
| 50˚C | 45.66 | 45.45 | 39.02 | 39.42 |
| 80˚C | ---- | ----- | 54.64 | 53.48 |

This trend was confirmed with measurements in the React-IR system with NDIL001 and NDIL006. This is shown in Table 25. However, the previously measured Henry's constant for the physically dissolved $CO_2$ in NDIL0045 (57 bar at 25 $^0$C) using React-IR calibrations did not agree with that predicted by the $N_2O$ analogy estimate (20 bar at 25 $^0$C). Thus, it was concluded that the IR calibration in ILs without chemical complexation may not be applicable for ILs with chemical complexation. Therefore, the physical solubility of $CO_2$ in NDIL00046 using FTIR spectroscopy was estimated, where the physically dissolved $CO_2$ shows a distinct band around 2300 cm$^{-1}$. Using this method, an estimate was made that the Henry's law constant for physically dissolved $CO_2$ in NDIL0046 at room temperature is 62 bar. As discussed below, high pressure experiments yielded a different value for the Henry's law constant.

Table 25: Comparison of Henry's Law Constants for $CO_2$ and $N_2O$ in NDIL0001 and NDIL0006 in units of bar, as measured by the React-IR system.

| | $CO_2$ | | $N_2O$ | |
|---|---|---|---|---|
| | 25 $^0$C | 50 $^0$C | 25 $^0$C | 50 $^0$C |
| NDIL001 | 31.6 ± 0.2 | 45.6 ± 0.3 | 29 | 46 |
| NDIL006 | 32.8 ± 0.2 | 46.2 ±0.3 | 28 | 44 |
| EMD0005 | | | 20 | 31 |
| EMD0006 | | | 25 | 39 |

Additional $CO_2$ uptake measurements were made for NDIL0058, NDIL0059 and NDIL0065. All three of these compounds are solid at room temperature, so the uptake curves were measured at 60°C. NDIL0065 contains a less expensive anion, which have not been investigated previously. NDIL0065 absorbed more carbon dioxide at higher

pressures than NDIL0058 and NDIL0059. However, at the low pressures of interest for post-combustion $CO_2$ capture, NDIL0058 had the highest capacity. The capacities would likely be closer to one mole $CO_2$/ mole IL at somewhat lower temperatures.
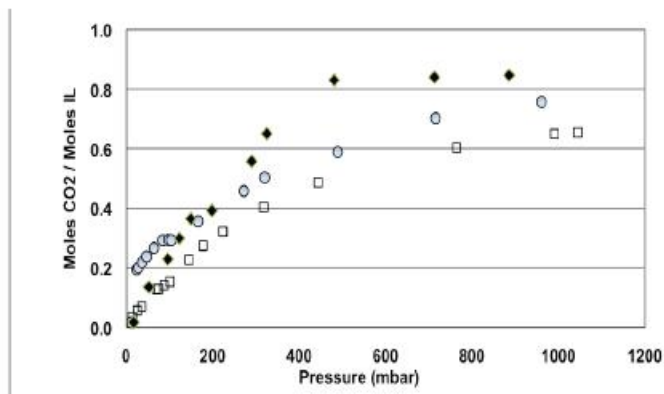


**Figure 70: Absorption isotherm of $CO_2$ in NDIL0065 (diamonds) , NDIL0058 (circles) and NDIL0059 (squares) performed at 60°C**

As discussed above, NDIL0046 was chosen to be the IL for which Trimeric performs a detailed systems analysis. Therefore, they need extensive property data to do the modeling. Therefore measurements of $CO_2$ uptake in this IL were begun. Figure 71 shows a number of isotherms for $CO_2$ in NDIL0046 as a function of temperature.
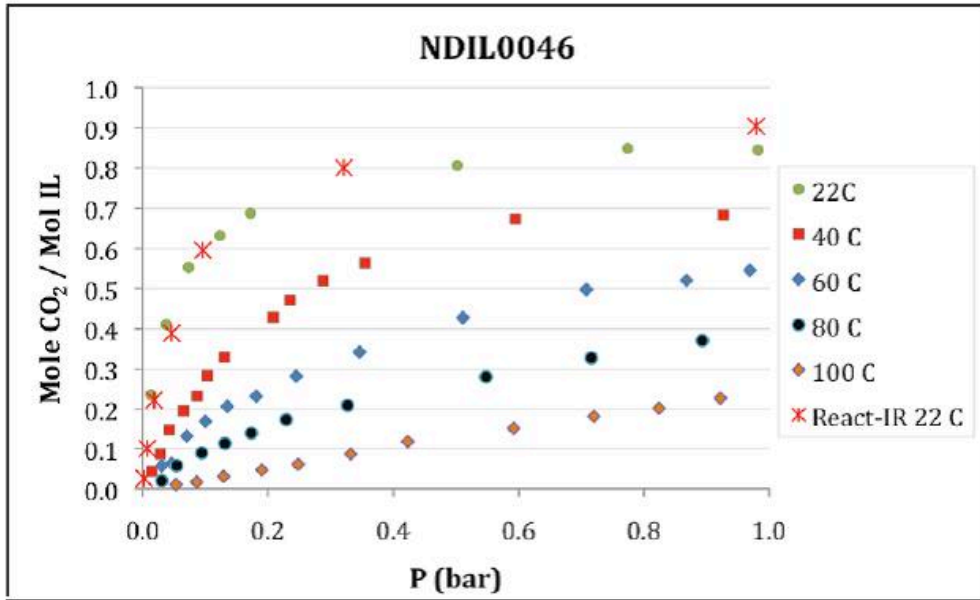
**Figure 71: CO$_2$ uptake curves for NDIL0046 as a function of temperature.**

These data needed to be fit to an analytic model so Trimeric could use the model in process simulations. The data were well-fit by the 3-parameter Langmuir model which had been developed; Figure 72 shows the quality of the fit.
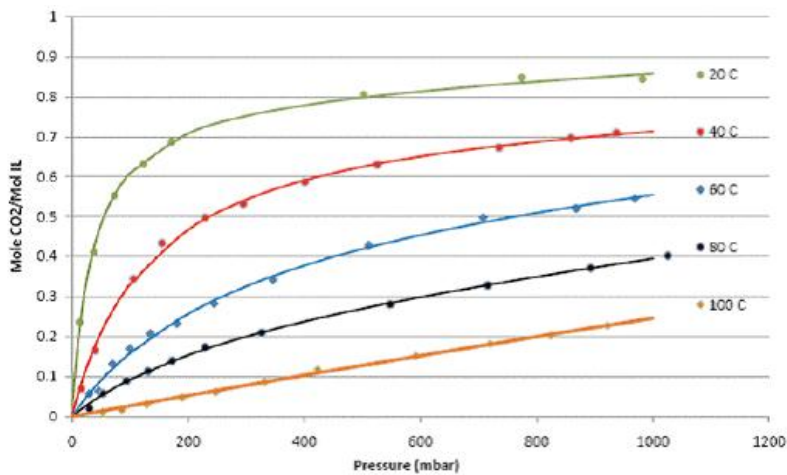


**Figure 72: Lines represent the fits to the experimental data (points) for CO$_2$ absorption in NDIL0046.**

$CO_2$ uptake data for NDIL0076 has been obtained, and these results, at 22 °C, are shown in Figure 73 in comparison to the data for NDIL0046 at the same temperature. Clearly, the uptake for NDIL0076 is much higher, approaching two moles of $CO_2$ per mole of IL. Note that $CO_2$ binds much more strongly to this IL than it does to NDIL0046.
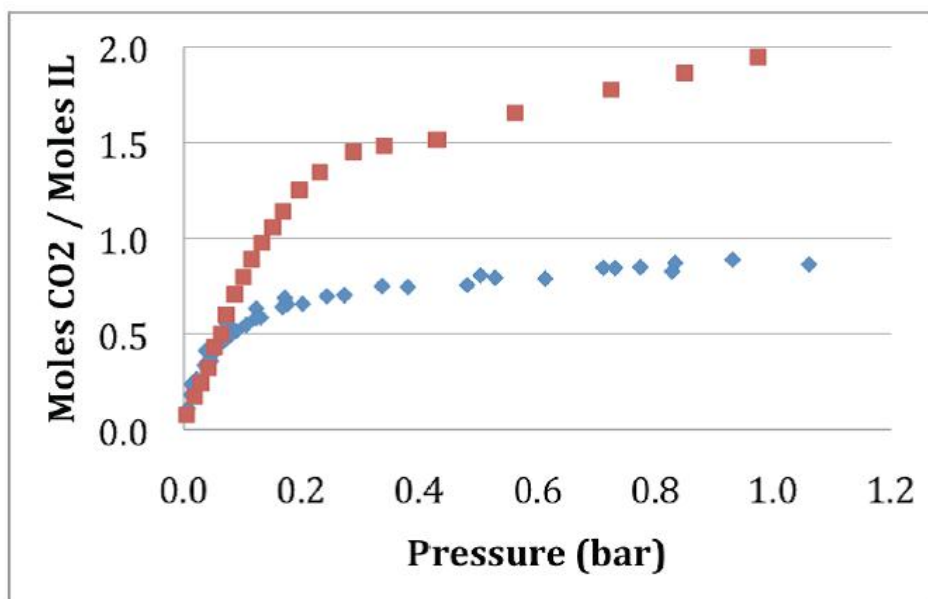


**Figure 73: The $CO_2$ uptake curve for NDIL0076 (red symbols) in comparison to NDIL0046 (blue squares) at 22 $^0$C.**

As a test of the estimate of the Henry's law constant for $CO_2$ in NDIL0046, pressure measurements of $CO_2$ solubility were made. After around 1 bar, the IL reaction with $CO_2$ will saturate and any additional uptake can be assumed to be physical. By measuring this high pressure uptake, an independent estimate of the $CO_2$ Henry's law constant can be obtained. A high pressure isotherm for NDIL0046 is shown in Figure 74.
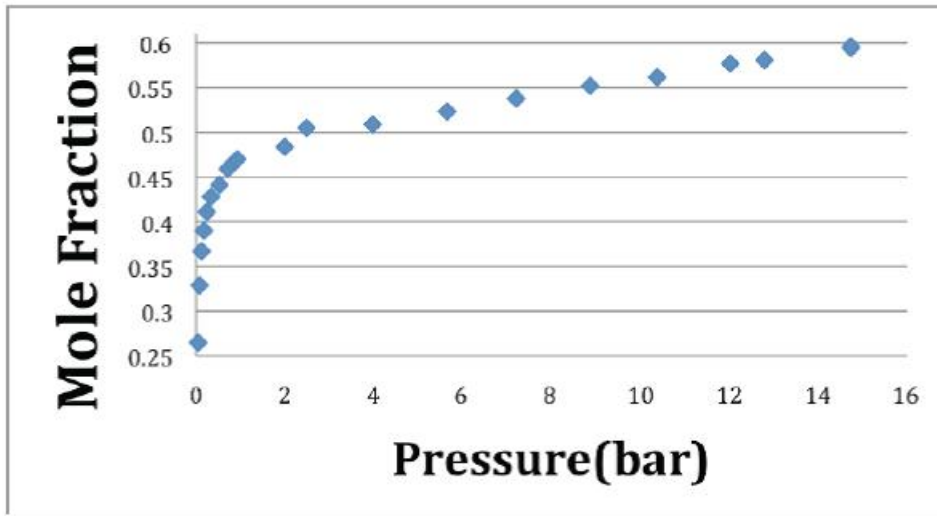
**Figure 74: High pressure uptake of $CO_2$ in NDIL0046 at 22 $^{o}$C.**

Note that the points above 2 bar are from a gravimetric apparatus, while the low pressure points are from the IR cell. The fact that the two data sets agree with one another is good confirmation of the reliability of these two methods. Unfortunately, the Henry's law constant estimated from these measurements is about half that obtained from the IR estimates. It was decided to use the estimate from the isotherm in the process simulations, as it is a physical measurement and does not rely on calibration as does the IR measurement.

The enthalpy of absorption was measured for several additional ILs with $CO_2$, as described previously, with the Setaram microDSCIII calorimeter. The results are shown in Table 26.

Table 26:  Heats of absorption of $CO_2$ in various ILs.

| Ionic Liquid | Heat of Absorption, kJ/mol $CO_2$ |
|---|---|
| NDIL0045 | -77 |
| NDIL0046 | -48 |
| NDIL0051 | -45 |
| NDIL0052/NDIL0047 | -18 |
| NDIL0043 | -64 |

It is important to note that NDIL0052/NDIL0047 is actually a mixture of approximately 87 % NDIL0052 and 13 % NDIL0047. The results shown in Table 26 agree remarkably well with the heat of reaction obtained from *ab initio* calculations.

Given its importance in the process modeling being performed by Trimeric, additional attention was given to the measurement of the enthalpy of reaction of NDIL0046. Multiple calorimetric measurements of the enthalpy of reaction of $CO_2$ with three different batches of NDIL0046 were performed using a Setaram microDSCIII calorimeter. The results are shown in Table 27. As can be seen, the results vary by about 5 kJ/mol and so this will be accounted for in the process modeling.

Table 27: Experimentally determined enthalpies of reaction for $CO_2$ in NDIL0046.

| Batch 1 Experiment # | $\Delta$Habs (kJ/mol$_{CO2}$) |
|---|---|
| 1 | -48 |
| 2 | -51 |
| 3 | -49 |
| 4 | -48 |

| Batch 2 Experiment # | $\Delta$Habs (kJ/mol$_{CO2}$) |
|---|---|
| 1 | -53 |
| 2 | -50 |
| 3 | -49 |

| Batch 3 Experiment # | $\Delta$Habs (kJ/mol$_{CO2}$) |
|---|---|
| 1 | -45 |
| 2 | -45 |

In an effort to increase the thermal stability of the ILs, gas chromatography – mass spectrometry (GC-MS) was used to analyze the thermal decomposition products of the ILs. In particular, two possible decomposition mechanisms were investigated, as shown schematically for a phosphonium salt in Figure 75. The potential mechanisms are: (1) a

nucleophilic substitution reaction at the R-carbon center, **[S$_N$(C)]**: where a nucleophilic anion like halide displaces a trialkylphosphine group. The oxidation state changes from the reactant (P at +5 oxidation state) to the product (P at +3 oxidation state); this reaction can also be regarded as a reductive elimination process, and (2) *β-elimination*, **E$_β$**: where the *β*-proton is abstracted by a base in concert with the expulsion of trialkylphosphine from the R-carbon.

$$R_3P \quad + \quad X-CH_2-CH_2-R' \qquad \textbf{(1)}$$

$$\textbf{[S}_N\textbf{(C)]} \quad \Big\uparrow \quad X^{\ominus}$$

$$\overset{\oplus}{R_3P}-CH_2-CH_2-R' \xrightarrow[\textbf{E}_\beta]{B^{\ominus}} \begin{array}{c} R_3P \\ + \\ CH_2{=}CH{-}R' \\ + \\ BH \end{array} \quad \textbf{(2)}$$
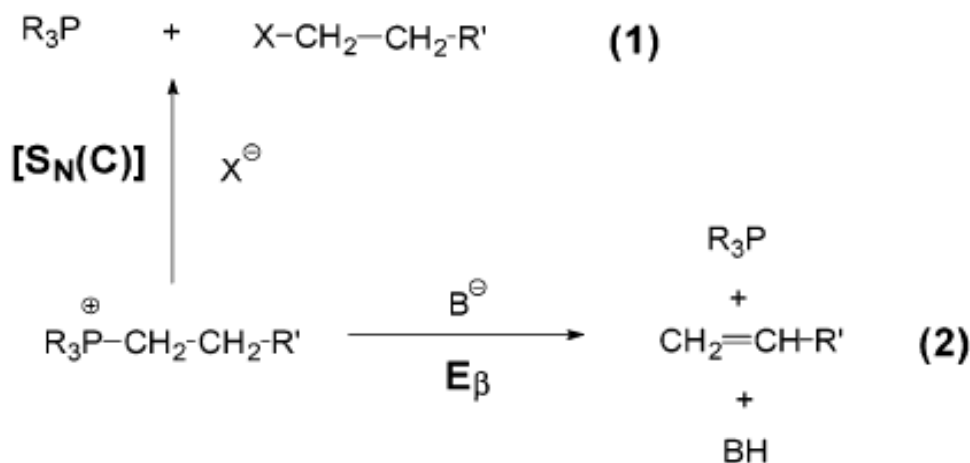
**Figure 75.  Possible decomposition mechanisms taken from *Xie et al , Chem. Mater., Vol. 14, No. 11, 2002.***

Decomposition temperatures were measured for a series of ILs using a TGA from Mettler Toledo, and the $T_{onset}$ was used to describe the IL's decomposition temperatures. IL having higher values of $T_{onset}$ typically means they have better thermal stability. Normally, IL thermal stability increases with the increase of anion size.  The glass transition ($T_g$), cold crystallization temperature ($T_{cc}$) and melting point ($T_m$) were measured with a DSC from Mettler Toledo. Many ILs tend to subcool easily to form glasses at very low temperatures rather than exhibiting crystallization or melting transitions. $T_g$ and $T_m$ values are important for determining the lower end of the operating range where the IL is liquid, and $T_{onset}$ can be regarded as the upper operating range since IL do not evaporate. A summary of the data are shown in Table 28. The results suggest that many of these liquids have an operating window well below -25 $^o$C and above 200 $^o$C.

Table 28:  $T_{onset}$ of IL under $N_2$ at ramp rate of 10 °C/min.

| IL | Batch | $T_{onset}$(°C) | $T_g$(°C) | $T_{cc}$(°C) | $T_m$(°C) |
|---|---|---|---|---|---|
| NDIL0054* | MFG24 | 274 | | | |
| NDIL0049* | MFG25 | 317 | | | |
| NDIL0059[a] | BEG24 | 273 | -67 | -14 | 17, 18, 29 |
| EMD0005 | BEG4 | 318 | -73 | | |
| NDIL0057 | BEG22 | 323 | -63 | | |
| NDIL0043 | EAP13 | 238 | -77 | | |
| NDIL0055 | LJAW3 | 252 | -73 | | |
| NDIL0046 | LJAW1 | 320 | -77 | | |
| NDIL0058[a] | BEG23 | 316 | | | 19, 37 |
| NDIL0035 | ---- | 340 | -86 | | |
| NDIL0056 | BEG21 | 339 | -66 | | |
| NDIL0063 | MFG 29 | 327 | -71 | | |
| NDIL0064* | FC7 | 319 | | | |
| NDIL0066 | LJAW6 | 317 | -52 | -7 | 45 |
| NDIL0051* | MFG26 | 260 | | | |
| NDIL0065 | MFG30 | 272 | -58 | -11 | 21 |
| NDIL0065 | LJAW20 | 266 | -62 | -19 | 14 |
| NDIL0065 | LJAW22 | 268 | -65 | | 14 |
| NDIL0065 | LJAW5 | 263 | -62 | | -46 |
| NDIL0066 | LJAW6 | 317 | -52 | -7 | 45 |
| NDIL0066 | MFG31 | 319 | -48 | 6 | 36 |
| NDIL0071 | SSM1 | 314 | -68 | | |
| NDIL0078 | SSM3 | 300 | -62 | | |
| NDIL0073* | SSM4 | 275 | | | -35/-1 |
| NDIL0061 | KMS12 | 332 | -73 | | |
| NDIL0031 | SSM | 275 | -73 | | |
| NDIL0076 | SSM6 | 213 | -64 | | |
| NDIL0072 | LJAW21 | 269 | -76 | | |
| NDIL0062 | KMS11 | 245 | -51 | | |

[a] Indicates that IL has multiple melting point.
* Indicates that IL has no DSC scan.

A detailed decomposition study of NDIL0046 was done, measuring the decomposition kinetics at five different temperatures.  The data were fit with zeroth order kinetics to obtain Arrhenius constants.  The data in both nitrogen (similar to the stripper conditions) and in air (more similar to the absorber conditions) are shown in Table 29.  Clearly, decomposition is significantly less in the inert atmosphere. This information will be used by Trimeric to estimate IL losses during use and the amount of makeup solvent that will be required for operation.

Table 29: Decomposition kinetics of NDIL0046.

| IL | Environment | Weight loss (%) at different temp for 16hr | | | | | Activation energy (kJ/mol) |
|---|---|---|---|---|---|---|---|
| | | 100 ℃ | 120 ℃ | 140 ℃ | 160 ℃ | 180 ℃ | |
| NDIL0046 | Air | 0.67 | 1.62 | 5.03 | 14.98 | 36.12 | 71.67 |
| | N2 | 0.86 | 1.57 | 2.57 | 3.74 | 5.12 | 31.44 |

Given the importance of IL viscosity on performance characteristics, a good deal of effort was expended to measure the viscosity of the neat and reacted ILs. The AHA ILs show very little increase in viscosity, even when reacted with $CO_2$ at 1 atmosphere of pressure. Specifically, the presence of carbon dioxide at room temperature raised the viscosity of NDIL0049 by only 33% and of NDIL0051 by only 50%.  These data are shown in Figures 76 and 77.  Despite having a larger capacity for $CO_2$ and larger percent increase than NDIL0049, the pure and $CO_2$-saturated viscosity of NDIL0051 were significantly lower than that for NDIL0049.  The viscosity of $CO_2$ saturated NDIL0051 was below 100 cP at and above 50°C.  NDIL0046 is the only previously reported NDIL to have a lower $CO_2$-saturated viscosity.
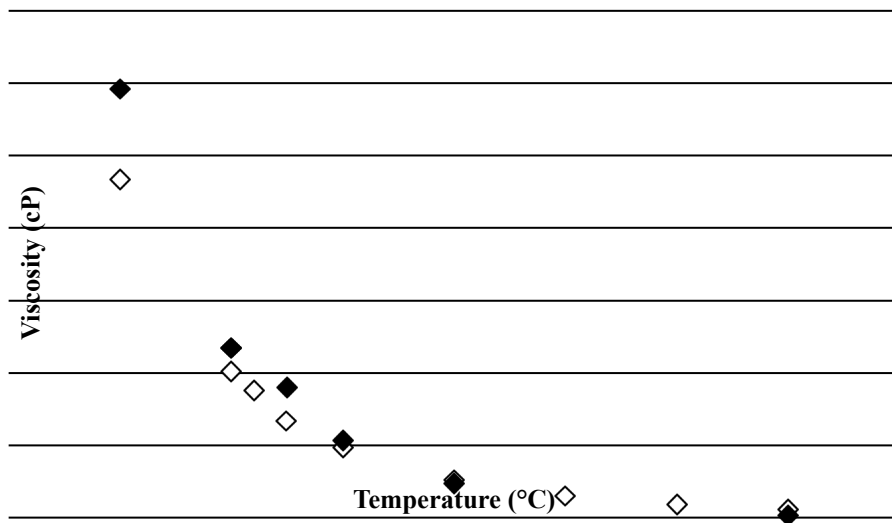
**Figure 76:** **Effect of carbon dioxide on the viscosity of NDIL0049. The empty diamonds represent the viscosity of the pure IL under one atmosphere of nitrogen. The black diamonds represent the viscosity of the saturated IL under one atmosphere of carbon dioxide.**
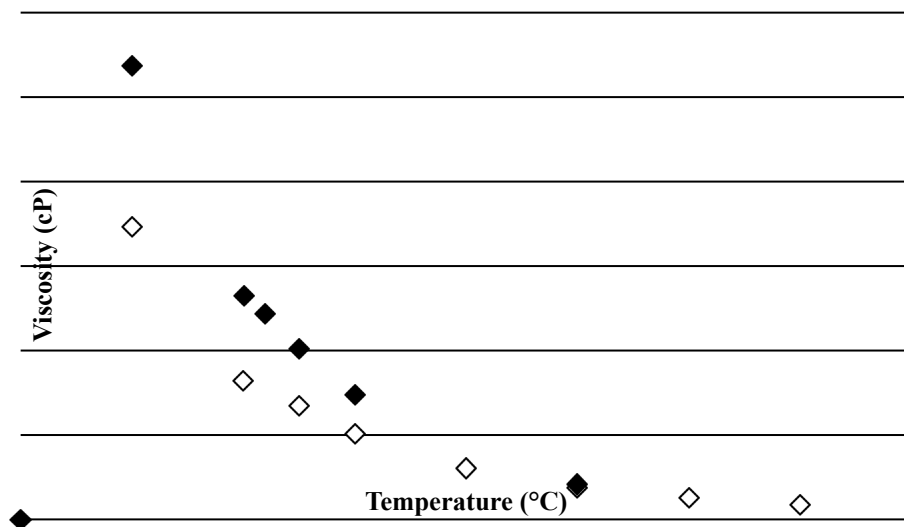


**Figure 77:** **Effect of carbon dioxide on the viscosity of NDIL0051. The empty diamonds represent the viscosity of the pure IL under one atmosphere of nitrogen. The black diamonds represent the viscosity of the saturated IL under one atmosphere of carbon dioxide.**

Figure 78 shows viscosity versus temperature data for NDIL0058 and NDIL0059. As can be seen, the phenomenon of not increasing viscosity with reaction with $CO_2$ is general and exhibited by more than one AHA IL. This is a significant breakthrough.
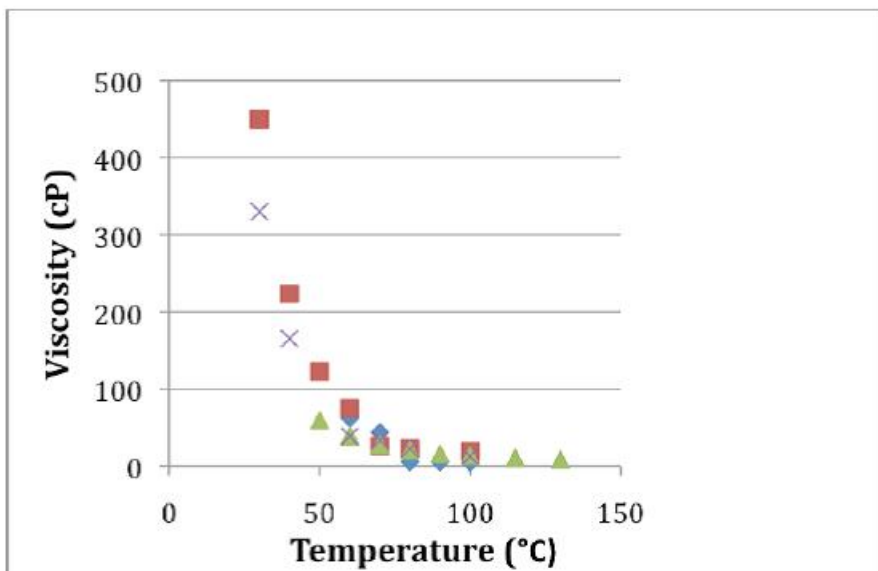
**Figure 78: Effect of carbon dioxide on the viscosity of NDIL0058 and NDIL0059. The blue diamonds and green triangles represent the viscosity of the pure ILs under one atmosphere of nitrogen. The red squares and crosses represent the viscosity of the saturated ILs under one atmosphere of carbon dioxide.**

Once again, there was interest in accumulating as much information about NDIL0046 as possible so that good data to Trimeric could be provided. In support of this, numerous measurements for different samples of NDIL0046, with and without $CO_2$ complexation and with varying amounts of water were made. The data are given in Figure 79. As can be seen, the primary effect on the viscosity is not $CO_2$, but the amount of water dissolved in the sample.
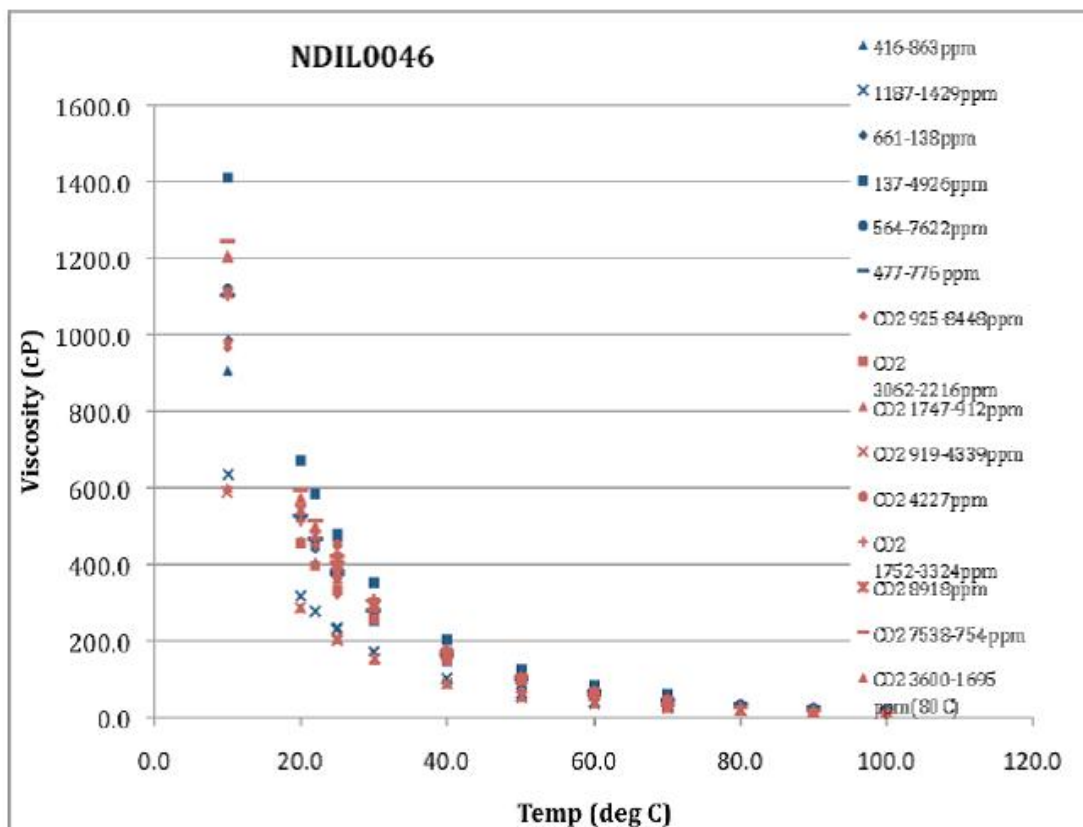
**Figure 79: Effect of carbon dioxide on the viscosity of NDIL0046. There is no discernible difference in the viscosity before and after complexation with CO₂. The primary difference in the measurements is the amount of water present in the sample, which ranges from a low of 137 ppm to a high of almost 9000 ppm. Dissolved water reduces the viscosity of the IL or IL/CO₂ mixture.**

The viscosities of NDIL0065, 0072, and 0076 were also measured, with the data shown in Figure 80. NDIL0076 was the least viscous of the three ILs and NDIL0065 and 0072 had about the same viscosity. NDIL0076 and NDIL0065 were selected for $CO_2$ absorption and the effect of $CO_2$ on the viscosity is shown in the Figure 81. NDIL0065 showed a 30% increase in viscosity at room temperature, and the viscosity of NDIL0076 doubled at room temperature. Despite having an extremely high $CO_2$ capacity, $CO_2$-saturated NDIL0076 had a very low viscosity at higher temperatures. Not only does it have a lower $CO_2$ saturated viscosity than NDIL0065, but it has the lowest $CO_2$ saturated viscosity of all the NDILs measured thus far in this project, with a viscosity below 100 cP at 40 °C.
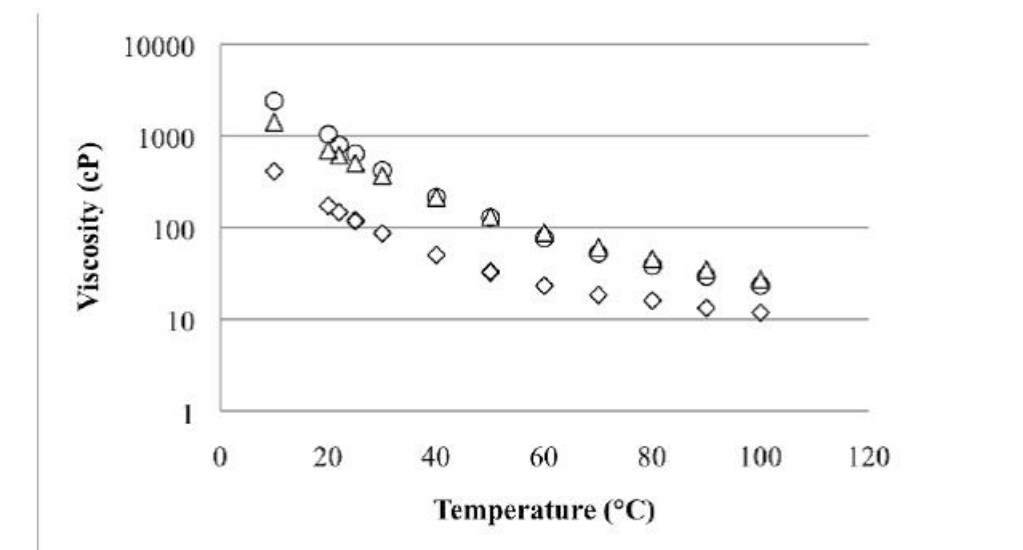
**Figure 80: Viscosity of neat NDIL0065 (circles), NDIL0072 (triangles), and NDIL0076 (diamonds).**
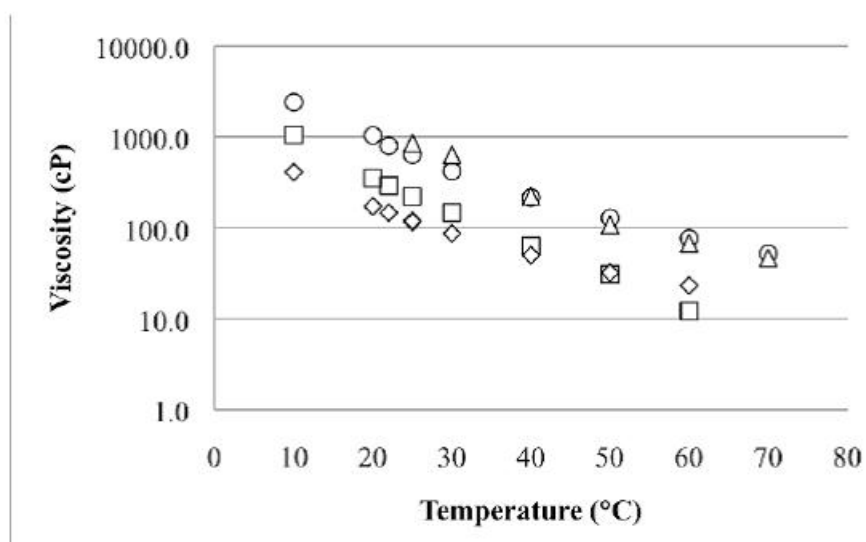


**Figure 81: Viscosity of NDIL0065, neat (circles) and $CO_2$ saturated (triangles), and NDIL0076, neat (diamonds) and $CO_2$ saturated (squares).**

An attempt was made to measure mass transfer coefficients, necessary for reaction rate analysis in the React-IR apparatus, using $N_2O$ as a non-reactive analogue to $CO_2$. Unfortunately, mass transfer correlations using the $N_2O$ analogy in a variety of ILs with widely varying viscosities did not yield a meaningful trend, as shown in Figure 82. The $CO_2$-$N_2O$ trends (not shown here) were consistent for the two low viscosity ILs,

126

NDIL001 and NDIL006. However, results with higher viscosity ILs did not give reasonable trends. For instance, $N_2O$ mass transfer in the highest viscosity IL (3543 cP) was greater than in the IL with a viscosity of 401 cP. The ILs used with their corresponding viscosities at experimental temperatures are summarized in Table 30. This clearly shows the necessity of including more parameters, which are not available, in the mass transfer correlation. Therefore, reaction conditions were modified to ensure that mass transfer limitations are not an issue.
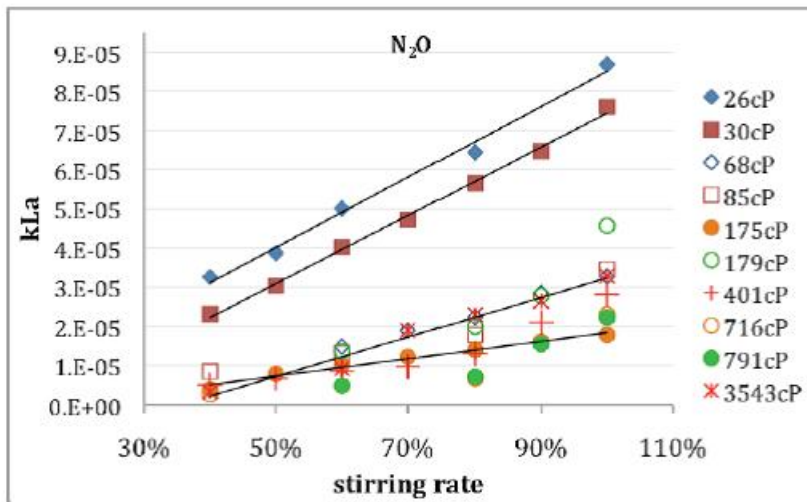


**Figure 82: Mass transfer coefficients of $N_2O$ obtained for ILs listed in Table 30.**

Table 30: The ILs analyzed for $CO_2$-$N_2O$ analogy for mass transfer correlations in React-IR system.

|  | Viscosity (cP) | |
|---|---|---|
|  | 25 $^0$C | 50 $^0$C |
| NDIL001 | 68 | 26 |
| NDIL006 | 85 | 30 |
| EMD0005 | 716 | 175 |
| EMD0006 | 791 | 179 |
| NDIL0039 | 3543 | |

The easiest way to eliminate mass transfer problems is to dilute the IL. $CO_2$ absorption experiments were performed with NDIL0057 and NDIL0058, diluted with tetraglyme, in the React-IR vessel at different stirring rates and liquid heights to see the effect of mass transfer. The gas space was charged with an initial pressure of 1.3 bar $CO_2$ at 25°C. Diluting the ILs with tetraglyme improved the mass transfer rates compared to pure ILs; however, it is still a function of stirring rate and liquid height, as seen in Figure 83.
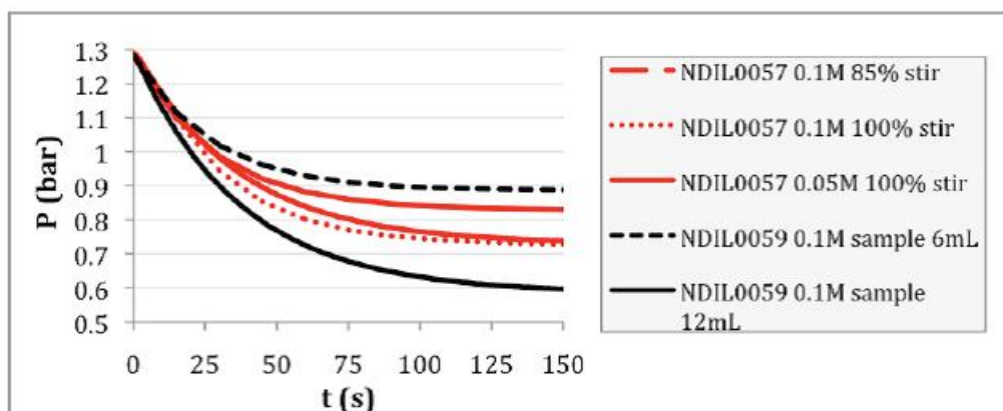


**Figure 83: CO$_2$ pressure trend at 25°C in the React-IR vessel for NDIL0057 and NDIL0058 diluted with tetraglyme.**

In order to enhance the absorption even further, in efforts to make it independent of stirring rate, a series of experiments were performed at 6 bar of initial $CO_2$ pressure with NDIL0058 samples at concentrations of 0.05, 0.1, 0.2 and 0.34 M (Fig. 84). The gas-liquid contact area was increased by using a new gas entrainment impeller (GEI) that rotates at 1000 rpm.
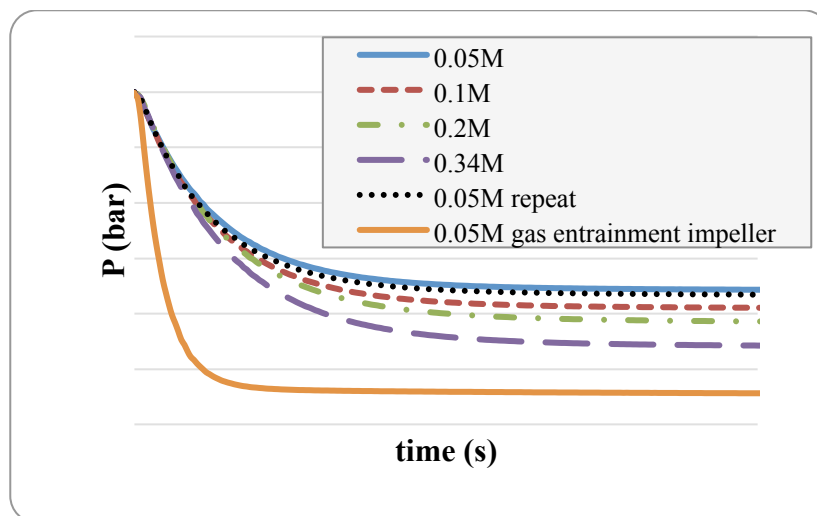
**Figure 84: CO$_2$ pressure trend in the React-IR vessel for NDIL0058 diluted with tetraglyme. The data was collected at 25 $^{o}$C.**

A linear trend was observed in total CO$_2$ uptake with increasing IL concentration that validates the consistency of the experiments. According to Figure 84, the first 15 s of the pressure trend is the same for all IL samples, except the GEI case. Based on the analysis of this region, mass transfer coefficients were estimated, and enhancement factors greater than 3 and 10, in the case of GEI, were obtained. The enhancement factor is the ratio of the amount of gas absorbed in the reactive liquid to the amount which would be absorbed if there were no reaction.

Benchmark reaction rate measurements were made using MEA solutions, which have known kinetic rates. The experimental setup was modified to carry out experiments at constant pressure while the pressure drop is measured in a gas supply vessel. Optimal mixing conditions and the gas-liquid surface area were determined by testing the unit with MEA solutions, with known reaction kinetic parameters, at different stirring rates, CO$_2$ pressures and concentrations. Accordingly, the experimental conditions were determined for diluted IL systems where the direct use of overall CO$_2$ absorption rate could be used to calculate the rate constant of the second order reaction between IL and CO$_2$.

A 0.09 M aqueous solution of EMD0005 was reacted with $CO_2$ at 22 °C and at a constant $CO_2$ pressure of 13 mbar. The second order reaction rate constant for EMD0005 was calculated to be 60,500 l/mol.s (with +/-65% uncertainty), compared to 5,400 l/mol.s for MEA(aq) at 22 °C. The contribution from the water reaction with $CO_2$ was neglected in the calculations. This suggests that the intrinsic reaction of $CO_2$ with this IL is quite fast, as was predicted from earlier quantum calculations. Given the viscosities, the rate of $CO_2$ uptake should be mass transfer limited and not reaction limited.

### 4.7 Systems and Economic Analyses Update

Properties of NDIL0046 necessary for the systems analysis were provided to Trimeric. Trimeric focused on completing its analysis by early in BP IV.

### 4.8 Project Management and Reporting.

The team maintained regular conference calls during this BP. Profs. Maginn and McCready attended the CCS conference in May and presented a paper on the project. They also visited B&W's facilities and worked with researchers there on the design of the lab-scale test unit. Air Products dropped out of the project due to cutbacks at its R&D center.

## 5. Budget Period IV: 8/1/10-9/30/12

Budget Period IV consists of four major tasks and several sub-tasks. The major task are: 1) Construct, start up and run lab-scale test system; 2) perform a final economic, engineering and systems analysis; 3) project management and reporting. An extension to this budget period was granted, and additional IL development and testing was added to the task list as item 4.

### 5.1 Lab-Scale Test System

The design and construction of the lab-scale test system at Notre Dame was completed, using the system at B&W as a guide. As mentioned in Section 4, the Notre Dame had more manual controls than the B&W system to minimize cost. Figure 85 shows a picture

of the rig. The Notre Dame lab scale unit was completely enclosed in a walk-in hood. It consists of an absorption column and a stripping column, each 8 cm in diameter and made of glass. Each column was made into three sections of length 1 m, 0.66 m and 0.33 m so different lengths of columns could be run for different experiments. Generally, the full 2m length was used for both columns. A custom packing was made of aluminum strips 4 mm wide and 5-6 cm long, rolled into strips, as can be seen in in Fig. 85. The column was run with counter current flow of the gas and liquid. The gas was injected at the bottom through the side leg of a T. The liquid was be pumped onto a distributor plate, which is a 1 cm metal circle with holes drilled in it sitting on top of the packing.

A test plan was also finalized that described all the experiments to be run on the system. The lab-scale test system was initially housed in Fitzpatrick Hall, but was then moved to a walk-in hood in Stinson-Remick Hall. Typical operating conditions are: inlet gas flows of 1.8 liters/s with a composition of 15% $CO_2$, 2% $H_2O$, and 83% $N_2$ and liquid flow rates of 5 ml/s.



**Figure 85: Photograph of the original lab-scale test system constructed at Notre Dame.**

Based on the test plan, a series of tests were run to break in the lab-scale unit. These included runs with glycerin and water, with varying mixtures having a range of viscosities. NaOH / water and MEA / water mixtures were also run prior to testing ILs.

Figure 86 shows an example of a fluid dynamics experiment with glycerin and water which enabled a determination of the pressure drop as a function of gas and liquid flowrates. A special aluminum packing was created for the column to minimize pressure drop.

It should be noted that loading occurred for more viscous (~200 cP and greater) solutions in a more densely packed area of the column. The nature of the packing prevents a perfect distribution of loading. Less viscous solutions did not cause loading to occur in the column at reasonable flowrates.

Heat transfer experiments were also performed. A heating cord, and insulation wrapped around the outside of the stripping unit, was used to heat up fluid while it is inside the column. Experiments were run to confirm that the liquid being stripped of $CO_2$ could be heated to a sufficiently high temperature of 70 $^o$C inside the unit. The top and middle segments of the column have similar heating cord arrangements but are managed by two separate temperature controllers, which allow for a temperature gradient to be achieved inside the stripping unit. Below each heated section a thermocouple inside the column can measure the temperature of the liquid as it flows down. While these experiments were performed with the glycerin and water solution and not the IL, the results confirmed that the liquid could be heated to 70 $^o$C. The previous bench-top experiments showed that $CO_2$ was stripped from the IL by heating it to 70 $^o$C before entering the column.

Solutions in a range from 10% to 17% MEA in water were used to evaluate column performance. This range was selected to give similar volumetric and molar flowrates to those of the IL at the designed conditions. The simulated flue gas entered the column with a 1.8 liters per second flowrate and a $CO_2$ concentration of 14%, which also

matched the design conditions. The height of the transfer unit is defined according to the following formula.

$$HTU = \frac{2\ meters}{NTU} = \frac{2\ meters}{\int_{CO2in}^{CO2out} \frac{dy}{(1-y)\ln\left(\frac{1}{1-y}\right)}}$$

For the same molar flow rate as those specified for the IL in the design conditions, an HTU of 5.1 meters was measured. This HTU, in the column, corresponds to nearly 40% removal of $CO_2$ from the simulated flue gas stream. Because the IL has achieved significantly better uptake than MEA in previous experiments, the expected HTU for 90% removal of $CO_2$ would equal the column height of 2 meters. Consequently, the initial MEA experiments, beyond providing a baseline performance for the column, are suggesting that the IL will behave as expected.
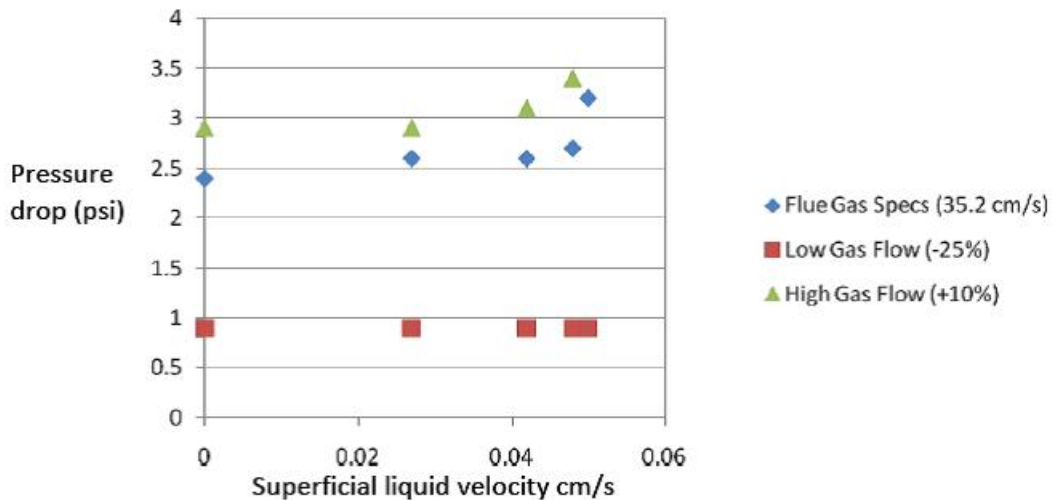


**Figure 86: Pressure drop for the lab-scale column as a function of liquid and gas velocities for a 200 cP glycerin/water mixture.**

Following these tests, solutions of water and MEA were used to characterize the packed column and provide insight into future IL absorption data. A series of experiments was completed which varied the molar flowrate MEA as well as the simulated flue gas flow

rate. At the specified gas stream conditions, the HTU values varied from 5.8 to 3.3 meters. The lowest HTU value of 3.3 meters is near the maximum absorption capability for MEA in this system. The 20 wt% solution of MEA provides a benchmark for performance comparison when using ILs in the system.

Solutions of water, sodium hydroxide, and glycerin (to enhance viscosity) were used to evaluate the physical absorption occurring within the packed column absorber. Using solutions of 1 M sodium hydroxide in 91 wt% glycerin (100-200 cP) at varying flow rates a limited amount of $CO_2$ was absorbed. At similar operating conditions the sodium hydroxide solutions gave HTU values that were 3 times greater than the corresponding MEA molar flow rates. The NaOH HTU value of 15 meters occurred while operating at a molar flowrate of .18 mols per minute. Further tests involving higher concentration sodium hydroxide solutions could cause unwanted reaction with aluminum packing so they were not conducted. This limited the maximum molar flowrate of NaOH. Figure 87 shows a comparison between the HTU values of the NaOH and MEA. Both the gas flow rates and the liquid flow rates were varied.
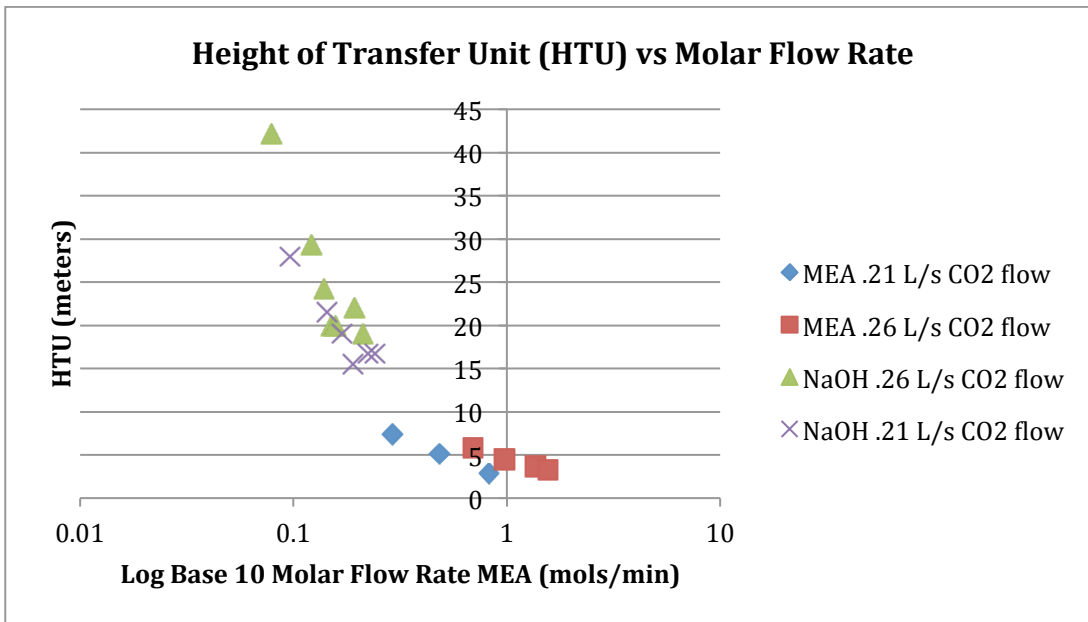


**Figure 87: A Comparison of HTU values for both MEA and NaOH over varying liquid and gas flow rates.**

A series of experiments using the EMD005 IL as the absorption solvent for $CO_2$ was conducted. These include both "open loop" where just the absorber or just the desorber is run as well as steady state, continuous experiments where the absorber and desorber were run together.

This series of experiments was intended to explore the experimental space sufficiently to determine what if any difficulties would arise with using EMD005 as the absorption solvent.

Open Loop Experiments

Given the limited amount of IL available, this set of experiments was done to determine how the absorption column would behave with EMD005 as the solvent.

The absorber was run with liquid flow rates between 1-3 ml/s and gas flow rates of 0.8 to 1.5 l/s. Up to 30% of the $CO_2$ was removed with HTU values of 6.5 to 16 m. These results are larger than expected and while not entirely infeasible, suggest that the while the EMD005 will work as a $CO_2$ absorption solvent from a chemical standpoint, the viscosity is too large for small absorption columns to function well. It could be possible to build a commercial scale absorber with a viscosity this large, but it will certainly be desirable to have a lower viscosity IL as the working solvent. Thus the initial hypothesis that this particular IL will have some performance problems due to its viscosity has been confirmed.

Steady State Experiments

In these experiments, the liquid flow rate was varied between 1 and 2.5 ml/s and the gas flow rate to the absorber varied between .3 and 1 l/s. Temperatures in the stripper varied from 120 to 180C. Under these conditions, the system could be operated continuously with reasonably steady conditions. Figure 88 shows the concentration versus time for the exit of the absorber and stripper for a run lasting ten hours. These data, and other runs, show that an IL solvent can be recycled continuously for $CO_2$ removal. A check of

the mass balance indicates that the amount of $CO_2$ being absorbed matches the amount being removed within 5-10%. This value is about the expected accuracy of the experiment given the need to control gas and liquid flow rates in two devices and measure the concentrations in both the stripper and absorber.

These initial experiments were successful in proving that continuous closed-loop operation of the system could be achieved. However, when operated this way, the measured values of HTU and NTU for both the absorber and desorber were not accurate enough to use for a design correlation.

Careful examination of the experimental system and data revealed two possible problems. First is that the high viscosity of the liquid was causing some accumulation in the absorption column, particularly at lower flow rates. (Even slight accumulation could affect the HTU values.) Hence, the apparent HTU was not a steady state value. A second problem was that a once-through pass of the desorber did not completely strip the $CO_2$ from the IL. Thus the measurements of absorber performance changed with flow rates, but not limited to the flow rates of the absorber.

To remedy this situation and get a preliminary design equation, a series of experiments were initiated running each column open-loop. It was verified that the IL was not fully stripped by a once--through pass. For future runs, it will be confirmed that the IL is fully-stripped by running it through the desorber column multiple times. The absorber is also monitored to make sure there is no apparent change in liquid holdup.

Experimental test conditions for new series of runs.

| Parameters | |
| --- | --- |
| Low Liquid Flow Rate | 0.9728 ml/sec |
| High Liquid Flow Rate | 1.345 ml/sec |
| Low Gas Flow Rate | 36.37 ml/sec |
| Mid Gas Flow Rate | 77.8 ml/sec |

High Gas Flow Rate                              120.9 ml/sec

Temp Setting on stripper                        120C (55C in column)

$N_2$ Fed to Stripper at                        1 PSI

$N_2$ Fed to Absorber at                        49 SLPM

These experiments produced HTU's in the low end of previous values, about 6 m.

| Low Liquid Low Gas run | yin | yout | NTU | HTU (m) |
|---|---|---|---|---|
| Run 1 | 2.34% | 1.73% | 0.3057 | 6.542 |
| Low Liquid High Gas run | yin | yout | NTU | HTU (m) |
| Run 2 | 10% | 7.27% | 0.3335 | 5.9962 |

Following this scouting work, approximately 20 runs of the absorber were completed using EMD0005.  It was found that the reliable, steady-state operating range of the column and flow system is relatively narrow.  This is gas flow rates of 35-120 ml/s (.01-.03 kg/m$^2$/s) and liquid flow rates of 1-1.5 ml/ sec (0.2-0.3 kg/m$^2$/s).  Higher liquid and gas flow rates are possible, but liquid accumulates in the column and unsteady behavior or greatly degraded performance occurs.
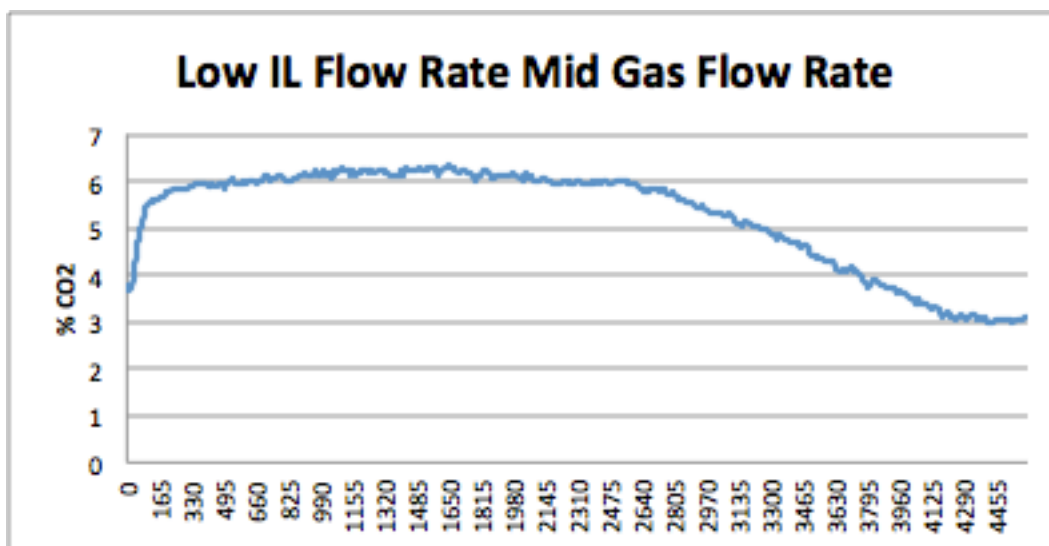
**Figure 88: CO$_2$ concentration versus time (in seconds) at good operating conditions.**

For good operating conditions, a steady CO$_2$ reading for time of ~1000 s or more was obtained, as shown in Figure 88. However, for other conditions, the concentrations will vary in a random fashion and never show a steady value.

For the smooth operation region, HTU values ranged from 3-6 m and the NTU values from 0.3 to 0.7. The best conditions were at the values of L = 1 ml/s and G = 36 ml/s where HTU was 2.8 m and the NTU was .7. At higher gas and liquid flow rates, HTU values as high as 30 m have been observed. This is probably not correct but was caused by unsteadiness in the gas flow caused by liquid accumulation in the column.

It was concluded that mass transfer rates are approximately what would be expected for any liquid of this viscosity, ~100 cP and to the degree that the viscosity could be reduced, the column would perform better.

Data from the best performance conditions are shown in Figure 89, which is the exit CO$_2$ composition, in mole %, as a function of time in seconds. The reading of close to 10% is before the liquid is turned on, and the reading just above 2 is (nominally) steady result for operation. (The spike in concentration at about 4000 seconds is a false reading – Figure 89 shows raw data). The liquid rate is 1.3 ml/s and the gas flow rate is 121ml/s. The

NTU value is 1.4, which gives an HTU 1.4 m, the lowest to have been measured up to this point. This is encouraging, and even better performance with NDIL0046 is anticipated, which has a lower viscosity than EMD0005.
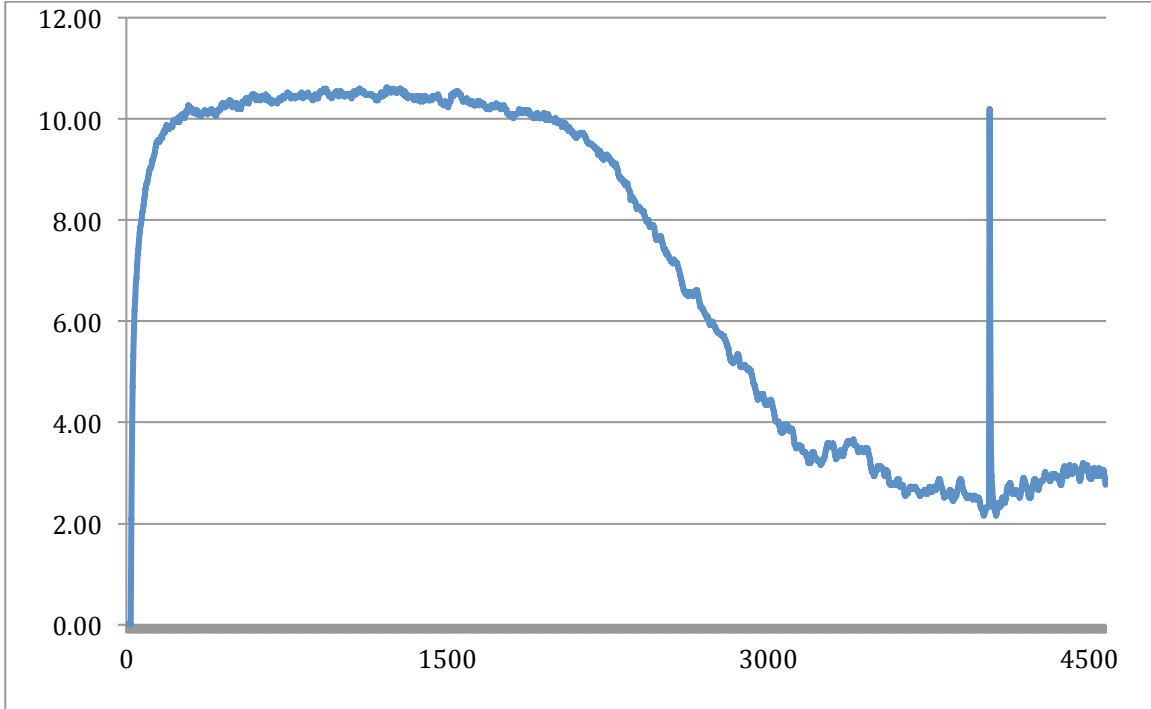


**Figure 89: Exit CO$_2$ composition from the column (mol %) as a function of time (seconds).**

Nominally steady operation at a gas flow rate of 216 ml/s was achieved, almost double the previous value that had been achieved while the liquid was at the highest value of steady operation of 1.3 ml/s.

Data from this highest gas flow rate are shown in Figure 90. The flow rates are 216 ml/s for the gas and 1.3 ml/s for the liquid. The performance degrades at this very high gas with an NTU value of .53, which gives an HTU of 3.8m. It is also seen that there is a very limited steady –state region.
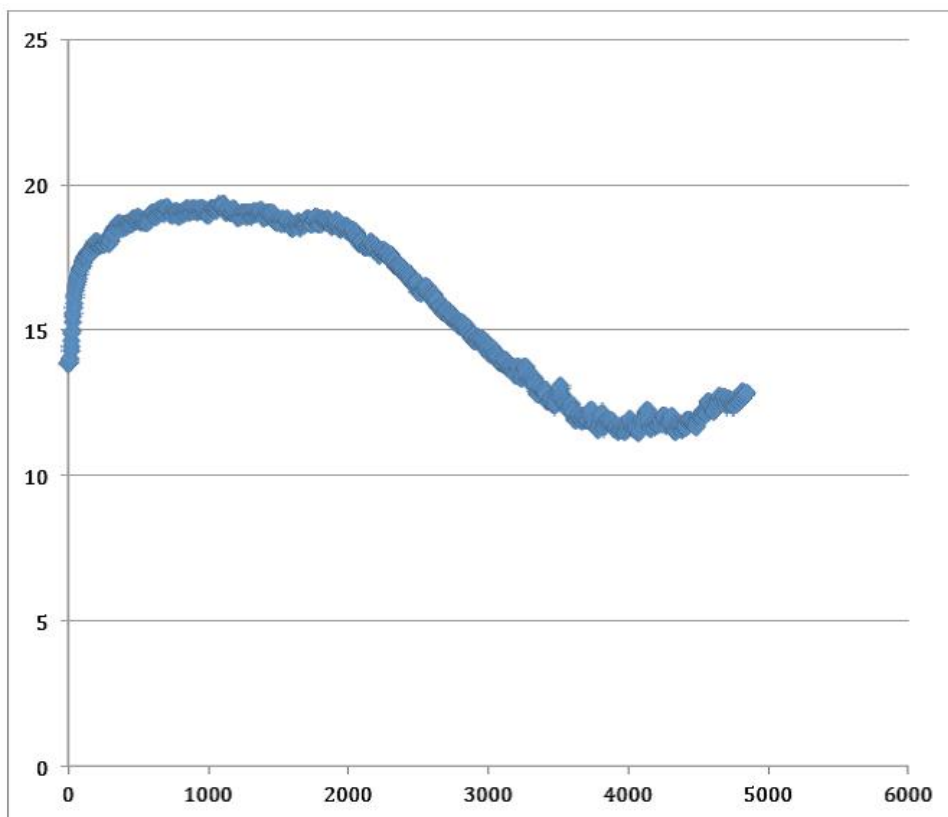
**Figure 90: Exit composition (mole fraction) versus time (seconds) at a gas flow rate of 216 ml/s and a liquid flow rate of 1.3 ml/s.**

In preparation for the lab-scale runs at B&W, the stability of a sample of plastic tubing in EMD0005 was examined. Short-term heating to $80^{\circ}C$ was performed as well as multi-week tests at room temperature. No evidence of degradation was observed, so it was concluded that this IL is compatible with their column.

During the last two quarters of BP IV, a sample was run of NDIL0046 provided to use by Koei Chemical (see below for a discussion of how this material was acquired). The viscosity was significantly higher than what had been made in the ND laboratories. This was attributed to the presence of impurities, most likely silver ions left over from the synthesis.

At room temperature, it was found that no matter what gas and liquid flow rates were tried, the IL was too viscous to distribute throughout the cross section of the column. As a result, the amount of $CO_2$ absorption was not very high. Figure 91 shows a plot of $CO_2$

140

concentration versus time for first the inlet and then the outlet of the column. The inlet $CO_2$ concentration is about 6.5%. The meter was switched to the outlet concentration at about 2800 s. Once the gas lines cleared, the exit concentration was about 5.8% and remained steady for 4000s. The HTU for this run is 12 m, which is not very good. The chemist who made the sample for Koei, Dr. Nishakawa, visited Notre Dame in July 2012, and it is now believed that the presence of impurities caused the unexpectedly high viscosity.
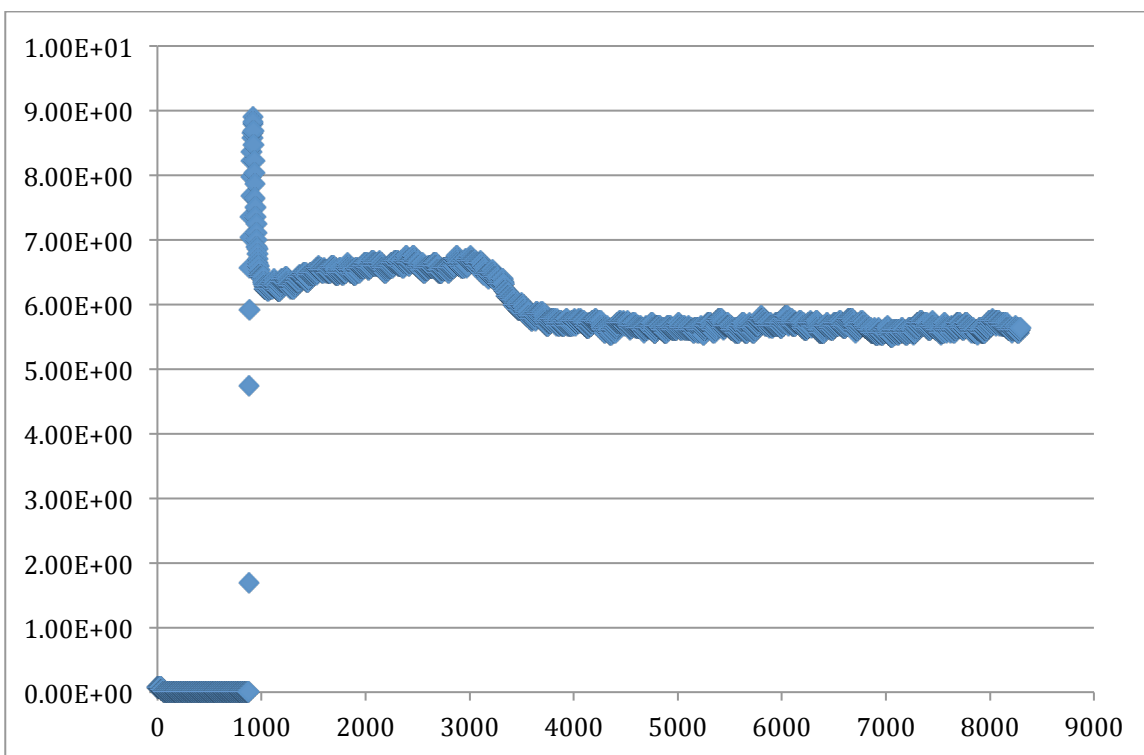


**Figure 91: Concentration of $CO_2$ (mole fraction) versus time (seconds) for lab scale system running NDIL0046**

Because of the high viscosity, it was decided to run the absorber only at temperatures above 40$^o$C. This change necessitated dismantling the system, as the heating for the column had to be re-done and the insulation attached. The heating of the storage tanks had to be increased as well to keep the liquid sufficiently warm.

Given the low mass transfer rates associated with the higher viscosity, it was decided to test whether the use of a low-viscosity diluent (the VMAS option originally suggested by

Air Products) might improve the performance characteristics. The column performance was characterized, using the HTU.

The definition of HTU was obtained from the following relation

$$Z = HTU * NTU, \quad NTU = \int_{y_{out}}^{y_{in}} \frac{dy}{(1-y)\ln\left(\dfrac{1}{1-y}\right)},$$

where Z is the height of the column packing and y is gas phase mole fraction. Figure 92 shows a plot of HTU versus molar flow rate for several different solvents evaluated in the Notre Dame column: NaOH in glycerine, 10 wt% and 20 wt% MEA solutions in water, NDIL0001 and NDIL0046 diluted with 10 wt% tetraglyme.

It can be seen that the HTU values for the MEA solutions ranged from about 3 to 8 m. Note that while these values are much higher than what would occur in a process scale column (because of the type of packing used in the lab scale unit to handle the relatively high viscosities encountered), they do provide a good baseline for comparison with other fluids.

The sodium hydroxide data are for different flow rates of a 1 M solution in glycerin (with a little water added to adjust the viscosity to 100cP and aid solubility). The performance of the NaOH solution is much worse than MEA because of the high viscosity and relatively low concentration of OH⁻ ions. However, these data show that the packing allowed column operation with liquids of 100cP.

The data for NDIL0001, a physically dissolving solvent, have higher HTU values than MEA. This is because the capacity of this IL is limited by physical absorption, and its viscosity is higher than the MEA solutions. It would be hard to justify use of this IL in large process over the conventional MEA solutions.

The last data set is NDIL0046, which reacts with $CO_2$ on 1 to 1 mole basis. As noted above, this IL has been diluted to 90% IL with tetraglyme (10wt%) so that the viscosity was about 100 cP. This was done because the sample of NDIL0046 provided by Koei

had a viscosity > 570cP at room temperature, which was too large to flow through the column and is about twice that of the NDIL0046 samples made by Notre Dame. The NDIL0046 HTU values are comparable to MEA, but at lower molar flow rates.  This occurs because, even when diluted, the 1-1 reaction stoichiometry allows a much higher $CO_2$ capacity than for MEA.  The HTU could probably be lowered further with some changes in liquid flow rate and viscosity, but time does not permit additional tests.

These last results suggest that the (calculated) energetics favoring the ND IL over MEA for $CO_2$ scrubbing could be realized in an *operable* process.  If a larger device were to be built, the packing material could be adjusted to work well for the viscosity of the chosen IL so that HTU values could be reduced further and most likely be made equivalent or better than MEA simply by increasing the liquid flow rate further (Note that the trend in all of the data is that HTU decreases with liquid flow rate).This suggests that larger scale testing with a mixture of IL and low volatility solvents are warranted.
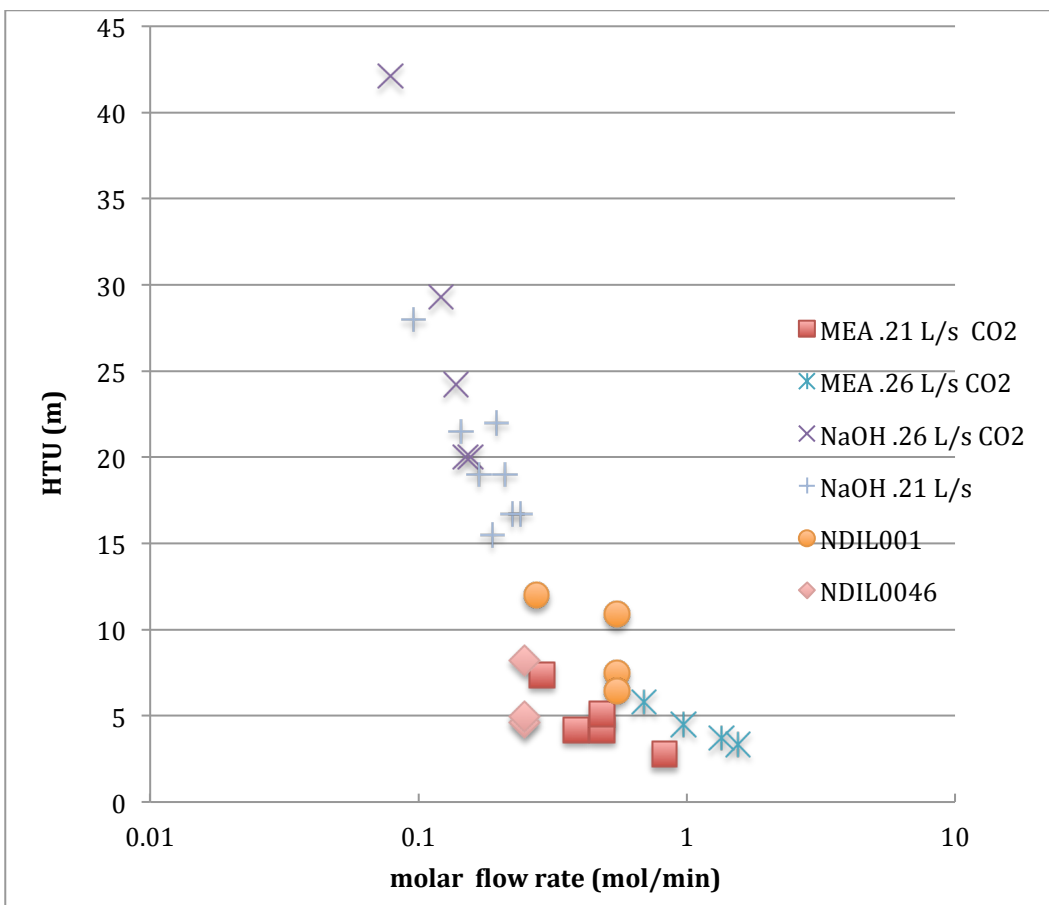
**Figure 92: Experimental HTU versus flow rate for various solvents tested at Notre Dame.**

B & W engineers visited Notre Dame laboratories in July of 2012, and plans were discussed for them to run this same IL in its absorption / stripping system as well as in a wetted wall column (WWC). Its system has a more elaborate temperature control system and can be operated at higher temperatures. A detailed report of the tests with NDIL0046 is given in Appendix II. A summary of the results is given here.

Approximately 14 liters of NDIL0046, synthesized by Koei Chemical, was provided to B&W (see Fig. 93). The IL was a dark brown color, which was caused by impurities (mainly silver).

**Figure 93: Image of totes used to send NDIL0046 to B&W.**

This particular IL was subjected to characterization tests at B&W using the WWC and RSAT Simulator in the $CO_2$ Control Lab and existing corrosion facilities to compare with previously tested solvents as well as substantiate performance claims.

B & W carried out experiments using a WWC to determine mass transfer behavior of $CO_2$ and NDIL0046 (see Fig. 94). The WWC is a differential gas-liquid reactor wherein $CO_2$ absorption or desorption can be studied under precisely controlled conditions. Capabilities include determining kinetic and thermodynamic information, which are key parameters in screening potential solvents for $CO_2$ capture. Contact times are typically on the order of 0.5 seconds, effectively simulating the hydraulics of a packed column. The main advantage is that, due to simple geometry, the area of contact between the gas and liquid is accurately known which makes calculations from first principles possible.

The column is housed in a circulating silicone oil bath, which is maintained isothermal by a temperature controller. Gravimetrically prepared solvent at some predefined $CO_2$ loading is charged to the system. The liquid is circulated using a magnetic drive gear

pump. While traditionally operated at a flow rate of 180mL/min, the high IL viscosity required a reduction of flow rate to 40 mL/min instead. As shown in Figure 95, solvent flows up through the vertical tube at the center, exits at the top, and continuously flows down over the outside surface of the tube in a thin film. The tube material of construction is stainless steel and has a diameter of 1.26 cm (0.5 inches). Solvent is counter-currently contacted with the gas, which rises through the annular space around the tube. Nitrogen and carbon dioxide are introduced to the system through separate mass flow controllers. Desired gas concentrations are achieved by adjusting the individual flow rates while maintaining the total gas flow rate at 4 slpm near atmospheric pressure. Varying the inlet $CO_2$ concentration allows testing under both absorption and desorption conditions. The exiting gas flows to an IR gas analyzer for outlet $CO_2$ measurement. A simplified system diagram is drawn in Figure 96; the entire apparatus is contained within a portion of an 8-foot fume hood.

Two $CO_2$ loading conditions at 0.1 and 0.3 mole $CO_2$/mole NDIL0046 were conducted at 40°C. In the rich $CO_2$ loading range near 5000 Pa where absorption rate is best compared, the liquid film mass transfer coefficient ($k_g$') can be evaluated against 30wt% MEA as a baseline comparison. The results were:  NDIL0046 $k_g$' = 1.4E-7 *mol/s·m²·Pa* versus MEA: $k_g$' = 3.5E-7 *mol/s·m²·Pa*.  This means that NDIL0046 had a slower mass transfer rate than MEA and indeed is slower than most of the aqueous amine-based solutions that have been tested previously by B&W. Mass transfer performance is similar to the mass transfer behavior of an unpromoted hindered amine. This is likely due to the higher viscosity of the liquid. A summary of the results for NDIL0046 plotted against a series of other solvents is provided in Figure 97.

**Figure 94: Picture of the B&W WWC apparatus.**
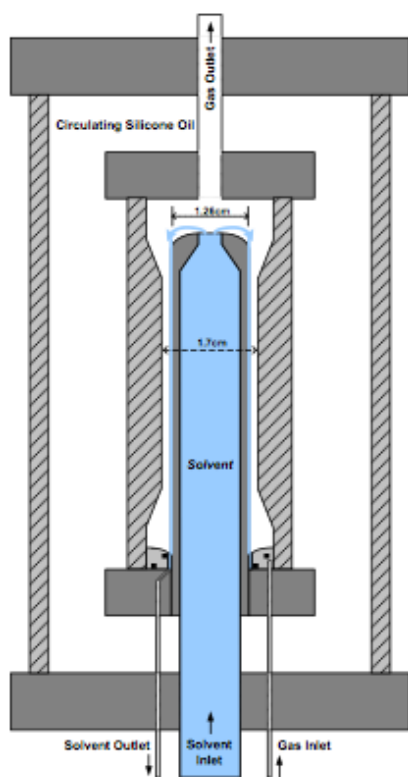


**Figure 95: Schematic of the WWC geometry.**
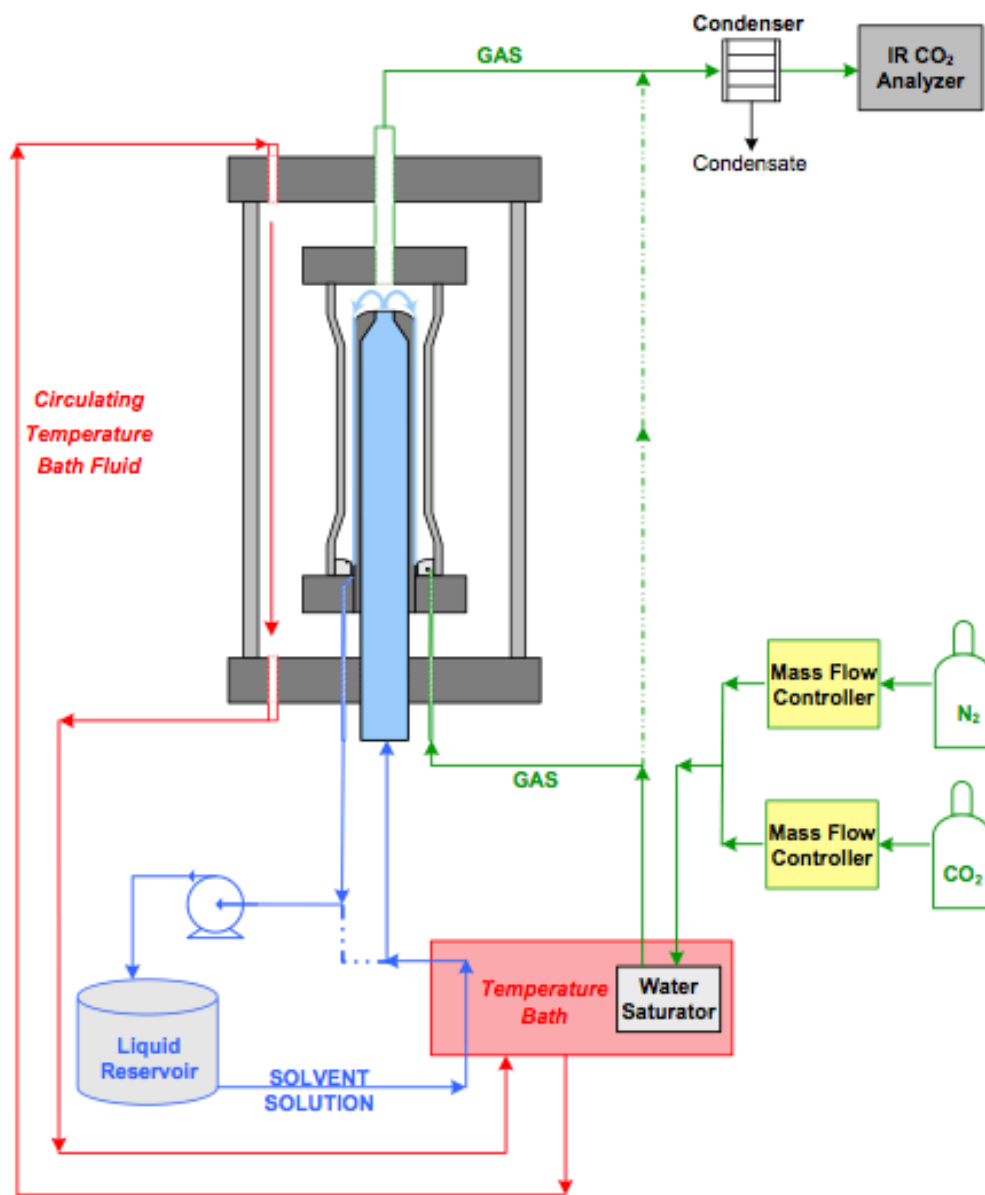
**Figure 96: Setup of the WWC experimental system.**
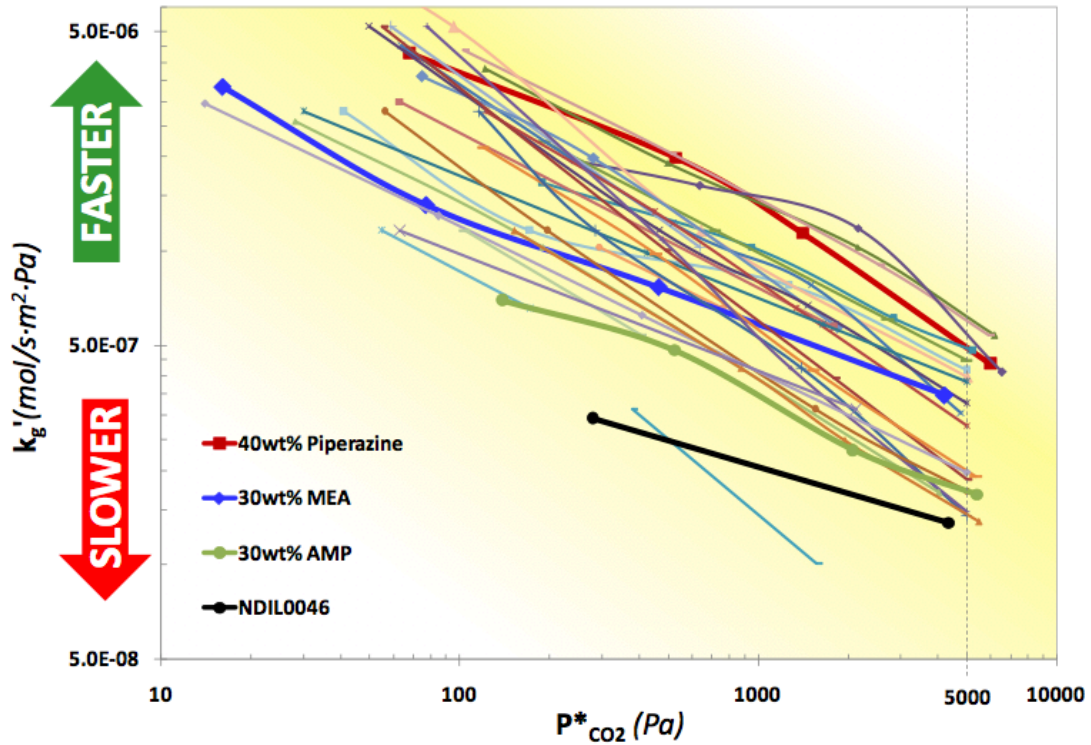
**Figure 97: WWC kinetic results for NDIL0046 compared to various other solvents.**

B & W also carried out performance testing using a simulated flue gas in a unit called RSAT™. RSAT™, a term coined by B&W, stands for their regenerable solvent absorption technology. The RSAT™ Simulator is the bench-scale absorption/stripping apparatus that was used as a model to construct a similar installation at the Notre Dame laboratory.
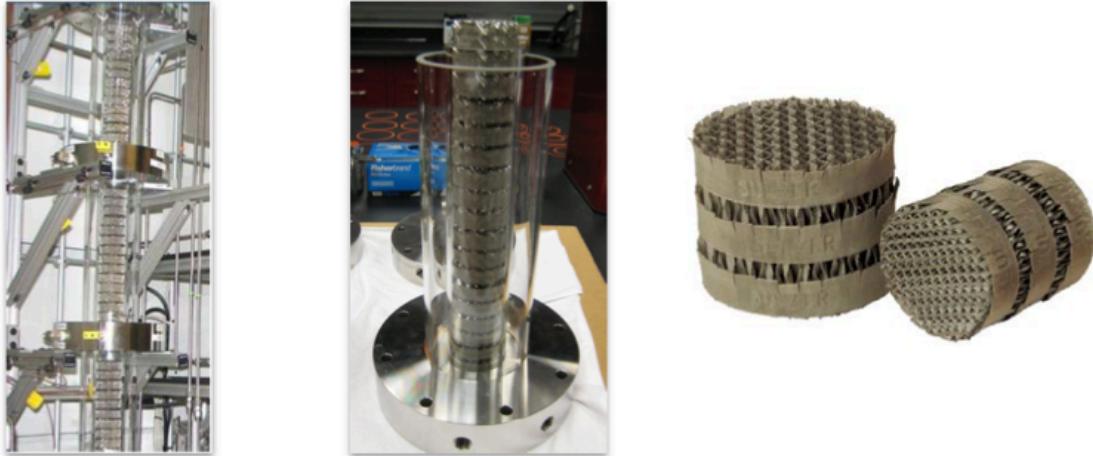
**Figure 98: Components of the RSAT apparatus. On the left are the modular columns; the middle image shows the concentric cylinders of the column and on the right is the structured packing that was used.**

The RSAT Simulator is completely contained inside an 8-foot distillation fume hood and constructed predominantly of glass and stainless steel components. The columns are a modular configuration consisting of 1-foot each glass sections joined by stainless steel flanges with penetrations, as shown in Figure 98 (left). The absorber column is 5-feet tall while the regenerator is only 4-feet in height due to the electrically powered reboiler at its base. Both columns have a 2-inch internal diameter and are embedded inside a concentric cylinder, allowing the outer glass to serve as a heating and/or insulation jacket as photographed in Figure 98 (middle). A customized DYM laboratory 316L structured packing made of sheet metal from Sulzer Chemtech, in Figure 98 (right), is especially designed for small laboratory applications and is installed for maximum gas-liquid contact efficiency. The system is designed to capture approximately 1 kilogram of $CO_2$ per hour. Note that this packing is best suited for lower viscosity fluids like liquid aqueous amines, and is not necessarily the type of packing that would be used for the higher viscosity IL fluids. A picture of the full system is shown in Figure 99.

**Figure 99: Picture of the installed RSAT simulator used at B&W.**

The unit proved challenging to operate in an integrated fashion with the installed equipment mainly due to high viscosity, which was not accounted for in the original design. Consequently, the system was decoupled, and the absorber column operated separately as a once-through batch process. Test conditions for liquid flow rate and flue gas composition closely matched a previous 30wt% MEA baseline case that achieved a 90% $CO_2$ removal rate at steady state. Comparatively, the NDIL0046 attained a 65% $CO_2$ removal rate near 30°C with a rich $CO_2$ loading of 0.52 mole $CO_2$/moleNDIL0046. Despite falling short of the targeted 90% $CO_2$ removal rate, the outcome was consistent with the mass transfer data obtained in the WWC and in Notre Dame's lab-scale unit, where it was found that the HTU of undiluted NDIL0046 is greater than that of aqueous MEA solutions. Again, this is thought to be due to the higher viscosity of the IL as compared to aqueous amines. Figure 100 shows a representative sample of the performance of NDIL0046 in the RSAT system. Table 31 lists the

operating conditions used in the test.
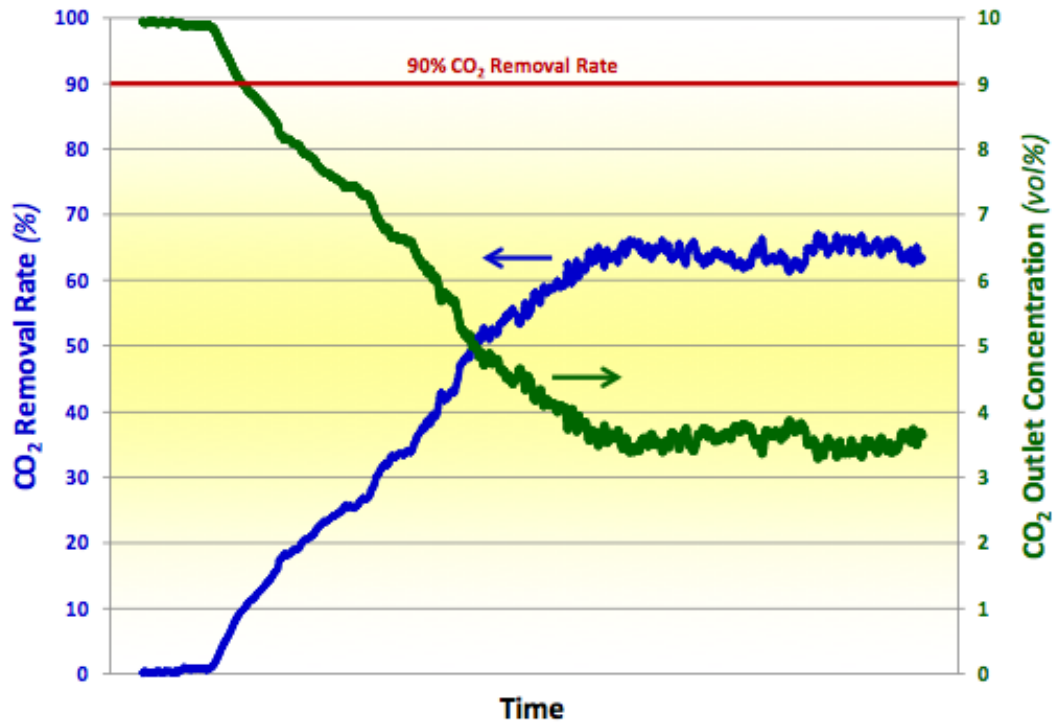


**Figure 100: NDIL0046 absorption performance in the B&W system.**

Table 31: RSAT simulator test conditions for NDIL0046 and a previous aqueous MEA run.

| | 30wt% MEA | NDIL0046 |
|---|---|---|
| | March 5, 2009 | September 11, 2012 |
| Liquid Flow Rate | 50 mL/min | 50 mL/min |
| Nitrogen Flow Rate | 6.5 slpm | 7.8 slpm |
| $CO_2$ Flow Rate | 0.75 slpm | 1.0 slpm |
| $CO_2$ Concentration | 10.3% | 11.3% |
| Gas Velocity | 0.22 ft/sec | 0.26 ft/sec |
| L/G | 5.2 | 4.4 |

Despite falling short of the 90% $CO_2$ removal rate, the outcome was consistent with the mass transfer data obtained in the WWC. Additional absorber packing height, which

translates to additional number of transfer units, would be required to achieve the desired target. The high viscosity was likely a detriment as well since the incoming streams were not maintained at 40°C due to the modified set-up. An absorber temperature profile is given in Figure 101 using the thermocouples placed along the height of the column. The incoming stream was approximately 25°C and reached a maximum of 36°C near the bottom of the column as can be seen with the exothermic temperature bulge from reaction.
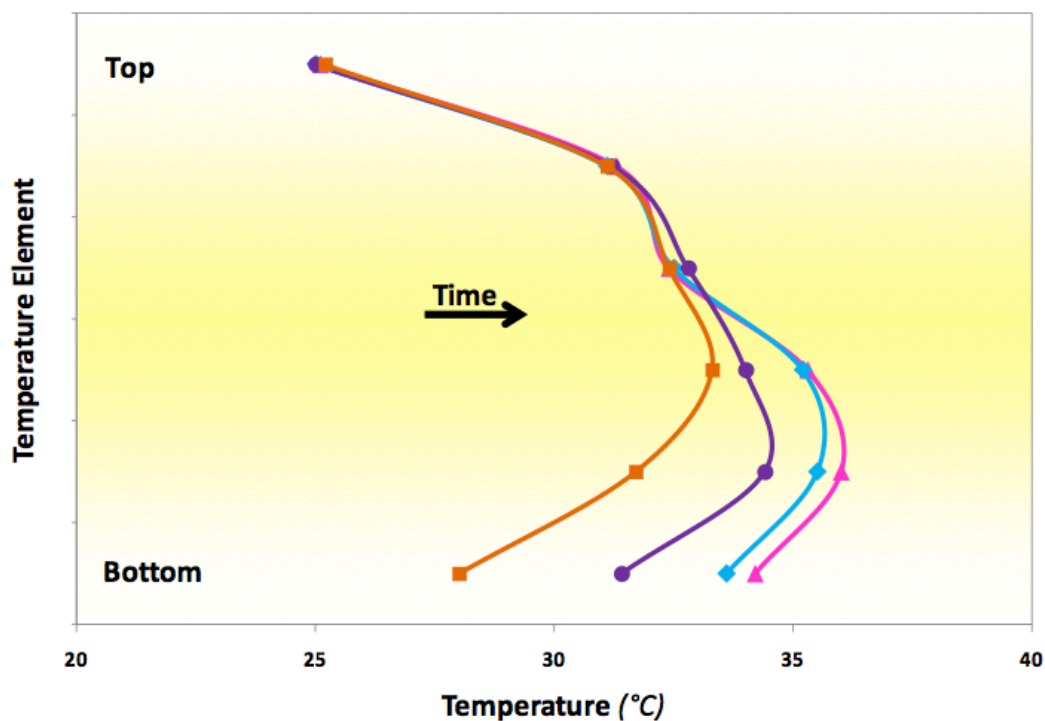


**Figure 101: NDIL0046 absorber temperature profile.**

Wet chemistry techniques using acid/base chemistry for $CO_2$ loading analysis such as is done for other solvent solutions could not be employed with the IL. Therefore, an absorber bottoms sample was collected after shut-down and sent to Notre Dame for $CO_2$ loading analysis. Results from thermal gravimetric analysis (TGA) revealed a $CO_2$ loading of 0.52 mole $CO_2$/mole NDIL0046. This result was higher than anticipated, suggesting that the system reached equilibrium within the RSAT system. B&W explained this result as arising from the long residence time within the column. They did not

attempt to compute the number of transfer units because of the proximity to equilibrium.

B&W also conducted corrosion tests on NDIL0046. Analyses consisted of linear polarization resistance (LPR) testing and potentiodynamic scans (PDs). LPR provides a corrosion rate (CR) that allows the tested materials to be compared among one another. The PDs supply general information regarding the corrosion behavior of the materials in the evaluated environments, including the probability of pitting to occur. The test plan consisted of testing 2 materials (carbon steel 1018-CS and stainless steel 304L-SS) in 2 different IL environments (neat and IL in the presence of $CO_2$) and 2 temperatures (room temperature and 150°C). No testing was conducted in the IL in the presence of $CO_2$ at 150°C since this particular IL can complex only low amounts of $CO_2$ at this temperature. Complete details of the tests are provided in Appendix III.

A summary of the average open circuit potential (OCP) values recorded before and after the LPRs along with the CRs calculated from the LPRs is displayed in Table 32 and Figure 102.

Table 32: Average OCP before and after LPRs and calculated CRs from LPRs.

| Carbon Steel 1018-CS | | | | |
|---|---|---|---|---|
| Test ID | Test Condition | $OCP_{ave}$ Before (V) | CR (mpy) | $OCP_{ave}$ After (V) |
| 1 | 25˚C, Neat | -0.262 | 0.01029 | -0.270 |
| 3 | 25˚C, $CO_2$ | -0.063 | 0.00068 | -0.072 |
| 5 | 150˚C, Neat | +0.076 | 0.09900 | +0.059 |
| Stainless Steel 304L-SS | | | | |
| Test ID | | $OCP_{ave}$ Before (V) | CR (mpy) | $OCP_{ave}$ After (V) |
| 2 | 25˚C, Neat | -0.174 | 0.00344 | -0.166 |
| 4 | 25˚C, $CO_2$ | -0.116 | 0.00136 | -0.102 |
| 6 | 150˚C, Neat | +0.030 | 0.07134 | +0.019 |
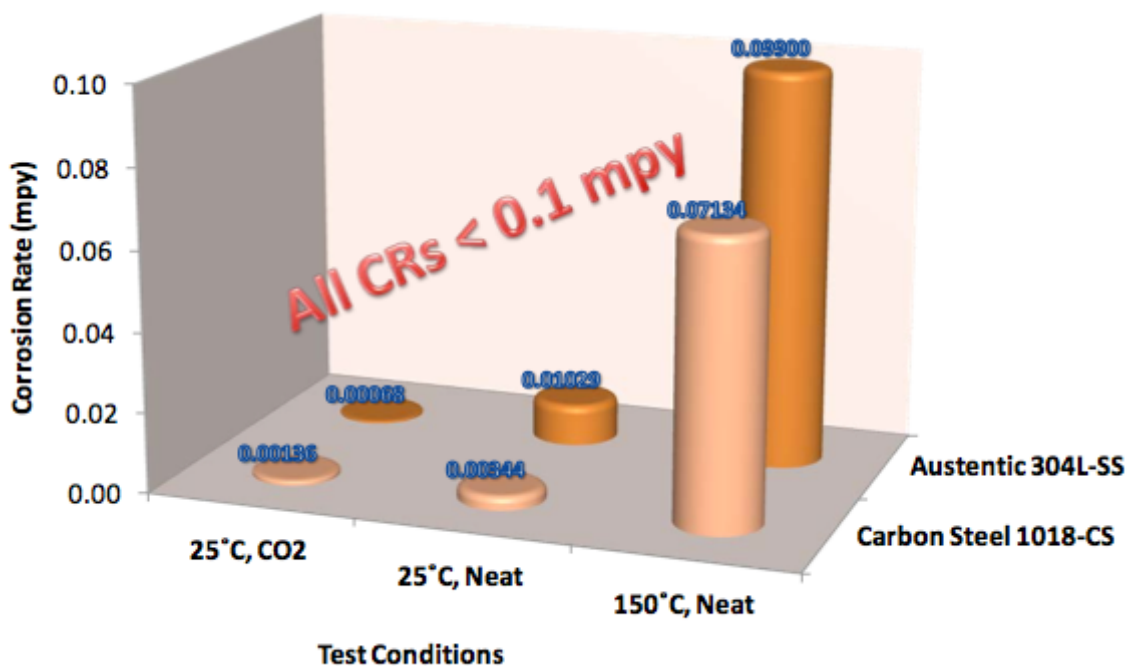
**Figure 102: Corrosion rates (CRs) measured by B&W.**

Analyses consisted of LPR testing and PDs on carbon steel 1018 and stainless steel 304L. CRs for both metals were 0.1 milli-inch per year (mpy) or less, indicating excellent corrosion behavior for NDIL0046 in each of the tested conditions. Generally speaking, CRs of 2 mpy or less are considered to be "excellent," while rates lower than 20 mpy are "good."

From Figure 102, it can be seen that tests in neat IL at $150^{\circ}$C exhibited the highest CRs; thus, this was the most aggressive condition from a corrosion standpoint. The second most aggressive condition was neat IL at room temperature. Lastly, the least aggressive condition was room temperature and IL in the presence of $CO_2$. The phenomenon of low corrosivity by ILs in the presence of $CO_2$ has been seen before in previous studies with different formulations of ILs. Overall, the corrosion behavior of carbon steel (1018-CS) was higher than stainless steel (304L-SS) in the case of the IL at room temperature and in the presence of $CO_2$. However, these values were so low that comparisons seem meaningless. It is expected that the sensitivity of the LPR technique does not permit accurate differentiation of CRs that are $< \sim 0.1$ mpy. In a practical sense, CRs of $< 0.1$

mpy can be considered essentially nil.

From a materials stand point, carbon steel and stainless steel should both exhibit excellent general corrosion resistance in all of the test conditions evaluated in the presence of NDIL0046. Based exclusively on general corrosion behavior, the test results indicate that carbon and stainless steel will perform excellent in these environments.

## 5.2 Additional IL Development and Testing

Based on process modeling by Trimeric, it was known at the start of BP IV that NDIL0046 was not the optimal IL for post-combustion $CO_2$ capture because it has a slightly too low enthalpy of reaction with $CO_2$, and therefore has a too low carrying capacity at conditions of interest. The project scope was therefore modified to allow Notre Dame researchers to continue to search for more optimal ILs as well as to make modifications to the lab-scale test unit to improve operational performance.

Synthesis

During this budget period, Notre Dame researchers synthesized five new ILs (NDIL0063, NDIL0071, NDIL0080, NDIL0088 and NDIL0094). All of these ILs were anticipated to have stronger binding energies with $CO_2$ than NDIL0046. Koei Chemical scientists were supposed to visit Notre Dame in February, 2011 to discuss efforts to synthesize new compounds that will be effective and low cost. Unfortunately, this visit was cancelled due to a serious illness of one of the scientists. Subsequently, a devastating earthquake and tsunami struck Japan and damaged some of Koei's facilities. Despite these problems, a conference call was held with the Koei Chemical scientists in March, 2011. Three anions were agreed on that would be cost effective to make and a few variations of the cation. The selected anions include one that has been incorporated in some of the ILs synthesized at Notre Dame, plus two new anions. Koei supplied Notre Dame researchers with 25 g samples of five different ILs (Koei001-Koei005). Koei001 used an anion that ND has investigated previously, but with a different cation. Both Koei002 and Koei003 employ new AHA-based anions. Koei004 and Koei005 contain an anion that ND has investigated previously, but with different cations. Unfortunately, NMR spectroscopy showed large quantities of unreacted starting materials in these last two samples.

<u>CO$_2$ Capacity</u>

CO$_2$ uptake results for NDIL0063 and NDIL0088 at room temperature are shown in
Figure 103 in comparison to NDIL0046.  As anticipated, these ILs show higher capacity
at lower CO$_2$ partial pressures, consistent with larger negative values of the heat of
reaction. With the stronger binding enthalpies with CO$_2$, special efforts have been made
to ensure that the ILs have not inadvertently picked up some CO$_2$ from the atmosphere
prior to testing.
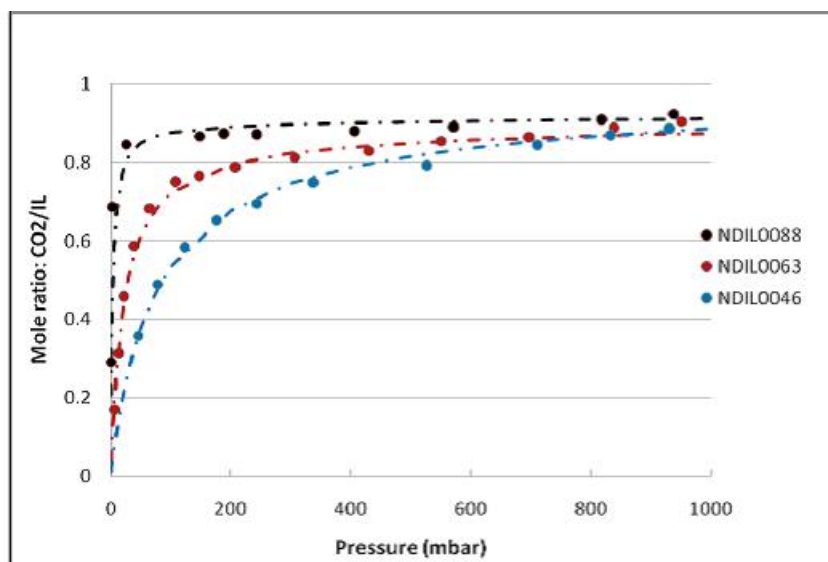


**Figure 103:  Solubility of CO$_2$ in two of the new ILs at room temperature in comparison to
NDIL0046.**

Later, CO$_2$ uptake was measured in NDIL0071 and NDIL0094. They also showed higher
binding for CO$_2$ compared to NDIL0046, as shown in Figure 104.
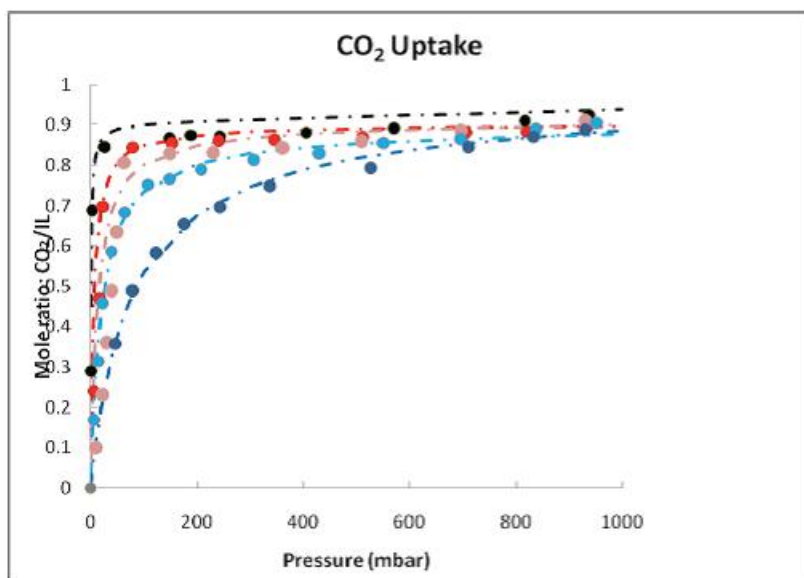
**Figure 104: CO$_2$ uptake curves for NDIL0046 (blue circles) and NDIL0088, 0071, 0094, and 0063.**

Note that all of these ILs are based in the AHA anion and all show uptakes approaching 1 mole CO$_2$ per mole IL.

CO$_2$ uptake results for Koei001, Koei002 and Koei003 at 22 ºC are shown in Figure 105. All three of these ILs show higher capacity at lower CO$_2$ partial pressures than the current baseline IL, NDIL0046, consistent with larger negative values of the heat of reaction.
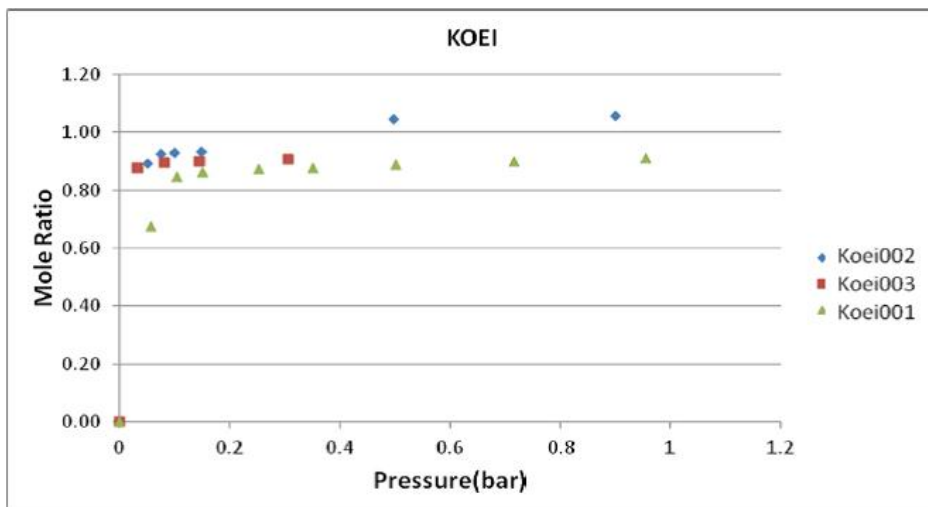
**Figure 105: Solubility of $CO_2$ in Koei001, Koei002 and Koei003 ILs at 22 $^o$C.**

Uptake results for Koei004 and Koei005 are shown in Figure 106. Note that these samples lost 20-40% of their weight during the outgas process before the mass leveled off, consistent with large quantities of neutral unreacted starting materials in the samples. The $CO_2$ uptakes for both samples level off well below the expected 1 mole of $CO_2$ per mole of IL. This is consistent with the samples containing nonvolatile impurities. Koei had difficulties synthesizing these compounds, and this is reflected in the less-than-perfect results obtained.
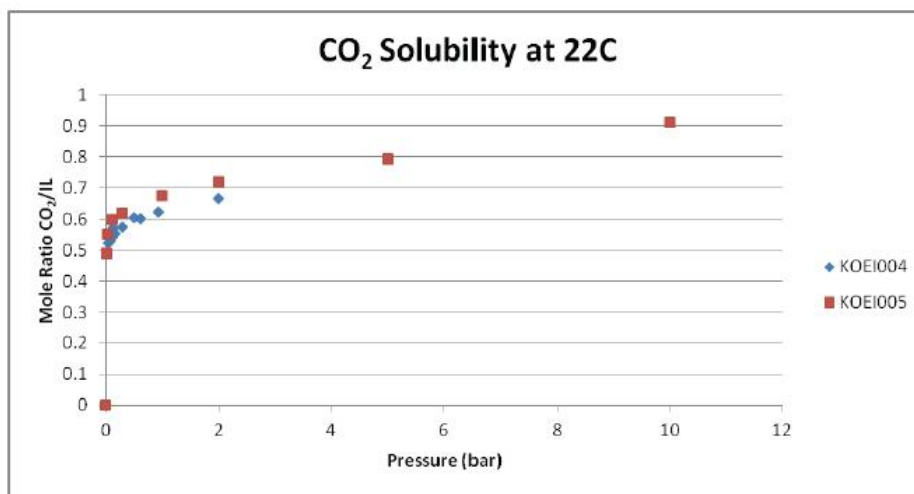


**Figure 106: Solubility of $CO_2$ in Koei004 and Koei005 at 22 $^o$C.**

159

Of interest also was seeing how these ILs took up $CO_2$ in the presence of water. The results are shown in Figure 107. The anion of this IL does not reprotonate in the presence of water or in the presence of a mixture of water and $CO_2$, as discussed above. Interestingly, the $CO_2$ capacity is higher when the water is present, especially at lower partial pressures of $CO_2$. It was hypothesized that the physical dissolution of water in the IL changes the activity coefficients of the IL and the IL-$CO_2$ complex, resulting in higher $CO_2$ uptake for a given temperature (and equilibrium constant).
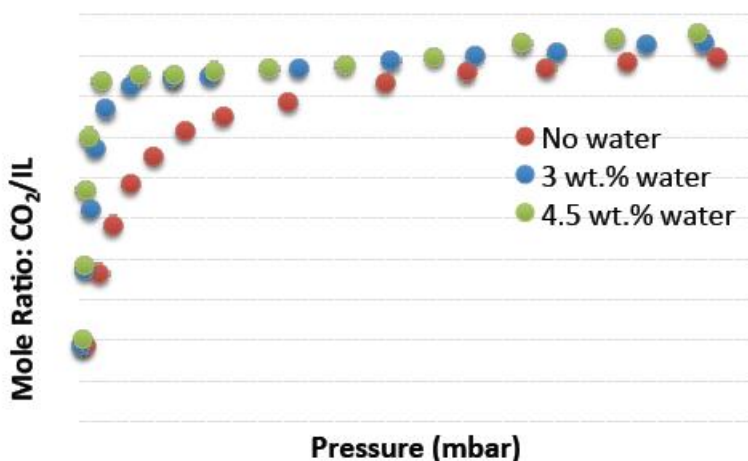


**Figure 107: $CO_2$ capacity of NDIL0046 with and without water.**

The $CO_2$ capacity of the NDIL0046 sample provided by Koei and used in the ND lab scale tests as well as in B&W's tests was measu. It was found that the $CO_2$ uptake was similar to that measured on the Notre Dame sample, and therefore the presence of large amounts of silver impurities had no impact on $CO_2$ uptake.

Viscosity

Viscosities of NDIL0088, 0071, 0094, and 0063 as a function of temperature have been completed for samples prior to exposure to $CO_2$ and after exposure to 1 bar $CO_2$ at room temperature. Viscosity increase is negligible for NDIL0071, 0094, and 0063; however, NDIL0088 increased in viscosity by about a factor of five. The viscosities of Koei001, Koei002 and Koei003 are shown in Figure 108. Overall, the viscosities of the Koei ILs are rather high, and this was attributed to the choice of cation. Detailed viscosity

measurements were not carried out on Koei004 and Koei005 because of their high impurity content.
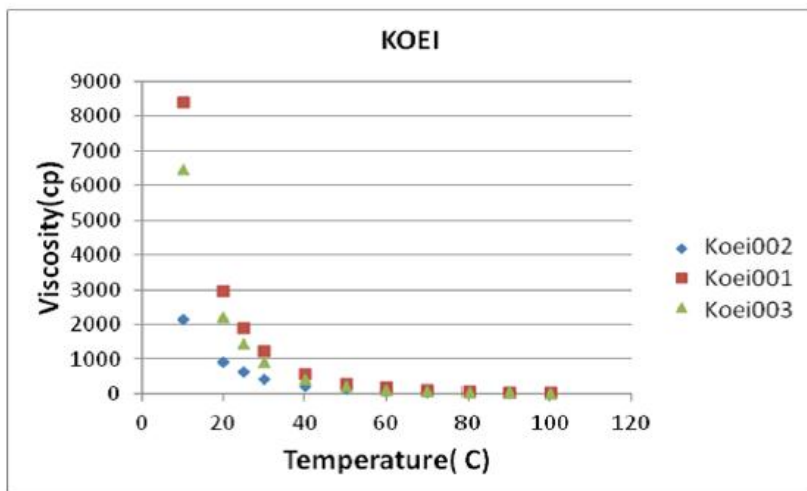


**Figure 108: Viscosity as a function of temperature of the three ILs from Koei Chemical.**

The influence of water on the viscosity of NDIL0046 was investigated. In Figure 109, the viscosity of the pure IL is shown as a function of temperature as the open squares. As shown in previous reports, the viscosity remains essentially unchanged when the IL complexes with $CO_2$. When water is added to the IL (no $CO_2$), the viscosity decreases. However, when water is present and the IL is exposed to and complexed with $CO_2$ at 1 bar $CO_2$ pressure, the viscosity actually increases somewhat, as shown by the triangles in Figure 109.
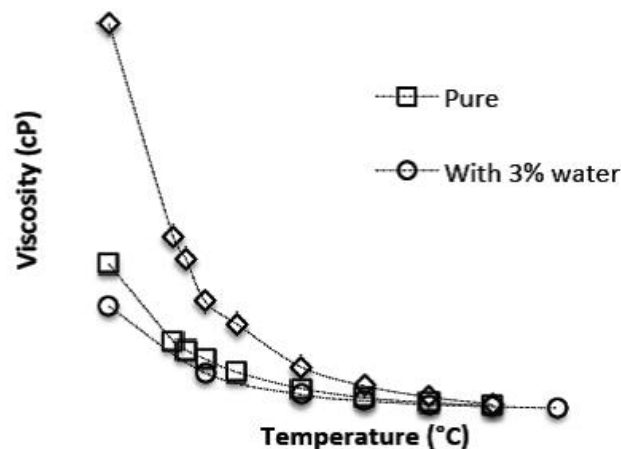
**Figure 109: Viscosity of NDIL0046 in the presence of $CO_2$ and water at room temperature.**

To further investigate this phenomenon, the effect of various concentrations of water on the viscosity of $CO_2$-complexed NDIL0046 and three other ILs was also examined. The results for NDIL0046 at room temperature are shown in Figure 110. The viscosity goes through a maximum around 0.75 moles of water/mole of IL. This is true for all of the ILs investigated thus far. It is hypothesized that the water provides hydrogen-bonding bridges between the $CO_2$-complexed anions of the ILs. Steric effects likely account for the maximum being somewhat below 1 mole of water/mole of IL.

Thermal Decomposition
Thermal decomposition temperatures were measured for the newly-synthesized ILs. Results are summarized in Table 33.

Table 33: Thermal decomposition temperatures of Notre Dame ILs.

| IL | $T_{decomp}$ (°C) |
|---|---|
| NDIL0063 | 323 |
| NDIL0071 | 312 |
| NDIL0080 | 272 |
| NDIL0088 | 296 |
| NDIL0094 | 267 |
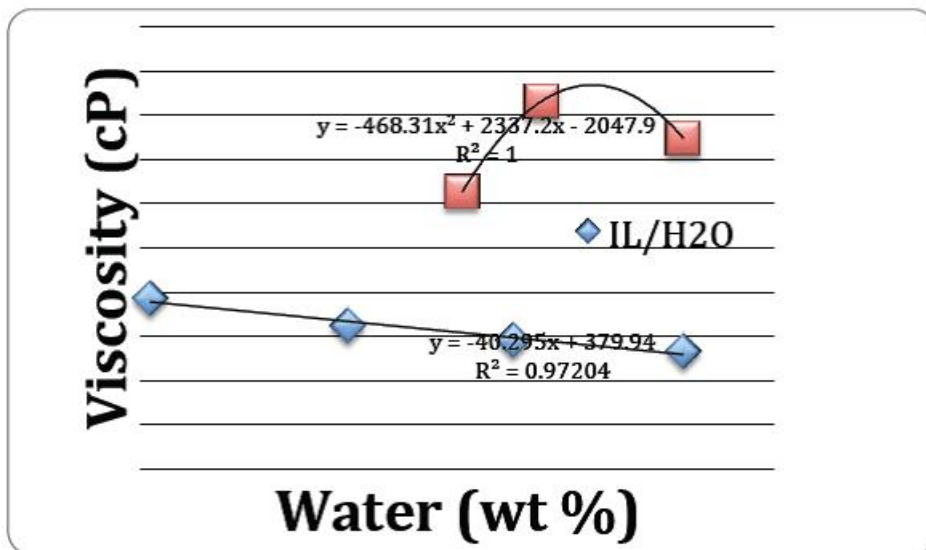
**Figure 110: Viscosity of NDIL0046 in the presence of various concentrations of water (blue diamonds) and in the presence of both water and $CO_2$ (red squares) at room temperature.**

For the Koei samples, thermal decomposition temperatures, heat capacities and glass transition temperatures are reported in Table 34. Note that because of the high impurity levels in Koei004 and Koei005, heat capacities were not measured, and it is believed that the decomposition temperatures are artificially low as a result of impurities.

Table 34: Decomposition temperatures, glass transition temperatures and heat capacities for the Koei samples.

| IL | $T_{onset}$/°C | | $T_g$/°C | $T_m$/°C | $C_p$/J·mol$^{-1}$·K$^{-1}$ | |
|---|---|---|---|---|---|---|
| | N$_2$ | Air | | | 25 °C | 50 °C |
| KOEI001 | 315 | 311 | -63 | -- | 939 | 992 |
| KOEI003 | 299 | 290 | -61 | -- | 951 | 1003 |
| KOEI002 | 308 | 297 | -73 | -- | 902 | 949 |
| KOEI004 | 262 | 219 | -81 | -47 | -- | -- |
| KOEI005 | 240 | 226 | -69 | 4 | -- | -- |

Reaction enthalpy
Reaction enthalpies with $CO_2$ were measured for these new ILs. The heat of reaction for NDIL0088, 0071, 0094 and 0063 were estimated, using the fits to the room temperature isotherms to obtain equilibrium constants. Since it is expected that the reactions with $CO_2$ will be similar for all of the AHA ILs, the entropy of reaction for NDIL0046 is then

163

used to estimate the heats of reaction for the other ILs.  They are all higher than the heat of reaction for NDIL0046 and match the values predicted computationally to within +/-10 kJ/mol.  The theoretical estimates of the heat of reaction of the three Koei samples with $CO_2$ range between -47 and -58 kJ/mole of $CO_2$, which are higher than the heat of reaction for NDIL0046 (experimentally determined as -43 kJ/mole of $CO_2$).  The steep $CO_2$ uptake isotherms for the Koei samples confirm strong binding with $CO_2$. The theoretical estimates of the heat of reaction of the last two Koei samples with $CO_2$ are expected to be about -70 kJ/mole of $CO_2$, which is higher than the heat of reaction for NDIL0046 (experimentally determined as -43 kJ/mole of $CO_2$).  The steep $CO_2$ uptake isotherms for the Koei samples confirm strong binding with $CO_2$.

Other Physical Properties

While investigating the behavior of these ILs in the presence of water, some indications were found that when $CO_2$ is also present, some of the ILs may reprotonate and therefore deactivate. The primary tool for these investigations is NMR spectroscopy.

For each test, about 1 g of IL was weighed into a test tube and about 1 g of millipore water was added to the vial and stirred vigorously with a stir bar for 30 minutes.  The resulting emulsion was allowed to settle at room temperature until phase splitting was observed: an aqueous layer and an "IL rich layer". For each IL, the analysis was done by $^1$H NMR of the IL rich phase in $DMSO_{d6}$ and the aqueous layer in $D_2O$.  Subsequently, $CO_2$ was bubbled at ambient temperature and pressure into the IL/$H_2O$ mixture for 30 minutes with vigorous stirring. Bubbling and stirring was ceased, the system was allowed to phase split and samples from the two layers were, once again, analyzed $^1$H NMR spectroscopy. When no phase-splitting was observed, a sample from the quasi-homogeneous mixture was recorded in both deuterated solvents. In addition, each IL (without water) was bubbled with $CO_2$ for 30 minutes and its NMR spectrum was recorded in both $D_2O$ and $DMSO_{d6}$, as control experiments.  The effect of a prolonged exposure of IL/$H_2O$ to $CO_2$ was also studied specifically for NDIL0046. In this case, $CO_2$ was bubbled at ambient temperature and pressure into the IL/$H_2O$ mixture for 12 h with vigorous stirring.  Additional water was introduced periodically to compensate for the

water that evaporated and to maintain a two phase system. As before, the samples of the two phases were analyzed by ^{1}H NMR. ^{1}H NMR spectra of the different pure ILs, as well as of the starting protonated-heterocyclic anions, were recorded in both $DMSO_{d6}$ and $D_2O$ as references.

The results were determined by comparing the ^{1}H NMR spectra of the IL-rich phase (in $DMSO_{d6}$) and the aqueous phase (in $D_2O$) after bubbling with $CO_2$ with the ^{1}H NMR spectra of the pure IL, protonated-heterocyclic anion, IL split phases after mixing with just water, and dry IL after bubbling with $CO_2$. Guided by the change in chemical shifts that are characteristic to each species in each part of these processes, as well as by the integrals that provide the relative numbers of chemically distinct hydrogens of each species, it was possible to make the following conclusions:

1) None of the ILs studied underwent protonation at the anionic heterocyclic moiety when mixed only with water.

2) ILs NDIL0063, NDIL0071, NDIL0080 and Koei001 experienced protonation when mixed with water and bubbled with $CO_2$ at the same time (which would form carbonic acid; thus, facilitating acid catalyzed reactions). This was made clear by comparing the ^{1}H NMR chemical shifts of the protonated-heterocyclic cation with the chemical shifts of aqueous phase after splitting.

3) ILs NDIL0046, Koei002 and Koei003 did not undergo protonation when mixed with water and $CO_2$.

4) Experiments with IL NDIL0094 were inconclusive. TGA of NDIL0094 revealed 5 wt % of starting protonated-heterocyclic unreacted starting material in that sample, which frustrated the analysis. Attempts to produce a protonated-anion-free IL have been unsuccessful. ^{1}H NMR spectra show the presence of the protonated-heterocyclic anion, but it cannot be discerned whether it is due to reprotonation or it is just part of the initial unreacted starting material impurity.

It has been found that NDIL0088, 0071, 0094, 0063 and 0046 are all stable in the presence of water at ambient conditions. However, in the presence of water and one atmosphere of $CO_2$, NDIL0063, 0071 and 0094 exhibit some evidence of protonation. This is not the case with NDIL0046 and 0088. Based on these studies, it has been

determined that the anions used in NDIL0063, NDIL0071, NDIL0080 and Koei001 are not appropriate for removal of $CO_2$ from wet post-combustion flue gas.

Based on these additional studies, Notre Dame identified NDIL0157 as the most promising IL and the one which should be used in the final systems analysis. Note that NDIL0157 was not made in the ND laboratory, but its properties can be well estimated from previous studies. The anion is the same as that in Koei003 and has the most favorable reaction characteristics with $CO_2$. Unfortunately, Koei was unable to produce more than a 25 g sample because of its prohibitive cost. The cation for NDIL0157 has also been made but with other anions. It is known from the previous work that the cation is a "spectator" and does not have any effect on the reaction of $CO_2$ with the anion. One simply needs to tune it so that the IL has a low heat capacity, low viscosity and wide liquidus range. Thus at the conclusion of this work, NDIL0157 was identified as the best available solvent, but additional process synthesis research will be necessary to see if a cheaper synthesis route can be discovered.

## 5.3 Economic, Engineering and Systems Analysis
### 5.3.1 Process Modeling
Trimeric delivered a report to Notre Dame on a systems analysis of using NDIL0157. During this time, Notre Dame researchers consulted extensively with Trimeric staff. A review of the report was conducted at Notre Dame in September. The full report was sent to David Lang, DOE program manager and is included in Appendix IV. The following is a brief summary of the major findings. Trimeric will participate in the final project review at NETL.

Process modeling and economic analysis were conducted for a $CO_2$ capture process using NDIL0157. Process simulations with mass and energy balances were prepared. Equipment in the process was then sized and selected, and purchased equipment costs were estimated from vendor information or costing software. Finally, capital costs, operating costs and COE were estimated. Costs for NDIL0157 were compared to a baseline case using MEA absorbent taken from the 2010 Cost and Performance Baseline[1]

and compared to costs for NDIL0046 evaluated in the previous milestone report for this project.[2]

The standard design basis for this evaluation is a 550 MW net supercritical coal-fired power plant using Illinois #6 subbituminous coal. The location for this greenfield plant is a generic plant site in Midwestern USA. A wet flue gas desulfurization (FGD) unit was assumed to be located upstream of the $CO_2$ capture unit. The target $CO_2$ removal was 90%. Any captured $CO_2$ was assumed to be delivered at pipeline pressure (15.2 MPa; 2215 psia), transported 80 kilometers (50 miles) and sequestered in a saline formation at a depth of 1,239 m (4,055 ft). The entire $CO_2$ capture system consisted of a single inlet gas conditioning train, multiple parallel capture units, and a single, common $CO_2$ compressor train.

Trimeric estimated that $CO_2$ capture increased the base COE from 5.89 ¢/kWh (Case 11 from the 2010 Cost and Performance Baseline) to 10.59 ¢/kWh for NDIL0157, assuming IL unit costs of $5,000/tonne and stainless steel materials of construction. In comparison, the COE for DOE Case 12 ($CO_2$ capture using Fluor's Econamine FG Plus$^{TM}$ process) was estimated by WorleyParsons to be 10.70 ¢/kWh.

Overall, the economics of using NDIL0157 were estimated to be comparable to the Fluor Econamine FG Plus$^{TM}$ process (DOE Case 12). Lower reboiler energy consumption for NDIL0157 was offset by higher compression energy requirements and higher capture and compression purchased equipment costs. The higher purchased equipment costs for NDIL0157 can be attributed primarily to the lean/rich cross-exchanger (due to the higher viscosity of NDIL0157) and compression equipment (due to the lower regeneration pressure for NDIL0157).

In addition to showing comparable cost performance to DOE Case 12, NDIL0157 exhibited superior performance to NDIL0046, which was studied in the prior systems analysis. Energy requirements were approximately 30% lower for NDIL0157 when compared to NDIL0046, and purchased equipment costs were approximately 36% lower.

Important parameters that influence the overall COE for the NDIL0157 $CO_2$ capture process include materials of construction, the viscosity of the IL, and the cost of the IL. The corrosion studies performed by B & W indicate that at temperatures below 100°C, CRs for ILs are less than CRs for MEA. This suggests that carbon steel is an acceptable material of construction for equipment operated at lower temperatures within the process. For example, if the IL absorber columns and packing were constructed of carbon steel instead of 316 stainless steel, the purchased equipment costs at 593 MW gross output would decrease by \$11.2 MM, and the overall COE at 550 MW net output would decrease from 10.59 ¢/kWh to 10.35 ¢/kWh.

In addition to the absorber, another large contribution to the overall capture purchased equipment costs was the rich/lean cross-exchanger. A 50% reduction in IL viscosity (when compared to the current values) would decrease cross-exchanger purchased equipment costs by approximately \$4.3 MM at 593 MW gross output, which results in a decrease in the COE from 10.59 ¢/kWh to 10.49 ¢/kWh. If the effects of reduced viscosity were combined with the effects of a carbon steel absorber, then overall COE at 550 MW net output would decrease from 10.59 ¢/kWh to 10.25 ¢/kWh.

The unit cost of ILs has a direct impact on the annual variable operations costs of the $CO_2$ capture system. Assuming a degradation rate of 0.23 kg IL/MT $CO_2$ and a unit cost of \$5/kg (or \$5,000/tonne), the annual cost of IL solvent replacement is approximately \$4.43 MM. If these unit costs were \$10/kg or \$15/kg, the annual cost of IL solvent replacement would increase to \$8.86 MM and \$13.29 MM, respectively. Assuming these unit costs, the overall COE at 550 MW net output would increase from 10.59 ¢/kWh to 10.77 ¢/kWh and 10.94 ¢/kWh, respectively.

### 5.3.2 Commercialization Report

Matric was contracted to complete a commercialization study for IL use in post-combustion $CO_2$ capture. This report was revised by Notre Dame in response to comments by the program manager and submitted to DOE in November, 2012. The major findings of this independent study are as follows.

Cost

Capture of carbon dioxide from coal-fired power plants has the potential to be less expensive using task-specific IL as a reactive sorbent rather than MEA. ILs are ionic compounds made with organic moieties which may be liquid even at room temperature and which are virtually non-volatile. Even with their use, energy consumption and overall cost of the separation process will be substantial.

Several aspects of commercialization of IL-based $CO_2$ capture were considered. First of all, the high cost of $CO_2$ capture implies that commercialization of any process will only occur by government mandate. A tax of at least \$45 and as much as \$60 per metric ton (tonne) of emitted $CO_2$ is necessary to spur commercialization. An extensive review of processes both for retrofit and for new plants revealed numerous candidate processes. Cost estimates are ambiguous for nearly all of them. A notable exception is the MEA process, which is in the most advanced stage of commercialization. Only two or three processes are deemed to have the potential for substantial cost reduction, and they each have significant technical risks. The IL-based process may reduce thermal energy usage by up to 64% compared to the MEA process. Significant savings in capital costs are unlikely, and non-energy operating costs will be higher.

Market

Market size for $CO_2$ capture processes such as the IL-based one is potentially huge. However, analysis suggests that a substantial number of old, inefficient, small, and/or geographically impractical coal-fired power plants are not candidates for retrofit. Combined with the recent dearth of construction of new plants, it is projected that the market for $CO_2$ capture processes for new plants as well as retrofits will be strong, given legislation mandating capture, or some mechanism for an appropriate cost of carbon dioxide emissions.

Technology Transfer

There are multiple possible technology transfer strategies for IL-based $CO_2$ capture. However, it is recommended that either licensing or a strategic alliance be pursued as the best possible avenue for commercialization because of the complexity, amount of capital required and technical skillset and knowledge base required by the commercializing entity. Possible licensing or strategic partners include:

- Large engineering firms with an energy focus
- Power equipment manufacturing companies
- Power plant owners and operators
- New carbon capture ventures with funding or partnerships

Scale-up

Scale-up of the IL-based $CO_2$ capture process to the point of full-scale demonstration is doable in ten years or less. Cost for a multi-step sequential scale-up, not including full-scale demonstration, is an estimated $60 million. Construction and 1 ½ years of operation of the full-scale demonstration separation process will cost roughly $600 million.

Recommendation

It is recommended that development of processes with the potential for a step-change reduction in cost be emphasized in spite of higher technical risks.

# Conclusions
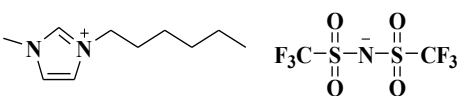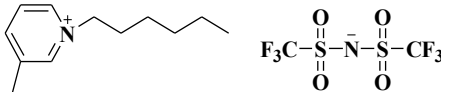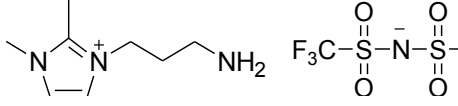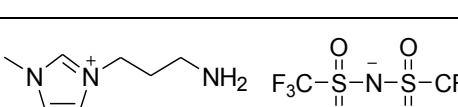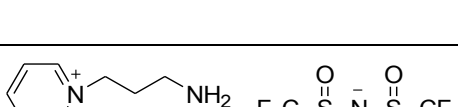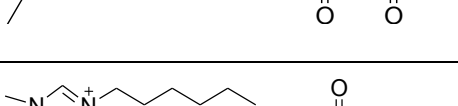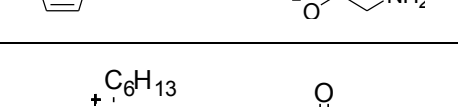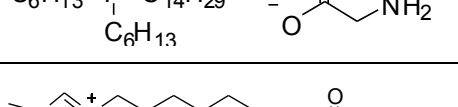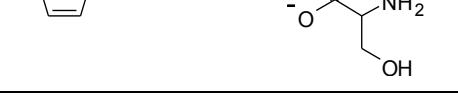
This project was successful in accomplishing all six of its basic objectives. A number of new molecular modeling techniques and experimental procedures were developed to design, synthesize and test new ILs with properties specifically tuned for post-combustion $CO_2$ capture. Along the way, several important discoveries were made.
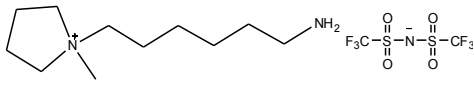
The chemistry of $CO_2$-IL reactions was elucidated such that a means was found for doubling the $CO_2$ carrying capacity of s ILs relative to the best available technology known at the start of the project. Note that the ILs developed in this project can react rapidly with a 1:1 stoichiometry of $CO_2$:reactive group in an anhydrous environment. The mechanism was discovered whereby viscosities were observed to increase when $CO_2$ reacts with an IL, and came up with an entirely new class of ILs that do not exhibit this viscosity increase. Using process modeling, it was learned that there is an optimum $CO_2$ binding energy with ILs that minimizes thermal regeneration duty and overall cost. Molecular modeling procedures were developed where accurate prediction of $CO_2$ binding energies from first principles could be predicted with no recourse to experimental data. Using this procedure, several new ILs were developed which had binding energies in the desired range. Many of these ILs were made, and subsequent tests validated the computational predictions. A host of physical property measurements were made on these ILs and computed many other properties. Lab-scale demonstration tests were carried out at Notre Dame and B & W and demonstrated that ILs can effectively remove $CO_2$ from a simulated flue gas. The efficiency of the IL relative to aqueous MEA is lower due to mass transfer limitations resulting from the relatively high viscosity of the ILs. It was discovered, however, that by diluting the IL with a suitable low viscosity, low volatility fluid, the performance could be made to approach that of MEA. The IL was found to have excellent corrosion behavior, such that carbon steel materials could probably be used in a process.
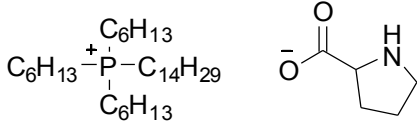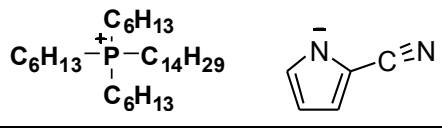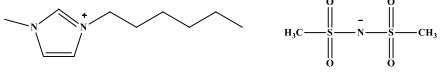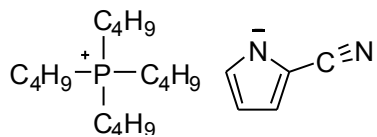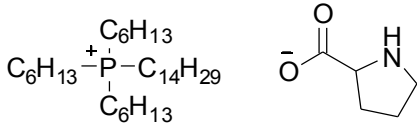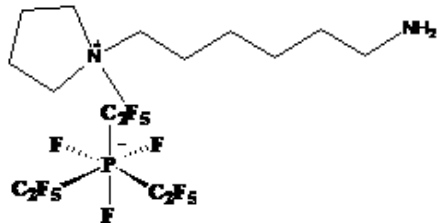
Trimeric's systems analysis indicates that the economics of using NDIL0157, the "best" IL identified in this work, are at least comparable to – and potentially better than -– the Fluor Econamine FG Plus$^{TM}$ process (DOE Case 12).  Additional work directed at

optimizing mass transfer, liquid viscosity, and the economics of IL manufacturing could improve the process economics further. Moreover, additional testing of NDIL0157 and other ILs in larger-scale gas contacting devices is recommended.

## List of major, non-proprietary ionic liquids developed and/or used in this project

| Structure | Name | Abbreviation | Code |
|---|---|---|---|
| | 1-hexyl-3-methylimidazolium bis(trifluoromethylsulfonyl)imide | [hmim][Tf₂N] | NDIL0001 |
| | 1-hexyl-3methylpyridnium bis(trifluoromethylsulfonyl)imide | [hmpy][Tf₂N] | NDIL0006 |
| | 1-(3-aminopropyl)-2,3-methylimidazolium bis(trifluoromethylsulfonyl)imide | [H₂NC₃H₆mmim][Tf₂N] | NDIL0016 |
| | 1-(3-aminopropyl)-3-methylimidazolium bis(trifluoromethylsulfonyl)imide | [H2NC3H6mim][Tf2N] | NDIL0017 |
| | 1-(3-aminopropyl)-3-methylpyridnium bis(trifluoromethylsulfonyl)imide | [H₂NC₃H₆mpy][Tf₂N] | NDIL0018 |
| | 1-hexyl-3-methylimidazolium glycinate | [hmim][Gly] | NDIL0028 |
| | Trihexyl(tetradecyl)phosphonium glycinate | [P₆₆₆₁₄][Gly] | NDIL0030 |
| | 1-hexyl-3-methylimidazolium serinate | [hmim][Ser] | NDIL0031 |
| | Trihexyl(tetradecyl)phosphonium Glutaminate | [P₆₆₆₁₄][Gln] | NDIL0032 |

| | | | |
|---|---|---|---|
| C$_6$H$_{13}$–P$^+$(C$_6$H$_{13}$)(C$_6$H$_{13}$)–C$_{14}$H$_{29}$ (alaninate anion) | Trihexyl(tetradecyl)phosphonium Alaninate | [P$_{66614}$][Ala] | NDIL0033 |
| C$_6$H$_{13}$–P$^+$(C$_6$H$_{13}$)(C$_6$H$_{13}$)–C$_{14}$H$_{29}$ (leucinate anion) | Trihexyl(tetradecyl)phosphonium Leucinate | [P$_{66614}$][Leu] | NDIL0034 |
| C$_6$H$_{13}$–P$^+$(C$_6$H$_{13}$)(C$_6$H$_{13}$)–C$_{14}$H$_{29}$ (isoleucinate anion) | Trihexyl(tetradecyl)phosphonium Isoleucinate | [P$_{66614}$][Ile] | NDIL0035 |
| C$_6$H$_{13}$–P$^+$(C$_6$H$_{13}$)(C$_6$H$_{13}$)–C$_{14}$H$_{29}$ (lysinate anion) | Trihexyl(tetradecyl)phosphonium Lysinate | [P$_{66614}$][Lys] | NDIL0036 |
| C$_6$H$_{13}$–P$^+$(C$_6$H$_{13}$)(C$_6$H$_{13}$)–C$_{14}$H$_{29}$ (threoninate anion) | Trihexyl(tetradecyl)phosphonium Threoninate | [P$_{66614}$][Thr] | NDIL0037 |
| C$_6$H$_{13}$–P$^+$(C$_6$H$_{13}$)(C$_6$H$_{13}$)–C$_{14}$H$_{29}$ (serinate anion) | Trihexyl(tetradecyl)phosphonium Serinate | [P$_{66614}$][Ser] | NDIL0038 |
| 1-(6-amino-hexyl)-1-methyl-pyrrolidinium cation with [Tf2N] anion | 1-(6-amino-hexyl)-1-methyl-pyrrolidinium bis(trifluoromethylsulfonyl)imide | [H2NC6H12mpyr][Tf2N] | EMD0004 |
| C$_6$H$_{13}$–P$^+$(C$_6$H$_{13}$)(C$_6$H$_{13}$)–C$_{14}$H$_{29}$ (taurinate anion) | Trihexyl(tetradecyl)phosphonium Taurinate | [P$_{66614}$][Tau] | NDIL0041 |
| C$_6$H$_{13}$–P$^+$(C$_6$H$_{13}$)(C$_6$H$_{13}$)–C$_{14}$H$_{29}$ (methioninate anion) | Trihexyl(tetradecyl)phosphonium methioninate | [P$_{66614}$][Met] | NDIL0043 |

174

| | | Trihexyl(tetradecyl)phosphonium prolinate | [P$_{66614}$][Pro] | NDIL0045 |
|---|---|---|---|---|
| | | Trihexyl(tetradecyl)phosphonium 2-(Cyano)pyrrolide | [P$_{66614}$][CNpyr] | NDIL0046 |
| | | 1-hexyl-3methylimidazolium bis(perfluoroethylsulfonyl)imide | [hmim][Beti] | NDIL0053 |
| | | Tetrabutylphosphonium cyanopyrrolide | [P$_{4444}$][CNpyr] | NDIL0058 |
| | | Trihexyl(tetradecyl)phosphonium prolinate | [P$_{66614}$][Pro] | EMD0005 |
| | | 1-(6-amino-hexyl)-1-methyl-pyrrolidinium tris(pentafluoroethyl)trifluoro-phosphate | [NH$_2$hmpyr] [eFAP] | EMD0006 |

# References

1. J. Kumelan, A. P. S. Kamps, D. Tuma, and G. Maurer, J. Chem. Thermodyn. 38, (2006) 1396.
2. S. N. V. K. Aki, B. R. Mellein, E. M. Saurer, and J. F. Brennecke, J. Phys. Chem. B 108, (2004) 20355.
3. A. Scurto, personal communication.
4. Wei Shi and Edward J. Maginn, *Journal of Computational Chemistry*, **2008**, 29, 2520-2530
5. Wei Shi and Edward J. Maginn, *Journal of Physical Chemistry B*, **2008**, 112, 2045-2055.
6. Keith Gutowski and Edward J. Maginn, *Journal of the American Chemical Society*, **2008**, 130, 14690-14704
7. Astrad, B., Bloom, R. and Swang, O., *J. Phys. Chem. A*, **111**, 1222-1228, 2007.
8. Kim, I.; Svendsen, H. F. *Ind. Eng. Chem. Res.* **2007**, *46*, 5803-5809.
9. Maham, Y.; Teng. T. T.; Hepler, L. G.; Mather, A. E. *Thermochimica Acta* **2002**, *386*, 111-118.
10. Otto, *et al.*, *Can. J. of Chem. Eng.* **1995**, *73*, 140-147
11. Marcos Perez-Blanco and Edward J. Maginn, *Journal of Physical Chemistry B* (cover article), **2010**, 36, 11827
12. Marcos Perez-Blanco and Edward J. Maginn, *Journal of Physical Chemistry B*, **2011**, 115, 10488-10499.

# Technology Transfer

Peer-reviewed publications resulting from this project

1. Christina Myers, Henry Pennline, David Luebke, Jeffery Ilconich, JaNeille K. Dixon, Edward J. Maginn and Joan F. Brennecke, "High Temperature Separation of Carbon Dioxide/Hydrogen Mixtures Using Facilitated Supported Ionic Liquid Membranes," J. Membrane Science, 322, 2008, 28-31.
2. Brett F. Goodrich, Juan C. de la Fuente, Burcu E. Gurkan, David J. Zadigian, Erica A. Price, Yong Huang, and Joan F. Brennecke, "Experimental Measurements of Amine-Functionalized Anion-Tethered Ionic Liquids with Carbon Dioxide," Ind. Eng. Chem. Res., 50(1), 2011, 111-118.
3. Joan F. Brennecke and Burcu E. Gurkan, "Ionic Liquids for $CO_2$ Capture and Emission Reduction," J. Phys. Chem. Let., 1(24), 2010, 3459-3464.
4. Brett F. Goodrich, Juan C. de la Fuente, Burcu E. Gurkan, Zulema K. Lopez, Erica A. Price, Yong Huang, and Joan F. Brennecke, "Effect of Water and Temperature on Absorption of $CO_2$ by Amine-Functionalized Anion-Tethered Ionic Liquids," J. Phys. Chem. B, 115, 2011, 9140-9150.
5. Mindrup, E.; Schneider, W. F. Computational Comparison of the Reactions of Substituted Amines with $CO_2$. *Chemsuschem* **2010**, *3*, 931–938.
6. Gurkan, B. E.; Goodrich, B. F.; Mindrup, E.; Ficke, L.; Masel, M.; Seo, S.; Senftle, T. P.; Wu, H.; Glaser, M. F.; Shah, J. K.; Maginn, E.; Brennecke, J.; Schneider, W. F. Molecular Design of High Capacity, Low Viscosity, Chemically Tunable Ionic Liquids for $CO_2$ Capture. *The Journal of Physical Chemistry Letters* **2010**, *1*, 3494–3499.
7. Gurkan, B. E.; la Fuente, de, J. C.; Mindrup, E. M.; Ficke, L. E.; Goodrich, B. F.; Price, E. A.; Schneider, W. F.; Brennecke, J. F. Equimolar CO 2Absorption by Anion-Functionalized Ionic Liquids. *Journal of the American Chemical Society* **2010**, *132*, 2116–2117.
8. Wu, C.; Senftle, T. P.; Schneider, W. F. First-principles-guided design of ionic liquids for $CO_2$ capture. *Phys. Chem. Chem. Phys.* **2012**, *14*, 13163.
9. Wei Shi and Edward J. Maginn, "Atomistic Simulation of the Absorption of Carbon Dioxide and Water in the Ionic Liquid 1-n-Hexyl-3-methylimidazolium Bis(trifluoromethylsulfonyl)imide ([hmim][Tf2N])", *Journal of Physical Chemistry B*, **2008**, 112, 2045-2055.
10. Keith Gutowski and Edward J. Maginn, "Amine-Functionalized Task-Specific Ionic Liquids: A Mechanistic Explanation for the Dramatic Increase in Viscosity Upon Complexation with $CO_2$ from Molecular Simulation", *Journal of the American Chemical Society*, **2008**, 130, 14690-14704.
11. Wei Shi and Edward J. Maginn, Molecular Simulation and Regular Solution Theory Modeling of Pure and Mixed Gas Absorption in the Ionic Liquids 1-n-Hexyl-3-methylimidazolium Bis(Trifluoromethylsulfonyl)amide ([hmim][Tf2N]), *Journal of Physical Chemistry B*, **2008**, 112, 16710-16720.
12. Marcos Perez-Blanco and Edward J. Maginn, "Molecular Dynamics Simulations of $CO_2$ at an Ionic Liquid Interface: Adsorption, Ordering and Interfacial Crossing", *Journal of Physical Chemistry B* (cover article), **2010**, 36, 11827.

13. Marcos Perez-Blanco and Edward J. Maginn, "Molecular Dynamics Simulations of Carbon Dioxide and Water at an Ionic Liquid Interface", *Journal of Physical Chemistry B*, **2011**, 115, 10488-10499

14. Thomas W. Rosch and Edward J. Maginn, "Reaction Ensemble Monte Carlo Simulations of Complex Molecular Systems", *Journal of Chemical Theory and Computation*, **2011**, 7, 269-279.

Patents

1. William F. Schneider, Joan F. Brennecke and Edward J. Maginn, "Ionic Liquids Comprising Heteroaromatic Anions," provisional patent filed 11/09; patent filed 11/10.

Invited Presentations

Joan Brennecke
1. "Gas Separations with Ionic Liquids," 2nd International Congress on Ionic Liquids, Yokohama, Japan, August 6-10, 2007.
2. "Ionic Liquids: Green Solvents for Reactions and Separations?" ACS Rocky Mountain Regional Meeting, Denver, CO, August 30, 2007.
3. "Carbon Dioxide Separations with Ionic Liquids," Department of Chemical Engineering, University of Rhode Island, October 4, 2007.
4. "Separation of Carbon Dioxide with Ionic Liquids," Department of Chemical Engineering, Carnegie Mellon University, October 25, 2007.
5. "Ionic Liquids for $CO_2$ Capture," Department of Chemical Engineering, West Virginia University, October 26, 2007.
6. "Ionic Liquids: Are They Worth Their Salt?" AIChE Annual Meeting, Professional Progress Award Lecture, November 5, 2007.
7. "Measurements of Gases in Ionic Liquids," Eastern Analytical Symposium, Somerset, NJ, Nov. 12, 2007.
8. "Ionic Liquids for Gas Separations," Department of Chemical Engineering, University of Michigan, January 10, 2008.
9. "Engineering Ionic Liquids for Separations," Department of Chemical and Biomolecular Engineering," University of Illinois at Urbana-Champaign, February 19, 2008.
10. "Ionic Liquids for Carbon Capture," Princeton Institute for the Science and Technologies of Materials, Princeton University, March 19, 2008.
11. "Ionic Liquids: Solvents for Reactions and Separations," MRSEC Spring 2008 Polymer Event, University of Massachusetts, May 14, 2008.
12. "Carbon Dioxide Capture Using Ionic Liquids," 236th ACS National Meeting, Philadelphia, PA, August 17, 2008.
13. "The Future of Carbon Dioxide Capture with Absorbents," CCR Niche Meeting on Carbon Capture and Sequestration, Rice University, October 13-14, 2008.

14. "Ionic Liquids: From Experimental Thermodynamics to Carbon Dioxide Capture," Department of Chemical Engineering and Applied Chemistry, University of Toronto, Toronto, CA, December 3, 2008.
15. "Design and Evaluation of Ionic Liquids as Novel $CO_2$ Absorbents," Electric Power Research Institute (EPRI) Workshop on Fundamental Challenges of $CO_2$ Capture, May 18-19, 2009.
16. "Engineering Gas Separations with Ionic Liquids," Plenary Lecture, 3$^{rd}$ International Congress on Ionic Liquids (COIL-3), Cairns, Australia, May 31-June 4, 2009.
17. "Separating Gases with Ionic Liquids," Department of Chemical Engineering, University of Southern California, October 8, 2009.
18. "Gas Separations with Ionic Liquids," Institute for Technical and Macromolecular Chemistry, RWTH Aachen, Aachen, Germany, June 22, 2010.
19. "Ionic Liquids: Potential for $CO_2$ Capture and other Separation Processes," Chevron Phillips Chemical Company, Bartlesville, OK, July 13, 2010.
20. Joan F. Brennecke, "Engineering Reactions with Ionic Liquids," session in honor of Roger Schmitz, AIChE Annual Meeting, Salt Lake City, UT, Nov. 7-12, 2010.
21. Joan F. Brennecke, "Thermodynamics and Phase Behavior of Ionic liquids with Gases, " session in honor of Stanley Sandler's 70$^{th}$ birthday II, AIChE Annual Meeting, Salt Lake City, UT, Nov. 7-12, 2010.
22. Joan F. Brennecke, "$CO_2$ Capture with Ionic Liquids: Reaction Enthalpy, Viscosity and Effect of Water," Jiaotong University, Xi'an, China, Sept. 14, 2012.
23. Sam Seo, Mauricio Quiroz-Quzman, Aruni DeSilva, Luke Simoni, Mark A. Stadtherr and Joan F. Brennecke, "$CO_2$ Capture: Ionic Liquids and Phase Change Ionic Materials," Green Solvents for Synthesis, Boppard, Germany, Oct. 8, 2012.

William Schneider
24. "First-Principles Evaluation Of $CO_2$ Complexation In Functionalized Ionic Liquids," (w/E. Mindrup), Symposium on Ionic Liquids: From Knowledge to Application, American Chemical Society National Meeting, Philadelphia, Pennsylvania, August 17-21, 2008.
25. "Ionic Liquids: A New Chemical Platform for $CO_2$ Separations," Indiana CCTR Advisory Committee Meeting, Indiana University, Bloomington, June 4, 2009.
26. "Ionic Liquids: A New Chemical Platform for $CO_2$ Separations," Pacific Northwest National Laboratory, Richland, Washington, January 7, 2010."Ionic Liquids: A New Chemical Platform for $CO_2$ Separations," Indiana University, Bloomington, Indiana, February 25, 2010.
27. "Ionic Liquids for $CO_2$ Capture from First-Principles," CECAM workshop on Carbon Capture, Lausanne, Switzerland, July 26-28, 2010.
28. "Chemically Complexing Ionic Liquids for Pre-Combustion $CO_2$ Capture," Global Climate and Energy Project Annual Meeting, Stanford, California, October 10, 2012.

Edward Maginn
29. "Carbon Dioxide Capture from Flue Gas Using Ionic Liquids: A Combined Molecular Modeling and Experimental Study" (Keynote Speaker), ASME 3rd Energy Nanotechnology International Conference, Jacksonville, FL, Aug. 10-14, **2008**.

30. "Using Molecular Simulations to Design New Ionic Liquids for Use in Energy and Propulsion Applications", University of Florida Chemical Engineering departmental seminar, February 3, **2009**.
31. "Development of Technologies for Carbon Dioxide Capture", Michiana Area Engineers Week, February 28, **2009**.
32. "Development of Technologies for Carbon Dioxide Capture", American Society of Heating, Refrigeration and Air Conditioning Engineers, South Bend, IN, March 19, **2009**.
33. "Ionic Liquids" Breakthrough Absorption Technology for Post-Combustion $CO_2$ Capture", NETL $CO_2$ Capture Conference, Pittsburgh, PA, March 24, **2009**.
34. "On the Use of Molecular Simulations for Computing Thermodynamic and Transport Properties of Ionic Liquids", Centre Europeen de Calcul Atomique et Moleculaire workshop, Dublin, Ireland, April 6, **2009**.
35. "Using Molecular Simulations to Design New Ionic Liquids for Use in Energy and Propulsion Applications", Department of Chemistry seminar, University of New Orleans, New Orleans, LA, April 17, **2009**.
36. "Design and Evaluation of Ionic Liquids as Novel $CO_2$ Absorbents", National Energy Technology Laboratory, Pittsburgh, PA, April 30, **2009**.
37. "Molecular Modeling of Solubility in Ionic Liquids", 8th World Congress on Chemical Engineering, Montreal, Quebec, Canada, August, **2009**.
38. "Developing New Ionic Liquids for $CO_2$ Capture: A Success Story for Thermodynamics and Computational Molecular Design", GE Global Research Symposium on Emissions and Aftertreatment, GE Global Research Center, Niskayuna, NY, Sept. 17, **2009**.
39. "Understanding Sorption and Diffusion in Ionic Liquids Via Molecular Simulation", Fakultät für Chemie und Mineralogie, Wilhelm-Ostwald-Institut für Physikalische und Theoretische Chemie, Universität Leipzig, Leipzig, Germany, Nov. 30, 2009.
40. "Understanding the behavior of chemically functionalized ionic liquids via molecular simulation", 239th American Chemical Society National Meeting, San Francisco, CA, March 21, **2010**.
41. "A Molecular Simulation Study of the Structure and Dynamics of Chemically Functionalized Ionic Liquids", 8th Liblice Conference on the Statistical Mechanics of Liquids, Brno, Czech Republic, June 15, **2010**.
42. "Molecular Simulation and Its Role in Energy and Environmental Research", Indo-US Workshop on Energy and Environment: Challenges and Research Opportunities, Delhi, India, Dec. 12, **2010**.
43. "Developing New Materials for Energy and Environmental Applications Via Molecular Simulation", University of Pennsylvania Department of Chemical and Biomolecular Engineering, Philadelphia, PA, January 26, **2011**.
44. "Developing New Materials for Energy and Environmental Applications Via Molecular Simulation", National University of Singapore Department of Chemistry, Singapore, February 17, **2011**.
45. "Development of New Ionic Liquids Solvents for $CO_2$ Capture", National University of Singapore Department of Chemical Engineering, Singapore, February 18, **2011**.

46. "Developing New Materials for Energy and Environmental Applications Via Molecular Simulation" University of Minnesota Department of Chemical Engineering and Materials Science, Minneapolis, MN, March 29, **2011**.
47. "How Molecular Simulations Can Save the World: Development of New Materials to Mitigate Greenhouse Gases", Vanderbilt University / Columbia University Molecular Modeling Cybercamp, Nashville, TN, June 3, **2011**.
48. "Developing New Materials for Energy and Environmental Applications Via Molecular Simulation", *Centennial Lecturer*, University of Alabama Chemical Engineering, Tuscaloosa, AL, Sept 22, **2011**.
49. "Developing New Materials for Energy and Environmental Applications Via Molecular Simulation", University of Washington Department of Chemical Engineering seminar, Seattle, WA, Nov. 14, **2011**.
50. "Developing New Materials for Energy and Environmental Applications Via Molecular Simulation", Louisiana State University Department of Chemical Engineering seminar, Baton Rouge, LA, January 20, **2012**.
51. "Using Molecular Simulation to Develop New Materials for Energy and Environmental Applications", Symposium on Chemical Physics of the Environment, Division of Chemical Physics of the American Physical Society, Boston, MA, Feb. 28, **2012**.
52. "Developing New Materials for Energy and Environmental Applications Via Molecular Simulation", MATGAS, Campus de la UAB, Bellaterra (Barcelona) – Spain, March 12, **2012**.
53. "Solubility and Interfacial Transport of $CO_2$ in Ionic Liquid Systems", ACS National Meeting, San Diego, CA, March 28, **2012**.
54. "Developing New Materials for Energy and Environmental Applications via Molecular Simulation", Department of Chemistry seminar, Monash University, Melbourne, Australia, May 8, **2012**.
55. "Ionic Liquid Research at Notre Dame: Carbon Capture and Other Applications", The Future of Energy Forum, Trinity College, Dublin, Ireland August 30, **2012**.


Contributed Presentations

1. Jessica L. Anderson, JaNeille K. Dixon, Mark J. Muldoon, Joan F. Brennecke, and Edward J. Maginn, "Ionic Liquids as $CO_2$ Capture Media," Chemrawn XVII Conference on Greenhouse Gases Mitigation and Utilization, Kingston, Ontario, Canada, July 11, 2007.
2. Jessica L. Anderson, JaNeille K. Dixon, Joan F. Brennecke and Edward J. Maginn, "Ionic Liquids as Suitable Media for $CO_2$ Capture," (poster presentation) 2nd International Congress on Ionic Liquids, Yokohama, Japan, August 6-10, 2007.
3. Jessica L. Anderson, JaNeille K. Dixon, Wei Shi, Kate E. Wilbanks, Edward J. Maginn, and Joan F. Brennecke, "Ionic Liquids as Absorption Media for Pure and Mixed Gas Capture," AIChE Annual Meeting, Salt Lake City, Utah, Nov. 4-10, 2007.
4. Edward J. Maginn, JaNeille K. Dixon, Elaine Mindrup, Wei Shi, Joan F. Brennecke, and William F. Schneider, "Evaluation of Ionic Liquids as Novel Post-Combustion

Carbon Dioxide Capture Solvents," Spring AIChE Meeting, New Orleans, LA, April 6-10, 2008.

5. Erica Price, Burcu Gurkan, Juan C. de la Fuente and Joan F. Brennecke, "Tuning Ionic Liquids for $CO_2$ Capture," poster presentation, Green Chemistry Summer School, Colorado School of Mines, July 9-18, 2008.

6. Brett F. Goodrich, Lindsay E. Ficke, and Joan F. Brennecke, "Experimental Measurements of Amine-Functionalized Ionic Liquids and Carbon Dioxide for Gas Separation," AIChE Annual Meeting, Nashville, TN, Nov. 8-13, 2009.

7. Brett F. Goodrich, Lindsay E. Ficke, Joan F. Brennecke, "Ionic liquids for post-combustion $CO_2$ capture: Tunable capacities and enthalpies," ACS National Meeting, San Francisco, CA, March 21-25, 2010.

8. Brett F. Goodrich and Joan F. Brennecke, "Experimental Measurements of Absorption Isotherms of Amine-Functionalized Ionic Liquids and Carbon Dioxide," 2010 Midwest Thermodynamics and Statistical Mechanics Conference, University of Notre Dame, June 1-3, 2010.

9. Burcu Gurkan and Joan F. Brennecke, "Kinetics of Carbon Dioxide Absorption by Chemically Reactive Ionic Liquids," 2010 Midwest Thermodynamics and Statistical Mechanics Conference, University of Notre Dame, June 1-3, 2010.

10. Samuel Seo and Joan F. Brennecke, "Carbon Dioxide Absorption by Amine Functionalized Ionic Liquids- Effect of Temperature and Water Content," poster presentation, 2010 Midwest Thermodynamics and Statistical Mechanics Conference, University of Notre Dame, June 1-3, 2010.

11. Marjorie Massel and Joan F. Brennecke, "Heat of Absorption Measurements of Carbon Dioxide in Novel Ionic Liquids Using Calorimetry," poster presentation, 2010 Midwest Thermodynamics and Statistical Mechanics Conference, University of Notre Dame, June 1-3, 2010.

12. Burcu E. Gurkan, Juan de la Fuente, Elaine M. Mindrup, Lindsay E. Ficke, Brett F. Goodrich, Erica A. Price, William F. Schneider, Edward J. Maginn and Joan F. Brennecke, "Chemically Complexing Ionic Liquids for Post-Combustion $CO_2$ Capture," Clearwater Clean Coal Conference, Clearwater, FL, June 6-10, 2010.

13. Brett Goodrich, Samuel Seo, Levi Wilson, Lindsay Ficke, Marjorie Massel, David Zadigian and Joan F. Brennecke, "Ionic liquids with aprotic heterocyclic anions for post-combustion $CO_2$ capture," ACS National Meeting, Boston, MA, Aug. 22-27, 2010.

14. Burcu Gurkan, Mark J. McCready and Joan F. Brennecke, "Physico-Chemical Properties of Functionalized Ionic Liquid Solutions for Kinetic Studies of $CO_2$ Absorption," AIChE Annual Meeting, Salt Lake City, UT, Nov. 7-12, 2010.

15. W. F. Schneider and E. Mindrup, "First-principles Design of Functionalized Ionic Liquids for $CO_2$ Separations," Division of Physical Chemistry, American Chemical Society National Meeting, San Francisco, California, March 21-25, 2010.

16. W. F. Schneider and E. Mindrup, "AHA! Computational design of aprotic heterocyclic anions for ionic-liquid-based $CO_2$ separations," Division of Fuel Chemistry, American Chemical Society National Meeting, Boston, Massachusetts, August 22-26, 2010.

17.	W. F. Schneider, E. Mindrup, and C. Wu, "Computational Design of Aprotic Heterocyclic Anions (AHAs) for Ionic-Liquid-Based $CO_2$ Separations," North American Catalysis Society Meeting, Detroit, Michigan, June 5-10, 2011.

18.	W. F. Schneider and C. Wu, "Theoretical investigation of Nitrogen-Heterocyclic Carbenes as reversible $CO_2$ capture reagents," Division of Physical Chemistry, American Chemical Society, San Diego, California, March 2012.

19.	Marcos Perez-Blanco and Edward J. Maginn, "Molecular dynamics simulations of $CO_2$ at an ionic liquid interface: adsorption, ordering and interfacial crossing", AIChE Annual Meeting, Nashville, TN, November 12, **2009**.

20.	Thomas Rosch, Wei Shi, Jindal Shah and Edward J. Maginn, "Improved Conformational Sampling for Reaction Ensemble Monte Carlo Simulations", AIChE Annual Meeting, Nashville, TN, November 12, **2009**.

21.	Edward J. Maginn, Joan Brennecke, William Schneider and Mark McCready, "Molecular Engineering of New Ionic Liquid Sorbents for $CO_2$ Capture", 9th Annual Carbon Capture and Sequestration Meeting, Pittsburgh, PA, May 11, **2010**.

22.	Marcos Perez-Blanco and Edward J. Maginn, "Molecular Dynamics Simulations of $H_2O$ and $CO_2$ at An Ionic Liquid Interface: Effect of a Third Component On $CO_2$ Absorption Dynamics", AIChE Annual Meeting, Salt Lake City, UT, November 9, **2010**.

# Appendices

Appendix I – Idealized $CO_2$ Capture Model

## 1.0    INTRODUCTION

Under a subgrant from the University of Notre Dame, Trimeric Corporation has completed this work to develop an idealized $CO_2$ capture model to document the minimum energy required to perform an ideal separation of $CO_2$ from flue gas and then compress the $CO_2$ to pipeline pressure (2205 psia) as specified in the DOE/NETL Systems Analysis Guidelines (DOE/NETL/ 2005).   This analysis will establish an appropriate benchmark and will provide context for current post-combustion $CO_2$ capture costs targeted by the DOE.

## 2.0    METHODOLOGY FOR THERMODYNAMIC ANALYSIS

Application of the first and second laws of thermodynamics provides a useful means of establishing the minimum amount of work that must be supplied to (or the maximum amount of work that can be produced from) a given process.  This constraint provides a benchmark for evaluating the energy efficiency of a particular process or for evaluating the thermodynamic feasibility of proposed processes.  In the case of post-combustion $CO_2$ capture from flue gas, thermodynamic analysis reveals the minimum amount of work or energy that must be supplied in order to separate the $CO_2$ from the flue gas and compress it for subsequent sequestration.  This minimum work requirement can then be used to estimate the amount of power that must be provided to the $CO_2$ capture unit from the electric power plant and the associated increase in the COE due to the de-rating of the power plant (not including capital costs).

Figure 1 shows a simple diagram of the steady-state $CO_2$ capture process which serves as a basis for the thermodynamic analysis.  The "system" is contained within the rectangle

and represents any hypothetical post-combustion $CO_2$ capture process. Material streams are exchanged between the system and the surroundings. Low level heat may be supplied to the system and heat may also be rejected to the surroundings. Work may be supplied to the system as well. The objective of the analysis is to calculate this minimum work requirement, given the specified material streams and the temperature at which heat is transferred to and from the surroundings.
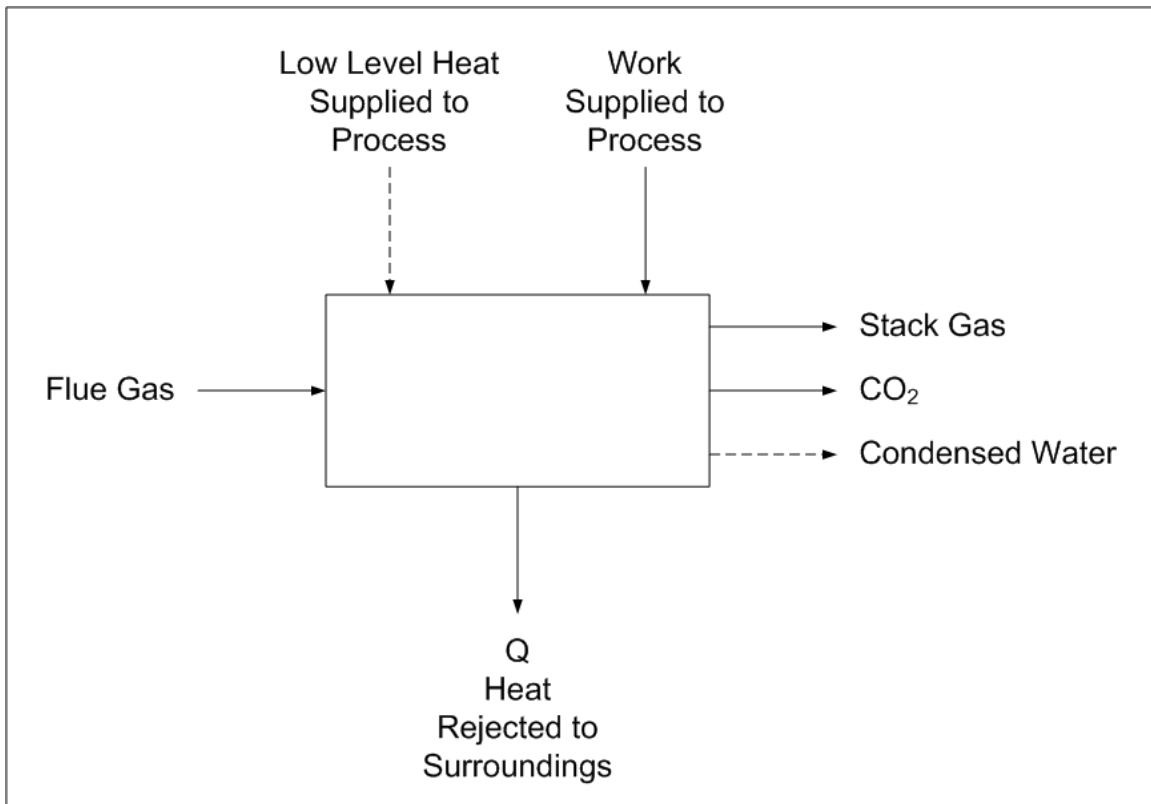
**Figure 1. $CO_2$ Capture Thermodynamic Analysis Schematic**

The thermodynamic analysis of processes is well-known and has been described in detail in chemical engineering literature (e.g., Smith and Van Ness, 1975) and therefore is not presented here in detail. The method generally requires constructing a hypothetical path using thermodynamically reversible steps and then adding up the minimum work

required for each step. Alternately, the minimum work can be calculated by examining the overall changes in entropy and enthalpy without the need to construct a hypothetical reversible process. The latter method is more convenient when a simple hypothetical process cannot be easily constructed or when the entropy and enthalpy of the entering and exiting streams can be readily calculated using a commercial process simulator.

For this simplified analysis, a 3-step hypothetical process using ideal reversible steps will be described. For this simplified model, it will be assumed that low level heat is not available and that no water is condensed or evaporated into the flue gas. The importance of these assumptions will be addressed later.

The three steps in the process were chosen for their computational simplicity and are given below:

- Cooling of the flue gas;
- Ideal reversible separation of $CO_2$ from the cooled flue gas; and
- Isothermal reversible compression of $CO_2$

The minimum work calculated for this three-step process is not dependent on the path chosen. For example, the minimum work calculated from this path would apply to real processes where compression requirements have been reduced (by regenerating a $CO_2$-laden solvent at high pressure, for example) even though the hypothetical calculation assumes that $CO_2$ compression begins at a pressure of one atmosphere. The minimum work for each step is described in the following paragraphs.

**Ideal Work for Process Step One: Cooling of Flue Gas**

The first step in the process involves reversible cooling the flue gas to the temperature at which it will be exhausted to from the process. The ideal work is calculated from the following well-known equation, sometimes referred to as the availability function:

$$W_{ideal} = T_o \Delta S - \Delta H \tag{1}$$

where

$W_{ideal}$ = Minimum ideal work required for this step (defined as negative if work is done on the system)

$T_o$ = Temperature of the surroundings

$\Delta S$ = Change in entropy of the system

$\Delta H$ = Change in enthalpy of the system

For this step the gas is assumed to behave as an ideal gas, such that:

$$W_{ideal} = T_o \int_{T_1}^{T_2} c_P \frac{dT}{T} - \int_{T_1}^{T_2} c_P dT \tag{2}$$

where

$c_p$ = The heat capacity at constant pressure for the flue gas

$T_1$ = The absolute temperature of the entering flue gas

$T_2$ = The absolute temperature of the cooled flue gas

**Ideal Work for Process Step Two: Separation of $CO_2$**

The ideal isothermal separation of flue gas into a vent stream and a pure $CO_2$ stream is given again by:

$$W_{ideal} = T_o \Delta S - \Delta H \tag{3}$$

For ideal gases, enthalpy is only a function of temperature. Therefore, for an isothermal process,

$$\Delta H = 0 \tag{4}$$

and

$$W_{ideal} = T_o \Delta S \tag{5}$$

The change in entropy for the system is calculated from the entropy of each stream:

$$\Delta S = S_{VentGas} + S_{CO_2} - S_{FlueGas} \tag{6}$$

For convenience, the reference state for each component is taken for each pure component at the temperature and pressure of the process. For ideal gases, the entropy of each stream is then given by:

$$S_i = -R \sum_i x_i \ln x_i \tag{7}$$

where $R$ is the gas constant.

For most separation processes, the thermodynamic efficiency is below 20 % and the actual work is significantly higher than that calculated from equation (5) (Shinnar, 2007).

**Ideal Work for Process Step Three: Isothermal Reversible Compression of $CO_2$**

The final step is the isothermal reversible compression of $CO_2$ to the final pressure of 2205 psia:

$$W_{ideal} = RT_2 \left[ \ln\left(\frac{P_1}{P_2}\right) + \ln\left(\frac{\phi_1}{\phi_2}\right) \right]$$  (8)

where

$P_1$     = Initial pressure (14.7 psia)

$\phi_1$     = Fugacity coefficient of $CO_2$ at the initial pressure and temperature

$P_2$     = Final pressure (2205 psia)

$\phi_2$     = Fugacity coefficient of $CO_2$ at the initial pressure and temperature

The first term in brackets of equation (8) is for an ideal gas while the second term corrects it to an actual gas. If $CO_2$ is treated as an ideal gas, the ideal work is about 20 % higher than if a more rigorous equation of state is used. Therefore, for these calculations the Peng Robinson equation of state was used to determine the fugacity coefficients and resulting minimum work for isothermal compression of $CO_2$.

## 3.0 MINIMUM WORK REQUIREMENTS FOR $CO_2$ CAPTURE AND COMPRESSION

Table 1 presents some example results for the calculation of the minimum work required to separate $CO_2$ from flue gas and compress it to 2205 psia using the previously described methodology.

Table 1. Minimum Work Requirements for Four Example Cases

|  | Case I | Case II | Case III | Case IV |
|---|---|---|---|---|
|  |  |  |  |  |
| Flue Gas Temperature, F | 140 | 300 | 140 | 300 |
| Stack Gas Temperature, F | 104 | 104 | 104 | 104 |
| Surroundings Temperature, F | 85 | 85 | 65 | 65 |
|  |  |  |  |  |
| Minimum Work, kJ/mol |  |  |  |  |
| Step 1: Cooling Flue Gas | 0.34 | 4.92 | 0.52 | 5.80 |
| Step 2: Separation of CO2 | -7.09 | -7.09 | -7.09 | -7.09 |
| Step 3: Compression of CO2 | -10.72 | -10.72 | -10.72 | -10.72 |
| Total: | -17.47 | -12.89 | -17.29 | -12.01 |

Case I represents a typical case where the flue gas is exiting a wet FGD unit at about 140 °F. Case II shows that the minimum work is lower if the process begins with hotter flue gas upstream of any desulfurization unit. Cases III and IV show the relative insensitivity to choice of ambient temperature at which heat is rejected to the surroundings.

The figures in Table 1 also assume that no "free" low level heat is available. The impact of having low level heat available depends primarily on how much heat is available and its temperature. The maximum amount of reduction in minimum work for the overall process that can be gained from use of low level heat is given by the following equation:

$$W_{ideal} = Q_w \left( \frac{T_w - T_o}{T_w} \right) \tag{9}$$

where

$Q_w$ = The amount of low level heat available

$T_w$ = The temperature at which low level heat is delivered to the process

$T_o$ = Temperature of the surroundings

One of the biggest potential sources of low level heat is the flue gas itself. As an example, if low level heat could be recovered by cooling the flue gas from 300 °F to 200 °F, this represents a potential heat source of about 14.7 kJ/mol of $CO_2$ captured, based on 13 % $CO_2$ in the flue gas and 90 % capture. Using an average temperature of 250 °F for $T_w$ and 85 °F for $T_o$ results in a potential reduction of minimum work of about 3.4 kJ/mol $CO_2$ captured. This represents about 19 % reduction in the total minimum work from a baseline requirement of 17.5 kJ/mole. This example, while not rigorous, shows that it takes a very large source of low level heat to cause a significant reduction in

the minimum work required for $CO_2$ capture. This example also shows that processes which could economically capture $CO_2$ from the hot flue gas have a thermodynamic advantage over those that rely on treating cooler gas (e.g., downstream of a wet FGD unit).

The simplified calculations in Table 1 did not include the effect of condensing water. If a process cools the flue gas and produces a condensed water stream, then the minimum work is slightly less than the values shown in Table 1. Although the calculations are more complex and not presented in detail here, the effect of accounting for the condensed water is to reduce the minimum work required by as much as 2 or 3 kJ/mole of $CO_2$ captured.

In conclusion, the minimum ideal work required to capture and compress $CO_2$ is in the range of about 10 – 17 kJ/mole $CO_2$ captured for the conditions studied, depending on whether or not water is condensed in the process and at what temperature the flue gas is fed to the $CO_2$ capture system. The next section shows what this range of minimum work translates to in terms of the COE

4.0    MINIMUM RESULTING IMPACTS ON COE

Supplying the minimum work required to capture and compress $CO_2$ and paying for the required equipment for the process will increase the COE. For this study, it is assumed that the minimum work will be provided from the associated power plant, either in the form of electricity to run compressors and other equipment, or in the equivalent amount of steam, or some combination of both. This demand for electricity or steam from the power plant effectively reduces the output of the power plant.

A typical coal-fired power plant has approximately 20,600 moles (gram-moles) of uncontrolled $CO_2$ emissions per net MW-hr electricity produced (DOE, 2006). If 90 % of this $CO_2$ is captured, then applying the estimated range of 10 – 17 kJ/mol $CO_2$ results in a minimum work requirement of 0.0515 – 0.08755 MW-hr per net MW-hr electricity

generated. For a net 500 MW plant this means that a minimum of 26 – 44 MW of work must be supplied to the $CO_2$ capture/compression system.

For each MW of work supplied to the $CO_2$ capture/compression system, some de-rating of the power plant will occur. The amount of de-rating will depend on the relative thermodynamic efficiencies of the power plant and the $CO_2$ capture/compression system. In addition, the de-rating will depend on how much of the work is supplied in the form of electricity versus the equivalent amount of heat (from a portion of the power generation steam or from other low level heat sources). If all of the minimum work is supplied in the form of electricity from the power plant, then the power plant would be de-rated by more than 1 MW for each MW of work required due to the thermodynamic inefficiencies of the $CO_2$ capture/compression system. For example, a typical electric-driven multistage compressor might be about 70 % efficient compared to the ideal minimum work of reversible isothermal compression, resulting in a de-rating of 1.45 MW per MW minimum work required.

Conversely, if all of the minimum work is supplied in the form of steam from the power plant, and further assuming that the thermodynamic efficiency of the $CO_2$ capture/compression system is the same as the thermodynamic efficiency of the power plant, then 1 MW of de-rating will occur for each MW of minimum work required. With this assumption, a net 500 MW plant would be de-rated by a minimum of 26 – 44 MW to a net output of 456.22 – 474.25 MW, resulting in a 5.4 - 9.6 % increase in COE due to the minimum work requirements (and not including any contribution from the capital cost of the equipment). In practice, the best estimates for commercial processes show much lower thermodynamic efficiencies, as evidenced by reductions in the overall power plant output in the neighborhood of 28 % , or about 140 MW for this example (DOE, 2006).

In conclusion, thermodynamic analysis of the $CO_2$ capture and compression process have shown that the minimum thermodynamic work required is equivalent to about 10 – 17 kJ/mol $CO_2$ captured. This leads to minimum expected increases in COE of about 5.4 – 9.6 % assuming 1 MW of de-rating of the power plant per MW of ideal work required

(not including the significant increases in COE that result from the capital cost for the $CO_2$ capture and compression equipment). Typical thermodynamic efficiencies for separation process (e.g. distillation) are less than 20 % (Shinnar, 2007). With typical thermodynamic efficiencies for separation processes included, the actual COE increase is expected to be 20 % or more. Capital costs for current absorption-based technology has been reported to be about $0.01/kWhr, or roughly another 20 % increase in COE (DOE, 2006).

## 5.0   ACKNOWLEDGEMENTS

## 6.0   REFERENCES

DOE/NETL. "Carbon Capture and Sequestration Systems Analysis Guidelines", April 2005.

Smith, J.M., and H.C. Van Ness. Introduction to Chemical Engineering Thermodynamics, 3rd ed., McGraw-Hill Book Company, New York, 1975.

DOE/NETL- 401/120106, "Carbon Dioxide Capture from Existing Coal-Fired Power Plants", December 2006.

Shinnar, R., and F. Citro. "Up Front, Efficient Technology Evaluation: It's What's Needed to Prevent Futile Investments", Chem. Engr. Prog., Feb. 2007.

Appendix II – Report from Babcock and Wilcox on Mass transfer and absorption performance

# IONIC LIQUIDS: BREAKTHROUGH ABSORPTION TECHNOLOGY FOR POST-COMBUSTION $CO_2$ CAPTURE

## $CO_2$ CONTROL LAB EXPERIMENTAL INVESTIGATION

**FINAL REPORT**

**PREPARED FOR:**
UNIVERSITY OF NOTRE DAME

**PREPARED BY:**
LISA M. RIMPF

DATE ISSUED: 2 NOVEMBER 2012

REPORT BWRC:2012:R002FP7006:03

**RCD1466**

**Babcock & Wilcox Research Center**
180 South Van Buren Avenue
Barberton, OH 44203-0622

## DISCLAIMER

This report was prepared by Babcock & Wilcox Power Generation Group, Inc. for the University of Notre Dame.  Neither Babcock & Wilcox Power Generation Group, Inc., the University of Notre Dame, nor any person acting on their behalf:

a)  Makes any warranty or representation, express or implied, or assumes any legal liability or responsibility for the accuracy, completeness, or usefulness or any information, apparatus, product, or process disclosed, or represents that its use would not infringe privately owned rights; or

b)  Assumes any liabilities with respect to the use of, or for damages resulting from the use of, any information, apparatus, method or process disclosed in this report.

# TABLE OF CONTENTS

# LIST OF FIGURES

# LIST OF TABLES

## 1.0 INTRODUCTION

### 1.1 BACKGROUND

Ionic liquids are molten organic salts in their pure state near ambient conditions due to a characteristic low melting point. These compounds are anhydrous, generally immiscible with water, and should not be mistaken for ionic solutions. They possess negligible vapor pressure and are therefore non-volatile. Ionic liquids (IL) have gained popularity in a variety of industrial applications because of the ability to tune physicochemical properties by selecting task specific cations and anions. Attributable to the variety of possible cation and anion combinations that can be paired, there are essentially an infinite number of molecules that can by synthesized. Termed "designer solvents," ionic liquids can be optimized for their intended purpose using chemistry fundamentals.

The Babcock & Wilcox Company (B&W) gained interest in ionic liquids for post-combustion $CO_2$ scrubbing at the *5th Annual Conference on Carbon Capture and Sequestration* in Washington D.C. after a presentation by Dr. Joan F. Brennecke from the University of Notre Dame. The talk, "*Carbon Dioxide Capture from Flue Gas Using Ionic Liquids,*" focused on a novel type of solvent which can be employed as an absorbent for $CO_2$ capture. This work, funded partially under a Phase I grant from the U.S. Department of Energy's (DOE) National Energy Technology Laboratory (NETL), demonstrated that ionic liquids have the potential to possess favorable attributes, and thus show promise for post-combustion $CO_2$ capture. Immediate interest led to on-site collaboration discussions followed by a more thorough technology evaluation.

Subsequently, B&W teamed with faculty from the Department of Chemical and Biomolecular Engineering at the University of Notre Dame and other industry partners in the preparation of a proposal entitled "*Ionic Liquids: Breakthrough Absorption Technology for Post-Combustion $CO_2$ Capture*" submitted in 2006 under the U.S. DOE solicitation DE-PS26-06NT42829-2, "*Novel Technology and Commercially Focused Approaches to $CO_2$ Capture and Separation for Existing and Future Carbon Based Electric Generation Power Plants.*" The project was successfully awarded to Dr. Edward Maginn as the Principal Investigator with contract DE-FC26-07NT43091 beginning on March 1, 2007. The contract was amended on multiple occasions to revise partnership changes, financial commitments, scope adjustments, and a schedule extension with completion date of September 30, 2012 nearly three years past the original timetable.

Separately, B&W continued along a parallel course of internal development aimed predominantly on aqueous amine-based solutions. The work to support this effort focused on finding better solvents along with improving process design and making better use of heat sources in the power plant to improve regeneration energy and the overall economics. A major endeavor was directed at identification, screening, and selection of an advanced solvent with beneficial corrosion characteristics, limited environmental impact, durability and longevity. RSAT, a term coined by B&W, stands for regenerable solvent absorption technology and refers to a class of post-combustion processes wherein $CO_2$ is removed from combustion flue gases using a liquid solvent through a traditional absorption-stripping scheme as drawn in Figure 1.
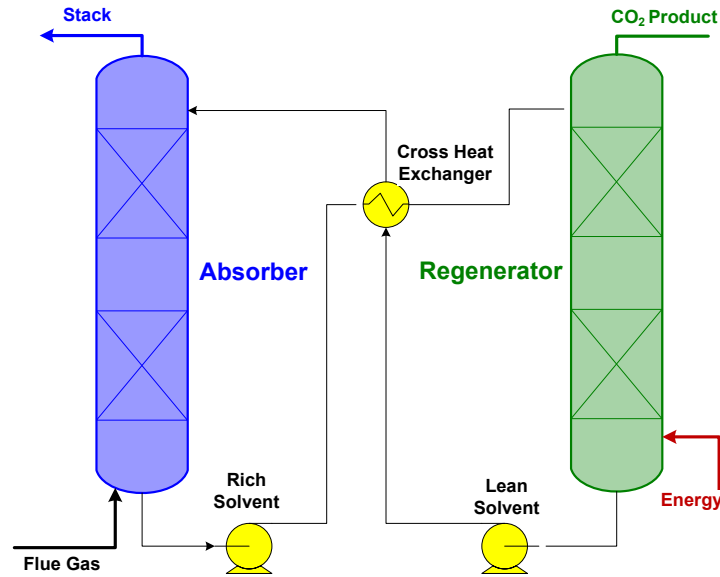
**Figure 1. Generic RSAT$^{TM}$ Process**

The development pathway, illustrated in Figure 2, depicts the stage-gate approach to carry ideas from discovery and screening through commercialization. A variety of tools, colored red, were put in place by B&W to support RSAT process development activities and gain direct, hands-on experience. Significant company resources and funding were devoted to the creation of these tools which strategically positioned B&W to conduct independent evaluation and characterization.
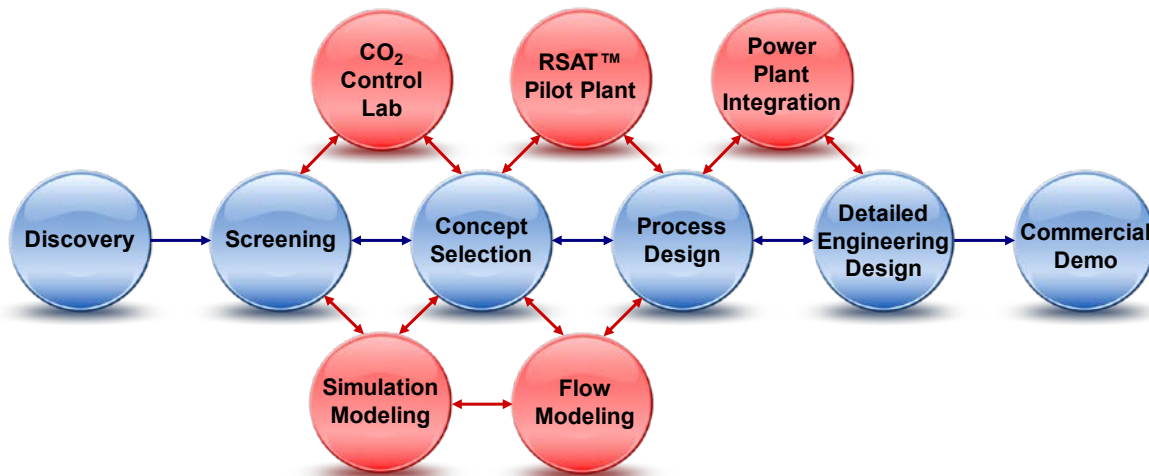


**Figure 2. B&W Development Program for RSAT Process with Tools**

It is the mutual interest in a superior regenerable solvent for post-combustion $CO_2$ capture from power plants where the synergy aligns between B&W and the University of Notre Dame ionic liquid project. The experience of B&W in the power generation industry along with the innovation of the University of Notre Dame researchers leverages the expertise to understand the challenges for large-scale deployment.

## 1.2   OBJECTIVE

The overall goal of the project is to develop an ionic liquid(s) that can capture at least 90% of the carbon in the fuel fed to a coal-fired power plant with economics that show promise toward meeting U.S. DOE program goals of no more than a 35% increase in cost of electricity.  A preliminary systems analysis study identified target properties of ionic liquids that should result in significant cost savings for $CO_2$ capture compared to traditional amine-based solvents.  The ideal absorbent possesses the beneficial properties of several different technologies without the drawbacks.  As with solid adsorbents, the ideal liquid absorbent should be non-volatile to simplify regeneration and minimize loss of material.  Like physical absorbents, it should have a low energy requirement for regeneration.  The capacity should be high and other physical properties of the absorbent such as viscosity, heat capacity, and decomposition temperature should be in a range so as to make the absorbent compatible with conventional processing equipment.  Finally, the ideal absorbent should have a reasonably low cost, be stable and non-corrosive.

To meet the objectives of the project, a research and development plan was outlined to:

- fundamentally design molecules through computer  simulations.
- synthesize promising compounds in the laboratory.
- measure or accurately estimate relevant physical properties, including: $CO_2$, $N_2$, $H_2O$, $NO_2$ and $SO_2$ solubility as a function of temperature and pressure, mixed gas solubility, viscosity, heats of absorption, heat capacity, mass transfer coefficients, reaction rates for chemically complexing systems, thermal decomposition, long-term chemical stability and corrosivity.
- complete a detailed systems and economic analysis study in accordance with U.S. DOE-NETL's Carbon Capture and Sequestration Systems Analysis Guidelines.
- demonstrate feasibility with a continuous lab-scale apparatus.
- develop a path forward for commercialization.

The success of ionic liquids as a viable technology requires increasing the knowledge base on the chemical characteristics and on the competitiveness of processes which utilize ionic liquid based absorbents for $CO_2$ capture from flue gas streams compared to commercial amine-based systems.

From B&W's perspective, the primary purpose of participating in this project was the opportunity to conduct a comprehensive evaluation of this emerging technology as it evolves, offer advice on practical power plant considerations, build a relationship with the project team and, if appropriate, negotiate a preferred position for commercialization in the marketplace.

## 1.3   SCOPE

The B&W Power Generation Group Research Contract Department committed to at least $200,000 of direct in-kind cost share through RCD1466 (R002FP7006) over the course of the program.  B&W's scope included participation in project planning and status meetings either via teleconference or in-person as deemed necessary, review and comment on results, along with providing realistic insights from an OEM (original equipment manufacturer) perspective.  In addition to general participation in project activities, B&W specifically provided guidance to design a laboratory-scale pilot test facility at the University of Notre Dame to quantify the performance of promising solvents in both the absorption and stripping processes under representative conditions.  Furthermore, corrosion screening analysis on multiple ionic liquid samples was also conducted.  After nearly six years of

development and testing, several breakthrough formulations were achieved in the University of Notre Dame laboratories. These innovative aprotic heterocyclic anion (AHA) compounds do not exhibit a viscosity increase after $CO_2$ absorption as was a previous difficulty with prior chemically complexing ionic liquids. Consequently, the scope of B&W's involvement was expanded as result of this promising discovery to include additional testing at the Babcock & Wilcox Research Center (BWRC) in Barberton, Ohio. This allowed for direct, hands-on experience and comparison with not only data from the University of Notre Dame but also with solvents previously investigated by B&W.

A single ionic liquid was identified by the University of Notre Dame for larger batch production based upon its favorable characteristics along with the ability to synthesize a 'significant' volume. The descriptive chemical name Trihexyltetradecylphosphonium 2-cyanopyrrolide can be more simply abbreviated as [P66614][2CNPYL] or [$P_{66614}$][2-CNpyr] and may also be referred to as NDIL0046 for intellectual property protection. Up to this point only gram quantities had been prepared and the challenge to synthesize 25 liters was a significant step-change. The proprietary and non-commercial research sample ionic liquid was manufactured under agreement by Koei Chemical Company, Limited in Japan at a cost of US$50,000 and shipped to the University of Notre Dame in June 2012. A photograph of the original bottle label is pictured in Figure 3. Approximately 14 Liters, nearly half of the total quantity, was sent as a hazardous material to BWRC in August 2012 using a 5-gallon tote, shown in Figure 4.



**Figure 3. Original Bottle Label**     **Figure 4. Sample Received at B&W**

This particular ionic liquid was subjected to characterization tests at B&W using the Wetted-Wall Column and RSAT Simulator in the $CO_2$ Control Lab and existing corrosion facilities to compare with previously tested solvents as well as substantiate performance claims. The primary content of this document encompasses the work conducted at BWRC in the $CO_2$ Control Lab.

## 2.0 METHODS

### 2.1  CO$_2$ CONTROL LAB

The CO$_2$ Control Lab was built in 2007 to support B&W's efforts to develop an RSAT process for the capture of CO$_2$ emitted from coal-fired power plants.  Activities in the CO$_2$ Control Lab focus on post-combustion capture by scrubbing with a liquid solvent.  The purpose of this laboratory is to provide information about solvent performance and create a normalized platform for the direct comparison of solvents under similar conditions employing the same installed equipment.  The facility is equipped with a LabVIEW™ and IOtech™ data acquisition system and is instrumented to gain key measurements.  Work is conducted in accordance with normal business practice outlined in the BWRC Standard Practice Quality Assurance Manual which is compliant to ISO-9001:2008.

### 2.1.1  Handling

A visit to the University of Notre Dame on July 16, 2012 by George Farthing and Lisa Rimpf allowed a preview of NDIL0046.  Ionic liquids were generally unfamiliar to B&W; therefore, speaking directly with the researchers and students offered insight regarding environmental, health and safety (EH&S) considerations and practical operating tips before receiving the sample in Barberton.  The dark-brown colored ionic liquid was observed flowing through the laboratory pilot system absorption column.  This apparatus is a simplified resemblance to the RSAT Simulator.  A few obvious challenges were identified.  The NDIL0046 is approximately 500 cP at room temperature and demonstrated a likeness to molasses while revealing its flooding potential.  However, there is data and experience that indicates the viscosity can be decreased to a more manageable range, closer to 100cP, by raising the temperature to nominal CO$_2$ absorption conditions of 40°C (1).  Furthermore, NDIL0046 is insoluble in water, so cleaning with an organic solvent is required.  Recommendations included methanol, ethanol, or acetone. This automatically implied a significant increase of hazardous waste generation volume.

A Safety and Environmental Evaluation Request (SEER) and Job Safety Analysis (JSA) were completed per BWRC project requirements.  While a copy of the material safety data sheet (MSDS) was provided, in Appendix 6.1, limited information is available based upon the developmental status of this compound.  Standard laboratory engineering controls, such as fume hoods, and personal protective equipment (PPE) like nitrile gloves, lab coat, and safety glasses per usual practice were deemed sufficient.  Any collected liquid waste was categorized hazardous for disposal and was subjected to third-party analytical testing for profiling.

The viscosity of NDIL0046 is significantly higher than previously investigated CO$_2$ capture solvents in the CO$_2$ Control Lab.  This raised some operability concerns since this was a 'first of a kind.'  Water soluble solutions to mimic the higher viscosity ionic liquid were first investigated to determine testing feasibility and facilitate cleaning. High-concentration aqueous sugar (sucrose) solutions were prepared at 65wt% and 70wt% according to Table 1 and observed for behavior.

**Table 1. Sucrose Solutions: Composition, Viscosity, Density at 20°C (2)**

| % Sucrose | Concentration | Viscosity | Density |
|:---:|:---:|:---:|:---:|
| *w/w* | *gm/L* | *μ* | *ρ* |
| 0 | 0 | 1.00 | 0.998 |
| 5 | 50.9 | 1.144 | 1.018 |
| 10 | 103.8 | 1.333 | 1.038 |
| 15 | 158.90 | 1.589 | 1.059 |
| 20 | 216.20 | 1.941 | 1.081 |
| 25 | 275.90 | 2.442 | 1.104 |
| 30 | 338.10 | 3.181 | 1.127 |
| 35 | 402.90 | 4.314 | 1.151 |
| 40 | 470.60 | 6.150 | 1.176 |
| 45 | 541.10 | 9.360 | 1.203 |
| 50 | 614.80 | 15.400 | 1.230 |
| 55 | 691.60 | 28.02 | 1.258 |
| 60 | 771.90 | 58.37 | 1.286 |
| **65** | **855.60** | **146.90** | 1.316 |
| **70** | **943.00** | **480.60** | 1.347 |
| 75 | 1034.00 | 2323.00 | 1.379 |

These sugar solutions were syrupy yet fluid and pourable; this was encouraging. Viscosities were estimated using a Cannon-Fenske Viscometer to be near the values in Table 1.  Initially the 65wt% sugar solution was charged to the WWC per normal operating protocol. The same was subsequently done with the 70wt% sugar solution. For each, the apparatus did function properly with a bit of coaxing.  The liquid film was quite thick but appeared stable.  The 4 standard liters per minute (slpm) gas flow rate would be maintained; however, the liquid flow rate was significantly reduced from the nominal 180mL/min to minimize pressure drop in the small-diameter stainless steel tubing supplying solvent to the WWC. The direct relationship between flow rate, viscosity and pressure drop is described by the Hagen-Poiseuille Equation, shown here:

$$\Delta P = \frac{32\mu\bar{V}L}{D^2} \tag{1}$$

where, $P$ = pressure
$\quad\quad\mu$ = viscosity
$\quad\quad\bar{V}$ = flow rate
$\quad\quad L$ = length of tube
$\quad\quad D$ = tube diameter

It was determined that NDIL0046 testing could be attempted in the Wetted-Wall Column and experiments would proceed with a reduced liquid flow rate to maintain a reasonable liquid pressure of ≤ 50 psig at the pump discharge.

Upon arrival, the NDIL0046 appeared more fluid than when observed at the University of Notre Dame and was easily transferred from the tote with a peristaltic pump and platinum-cured flexible silicone tubing. The sample was first manipulated by simple agitation on a stirring plate; there was at least some indication that the material could be shear thinning although this was not investigated in detail. A 100mL graduated cylinder was then filled with 0.24-inch random laboratory Pro-Pak Distillation Packing from the Cannon Instrument Company as shown in Figure 5.



**Figure 5. Laboratory Random Packing**

Approximately 50mL of ionic liquid was poured over the packing to observe the behavior. A small amount of flooding presented even at a slow pour rate likely due to vapor lock. Channeling was also evident as some pieces were not wetted. The ionic liquid did flow better than expected based upon previous observation. However, the 'sticky' behavior was apparent as the ionic liquid adhered to the glass and tubing walls.

Gas washing bottles are used to gravimetrically prepare solvents with accurate $CO_2$ loading at room temperature. A known mass of solvent is charged to the vessel. Pure $CO_2$ is sparged to the bottom through a perforated glass frit. Gas bubbles rise through the batch of solvent and the absorption reaction takes place. The gas washing bottle placed on a balance measures the $CO_2$ mass uptake.
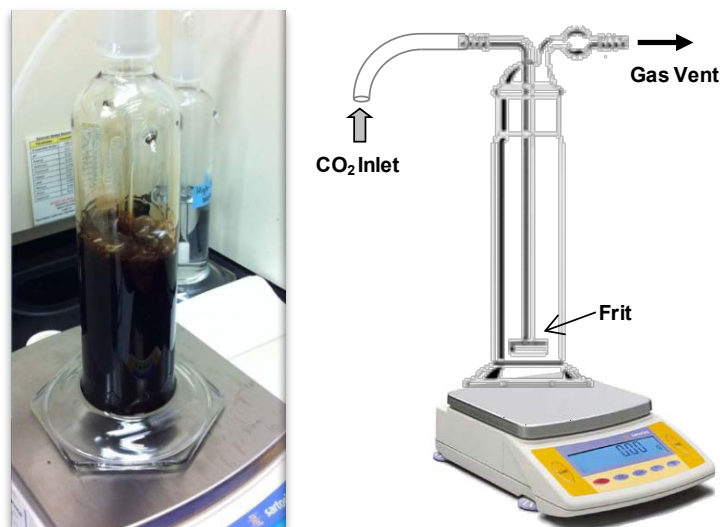


**Figure 6. Gravimetric $CO_2$ Loading**

It was unclear if this technique would be valid for the NDIL0046 based upon modest heat of reaction and concerns of off-gassing.  To verify that this standard practice was still viable, $CO_2$ was supplied to 250 grams NDIL0046, as shown in Figure 6, and the mass increase recorded with time until saturated at 16.3 grams.   This equated to a $CO_2$ loading of 0.852 mole $CO_2$/mole NDIL0046, nearly maximum capacity (1).  Foaming tendency was evident as larger bubbles formed at the surface and smaller pin-hold bubbles were present in the bulk.  The gas washing bottle remained on the balance overnight undisturbed to observe if any weight loss occurred; no change was documented at ambient conditions.  Furthermore, the viscosity remained unchanged as anticipated.

The method of gravimetric $CO_2$ loading calculation is shown here for example:

$$CO_2 \ Loading = \ \alpha = \frac{mole \ CO_2}{mole \ active \ site} \qquad (2)$$

$$NDIL0046 \ Molecular \ Weight = \ 574.95 \ gram/mole \qquad (3)$$

$$CO_2 \ Molecular \ Weight = \ 44.01 \ gram/mole \qquad (4)$$

$$NDIL0046 = \ 250g \cdot \frac{mole}{574.95 \ g} = 0.435 \ mole \qquad (5)$$

$$CO_2 = \ 16.3g \ \cdot \frac{mole}{44.01 \ g} = 0.370 \ mole \qquad (6)$$

$$\alpha = \frac{0.370 \ mole \ CO_2}{0.435 \ mole \ IL} = 0.852 \ \frac{mole \ CO_2}{mole \ IL} \qquad (7)$$

Initial screening assessments confirmed some of the obstacles, including: high viscosity, foaming tendency, stickiness, dark staining on some surfaces, and cleaning challenges.  Experiencing them personally was certainly beneficial to better understand potential limitations and handling techniques.  Yet, these scoping tasks also provided a sense of reassurance that continuing with testing in the Wetted-Wall Column, as proposed, was even possible before uploading in the system.

### 2.1.2   Wetted-Wall Column

The Wetted-Wall Column (WWC) is a bench-scale apparatus that is useful in evaluating and designing reactive absorption processes.  It is a differential gas-liquid reactor wherein $CO_2$ absorption or desorption can be studied under precisely controlled conditions. Capabilities include determining kinetic and thermodynamic information, which are key parameters in screening potential solvents for $CO_2$ capture.  Contact times are typically on the order of 0.5 seconds, effectively simulating the hydraulics of a packed column. The main advantage is that, due to simple geometry, the area of contact between the gas and liquid is accurately known which makes calculations from first principles possible.

The column is housed in a circulating silicone oil bath which is maintained isothermal by a temperature controller. Gravimetrically prepared solvent at some predefined $CO_2$ loading is charged to the system. The liquid is circulated using a magnetic drive gear pump. While traditionally operated at a flow rate of 180mL/min, the high ionic liquid viscosity required a reduction of flow rate to 40 mL/min instead. As shown in Figure 7, solvent flows up through the vertical tube at the center, exits at the top, and continuously flows down over the outside surface of the tube in a thin film. The tube material of construction is stainless steel and has a diameter of 1.26 cm (0.5 inches). Solvent is counter-currently contacted with the gas which rises through the annular space around the tube.
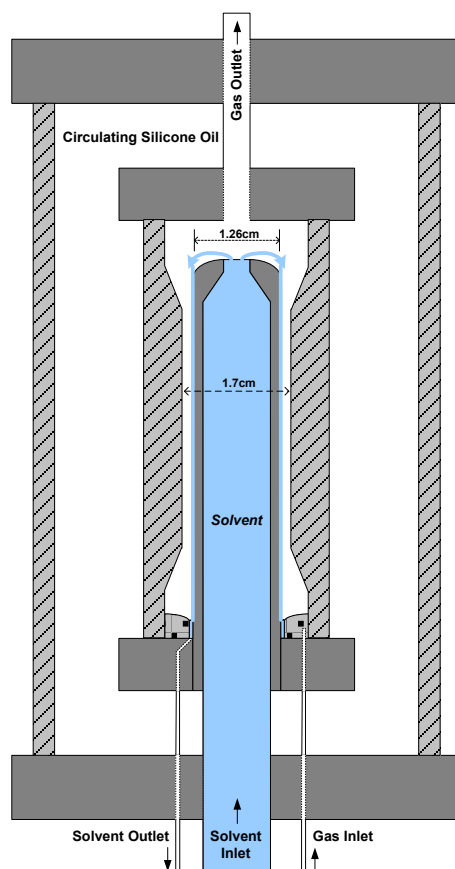


**Figure 7. Wetted-Wall Column Geometry**

Nitrogen and carbon dioxide are introduced to the system through separate mass flow controllers. Desired gas concentrations are achieved by adjusting the individual flow rates while maintaining the total gas flow rate at 4 slpm near atmospheric pressure. Varying the inlet $CO_2$ concentration allows testing under both absorption and desorption conditions. The exiting gas flows to an infrared (IR) gas analyzer for outlet $CO_2$ measurement. A simplified system diagram is drawn in Figure 8; the entire apparatus is contained within a portion of an 8-foot fume hood.
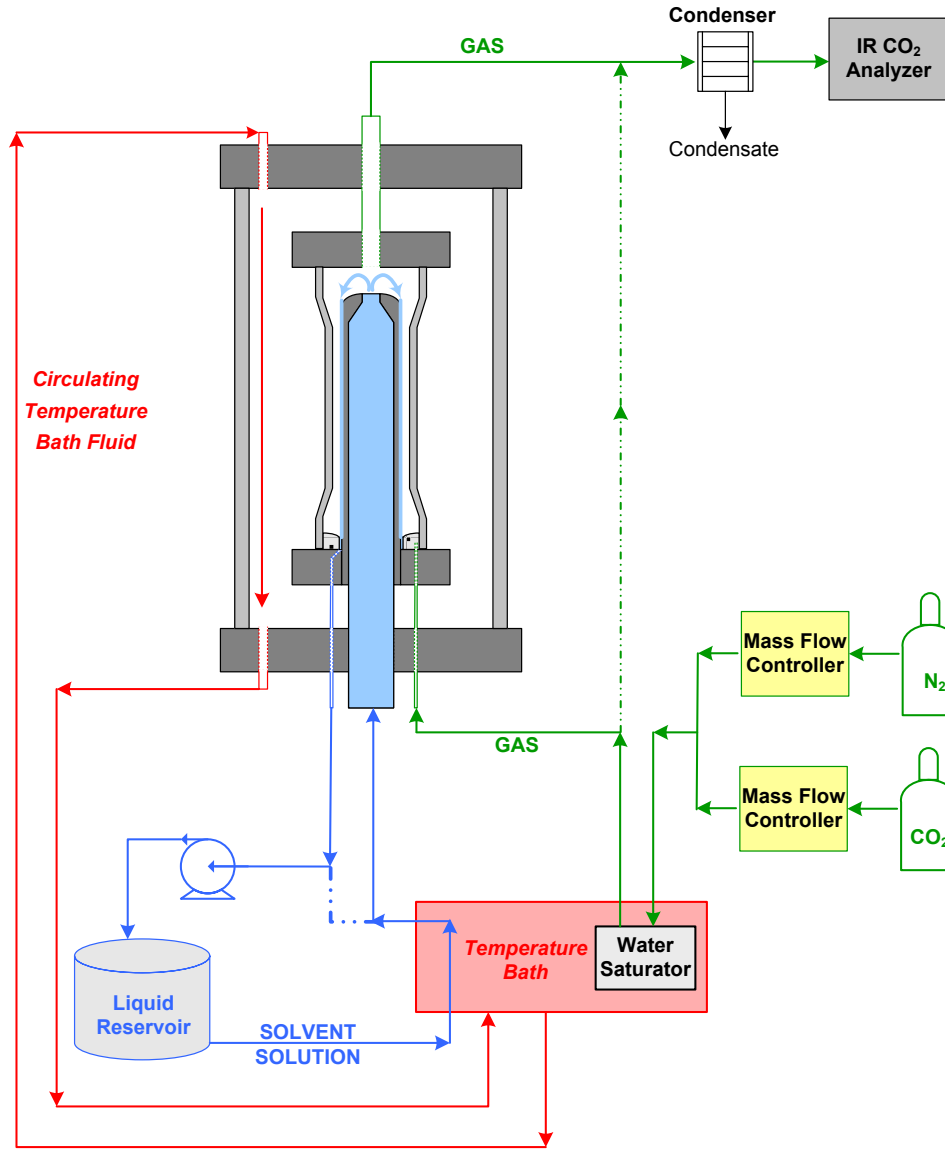
**Figure 8. Wetted-Wall Column Simplified System Diagram**

The $CO_2$ flux, $N$, is calculated for each data point by taking the difference in partial pressure at the gas inlet and outlet of the column; this represents the rate at which $CO_2$ is either absorbed or desorbed from the solvent and can be expressed with Equation (8) :

$$N = K_G A(P_{CO_2} - P^*_{CO_2}) \qquad\qquad \textbf{(8)}$$

Plotting flux as a function of $CO_2$ partial pressure in the gas phase, $P_{CO_2}$, forms a straight line. A sample of this plot can be seen in Figure 9.
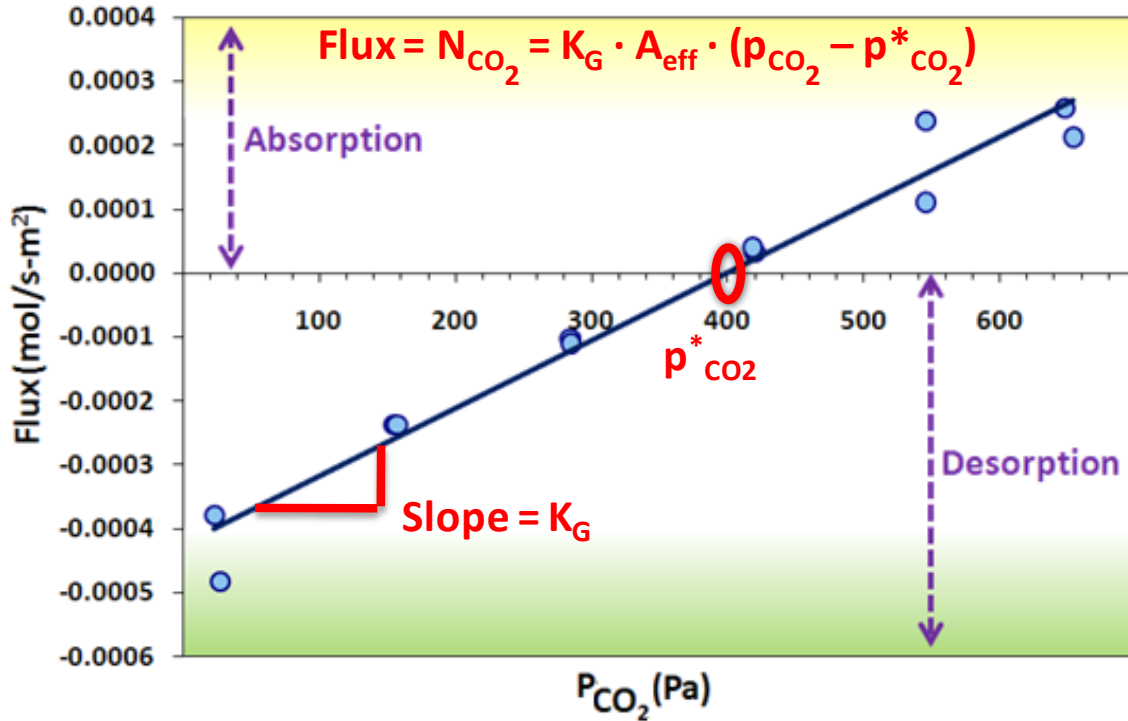
**Figure 9. Sample Wetted-Wall Column Data**

Since the area of gas-liquid contact is known by design, the overall mass transfer coefficient, $K_G$, can be extracted from the slope of the line. The point at which the line intercepts the x-axis defines the thermodynamic equilibrium value of $CO_2$ vapor pressure, $P_{CO_2}^*$, in the liquid phase for the given conditions. The equilibrium partial pressure is when the solvent neither absorbs nor desorbs and is unique for each solvent, concentration, $CO_2$ loading and temperature combination.

Liquid film mass transfer coefficient enhanced with reaction, $k_g'$, can be extracted by applying Equation (9),

$$\frac{1}{K_G} = \frac{1}{k_g} + \frac{1}{k_g'} \tag{9}$$

where $k_g$ is the gas film mass transfer coefficient whose correlation was obtained through a separate study with good accuracy (3). This $k_g$ correlation has been used for all data analysis and is unique to the apparatus.

Under pseudo-first order reaction assumptions, the kinetic reaction rate constant is embedded within the $k_g'$ term (3). Initial evaluation of solvent performance can be approximated by $k_g'$ comparison.

### 2.1.3    RSAT™ Simulator

The RSAT Simulator is a fully-functional RSAT process, albeit at very small scale.  The test facility is used to investigate promising solvents which have shown encouraging results in the Wetted-Wall Column. The system contains most of the unit operations equipment that would be installed at larger scale and offers the versatility to operate in a variety of modes thereby providing excellent flexibility for development work.  Solvent recycled through the entire system in a fully-integrated scheme allows the process to be studied under realistic conditions for the first time.  Conversely, decoupling to a batch-wise configuration permits the analysis of absorption or stripping independently.

One of the main objectives of conducting solvent studies with the RSAT Simulator is to evaluate solvent performance in a timely manner by using reasonable liquid quantities, especially when solvent price and availability is a limiting factor. The level of commitment for operation requires a significant effort increase over beaker-type quantities but provides both qualitative and quantitative data that closes the gap between fundamental experiments and the step-change leap to a pilot plant.

The RSAT Simulator is completely contained inside an 8-foot distillation fume hood and constructed predominantly of glass and stainless steel components.  The columns are a modular configuration consisting of 1-foot each glass sections joined by stainless steel flanges with penetrations, as shown in Figure 10.  The absorber column is 5-feet tall while the regenerator is only 4-feet in height due to the electrically powered reboiler at its base.  Both columns have a 2-inch internal diameter and are embedded inside a concentric cylinder, allowing the outer glass to serve as a heating and/or insulation jacket as photographed in Figure 11.  A customized DYM laboratory 316L structured packing made of sheet metal from Sulzer Chemtech, in Figure 12, is especially designed for small laboratory applications and is installed for maximum gas-liquid contact efficiency.  The system is designed to capture approximately 1 kilogram of $CO_2$ per hour.



**Figure 10. Modular Columns**     **Figure 11. Concentric Cylinders**     **Figure 12. Structured Packing**
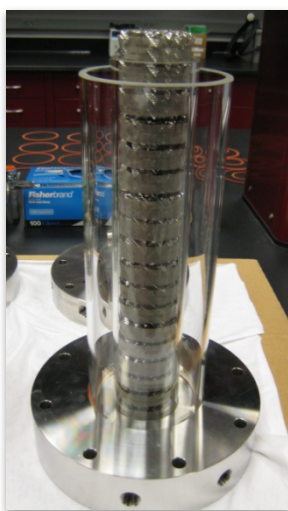
The main advantage of using glass is to conduct visual observations of hydraulics within the columns, such as: wettability, flooding, viscosity, foaming, and precipitation/crystallization along with other affects such as color change due to degradation on a real-time basis.

The process is manually controlled to manage temperatures, flows, and under most instances water balance. The generally employed flow sheet is shown in Figure 13 as utilized for previous test campaigns with aqueous solvent solutions.
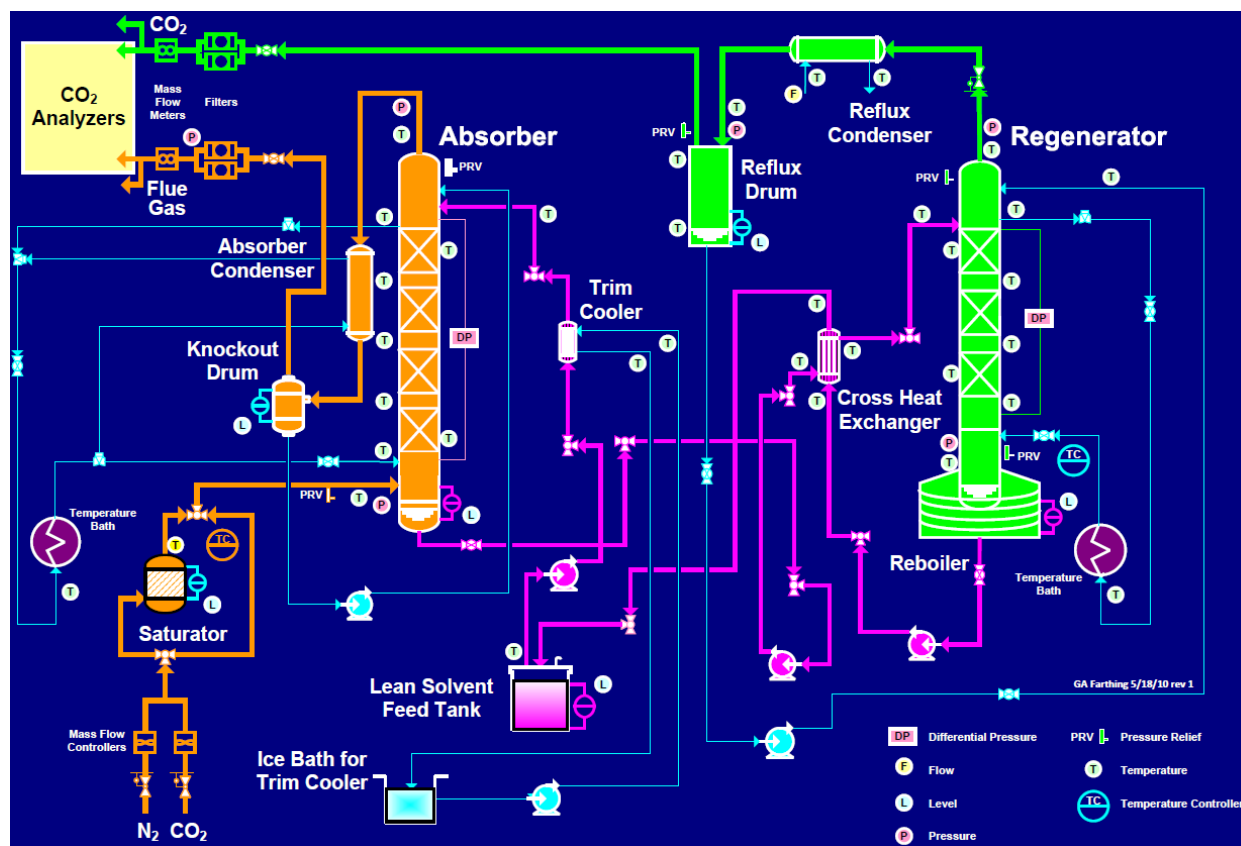


**Figure 13. RSAT Simulator Flow Sheet Schematic**

Lean solvent is fed from an inventory tank into the top of the absorber column; this incoming temperature can be controlled by use of a trim cooler. The liquid flowing down the packing is counter-currently contacted with a water saturated synthetic mixture of $CO_2$ and nitrogen that mimics typical power plant composition which enters the bottom of the absorber column. Absorber overhead condensate, captured by a heat exchanger, collects in a knockout drum and is returned to the absorber. The scrubbed outlet flue gas is sent to an IR gas analyzer to measure the reduced $CO_2$ concentration which can be directly translated to removal rate.

The rich solvent is withdrawn from the bottom of the absorber through a shell-and-tube cross heat exchanger and fed to the top of the regenerator column. The $CO_2$ is distilled via heating with a reboiler. Heating the solution not only causes the equilibrium solubility of $CO_2$ to decrease, but also evaporates some of the water. The water vapor reduces the partial pressure of $CO_2$ in the gas phase, thereby increasing the driving force for $CO_2$ desorption. The regenerated lean solvent passes through the opposing side of the previously mentioned cross heat exchanger and is recycled back to the liquid feed tank, making the process integrated by constant recirculation of the liquid solvent. The regenerator overhead flows through a cooling heat exchanger and condensate is collected in a reflux drum before returned to the column based on water balance and concentration requirements. The nearly pure $CO_2$ stream is exhausted to gas analysis.

Testing protocols were developed during 30wt% monoethanolamine (MEA) baseline characterization to evaluate operational performance. Parametric variations of liquid flow rate, superficial gas velocity, liquid-to-gas (L/G) ratio, and temperatures were adjusted to understand system limitations and capabilities. This approach laid the groundwork for future solvent evaluation and comparison. Absorber temperature profile, $CO_2$ removal rate in relation to the 90% target, and off-line chemical analysis for $CO_2$ loading, carrying capacity and solvent concentration offered quantitative insight regarding solvent behavior. Realistic energy penalties cannot be estimated due to limited resolution with reboiler power and heat losses due to conduction, large exposed surface area, and fume hood air movement.



**Figure 14. Installed RSAT Simulator**

The RSAT Simulator facility, pictured in Figure 14, was used as a model to construct the similarly assembled laboratory-scale absorption/regeneration system at the University of Notre Dame. As outlined in the Statement of Project Objectives, B&W served as an advisor to aid in the construction of this unit. Iterative discussions and visits back-and-forth between 2008 and 2010 focused on design considerations. A memo issued by B&W in May 2010 summarized equipment vendors, cost estimates, design files, and detailed photos to finalize installation plans.

## 2.2  CORROSION TESTING

Evaluation of corrosivity is reported elsewhere by E. Purusha Bonnin-Nartker in reports BWRC:2012:R002FP7006:01 and BWRC:2012:R002FP7006:02.

## 3.0 RESULTS AND DISCUSSION

### 3.1    WETTED-WALL COLUMN

The NDIL0046 was successfully tested in the Wetted-Wall Column at 40°C with two $CO_2$ loading conditions.  Although not without some challenges due to the high viscosity and foaming tendency, a bit of finesse compensated to achieve a smooth and stable film.  Concessions were made with a lower solvent flow rate of 40mL/min to manage the pressure drop, but this did not affect the outcome. Figure 15 captures images of NDIL0046 during operation.



**Figure 15. Wetted-Wall Column NDIL0046 Testing Images**

$CO_2$ loadings of 0.1 and 0.3 mole $CO_2$/mole NDIL0046 were selected based upon measured $CO_2$ absorption capacities to represent potential lean and rich conditions in the absorber (1).  While testing at 60°C would normally follow in progression, it was not evident that absorption was even possible given the isotherms (1).  Schedule limitations prevented additional experiments to further investigate. However, with these introductory data points, insight on performance for solvent comparison was achieved.

Figure 16 is a compilation of kinetic data obtained at 40°C for various solvents. The x-axis is the equilibrium partial pressure of $CO_2$ which corresponds to different $CO_2$ loading conditions. The y-axis plots liquid film mass transfer coefficient as $k_g^{'}$.  A higher $k_g^{'}$ value generally indicates faster kinetics and is primarily a function of $CO_2$ loading.  For the same solvent, the higher the $CO_2$ loading, the smaller the $k_g^{'}$ value will be.  Solvents with faster kinetics generally show consistently strong $k_g^{'}$ throughout the entire operational loading range.  However, $CO_2$ absorption kinetics are generally considered more important in the rich loading range than in the lean loading range mainly because $CO_2$ loading has a significant impact on absorption rate.  Therefore, comparison of $k_g^{'}$ at a $CO_2$ equilibrium partial pressure of 5000 Pa, indicated with a dotted line, gives a more straightforward rank of absorption kinetics for candidate solvents.
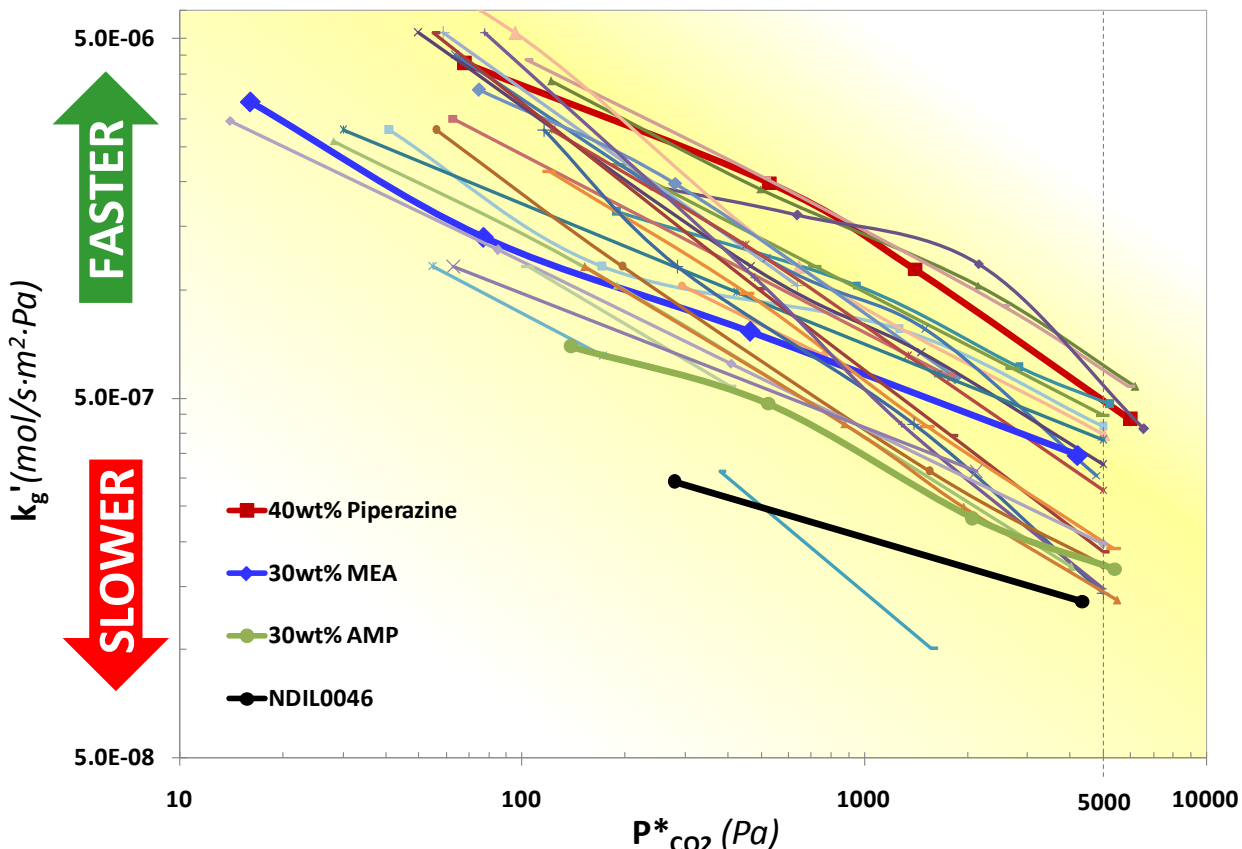
**Figure 16. Wetted-Wall Column Solvent Kinetics Comparison at 40°C**

The industry benchmark solvent, 30wt% MEA, appears in the middle of the graph. A number of advanced formulations demonstrate improved kinetic performance over this standard, including 40wt% Piperazine. Comparatively, NDIL0046 is slower than most of the previous amine-based solutions tested by B&W. Results are similar to the behavior of an unpromoted hindered amine as can be seen by the proximity to 30wt% AMP (2-amino-2-methyl-1-propanol). However, it is unclear if the poor performance is a result of high viscosity restricting mass transfer, chemical functionality impacting kinetics, or some combination of both. Either of these deficiencies could likely be adjusted by further selective tuning on the molecular design to improve upon NDIL0046.

Although there was still some apprehension regarding feasibility of operation, a decision was made to proceed with RSAT Simulator testing following completion of WWC experiments and clean-up.

## 3.2    RSAT™ SIMULATOR

The RSAT Simulator was configured with minor adaptations from its conventional scheme to facilitate testing of the NDIL0046. The top annular section of the absorber column was plumbed to circulate water at 40°C and help control the incoming solvent temperature. The regenerator column jacket was maintained at 120°C using a silicone oil bath to promote $CO_2$ desorption. Similarly, the reboiler was programmed with this same 120°C set point engaging only the bottom heating band. The water saturator on the incoming flue gas line was bypassed to avoid a separate water phase. The lean solvent tank was removed to reduce solvent hold-up; nearly 6 liters, compared to the normal 10-12 liters, was charged directly to the reboiler.

The RSAT Simulator proved challenging to operate in an integrated fashion with the NDIL0046, although several attempts with reasonable and timely modifications were undertaken. Limitations stemmed from the original design which anticipated operation with low viscosity fluids on the order of approximately ≤ 15cP. Liquid circulation rate with the installed peristaltic pumps was constrained by viscosity and pressure drop through the existing network of nominal 1/4-inch tubing diameter and even smaller heat exchanger restrictions. Minimal liquid flow rates and a high molecular weight did not encourage $CO_2$ absorption even when 100% $CO_2$ was supplied at 3 slpm. Taking measurements proved impractical since instruments, like mass flow meters and gas analyzers, were out of range under these conditions. On a more optimistic note, flooding was not observed and the ionic liquid flowed through the packing fairly well – better than expected, as shown in Figure 17.



**Figure 17. Wetted Packing**

Before shutting down, a tube from the regenerator overhead vent was redirected to a beaker of water where exhausting bubbles slowly evolved; this was a positive indication that $CO_2$ desorption was actually taking place. In an attempt to quantify this qualitative observation, a Bios Defender 530H external primary flow standard was connected and measured an average of 0.07 slpm $CO_2$ outlet flow. Recovered $CO_2$ was less than 3% of the supply to the absorber.

The system was decoupled and the absorber column operated separately as a once-through batch process. Neat ionic liquid was withdrawn directly from the 5-gallon tote using a magnetically driven gear pump and transported via a flexible 3/8-inch Teflon® lined stainless steel hose to the absorber inlet at the top of the column. This approach drastically minimized line restrictions and permitted unhindered flow. Figure 18 illustrates this arrangement.



**Figure 18. Decoupled Absorber Batch Configuration**

Conditions were carefully selected to align with a similar test case from the 30wt% MEA baseline characterization campaign, as can be seen in Table 2.

**Table 2. RSAT Simulator Test Conditions**

|  | 30wt% MEA | NDIL0046 |
|---|---|---|
|  | March 5, 2009 | September 11, 2012 |
| Liquid Flow Rate | 50 mL/min | 50 mL/min |
| Nitrogen Flow Rate | 6.5 slpm | 7.8 slpm |
| $CO_2$ Flow Rate | 0.75 slpm | 1.0 slpm |
| $CO_2$ Concentration | 10.3% | 11.3% |
| Gas Velocity | 0.22 ft/sec | 0.26 ft/sec |
| L/G | 5.2 | 4.4 |

Although there were some distinct differences, particularly that the MEA test was an integrated absorption/stripping process operated at steady state, a comparison of $CO_2$ removal rate provided the best appraisal. The $CO_2$ removal rate is calculated by using the difference in the $CO_2$ concentrations in the gas streams entering and exiting the absorber. The analogous MEA condition achieved 90% $CO_2$ removal. The NDIL0046 achieved an averaged 65% $CO_2$ removal rate as can be seen in Figure 19 where $CO_2$ removal is graphed with a blue colored line versus time as the experiment progressed. Outlet $CO_2$ concentration is also plotted on the secondary y-axis in green and decreases to approximately 3.6% $CO_2$ during the course of the experiment. The plots are inversely related, such that as $CO_2$ removal increases, the outlet $CO_2$ concentration decreases.
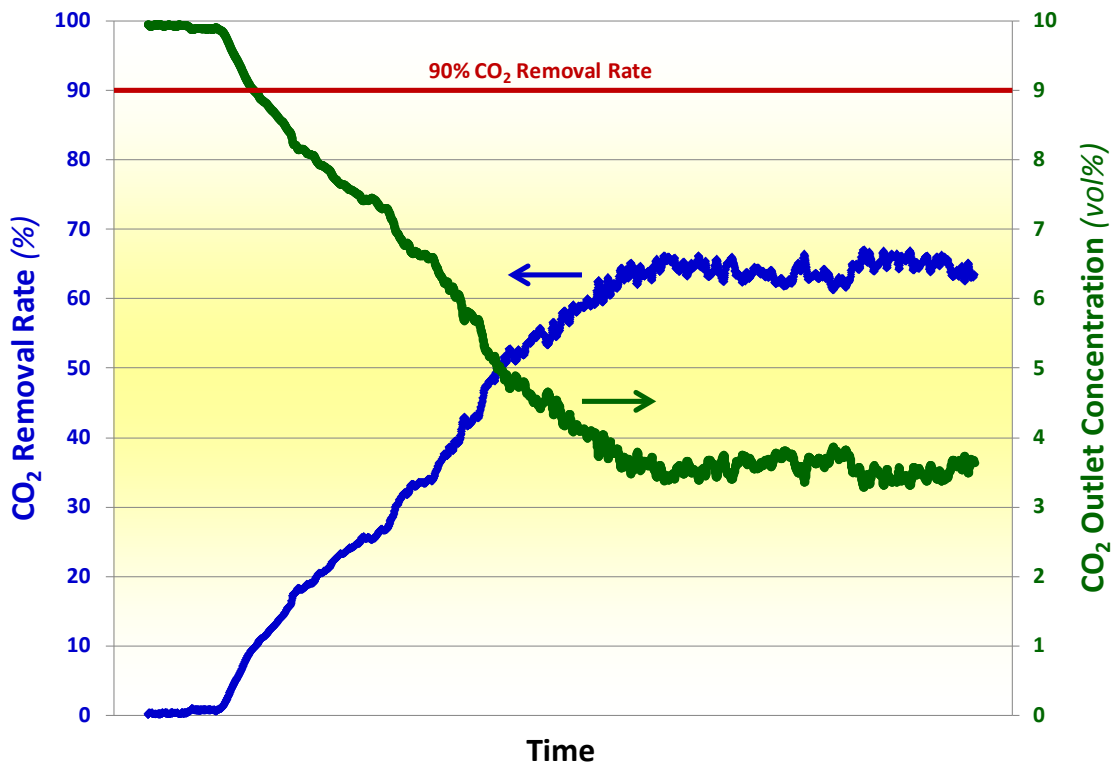


**Figure 19. NDIL0046 Absorption Performance**

Despite falling short of the 90% $CO_2$ removal rate, the outcome was consistent with the mass transfer data obtained in the Wetted-Wall Column. Additional absorber packing height, which translates to additional number of transfer units, would be required to achieve the desired target. The high viscosity was likely a detriment as well since the incoming streams were not maintained at 40°C due to the modified set-up, although the colder temperatures likely favored better absorption. An absorber temperature profile is given in Figure 20 using the thermocouples placed along the height of the column. The incoming stream was approximately 25°C and reached a maximum of 36°C near the bottom of the column as can be seen with the exothermic temperature bulge from reaction.
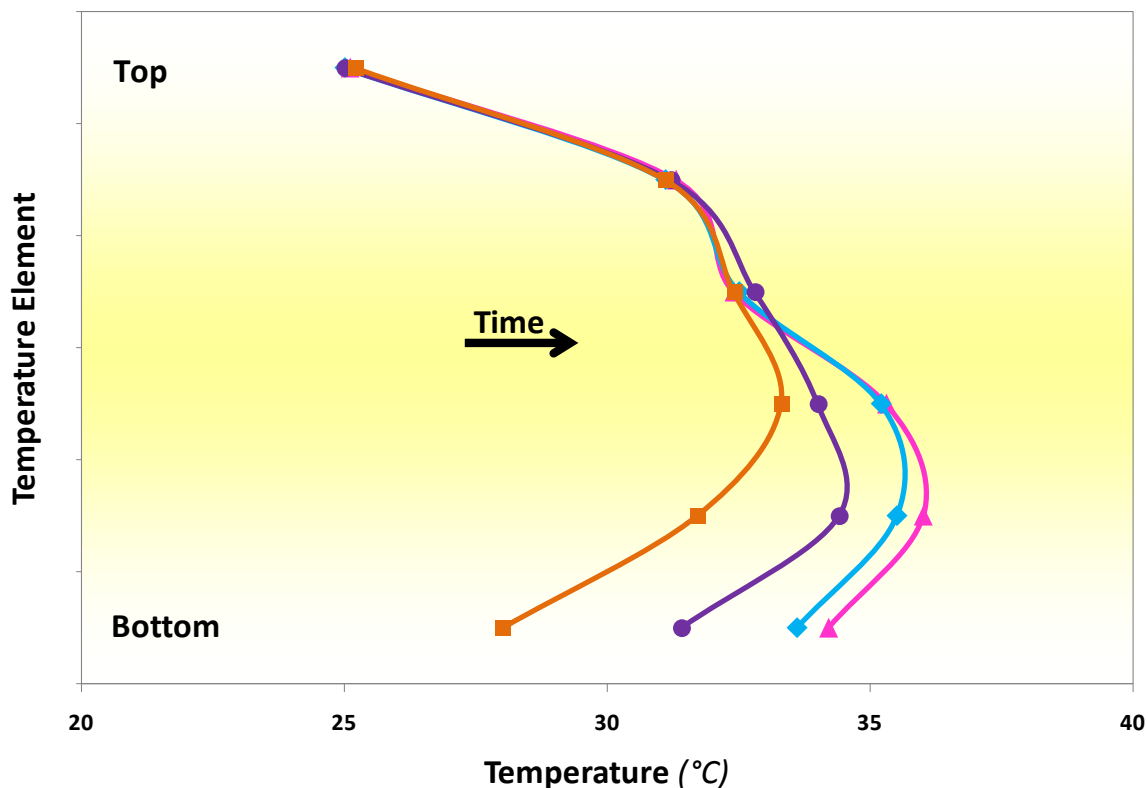


**Figure 20. NDIL0046 Absorber Temperature Profile**

Wet chemistry techniques using acid/base chemistry for $CO_2$ loading analysis like is done for other solvent solutions could not be employed with the ionic liquid. Therefore, an absorber bottoms sample was collected after shut-down and sent to the University of Notre Dame for $CO_2$ loading analysis. Results from thermal gravimetric analysis (TGA) revealed a $CO_2$ loading of 0.52 mole $CO_2$/mole NDIL0046. This result was higher than anticipated. Further examination of the literature data for absorption capacity versus the RSAT Simulator experimental conditions for temperature and $CO_2$ concentration is shown in Figure 21 (1).
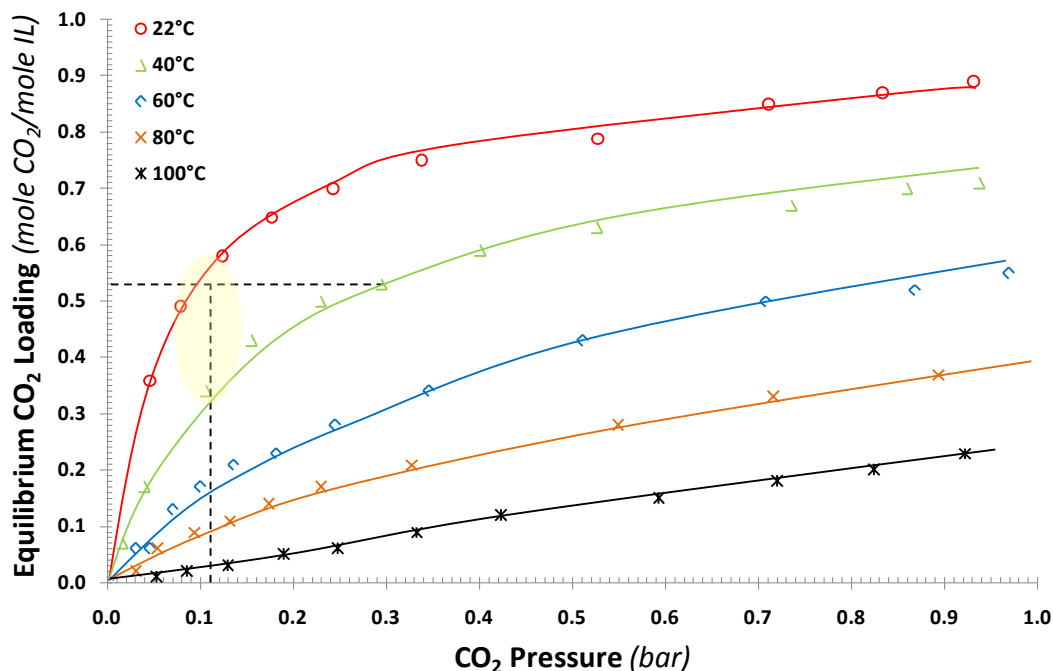
**Figure 21. CO$_2$ Uptake Capacity from Closed, Stirred Variable Temperature Absorption Cell (1)**

Visually interpolating between the isotherms of 22°C and 40°C drawn in Figure 21 using the temperatures given in Figure 20 suggests that a CO$_2$ loading of 0.52 mole CO$_2$/mole NDIL0046 is indeed possible.  However, it is a bit surprising that an apparent equilibrium condition was attained during testing.  This could perhaps be explained by the long residence time in the column due to the slow liquid flow rate and high efficiency of the laboratory structured packing. Calculating the number of transfer units did not prove useful because of the proximity to equilibrium.

For the most part, the NDIL0046 functioned as a CO$_2$ absorbing liquid solvent and could be measured using approximately the same scale as well-known amine-based formulations.  However, the ability to regenerate a pure stream of CO$_2$ was not proven herein and needs to be demonstrated in a process scheme to determine overall feasibility.

## 3.3    SOLVENT MANAGEMENT

The NDIL0046 was returned to the University of Notre Dame by combining the separately used liquid volumes together in the received tote container.  The mixture had some unknown CO$_2$ loading. Separate sample vials collected at the conclusion of experiments were labeled and returned as well.

After draining, laboratory glassware and equipment were cleaned thoroughly with either methanol and/or ethanol to eliminate residual ionic liquid before water washing.  Many rinses were required to restore facilities back to a neutral condition.  The sequestered waste was deemed hazardous for ignitability due to flash point (less than 60°C) of the organic solvents.  Silver contamination from NDIL0046 synthesis, as disclosed in Section 6.2 - Certificate of Analysis, dictated a Toxicity Characteristic Leaching Procedure (TCLP).  A third-party analytical chemistry laboratory verified the waste stream silver concentration as 2.6 mg/L (ppm).  The Environmental Protection Agency (EPA) regulatory limit is 5 ppm. Thus, the level for silver toxicity was under the reporting threshold.

**4.0 CONCLUSIONS**

**4.1    SUMMARY**

The Babcock & Wilcox Company was able to independently evaluate a revolutionary compound invented by University of Notre Dame researchers for post-combustion $CO_2$ capture.  The innovative aprotic heterocyclic anion (AHA) ionic liquid identified as NDIL0046 was tested during August and September, 2012 using established facilities at the B&W Research Center to evaluate performance.

The Wetted-Wall Column is a differential gas-liquid reactor wherein $CO_2$ absorption or desorption can be studied under precisely controlled conditions.  Two $CO_2$ loading conditions at 0.1 and 0.3 mole $CO_2$/mole NDIL0046 were conducted at 40°C.  In the rich $CO_2$ loading range near 5000 Pa where absorption rate is best compared, the liquid film mass transfer coefficient ($k_g'$) can be evaluated against 30wt% MEA as a baseline comparison, where NDIL0046: $k_g'$ = 1.4 x10$^{-7}$ mol/s·m$^2$·Pa versus MEA: $k_g'$ = 3.5 x10$^{-7}$ mol/s·m$^2$·Pa.  NDIL0046 was slower than most of the aqueous amine-based solutions that have been tested previously by B&W, similar to the mass transfer behavior of an unpromoted hindered amine.

The RSAT™ Simulator is the bench-scale absorption/stripping apparatus that was used as a model to construct the similar installation at the University of Notre Dame laboratory.  The unit proved challenging to operate in an integrated fashion with the installed equipment mainly due to high viscosity which was not accounted for in the original design.  Consequently, the system was decoupled and the absorber column operated separately as a once-through batch process.  Test conditions for liquid flow rate and flue gas composition closely matched a previous 30wt% MEA baseline case which achieved a 90% $CO_2$ removal rate at steady state.  Comparatively, the NDIL0046 attained a 65% $CO_2$ removal rate near 30°C with a rich $CO_2$ loading of 0.52 mole $CO_2$/moleNDIL0046.  Despite falling short of the targeted 90% $CO_2$ removal rate, the outcome was consistent with the mass transfer data obtained in the Wetted-Wall Column.

Electrochemical evaluations were used to understand corrosivity toward commonly used materials of construction in the process industry.  Analyses consisted of linear polarization resistance (LPR) testing and potentiodynamic scans (PDS) on carbon steel 1018 and stainless steel 304L.  Corrosion rates for both metals were 0.1 mpy or less, indicating excellent corrosion behavior for NDIL0046 in each of the tested conditions.  The details are reported elsewhere.

Overall, both the quantitative and qualitative results are intriguing and entice more questions regarding application of this novel technology to $CO_2$ scrubbing.  This particular class of AHA ionic liquid compounds has several appealing properties akin to solid sorbents. The non-volatile nature was particularly remarkable.  An obvious absence of odor, no worry of evaporation and general lack of flammability are attractive characteristics, without the drawbacks of solids handling and transport. The traditional water wash section(s) can likely be eliminated and a lower make-up solvent supply can potentially be realized from the diminished emissions escaping through the exhausting stack. Implications regarding corrosion and materials of construction are also favorable. From a capital investment point of view, it is possible that lower grade and cheaper materials could be employed. Nonetheless, there are still distinct tradeoffs that cannot be neglected.  High viscosity, poor mass transfer, cleaning with organic solvents and disposal remain of practical concern.  More information is crucial pertaining to environmental release, such as toxicological and ecological impacts, energy

penalty ramifications which were not quantified herein, and degradation products in the presence of flue gas contaminants. The balance between pros and cons insinuates that ionic liquids could still be a viable future technology and should not be dismissed without further investigation.

Taking into account that the scope of these tests focused on a particular ionic liquid compound, NDIL0046, there is likely still room to maneuver with these tunable molecules to improve upon deficiencies. This particular compound was by no means identified as a 'silver bullet' or optimal formulation.

## 4.2    RECOMMENDATIONS

As this particular project comes to a close, recommendations for ongoing development needs are identified as follows:

Although the viscosity has been drastically reduced over the course of this program by orders of magnitude, another step-change improvement would significantly enhance mass transfer along with the ability to pump more effectively.

Exploring ionic liquid synthesis techniques to minimize cost and adverse impurities would help to make this solvent a more attractive option.

The regeneration step requires exploration either to identify an inert diluent which can provide sufficient driving force for $CO_2$ desorption and/or a modified process concept to take advantage of the non-aqueous nature of the ionic liquid.

A continued collaboration relationship and discussions to seek opportunities for partnership should be maintained.

## 4.3    ACKNOWLEDGEMENTS

A special thank you is owed to Babcock & Wilcox Research Center colleagues who participated in this program. Without everyone's teamwork and can do attitude, accomplishing this ionic liquid testing in such short order would not have been possible.

Grateful appreciation is extended for the collective effort, troubleshooting, expertise, advice and assistance offered by fellow chemical engineers George Farthing, Mike Klidas, Lei Ji, Ruby Zhang, and co-op student Victoria Wilson in the $CO_2$ Control Lab. Technician, Jeff Peterson quickly provided equipment alterations and repairs with craft and urgency to implement requested changes.

Corrosion experiments led by Jeff Sarver and E. Purusha Bonnin-Nartker and supported by Dan Panaia and Bob Pelger offered new insight into how ionic liquids react with various metals that could be used for materials of construction.

Environmental, Health and Safety Specialist, Lindsey Larson is recognized for her overall guidance with respect to employee and environmental welfare when handling a new chemical and ensuring that all regulatory requirements were followed.

## 5.0 REFERENCES

1. *Molecular Design of High Capacity, Low Viscosity, Chemically Tunable Ionic Liquids for CO2 Capture.* **B. Gurkan, B.F. Goodrich, E.M. Mindrup, L.E. Ficke, M. Massel, S. Seo, T.P. Senftle, H. Wu, M.F. Glaser, J.K. Shah, E.J. Maginn, J.F. Brennecke, W.F. Schneider.** Notre Dame : s.n., 2010, The Journal of Physical Chemistry Letters, pp. 3494-3499.

2. **Instrumentation Specialties Company.** *ISCOtables: A Handbook of Data for Biological and Physical Scientists.* [ed.] Gunter Hofmann. 7th Edition. Lincoln : s.n., 1977.

3. *CO2 Chemical Solvent Screening at The Babcock & Wilcox Company.* **L. Ji, S.J. Miksche, L.M. Rimpf, G.A. Farthing.** Pittsburgh : s.n., 2009. 8th Annual Conference on Carbon Capture and Sequestration. BR-1823.

## 6.0 APPENDIX

### 6.1    MATERIAL SAFETY DATA SHEET (MSDS)

[P66614]2CNPYL  KOEI CHEMICAL COMPANY, LIMITED          W6612-1  2012/05/09

# KOEI

## Material Safety Data Sheet

Date of preparation    2012/05/09

### 1.CHEMICAL PRODUCT AND COMPANY IDENTIFICATION

| | |
|---|---|
| Product name: | Trihexyltetradecylphosphonium 2-cyanopyrrolide |
| Company name: | KOEI CHEMICAL COMPANY, LIMITED |
| Address: | Shionogi Honcho Kyodo Building, 7-2, Nihonbashi-Honcho 3-chome, Chuo-ku, Tokyo, Japan<br>Information and emergency phone during business hour<br>Telephone number +81-3-6667-8271<br>FAX number +81-3-6667-8289 |
| Remarks: | Transport emergency telephone<br>CHEMTREC<br>800-424-9300(The United States or Canada, toll-free)<br>+1-703-527-3887(Outside the United States or Canada, collect calls accepted) |
| Product code: | W6612 |
| Recommended use and restrictions: | · General chemical material |

### 2.HAZARDS IDENTIFICATION

GHS classification:

Physical hazards:

Pyrophoric liquids:                          Not classified

Health hazards:

Enviromental hazards:

Hazardous to the aquatic enviroment-chronic:        Category 2

For those hazards do not list above are "not applicable" or "classification not possible".

GHS label element:

Pictogram:



Signal word:                       '

Hazard statements:          ·  Toxic to aquatic life with long lasting effects

Precautionary statement:

Prevention:                ·  Avoid release to the environment.
·  [Supplemental information]
·  Do not handle until all safety precautions have been read and understood.
·  Keep away from heat/sparks/open flames/hot surfaces.-No smoking.
·  Avoid breathing dust/fume/gas/mist/vapours/spray.
·  Do not get in eyes, on skin, or on clothing.
·  Wear protective gloves/protective clothing/eye protection/face protection.
·  Wash thoroughly after handling.

Response:                ·  Collect spillage.

[P66614]2CNPYL  KOEI CHEMICAL COMPANY, LIMITED                W6612-1  2012/05/09

- [Supplemental information]
- In case of fire: Use appropriate media for extinction.
- IF INHALED: Remove victim to fresh air and keep at rest in a position comfortable for breathing.
- IF ON SKIN: Wash with plenty of soap and water.
- If skin irritation occurs: Get medical advice/attention.
- IF IN EYES: Rinse cautiously with water for several minutes. Remove contact lenses, if present and easy to do. Continue rinsing.
- If eye irritation persists: Get medical advice/attention.
- IF SWALLOWED: Call a POISON CENTER or doctor/physician if you feel unwell.

Storage:
- [Supplemental information]
- Store in a well-ventilated place. Keep container tightly closed.

Disposal:
- Dispose of contents/container in accordance with local/regional/national/international regulations.

## 3.COMPOSITION/INFORMATION ON INGREDIENTS

Discrimination of single substance or mixture:    Single substance

Chemical name or common name:    Trihexyltetradecylphosphonium salt with 1H-pyrrole-2-carbonitrile(1:1)

Chemical characteristic (chemical formulas):    $C_{32}H_{68}P \cdot C_5H_3N_2$ (M.W. 574.95)

Abbreviation:    [P66614]2CNPYL

Ingredient:

| No. | Ingredient name | CAS number | Chemical formulas | Concentration or concentration range |
|-----|-----------------|------------|-------------------|--------------------------------------|
| 1 | Trihexyltetradecylphosphonium 2-cyanopyrrolide | 1259948-56-5 | $C_{32}H_{68}P \cdot C_5H_3N_2$ (M.W. 574.95) | ≥ 97 % |

Others:

## 4.FIRST-AID MEASURES

If inhaled:
- Immediately remove to fresh air. Keep victim warm. Get medical attention immediately. If not breathing, give artificial respiration or give oxygen.(by trained personnel)

If on skin:
- Immediately flush skin with plenty of water or shower. Remove contaminated clothing and shoes. Protect yourself by wearing gloves. Get medical attention immediately.

If in eyes:
- Immediately flush eyes with plenty of water for at least 15 minutes. Get medical attention immediately.

If swallowed:
- Rinse mouth with water. Get medical attention immediately. Give one or two glasses milk or water to drink. Never give anything by mouth to unconscious person.
- Do not induce vomiting and get medical attention immediately.

## 5.FIRE-FIGHTING MEASURES

Suitable extinguishing media:
- Dry chemical powder, foam and carbon dioxide

Banned extinguishing media:
- Solid streams of water

Specific hazards:
- On combustion, forms harmful gases.

Special fire-fighting procedures, protection of fire-fighters:
- In case of fire in the surroundings, move container from fire areas.
- Apply water from a safe distance to cool and protect surrounding area.
- Wear proper protective equipment. Keep personnel removed and upwind of fire.

[P66614]2CNPYL  KOEI CHEMICAL COMPANY, LIMITED                    W6612-1  2012/05/09

## 6.ACCIDENTAL RELEASE MEASURES

| | |
|---|---|
| Personal precautions, protective equipment and emergency procedures: | • Wear proper protective equipment.<br>• Evacuate personnel downwind.<br>• Isolate hazard area. Keep unnecessary and unprotected personnel from entering.<br>• Shut off all sources of ignition.<br>• Prepare extinguishing media. |
| Environmental precautions: | • Do not let this chemical enter the environment. |
| Methods and materials for containment and cleaning up: | • Collect leaking and spilled liquid in sealable containers as far as possible. Absorb remaining liquid in sand or inert absorbent and remove to safe place. |
| Prevention of secondary hazards: | • Immediately eliminate all sources of ignition(Prohibit smoking, sparks or open flame around the area). |

## 7.HANDLING AND STORAGE

Handling:

| | |
|---|---|
| Technical measures: | • Technical measures : Implement technical measure and use personal protection mentioned in'Section 8. EXPOSURE CONTROLS AND PERSONAL PROTECTION'. |
| Local and general ventilation: | • Local exhaust or general ventilation : Implement local exhaust or general ventilation mentioned in'Section 8. EXPOSURE CONTROLS AND PERSONAL PROTECTION'. |
| Safe handling instructions: | • To prevent inhalation and skin absorption, wear personal protective equipment.<br>• Wash thoroughly after handling.<br>• Use only in a well-ventilated area.<br>• Shut off all gas pilot and electrical(spark or hot wire)igniters and other sources of ignition during use and until all vapours(odours)are gone. Keep away from heat, sparks and flame. |

Storage:

| | |
|---|---|
| Technical measures: | • Keep away from sources of ignition such as heat, flame, open flame. -No smoking. |
| Storage condition: | • Keep container closed when not in use.<br>• Keep in the dark.<br>• Keep in a well-ventilated room. |
| Safe packing materials: | • Use containers prescribed in UN Transport Regulation. |

## 8.EXPOSURE CONTROLS AND PERSONAL PROTECTION

| | |
|---|---|
| Engineering controls: | • Use with local exhaust ventilation or in closed systems. |

Personal protective equipment:

| | |
|---|---|
| Respiratory protection: | • Wear chemical-cartridge respirator with an organic vapour cartridge or canister, air-supplied respirator(hose mask, air-line respirator). Wear self-contained respirator(air-supplied respirator, oxygen respirator)with emergency escape provisions. |
| Hand protection: | • Chemical resistant gloves |
| Eye protection: | • Safety spectacles with side shields(or goggles) |
| Skin and body protection: | • Impervious boots, impervious clothing, head gear |
| Hygiene measures: | • Wash hands throughly after handling. |
| Others: | • ACGIH(2011), OSHA-PEL(2006) Not established |

[P66614]2CNPYL  KOEI CHEMICAL COMPANY, LIMITED                      W6612-1  2012/05/09

## 9.PHYSICAL AND CHEMICAL PROPERTIES

The appearance:

| | |
|---|---|
| Physical state, shape, color etc: | Dark yellow red clear liquid to very dark yellow red liquid |
| Odour: | Characteristic odour |
| pH: | No data |
| Melting point/freezing point: | No data |
| Initial boiling point and boiling range: | No data |
| Flash point: | No data |
| Auto-ignition temperature: | No data |
| Flammability (solid, gas): | — |
| Upper/lower flammability or explosive limits: | No data |
| Vapor pressure: | No data |
| Vapour density: | No data |
| Evaporation speed: | No data |
| Relative density: | No data |
| Solubility: | |
| For the water: | No data |
| For the water: | No data |
| For the solvent: | No data |
| For the solvent: | No data |
| Partition coefficient n-octanol/water: | No data |
| Decomposition temperature: | No data |
| Others: | No data |

## 10.STABILITY AND REACTIVITY

## 11.TOXICOLOGICAL INFORMATION

## 12.ECOLOGICAL INFORMATION

- Spilled material or waste material may cause environmental damage. Handle carefully. Do not throw washing water and product on ground, into river and into waterways directly.

| Hazardous to the aquatic environment chronic hazard: | · Category 2 |
|---|---|

## 13.DISPOSAL CONSIDERATIONS

| Residual waste: | · In accordance with local and national regulations. |
|---|---|
| | · Attention of the recipient should be drawn to the possible existence of local disposal regulations. |
| Contaminated container and packaging: | · Handle and dispose an empty container after contents in container are removed completely. |

[P66614]2CNPYL　KOEI CHEMICAL COMPANY, LIMITED　　　　　　　　　W6512-1　2012/05/09

> · Contract with an industrial waste disposal contractor who obtains permission, and entrust such handling and disposal of waste material.

## 14.TRANSPORT INFORMATION
International regulations:

| | | |
|---|---|---|
| Marine transport: | · | IMO |
| UN number: | · | 3082 |
| Proper shipping name: | · | ENVIRONMENTALLY HAZARDOUS SUBSTANCE, LIQUID, N.O.S. |
| Class: | · | 9 |
| Packing group: | · | Ⅲ |
| Marine pollutant: | · | Applicable |
| Air transport: | · | ICAO/IATA |
| UN number: | · | 3082 |
| Proper shipping name: | · | Environmentally hazardous substance, liquid, n.o.s. |
| Class: | · | 9 |
| Packing group: | · | Ⅲ |

## 15.REGULATORY INFORMATION

## 16.OTHER INFORMATION

The reference of mention contents:

| | |
|---|---|
| Company name: | KOEI CHEMICAL COMPANY, LIMITED |
| Division in charge: | Responsible Care Office |
| E-mail address: | sdsinfo_rc@koeichem.co.jp |

Description in this MSDS has been prepared based on references, information and data which are available to data, however, concentrations of ingredients, physical-chemical properties and dangerous hazard information are not guaranteed value. Please note that the precautions only cover normal handling conditions and additional safety measures which are suitable for your own uses or purposes should be applied for unusual handling conditions.

## 6.2   CERTIFICATE OF ANALYSIS

# KOEI   KOEI CHEMICAL COMPANY, LIMITED

MARKETING & DEVELOPMENT
SHIONOGI HONCHO KYODO BLDG.
3 - 7 - 2, NIHONBASHI HONCHO,
CHUO-KU, TOKYO, JAPAN 103-0023
TELEPHONE : +81 3 6667 8271
FACSIMILE : +81 3 6667 8289

QUALITY ASSURANCE OFFICE
25, KITASODE, SODEGAURA CITY
CHIBA, JAPAN 299-0266
TELEPHONE : +81 438 63 5511
FACSIMILE : +81 438 63 5546

To whom it may concern :                                15-Jun-2012
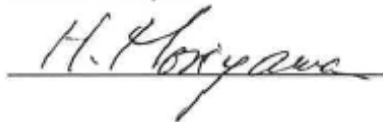
## CERTIFICATE OF ANALYSIS

Inspections were conducted at our laboratory and the results are as follows:

| Commodity | | : Trihexyltetradecylphosphonium 2-cyanopyrrolide |
|---|---|---|
| Lot No. | : | 20601K |
| Quantity | kg : | 22.25 |
| Characteristic | | Result |
| Appearance | : | Dark brown liquid |
| Water content | ½ : | 0.15 |
| Ag (ICP) | ppm : | 4600 |
| Cl⁻(IC) | ppm : | 530 |
| Viscosity (25℃) | mPa · s : | 571 |

We as the manufacturer, do hereby certify that the above mentioned is true and authentic.

Quality Assurance Group
Manager
Hiroshi Moriyama

Appendix III – Report from Babcock and Wilcox on corrosion studies

# CORROSION TESTING OF IONIC LIQUID NDIL0046

**FINAL REPORT**

**PREPARED BY:**

PURUSHA BONNIN-NARTKER

DATE ISSUED: 18 SEPTEMBER 2012

REPORT NO. BWRC:12:R002FP7006:01

**The Babcock & Wilcox Research Center**
180 South Van Buren Avenue
Barberton, OH 44203-0622

**DISCLAIMER**

This report was prepared by Babcock & Wilcox Power Generation Group, Inc. for the University of Notre Dame.  Neither the Babcock & Wilcox Power Generation Group, Inc., the University of Notre Dame, nor any person acting on their behalf:

a) Makes any warranty or representation, express or implied, or assumes any legal liability or responsibility for the accuracy, completeness, or usefulness or any information, apparatus, product, or process disclosed, or represents that its use would not infringe privately owned rights; or

b) Assumes any liabilities with respect to the use of, or for damages resulting from the use of, any information, apparatus, method or process disclosed in this report.

# TABLE OF CONTENTS

# LIST OF FIGURES

# LIST OF TABLES

**Table**                                                                                      **Page**

# NOMENCLATURE

| | |
|---|---|
| $Ag$ | Silver |
| $Al$ | Aluminum |
| $C$ | Carbon |
| $CE$ | Counter Electrode |
| $Cl^-$ | Chloride |
| $Co$ | Cobalt |
| $Cr$ | Chromium |
| $CR$ | Corrosion Rate |
| $CRs$ | Corrosion Rates |
| $Cu$ | Copper |
| $E_{rev}$ | Reversible Potential |
| $Fe$ | Iron |
| $IL$ | Ionic Liquid |
| $LPR$ | Linear Polarization Resistance |
| $Mn$ | Manganese |
| $Mo$ | Molybdenum |
| $mPa \bullet s$ | Mega Pascal per Second |
| $N$ | Nitrogen |
| $Nb$ | Niobium |
| $Ni$ | Nickel |
| $OCP$ | Open Circuit Potential |
| $P$ | Phosphorous |
| $PDS$ | Potentiodynamic Scan |
| $ppm$ | Parts per Million |
| $PS$ | Potentiostatic Hold |
| $RE$ | Reference Electrode |
| $S$ | Sulfur |
| $scfh$ | Standard Cubic Feet per Hour |
| $Si$ | Silicon |
| $Ti$ | Titanium |
| $WE$ | Working Electrode |

## 1.0 INTRODUCTION

### 1.1 BACKGROUND

A new class of Ionic Liquid (IL) was provided by the University of Notre Dame to The Babcock & Wilcox Research Center (BWRC) on August 14, 2012. The purpose of the analyses was to determine the corrosion behavior of materials in contact with the IL identified as NDIL0046 at different testing conditions.

This was part of an extended effort of evaluating several classes of ILs to further understand their corrosivity toward commonly used materials of construction in the process industry. For that reason electrochemical corrosion evaluations were used to accomplish this task.

### 1.2 OBJECTIVE

Analyses consisted of linear polarization resistance (LPR) testing and potentiodynamic scans (PDS). LPR provides a corrosion rate (CR) that allows the tested materials to be compared amongst one another. The PD scans supply general information regarding the corrosion behavior of the materials in the evaluated environments, including the probability of pitting to occur.

### 1.3 SCOPE

The proposed test plan consisted of testing 2 materials (carbon steel 1018-CS and stainless steel 304L-SS) in 2 different IL environments (neat and IL in the presence of $CO_2$) and 2 temperatures (room temperature and 150$^o$C). No testing was conducted in the IL in the presence of $CO_2$ at 150°C since this particular IL can complex only low amounts of $CO_2$ at this temperature. The test matrix and a description of test conditions is found later in this document.

## 2.0 EXPERIMENTAL METHOD

### 2.1 MATERIALS

Tests were performed on 1018-CS carbon steel and type 304L-SS stainless steel. The composition of these materials is shown in Table 2.1.

**Table 2.1: Composition of Test Materials**

| Material | Heat # | Elements (Weight %) | | | | | | | | | | | | | |
|---|---|---|---|---|---|---|---|---|---|---|---|---|---|---|---|
| | | C | Mn | P | S | Si | Ni | Cr | Mo | Cu | Al | Ti | N | Co | Nb | Fe |
| 1018-CS | 233383 | 0.150 | 0.680 | 0.005 | 0.022 | 0.250 | 0.080 | 0.040 | 0.015 | 0.160 | 0.001 | --- | --- | --- | --- | 98.597 |
| 304L-SS | 14702 | 0.022 | 1.720 | 0.025 | 0.027 | 0.620 | 9.880 | 18.380 | 0.330 | 0.090 | --- | 0.003 | 0.063 | 0.120 | 0.020 | 68.700 |

The test specimens were purchased from Metal Samples and their geometrical shape comprised of rods 4 mm in diameter and 90 mm long. These materials were purchased for previous IL testing, but were not used.

Other materials used throughout the testing program included a Ni wire loop as the counter electrode (CE) and a silver (Ag) wire as the reference electrode (RE). These two electrode materials were used in the electrochemical test cell which will be described in Section 2.2.

### 2.2 ELECTROCHEMICAL TEST CELL

The electrochemical tests were performed using a PAR Model K0264 Micro-Cell Kit to minimize the volume of IL required for each tests. The test cell consisted of a glass cell bottom, a Ag wire RE, and a coiled Ni wire CE. A rod of the test material acted as the working electrode (WE). For tests that were conducted in saturated $CO_2$ conditions, a $CO_2$ purge tube was also placed in the test cell. The components of the test cell were configured as shown in Figure 2.1[1].
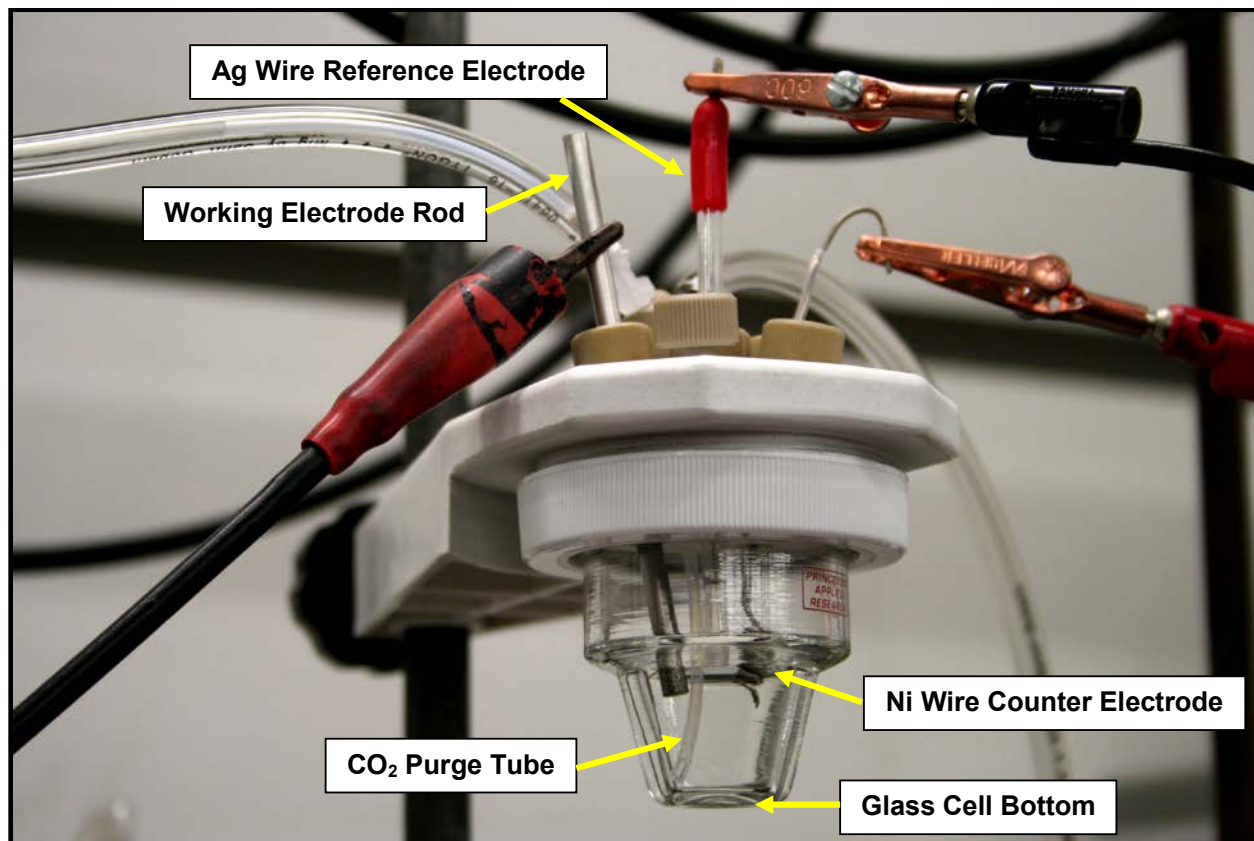
**Figure 2.1: Electrochemical Test Cell Configuration**

Test solution volume included 15 ml of NDIL0046 per each test conducted. IL solution was poured into the cell bottom for each test run. Initially, the fritted glass cylinder housing the Ag wire RE was to be filled with the test solution but due to the high viscosity exhibited by NDIL0046, the electrochemical measurements showed excess noise, providing increased difficulty in the interpretation of results. For that reason, it was decided to leave the Ag wire exposed to the IL without utilizing the housing. Lastly, the WE rod was inserted into the solution such that the exposed surface area was 1.38 $cm^2$ for each test.

## 2.3   TEST INSTRUMENTATION

The electrochemical measurements were performed using a Gamry Instruments, Inc. Potentiostat Model PCI4G/750 and Gamry Echem Analyst control and analysis software version 5.68.

Temperature of the IL during the corrosion testing was measured with a traceable digital Fluke 52 K/J Type Thermometer.

Measurement of solution volume and weight was conducted gravimetrically to increase accuracy with a Mettler Toledo Balance Model PM6100.

## 2.4   TEST CHEMICAL

The University of Notre Dame provided the IL that was tested in this program to BWRC. The specific properties of the IL that was provided are listed in Table 2.2.

### Table 2.2:  Properties of IL NDIL0046

| Ionic Liquid | Appearance | State | Viscosity (25$^o$C) (mPa•s) | Water Content (%) | Ag (ICP) (ppm) | Cl$^-$ (IC) (ppm) |
|---|---|---|---|---|---|---|
| [P66614][2CNPYL] NDIL0046 | Dark Brown | Liquid | 571 | 0.15 | 4600 | 530 |

For the IL specified above, four tests were performed in the neat liquid and two tests were conducted by bubbling $CO_2$ continuously through the liquid solution during the tests to insure that the IL was completely saturated with the gas.  For the tests performed under the $CO_2$ condition, the gas was bubbled through the IL overnight before testing.  Bone dry $CO_2$ research grade from Airgas was used to saturate the IL.  The $CO_2$ had a certified concentration of 99.999% $CO_2$ and trace impurities of <1.0 ppm argon + oxygen + carbon monoxide, <1.0 ppm of total hydrocarbons, <3.0 ppm of moisture, and <5.0 ppm of nitrogen.

## 2.5    TEST PROCEDURES

The text matrix used in this test program (including the evaluated conditions, temperature, IL solution environment, and tested materials) can be seen in Table 2.3.

### Table 2.3:  Text Matrix of Corrosion Testing

| Environment | IL (Neat) | | IL + CO$_2$ | |
|---|---|---|---|---|
| Temperature ($^o$C) | Carbon Steel 1018-CS | Stainless Steel 304L-SS | Carbon Steel 1018-CS | Stainless Steel 304L-SS |
| Room | T1[1] | T2[1] | T3[1] | T4[1] |
| 150 | T5[1] | T6[1] | --- | --- |

[1] T# = Test Number

The specific test procedures used in this test program, including the necessary inputs to convert the LPR data to CR, are present in Appendix 8.1.  The test procedure consisted of the following sequence:

1.  Delay the system for 30 seconds in standby mode prior to initiation of testing.

2.  Measure the open circuit potential (OCP) of the test material versus the RE for 30 minutes.

3.  Hold the potential at -0.02 V versus OCP for 3 minutes to prepare the system for the next step.

4.  Perform a LPR scan from OCP -0.02 V to OCP +0.02 V, then back to OCP -0.02 V at a rate of 0.1 mV/second.

5.  Measure the OCP of the test material versus the RE for 30 minutes.

6.  Perform a PDS from OCP -0.05 V to OCP +1.0 V, then back to OCP -0.05 V at a rate of 0.1667 mV/second.

Following each test sequence, the test specimen was removed from the holder and rinsed.  A photograph of the test specimen and the post test IL solution was taken.  The test solution was poured into a labeled glass vial and sealed.  The glass vials with the IL post test solutions were

identified with date, IL name, and test number for consistency. All test materials were cleaned using methanol or acetone due to the IL insolubility in water.

Prior to initiating Test 3 (see Table 2.3), conducted in the presence of $CO_2$, high purity $CO_2$ was bubbled through the IL solution overnight. Then, the $CO_2$ gas was continuously flowed through the test cell during the test. For the additional IL inventory previously saturated with $CO_2$, and prior to conducting Test 4, a $CO_2$ cover gas was flowed through the test cell to maintain its saturation condition before the solution was use for the test. Once again, the $CO_2$ gas was continuously flowed through the test cell during the test. Figure 2.2 illustrates the IL during the $CO_2$ loading process.
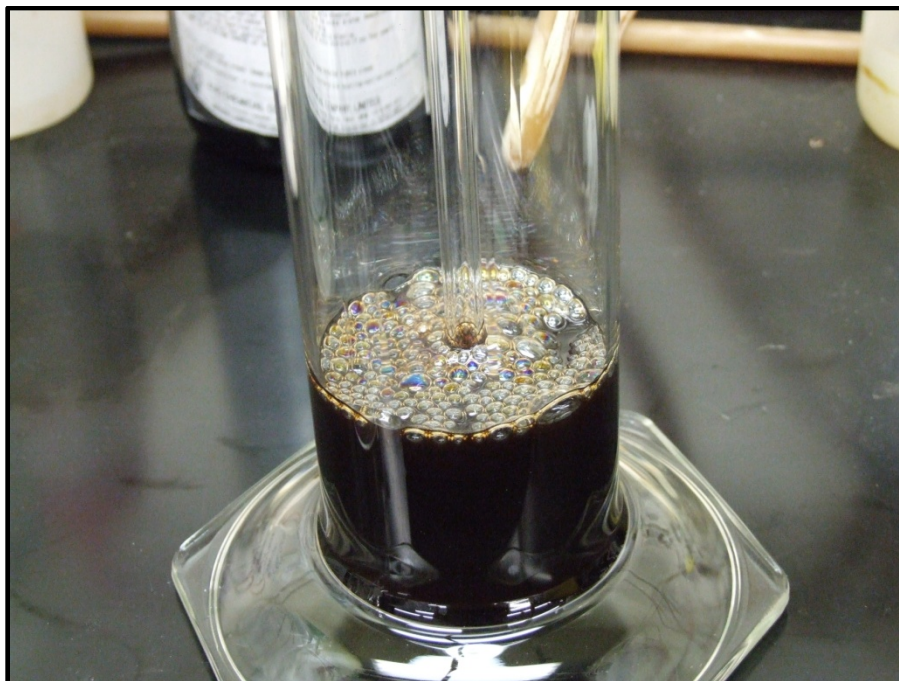


**Figure 2.2: $CO_2$ Loading Process**

For the tests conducted at $150^{\circ}C$ (Tests 5 and 6), a sand heating bath was utilized and the temperature inside of the test cell was continuously monitored. No temperature control was utilized during the room temperature tests (Tests 1-4); however, the temperature inside of the test cell was continuously monitored. The average test temperatures measured during the six tests are reported in Table 2.4. Additionally, Figure 2.3 illustrates the experimental setup with the utilization of the sand bath.

**Table 2.4:  Average Test Temperature Measured at Specific Test Conditions**

| Test No. | Material | Environment | Average Temperature ($^o$C) |
|----------|----------|-------------|------------------------------|
| 1 | Carbon Steel 1018-CS | Neat | 23.1 |
| 2 | Austentic 304L-SS | Neat | 22.8 |
| 3 | Carbon Steel 1018-CS | $CO_2$ | 23.7 |
| 4 | Austentic 304L-SS | $CO_2$ | 22.8 |
| 5 | Carbon Steel 1018-CS | Neat | 148.7 |
| 6 | Austentic 304L-SS | Neat | 147.8 |
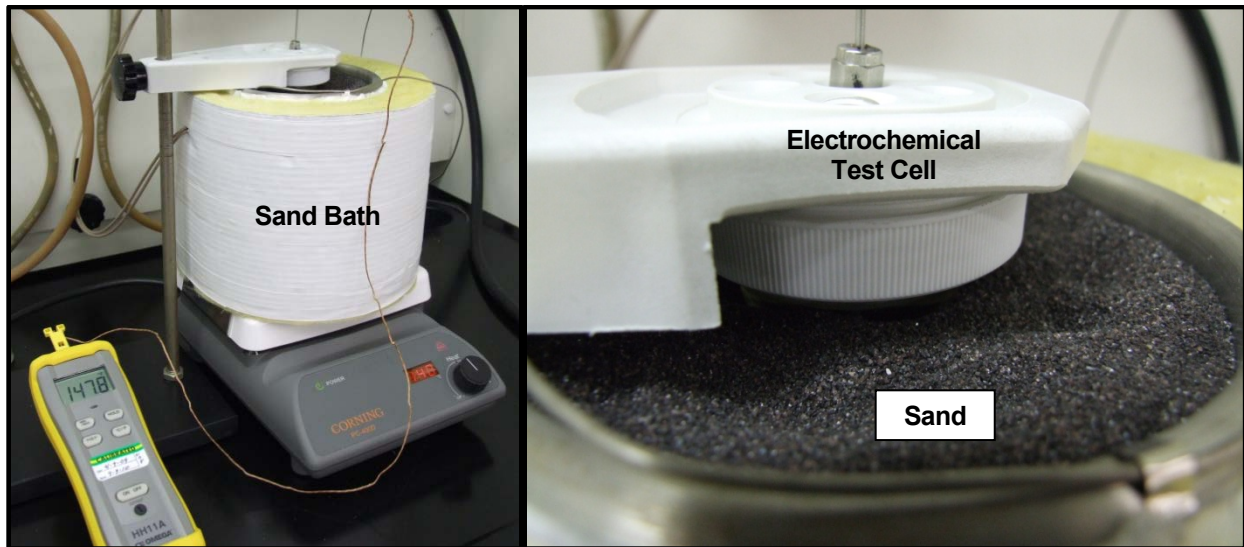


**Figure 2.3:  Experimental Setup including Sand Bath and Other Accessories**

## 3.0 RESULTS

### 3.1 OCP AND LPR MEASUREMENTS

A summary of the average OCP values recorded before and after the LPR scans along with the CRs calculated from the LPR scans is displayed in Table 3.1 and Figure 3.1.

**Table 3.1: Average OCP Before and After LPR Scans and Calculated CRs from LPR Scans**

| Test ID | Test Condition | $OCP_{ave}$ Before (V) | CR (mpy) | $OCP_{ave}$ After (V) |
|---|---|---|---|---|
| **Carbon Steel 1018-CS** | | | | |
| 1 | 25°C, Neat | -0.262 | 0.01029 | -0.270 |
| 3 | 25°C, $CO_2$ | -0.063 | 0.00068 | -0.072 |
| 5 | 150°C, Neat | +0.076 | 0.09900 | +0.059 |
| **Stainless Steel 304L-SS** | | | | |
| 2 | 25°C, Neat | -0.174 | 0.00344 | -0.166 |
| 4 | 25°C, $CO_2$ | -0.116 | 0.00136 | -0.102 |
| 6 | 150°C, Neat | +0.030 | 0.07134 | +0.019 |



**Figure 3.1: CRs Calculated from LPR Scans**

## 3.2    PDS MEASUREMENTS

Complete results from the 6 test sequences that were performed in this program, including the post-test solution and test specimen photographs are contained in Appendix 8.2.

A summary of the information obtained from the PDS is displayed in Table 3.2.  The values displayed in Table 3.2 are explained in the simulated PDS shown in Figure 3.2.

**Table 3.2:  Information from PDS Results**

| Test ID | Material | $E_{rev}$ Anodic (V) | Active Peak Current Density (A/cm$^2$) | Passive Potential Range (V) | Current Density @ OCP+1V (A/cm$^2$) | Hysteresis | $E_{rev}$ Cathodic (V) |
|---|---|---|---|---|---|---|---|
| 1 | Carbon Steel 1018-CS | -0.28 | ---- | ---- | 4.17E-06 | No | +0.07 |
| 2 | Austentic 304L-SS | -0.18 | ---- | ---- | 6.42E-06 | No | +0.24 |
| 3 | Carbon Steel 1018-CS | -0.10 | ---- | ---- | 1.08E-06 | No | +0.28 |
| 4 | Austentic 304L-SS | -0.12 | ---- | ---- | 1.55E-06 | No | +0.26 |
| 5 | Carbon Steel 1018-CS | +0.05 | ---- | ---- | 1.78E-04 | No | +0.09 |
| 6 | Austentic 304L-SS | +0.01 | ---- | ---- | 1.74E-04 | No | +0.04 |
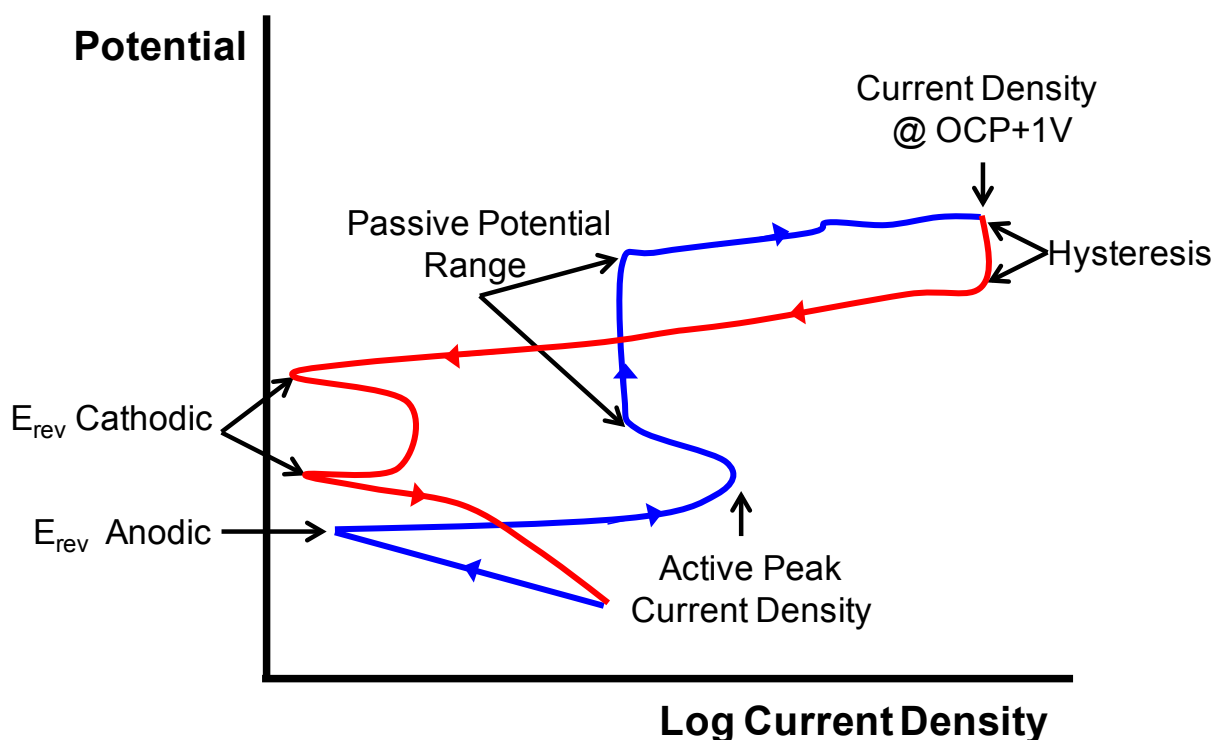


**Figure 3.2:  Values Recorded from Potentiodynamic Scans in Table 3.2**

## 3.3    OTHER OBSERVATIONS

Other observations from the test sequences are denoted below:

**Test Solution Color:**  All of the test solutions were dark brown as was shown in Figure 2.2.  The post test solution color did not change regardless of the different test conditions and/or test materials.  Examples of the post-test solution color can be seen in Figure 3.3.



**Figure 3.3:  Post-Test NDIL0046 Solution Color**

**Likely Electro-deposition of Ionic Metallic Species on the CE:**  The Ni CE used during Tests 5 and 6 performed at $150^{\circ}$C in the neat IL was observed to have changed appearance.  Figure 3.4 illustrates that the CE coil section surface color appeared dull relative to the rest of the electrode which looked shiny silver, as it did originally.  The coil section was immersed in the IL test solution during the tests.  Additionally, Figure 3.5 shows residues left at the bottom of the test cells after both Tests 5 and 6 were complete.  While no analyses were conducted on these residues, it is believed that possible metallic species from the IL solution may have electro-deposited on the Ni CE (the CE is held at cathodic potentials during the exposures which promotes plating reactions), thus changing its surface appearance.  It is known that NDIL0046 contains 4600 ppm of Ag (Table 2.2) which could have been the metallic specie that participated in the plating phenomenon.  It is unlikely that the observed residues came from the test specimens since their appearance after the tests seemed new and their corrosion rates were nil.   Appendix 8.2 illustrates the post-test appearance of the specimens.

Following Test 5 and 6, the CE was replaced with a new Ni CE wire coil to avoid associated interferences during subsequent tests.
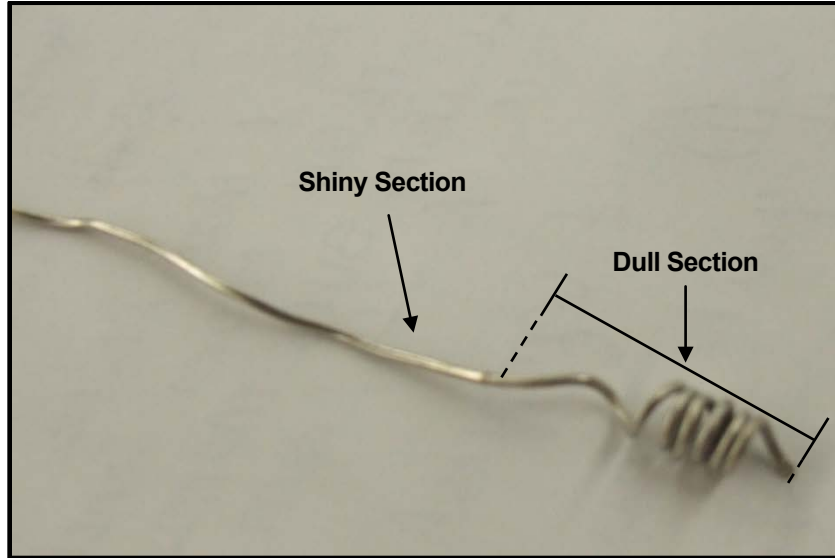
**Figure 3.4:  Ni CE Appearance after Tests 5 and 6 (Neat IL at 150$^{\circ}$C)**
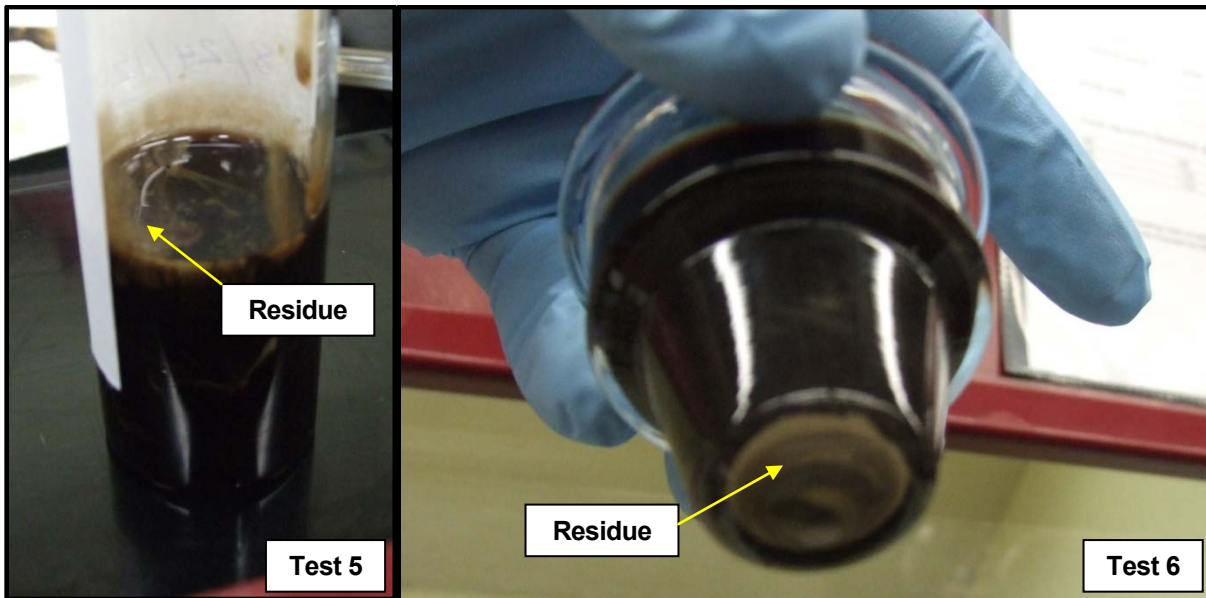


**Figure 3.5:  Residues Found in Post-Tests 5 and 6 IL Solutions**

## 4.0 DISCUSSION

Corrosion rates are generally classified as follows[1]:

|           |                |
|-----------|----------------|
| < 2 mpy   | Excellent      |
| < 20 mpy  | Good           |
| < 50 mpy  | Satisfactory   |
| > 50 mpy  | Unsatisfactory |

From the results presented in Table 3.1 and Figure 3.1, the CRs for carbon steel and stainless steel in all of the test conditions were 0.1 mpy or less, indicating excellent corrosion behavior for these materials in IL NDIL0046.  It was observed from Table 3.1 that the OCP before and after the corrosion evaluation via LPR scans were almost identical.  Results indicated that this average OCPs varied only less than 0.02 mV which shows great reproducibility of these results.

From Figure 3.1, it can be seen that tests in neat IL at 150°C exhibited the highest CRs, thus this was the most aggressive condition from a corrosion standpoint.  The second most aggressive condition was neat IL at room temperature.  Lastly, the least aggressive condition was room temperature and IL in the presence of $CO_2$.  The phenomenon of low corrosivity by ILs in the presence of $CO_2$ has been seen before in previous studies with different formulations of ILs(1).  Overall, the corrosion behavior of carbon steel (1018-CS) was higher than stainless steel (304L-SS) in the case of the IL at room temperature and in the presence of $CO_2$.  However, these values were so low that comparisons seem meaningless.  It is expected that the sensitivity of the LPR technique does not permit accurate differentiation of CRs that are < ~0.1 mpy.  In a practical sense, CRs of < 0.1 mpy can be considered essentially nil.

From a materials stand point, carbon steel and stainless steel should both exhibit excellent general corrosion resistance in all of the test conditions evaluated in the presence of NDIL0046.  Based exclusively on general corrosion behavior, the test results indicate that carbon and stainless steel will perform excellent in these environments.

The PDS data contained in Table 3.2 and the potential versus the log current density plots included in Appendix 8.2 provides additional information regarding the behavior of carbon steel and stainless steel in the NDIL0046 test solution at the different evaluated conditions.  The lack of hysteresis in all of the scans indicates that none of the materials will be expected to undergo localized forms of attack, such as pitting, in the tested conditions.

From Table 3.2, Tests 1 and 2 in neat IL at room temperature showed reversible potentials ($E_{rev}$ anodic) less anodic (more negative) than that of Tests 5 and 6 in neat IL at 150°C.  Maximum current density at OCP +1V for Tests 1-4 were 2 order of magnitude lower than that of Tests 5 and 6 at high temperature.

Overall, there was no active-passive behavior observed in any of the tests conducted.  The lack of active-passive behavior and nil CRs exhibited by both tested material suggest that a very thin protective oxide formed in all environments almost immediately after the materials were anodically polarized.  PDS were very reproducible within the same test condition, indicating almost no

differences associated with the material composition (carbon steel and stainless steel). Tests performed in neat IL at high temperature yielded the most anodic reversible potentials (highest values), with the highest current densities throughout the entire test program. The reproducibility effect can be seen in Figure 4.1, Figure 4.2, and Figure 4.3.

Based on the chemical composition of the IL, it appears that having the presence of 530 ppm of Cl⁻, a well known corrosive, did not have an effect on the corrosivity of the IL. Similarly, the lower water content in the IL (0.15%) may also have contributed to the reduced corrosivity.

Based on the electrochemical test results presented in this document, the overall corrosivity of the NDIL0046 would be classified as excellent. No rankings were established between different test conditions as CR values were considered nil.
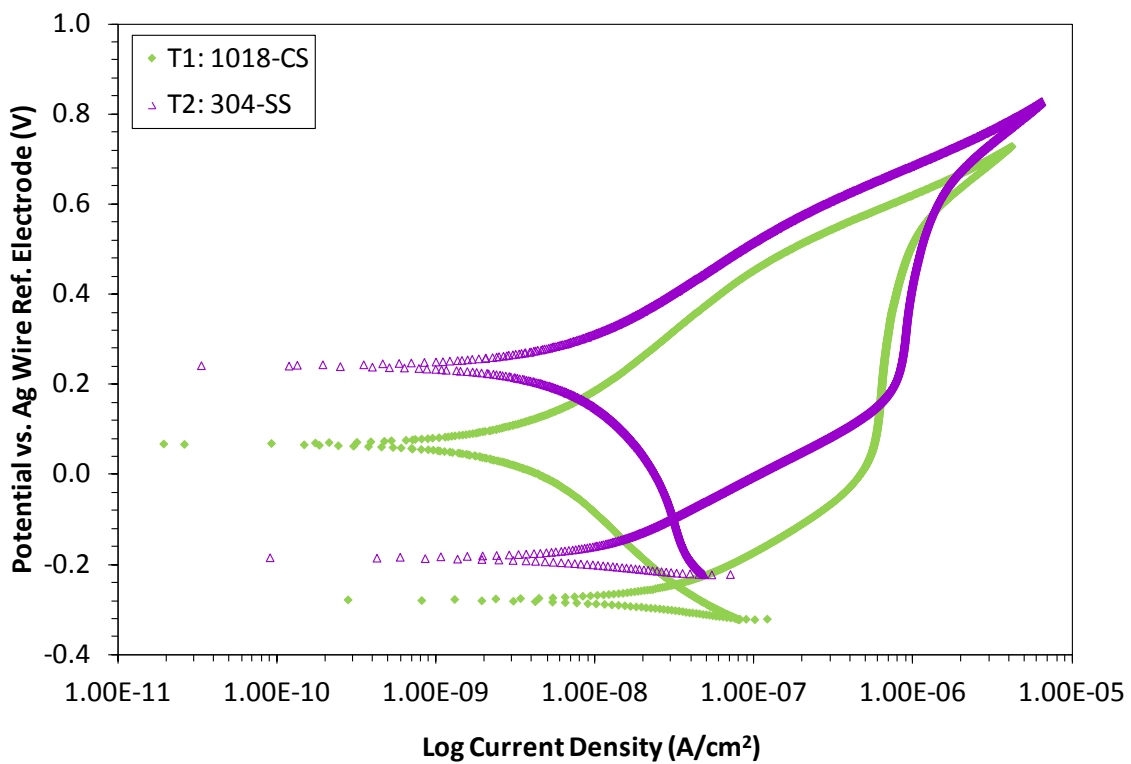


**Figure 4.1: PDS of Various Materials on Neat IL NDIL0046 at 25$^{o}$C**
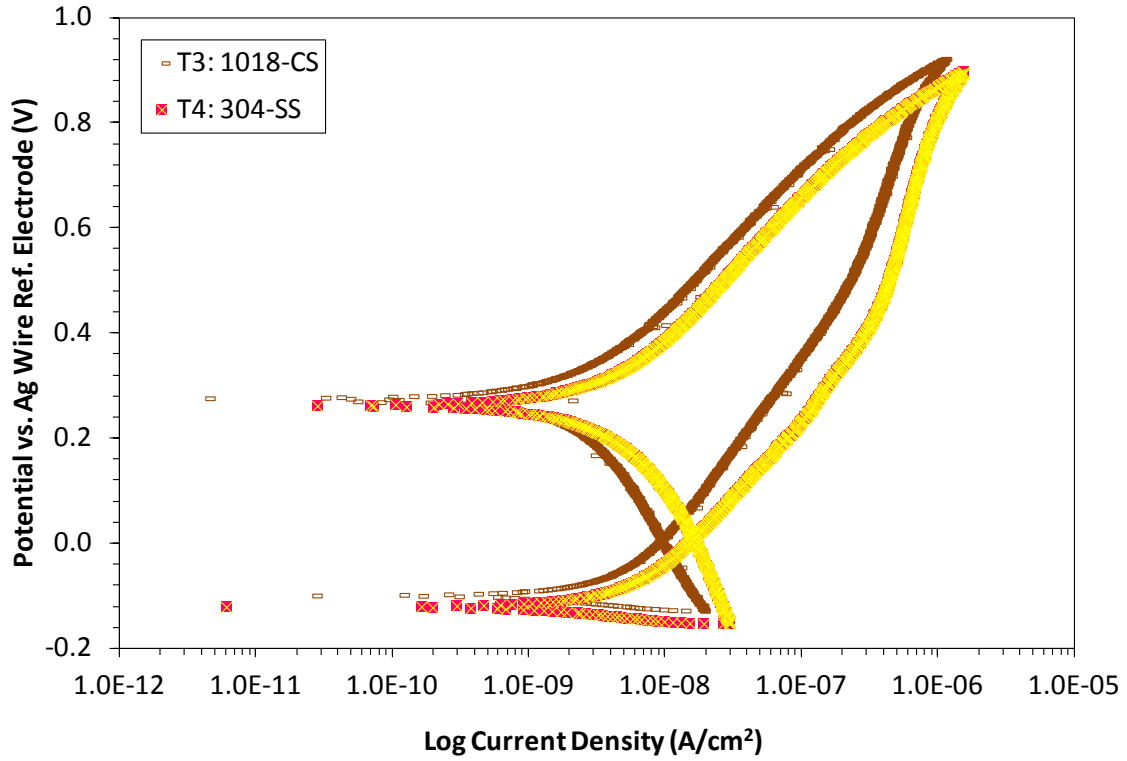
Figure 4.2: PDS of Various Materials on IL NDIL0046 and $CO_2$ at 25$^o$C
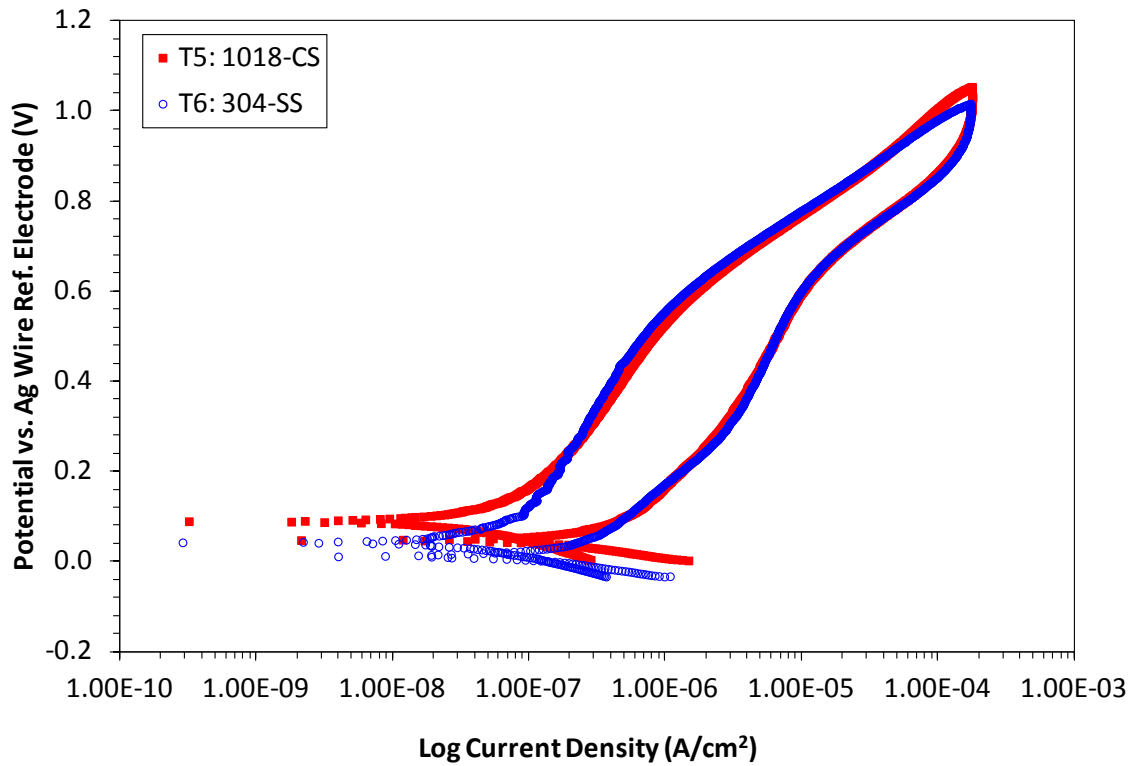


Figure 4.3: PDS of Various Materials on Neat IL NDIL0046 at 150$^o$C

## 5.0 CONCLUSIONS

The CRs for carbon steel and stainless steel were 0.1 mpy or less, indicating excellent corrosion behavior for these materials in IL NDIL0046 in all the tested conditions.

The test program provided results with high reproducibility in all the evaluated electrochemical corrosion techniques.

The corrosion behavior of carbon steel was higher than stainless steel in the case of IL in the presence of $CO_2$ at room temperature. CR values were so low that comparisons between materials were meaningless.

The least corrosivity was displayed by the IL in the presence of $CO_2$ at room temperature indicating that this was the least aggressive condition.

Carbon steel and stainless steel displayed no tendency to experience localized forms of attack, such as pitting, in any of the tested conditions.

There seemed to have been a temperature effect in the corrosivity of the NDIL0046 as this proved the most aggressive condition in both LPR and PDS evaluated techniques.

## 6.0 ACKOWLEDGEMENTS

The author would like to thank Dan Panaia for their assistance and expertise in performing the electrochemical test program.

Thanks to Jeff M. Sarver for his expertise and constant analysis, especially in the determination of possible tests to conduct, and analysis of observations and results.

## 7.0 REFERENCES

1. **Sarver, Jeff M.** *Final Report: Corrosion Screening Analyses for Ionic Liquids.* Barberton : The Babcock & Wilcox Research Center, 2009. RCD 4357.

**8.0 APPENDIX**

## 8.1 SPECIFIC ELECTROCHEMICAL TEST PROCEDURES

### 8.1.1 General Information

- Familiarize with the chemical physical and chemical properties by reading the MSDS.
    - IL stains, so take precautions to avoid spills and contain leaks
    - IL is not soluble with water. For this reason acetone/methanol should be used when cleaning is necessary.
    - IL color is dark brown
    - IL presents high viscosity. For this reason, transfers of the IL into various containers should be avoided as possible.
- Wear proper Personal Protective Equipment (PPE) as recommended: safety glasses, lab coat, and nitrile gloves.
- Make sure to wear nitrile gloves when handling the IL and/or the testing materials to avoid depositing skin oils into the material or cross-contaminating the test setup with the IL.
- Testing will be conducted in the electrochemical fume hood of the chemical lab. IL transfers from temporary into permanent storage containers should occur inside the fume hood at all times.
- An "Unattended Test Equipment Notice" should be filled and attached to the fume hood window should any testing be conducted over night or in an unattended fashion. See Purusha Bonnin-Nartker to fill this form.
- When working at high temperature conditions, make sure to display a "HOT" sign in the window of the fume hood to alert others that may be working nearby. Additionally, use gloves rated for high temperature when removing the test cell from the electrode holder (assembly).

### 8.1.2 Test Procedure for Test 1 and Test 2 (Neat IL at Room Temperature)

The following steps are to be followed in order to conduct electrochemical corrosion testing of Ionic Liquid NDIL0046.

1. Ensure that the test sequence has been entered into the software per the setup tables at the Gamry Potentiostat designated for this testing. Ensure that the data will be stored to unique file names. See Table 8.1 for material properties and Table 8.2 for the test sequence summary.
2. Clean portion of the WE to be tested with 600 grit paper, wipe, rinse with water and acetone, air dry.
3. Rinse CE and RE wires with acetone, and test cell with acetone and water. Dry with air to eliminate any possible residues.
4. Insert WE, CE, and RE into electrode holder as shown below in Figure 8.1.
5. Insert the Ag wire RE into the glass tube.
6. Insert the RE glass tube into the electrode holder as shown above. See also Figure 8.1 for a more detailed look of how to position the electrodes within the assembly.

**Table 8.1:  Material Properties**

| Test Parameter | Carbon Steel 1018-CS | Stainless Steel 304L-SS |
|---|---|---|
| Surface Area (cm$^2$) | 1.38 (insert rod 1 cm inside the liquid, such that 37 mm extends above the top of the ferrule | |
| Density (g/cm$^3$) | 7.87 | 7.94 |
| Equivalent Weight (g) | 18.88 | 19.66 |
| Stern-Geary Coefficient (mV) | 26 | |
| Reference Type | User Define | V vs. NHE = 0 |
| Polarity Conversion | Potential O$_2$$^+$ | Current O$_2$$^+$ |
| Corrosion Units | MPY | |

**Table 8.2:  Test Sequence Summary**

| Test | Approximate Time | No. of Points Collected | Sample Period (Pt/sec) |
|---|---|---|---|
| Delay | 30 sec | N/A | 1 |
| OCP 1 | 1800 sec = 30 min | 1800 | 1 |
| PS | 180 sec = 3 min | 180 | 1 |
| LPR | ~360 sec = 6 min | ~360 | 1 |
| OCP 2 | 1800 sec = 30 min | 1800 | 1 |
| PDS | ~12598 sec = 210 min = 3.5 h | ~2100 | 1 Pt / 6 sec |
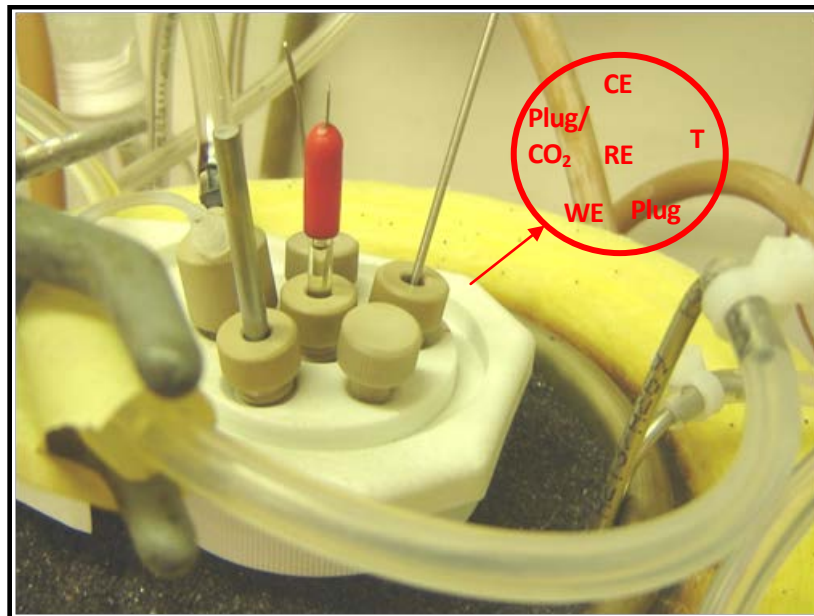


**Figure 8.1:  Visual Instructions for Electrode Positioning**

7.  Insert the thermocouple (T) and connect it to a calibrated thermometer.  Since these tests are specified at room temperature, the thermometer will be used to record the actual minimum and maximum temperature of the test.  Instructions on how to record these temperatures are explained further in this document.

8.  Fill the test cell with 15 ml of solution and secure test cell to the electrode holder.  To measure the volume of IL, place the test cell in a balance and tare.  Using a disposable plastic pipette, start adding IL into the test cell until the balance indicates 15 gr.

9.  Position the WE such that 1 cm extends inside the IL, all of the CE coils extend into the IL, and at least 0.5 cm of the RE tube extends into the IL.  Tighten the electrode fittings to insure that the electrodes do not move during the test.  See Figure 8.2 for details on this assembly.
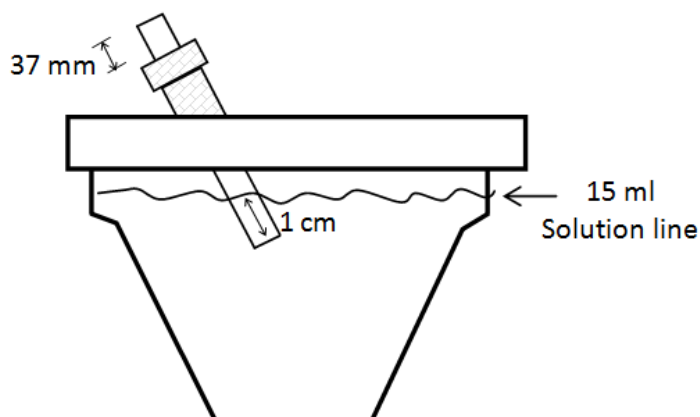


**Figure 8.2:  Details on WE Assembly**

10. Plug all other openings in the electrode holder (assembly).

11. Make connections between electrodes and potentiostat as follow:
   - WE connected to the green (working) and blue (working sense) cables
   - CE connected to the red (counter) cable
   - RE connected to the white (reference) cable
   - Keep the orange (counter sense) cable connected to itself
   - Keep the black (floating ground) cable connected to itself
   - Be cautious not to interconnect cables within each other or not to establish any kind of electrical connection outside from the specifications above to avoid electrical circuits.
   - Cables must not be connected and/or disconnected while a test is running in the potentiostat.  This could produce a short circuit to the operator.
   - Be cautious when handling the cables and maintain housekeeping around the assembly.  This is to avoid that cables get caught and snap from the assembly, or assembly support gets compromised.

12. Initiate test sequence.

13. Start recording IL temperature at the thermometer for minimum and maximum values.  This is done by clicking the "record" button at the instrument keypad.  Make sure the button selected is the one corresponding to the connected thermocouple.

14. After completion of the test sequence, disconnect potentiostat connection cables.

15. Remove test cell bottom and WE.  Rinse WE with acetone and dry it with air or paper. Photograph test solution and test specimen.  Make sure that specimen photographed corresponds to the actual exposed side of the material.  Label the solution sample to show in the photo: date (MMDDYY), IL Name ([P66614][2CNPYL]), and test number (T#).  Keep consistency within the different tests since these photographs will be shown in a final report.

16. Mark the expose side of the WE specimen with test number as "T#".  Cover specimen in paper and plastic bags and store in the desiccator for later use.  If same material is to be used in a later test, use the non-expose side of the specimen before using a brand new specimen.

17. Pour solution into a marked glass bottle.  Keep the same labeling system described in item 15.

18. Remove Ag wire RE from glass tube.

19. Remove electrodes from test cell by loosening fittings and pushing electrodes down. Rinse electrodes with acetone and dry them with air or paper.  Additionally, rinse test cell, hypodermic needle, and all other glassware thoroughly with water and/or acetone. Fittings, ferrules, and other equipment parts could be soaked in acetone inside a beaker for a few minutes.  The ultrasound bath could also be used for this purpose, especially if darker residues from the IL are observed in the accessories.

20. Acetone/methanol and IL waste should be segregated in a temporary container and dispose at the hazardous chemical waste drum located in the CO2 Control Lab.  Make sure to identify the correct waste drum as there are 2 adjacent drums with different purposes.

21. Contaminated napkins with IL and other chemicals could be safely disposed in the regular trash cans located in the laboratory areas.  Make sure trash cans are cleaned regularly to avoid the developing of odors characteristic of these chemicals, if any.

22. Store test solution in containers in the well-ventilated and dark cabinet underneath the fume hood.  Solution to be tested could also be stored in the same cabinet.  Make sure there are no acids in the same cabinet as these are incompatible with the IL.

### 8.1.3   Test Procedure for Test 5 and Test 6 (Neat IL at 150$^{o}$C)

The following steps are to be followed in order to conduct electrochemical corrosion testing of Ionic Liquid NDIL0046.

1. Ensure that the test sequence has been entered into the software per the setup tables at the Gamry Potentiostat designated for this testing. Ensure that the data will be stored to unique file names.  See Table 8.1 for material properties and Table 8.2 for the test sequence summary.

2. Clean portion of the WE to be tested with 600 grit paper, wipe, rinse with water and acetone, air dry.

3. Rinse CE and RE wires with acetone, and test cell with acetone and water.  Dry with air to eliminate any possible residues.

4. Insert CE and RE into electrode holder as shown below in Figure 8.1.

5. Insert the Ag wire RE into the glass tube.

6. Insert the RE glass tube into the electrode holder as shown above.  See also Figure 8.1 for a more detailed look of how to position the electrodes within the assembly.  Note that initially, the position for the WE will be plugged and WE will be added in a later step.

7. Insert the thermocouple (T) and connect it to a calibrated thermometer.  Since these tests are specified at 150$^o$C, the thermometer will be used to record the actual minimum and maximum temperature of the test.  Instructions on how to record these temperatures are explained further in this document.

8. Fill the test cell with 15 ml of solution and secure test cell to the electrode holder.  To measure the volume of IL, place the test cell in a balance and tare.  Using a disposable plastic pipette, start adding IL into the test cell until the balance indicates 15 gr.

9. Tighten the electrode fittings to insure that the electrodes do not move during the test.

10. Plug all other openings in the electrode holder (assembly).

11. Insert test cell and electrode holder into the sand (aluminum oxide - $Al_2O_3$) bath.  The sand bath should be located on top of a hot plate.  The hot plate will supply heat to the bottom of the sand bath (metal beaker containing the sand).  See Figure 8.3 for assembly details.
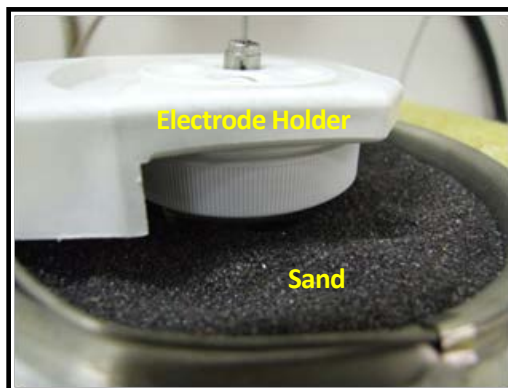


**Figure 8.3:  Details of Electrode Holder Assembly into the Sand Bath**

12. Plug the hot plate and set temperature as indicated in the Table 8.3.  Connect the sand bath internal heating element to the back of a temperature controller.  Temperature controller provides radial heat to the metal beaker via a heat tape to which is connected. Additionally, connect the internal sand bath thermocouple located along the metal beaker wall, to the back of the temperature controller.  Set the temperature controller as indicated in the table below.  See also Figure 8.4 that provides some insight on how these parts are interconnected.

**Table 8.3:  Temperature Setpoints for IL, Hot Plate, and Temperature Controller**

| Target IL Temperature | Hot Plate Temperature Setpoint | Temperature Controller Setpoint |
|---|---|---|
| 150$^o$C (302$^o$F) | 140$^o$C (284$^o$F) | 269$^o$C (516$^o$F) |
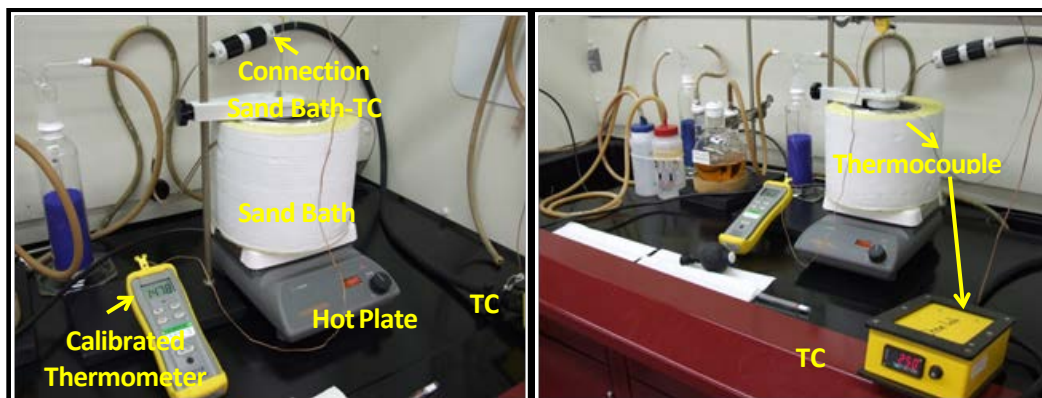
**Figure 8.4: Experimental Setup and Parts Connections**

13. Once the target IL temperature has been reached, unplugged the WE port and position the WE such that 1 cm extends inside the IL, all of the CE coils extend into the IL, and at least 0.5 cm of the RE tube extends into the IL. Tighten the electrode fittings to insure that the electrodes do not move during the test. See Figure 8.2 for details on this assembly.

14. Make connections between electrodes and potentiostat as follow:
    - WE connected to the green (working) and blue (working sense) cables
    - CE connected to the red (counter) cable
    - RE connected to the white (reference) cable
    - Keep the orange (counter sense) cable connected to itself
    - Keep the black (floating ground) cable connected to itself
    - Be cautious not to interconnect cables within each other or not to establish any kind of electrical connection outside from the specifications above to avoid electrical circuits.
    - Cables must not be connected and/or disconnected while a test is running in the potentiostat. This could produce a short circuit to the operator.
    - Be cautious when handling the cables and maintain housekeeping around the assembly. This is to avoid that cables get caught and snap from the assembly, or assembly support gets compromised.

15. Initiate test sequence.

16. Start recording IL temperature at the thermometer for minimum and maximum values. This is done by clicking the "record" button at the instrument keypad. Make sure the button selected is the one corresponding to the connected thermocouple.

17. After completion of the test sequence, disconnect potentiostat connection cables.

18. Remove test cell bottom and WE. Use gloves rated for high temperature when removing the test cell from the electrode holder (assembly). Rinse WE with acetone and dry it with air or paper. Photograph test solution and test specimen. Make sure that specimen photographed corresponds to the actual exposed side of the material. Label the solution sample to show in the photo: date (MMDDYY), IL Name ([P66614][2CNPYL]), and test number (T#). Keep consistency within the different tests since these photographs will be shown in a final report.

19. Mark the expose side of the WE specimen with test number as "T#". Cover specimen in paper and plastic bags and store in the desiccator for later use. If same material is to be used in a later test, use the non-expose side of the specimen before using a brand new specimen.

20. Pour solution into a marked glass bottle. Keep the same labeling system described in item 18.

21. Remove Ag wire RE from glass tube.

22. Remove electrodes from test cell by loosening fittings and pushing electrodes down. Rinse electrodes with acetone and dry them with air or paper. Additionally, rinse test cell, hypodermic needle, and all other glassware thoroughly with water and/or acetone. Fittings, ferrules, and other equipment parts could be soaked in acetone inside a beaker for a few minutes. The ultrasound bath could also be used for this purpose, especially if darker residues from the IL are observed in the accessories.

23. Acetone/methanol and IL waste should be segregated in a temporary container and dispose at the hazardous chemical waste drum located in the $CO_2$ Control Lab. Make sure to identify the correct waste drum as there are 2 adjacent drums with different purposes.

24. Contaminated napkins with IL and other chemicals could be safely disposed in the regular trash cans located in the laboratory areas. Make sure trash cans are cleaned regularly to avoid the developing of odors characteristic of these chemicals, if any.

25. Store test solution in containers in the well-ventilated and dark cabinet underneath the fume hood. Solution to be tested could also be stored in the same cabinet. Make sure there are no acids in the same cabinet as these are incompatible with the IL.

### 8.1.4   Test Procedure for Test 3 and Test 4 (IL and $CO_2$ at Room Temperature)

The following steps are to be followed in order to conduct electrochemical corrosion testing of Ionic Liquid NDIL0046.

1. Saturate 30 ml of IL solution with pure $CO_2$ gas immediately before performing the tests. Saturation will be accomplished by bubbling $CO_2$ through the solution overnight prior to starting a test. Cover the container and continue bubbling $CO_2$ through the remainder of the solution until all of the tests in this solution are completed.

2. Select a small $CO_2$ volumetric flow of approximately 0.4 scfh (standard cubic feet per hour) at the rotameter to have a slow but constant gas flow.

3. Ensure that the test sequence has been entered into the software per the setup tables at the Gamry Potentiostat designated for this testing. Ensure that the data will be stored to unique file names. See Table 8.1 for material properties and Table 8.2 for the test sequence summary.

4. Clean portion of the WE to be tested with 600 grit paper, wipe, rinse with water and acetone, air dry.

5. Rinse CE and RE wires with acetone, and test cell with acetone and water. Dry with air to eliminate any possible residues.

6. Insert WE, CE, RE, and $CO_2$ gas into the electrode holder as shown in Figure 8.1.

7. Insert the Ag wire RE into the glass tube.

8. Insert the RE glass tube into the electrode holder as shown above. See also Figure 8.1 for a more detailed look of how to position the electrodes within the assembly.

9.  Insert the thermocouple (T) and connect it to a calibrated thermometer. Since these tests are specified at room temperature, the thermometer will be used to record the actual minimum and maximum temperature of the test. Instructions on how to record these temperatures are explained further in this document.

10. Fill the test cell with 15 ml of solution and secure test cell to the electrode holder. To measure the volume of IL, place the test cell in a balance and tare. Using a disposable plastic pipette, start adding IL into the test cell until the balance indicates 15 gr.

11. Position the WE such that 1 cm extends inside the IL, all of the CE coils extend into the IL, and at least 0.5 cm of the RE tube extends into the IL. Tighten the electrode fittings to insure that the electrodes do not move during the test. See Figure 8.2 for details on this assembly.

12. Plug all other openings in the electrode holder (assembly).

13. Initiate $CO_2$ gas at a volumetric flow of approximately 0.4 scfh at the rotameter to have a slow but constant flow.

14. Make connections between electrodes and potentiostat as follow:
    - WE connected to the green (working) and blue (working sense) cables
    - CE connected to the red (counter) cable
    - RE connected to the white (reference) cable
    - Keep the orange (counter sense) cable connected to itself
    - Keep the black (floating ground) cable connected to itself
    - Be cautious not to interconnect cables within each other or not to establish any kind of electrical connection outside from the specifications above to avoid electrical circuits.
    - Cables must not be connected and/or disconnected while a test is running in the potentiostat. This could produce a short circuit to the operator.
    - Be cautious when handling the cables and maintain housekeeping around the assembly. This is to avoid that cables get caught and snap from the assembly, or assembly support gets compromised.

15. Initiate test sequence.

16. Start recording IL temperature at the thermometer for minimum and maximum values. This is done by clicking the "record" button at the instrument keypad. Make sure the button selected is the one corresponding to the connected thermocouple.

17. After completion of the test sequence, disconnect potentiostat connection cables.

18. Remove test cell bottom and WE. Rinse WE with acetone and dry it with air or paper. Photograph test solution and test specimen. Make sure that specimen photographed corresponds to the actual exposed side of the material. Label the solution sample to show in the photo: date (MMDDYY), IL Name ([P66614][2CNPYL]), and test number (T#). Keep consistency within the different tests since these photographs will be shown in a final report.

19. Mark the expose side of the WE specimen with test number as "T#". Cover specimen in paper and plastic bags and store in the desiccator for later use. If same material is to be used in a later test, use the non-expose side of the specimen before using a brand new specimen.

20. Pour solution into a marked glass bottle. Keep the same labeling system described in item 18.

21. Remove Ag wire RE from glass tube.

22. Remove electrodes from test cell by loosening fittings and pushing electrodes down. Rinse electrodes with acetone and dry them with air or paper. Additionally, rinse test cell, hypodermic needle, and all other glassware thoroughly with water and/or acetone. Fittings, ferrules, and other equipment parts could be soaked in acetone inside a beaker for a few minutes. The ultrasound bath could also be used for this purpose, especially if darker residues from the IL are observed in the accessories.

23. Acetone/methanol and IL waste should be segregated in a temporary container and dispose at the hazardous chemical waste drum located in the $CO_2$ Control Lab. Make sure to identify the correct waste drum as there are 2 adjacent drums with different purposes.

24. Contaminated napkins with IL and other chemicals could be safely disposed in the regular trash cans located in the laboratory areas. Make sure trash cans are cleaned regularly to avoid the developing of odors characteristic of these chemicals, if any.

25. Store test solution in containers in the well-ventilated and dark cabinet underneath the fume hood. Solution to be tested could also be stored in the same cabinet. Make sure there are no acids in the same cabinet as these are incompatible with the IL.

## 8.2  COMPLETE ELECTROCHEMICAL TEST RESULTS

### 8.2.1  Test 1: Carbon Steel in Neat IL at Room Temperature

LPR CR = 0.01029 mpy
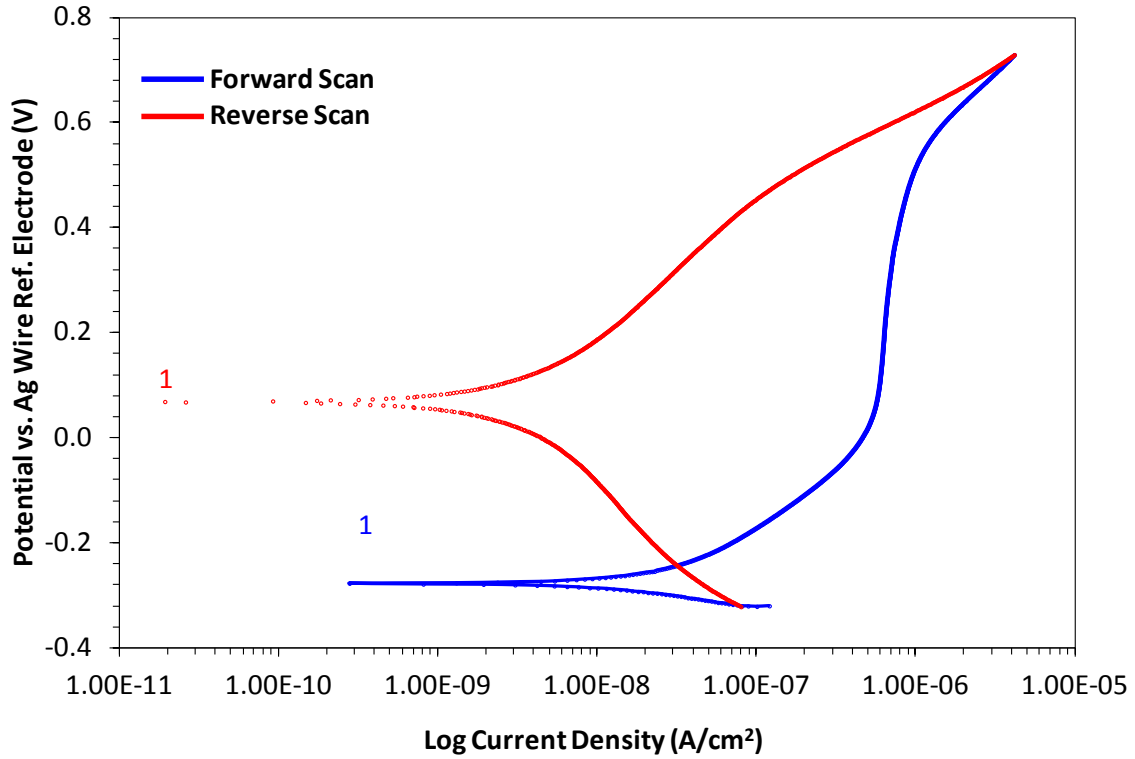


**Figure 8.5:  Carbon Steel 1018-CS in Neat IL NDIL0046 at 25$^{\circ}$C**



**Figure 8.6:  Post-Test 1 Neat IL NDIL0046 and 1018-CS Test Specimen**

### 8.2.2 Test 2: Stainless Steel in Neat IL at Room Temperature

LPR CR = 0.00344 mpy
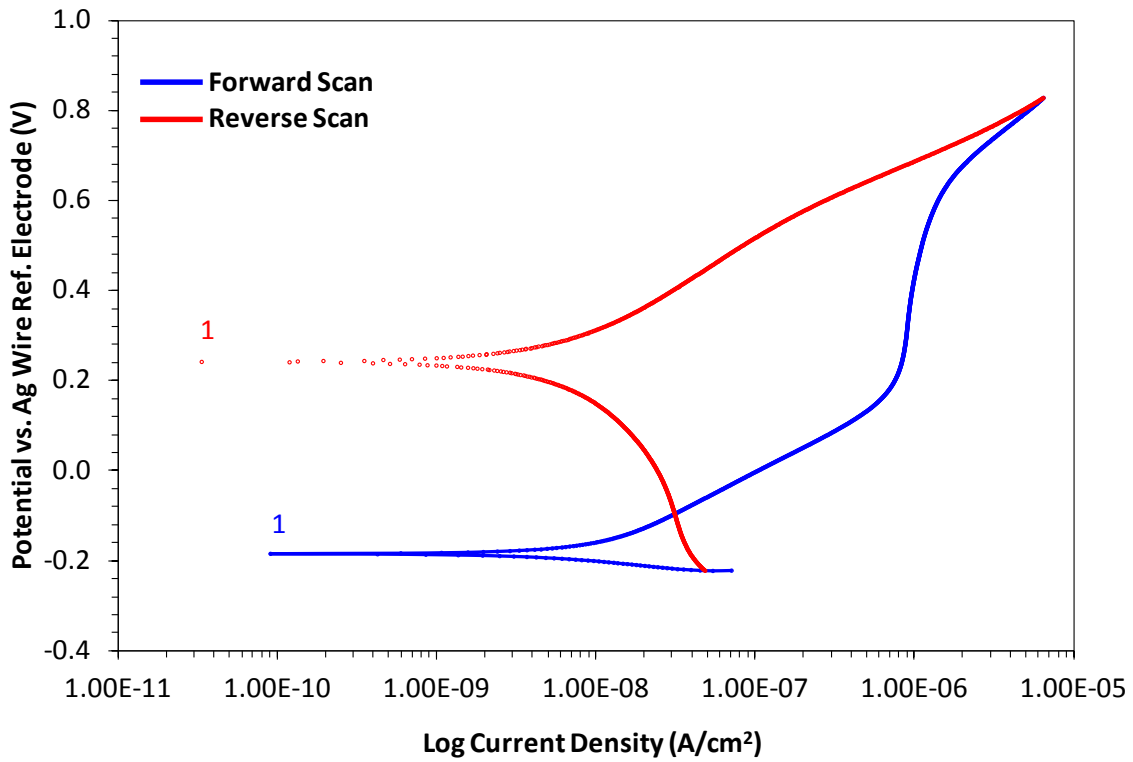


**Figure 8.7: Stainless Steel 304L-SS in Neat IL NDIL0046 at 25$^o$C**
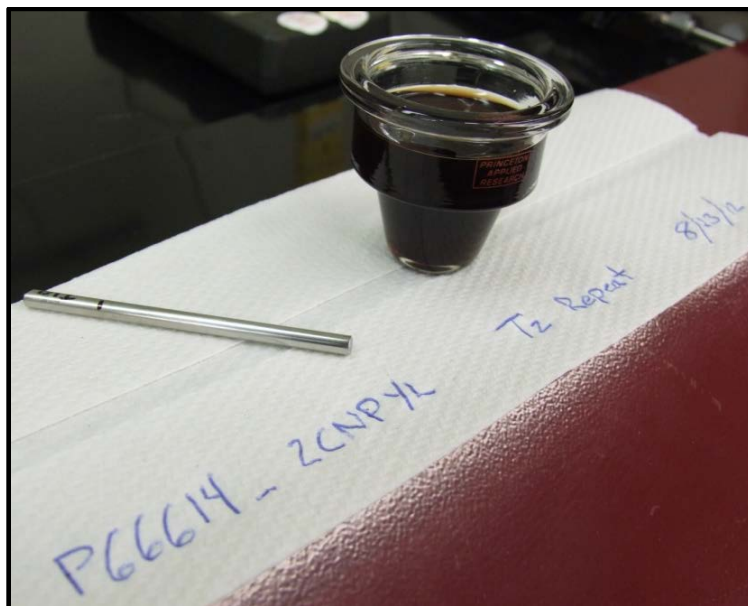


**Figure 8.8: Post-Test 2 Neat IL NDIL0046 and 304L-SS Test Specimen**

### 8.2.3 Test 3: Carbon Steel in IL and $CO_2$ at Room Temperature

LPR CR = 0.00068 mpy
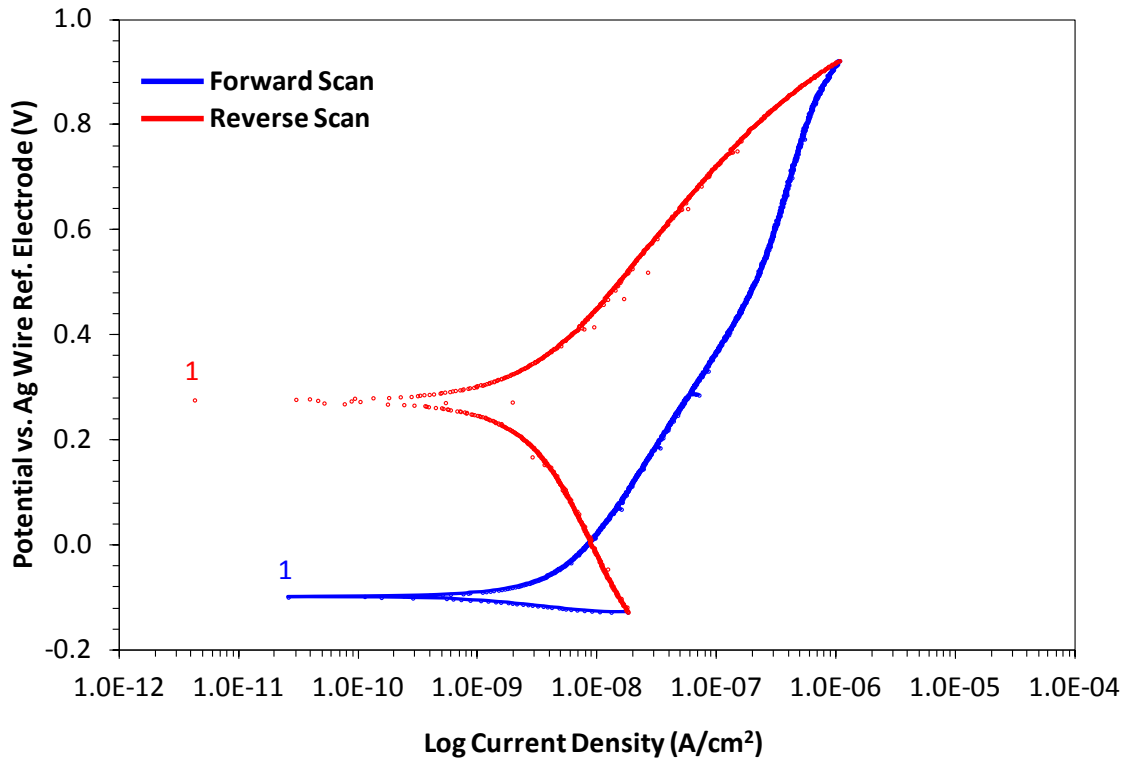


**Figure 8.9: Carbon Steel 1018-CS in IL NDIL0046 and $CO_2$ at 25$^o$C**



**Figure 8.10: Post-Test 3 IL NDIL0046, $CO_2$, and 1018-CS Test Specimen**

### 8.2.4    Test 4: Stainless Steel in IL and CO$_2$ at Room Temperature

LPR CR = 0.00136 mpy
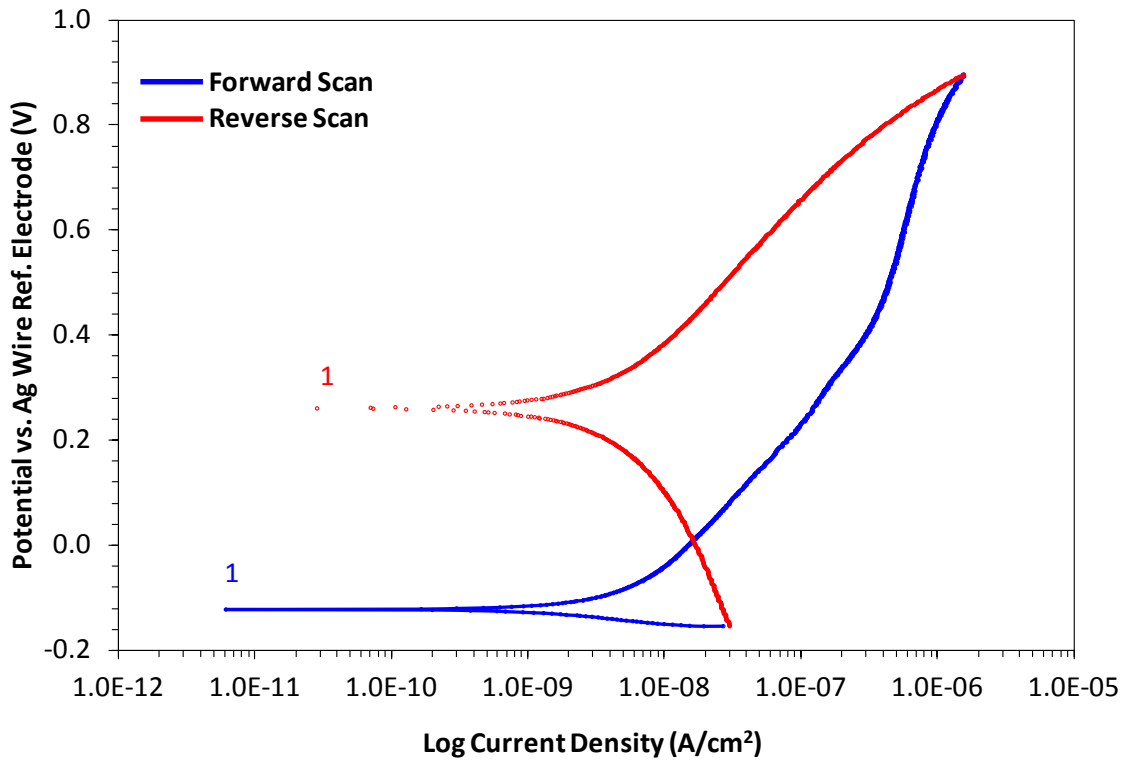


**Figure 8.11:  Stainless Steel 304L-SS in IL NDIL0046 and CO$_2$ at 25$^{\text{o}}$C**
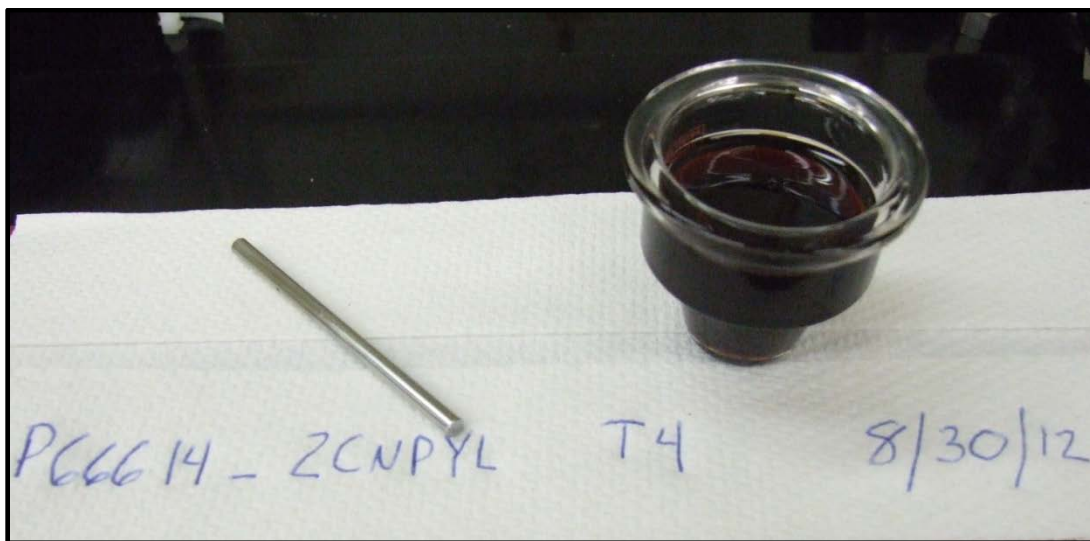


**Figure 8.12:  Post-Test 4 IL NDIL0046, CO$_2$, and 304L-SS Test Specimen**

### 8.2.5   Test 5: Carbon Steel in Neat IL at 150°C

LPR CR = 0.099 mpy
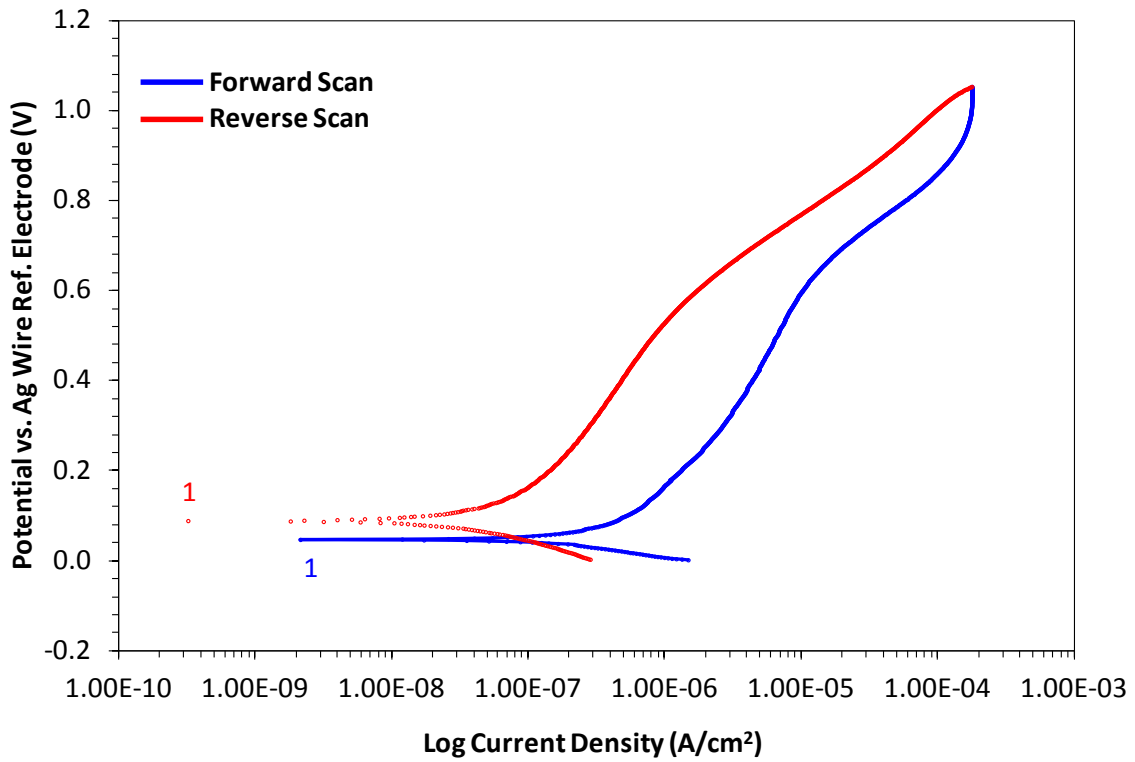


**Figure 8.13:  Carbon Steel 1018-CS in Neat IL NDIL0046 at 150°C**



**Figure 8.14:  Post-Test 5 Neat IL NDIL0046 and 1018-CS Test Specimen**

### 8.2.6  Test 6: Stainless Steel in Neat IL at 150$^o$C

LPR CR = 0.07134 mpy
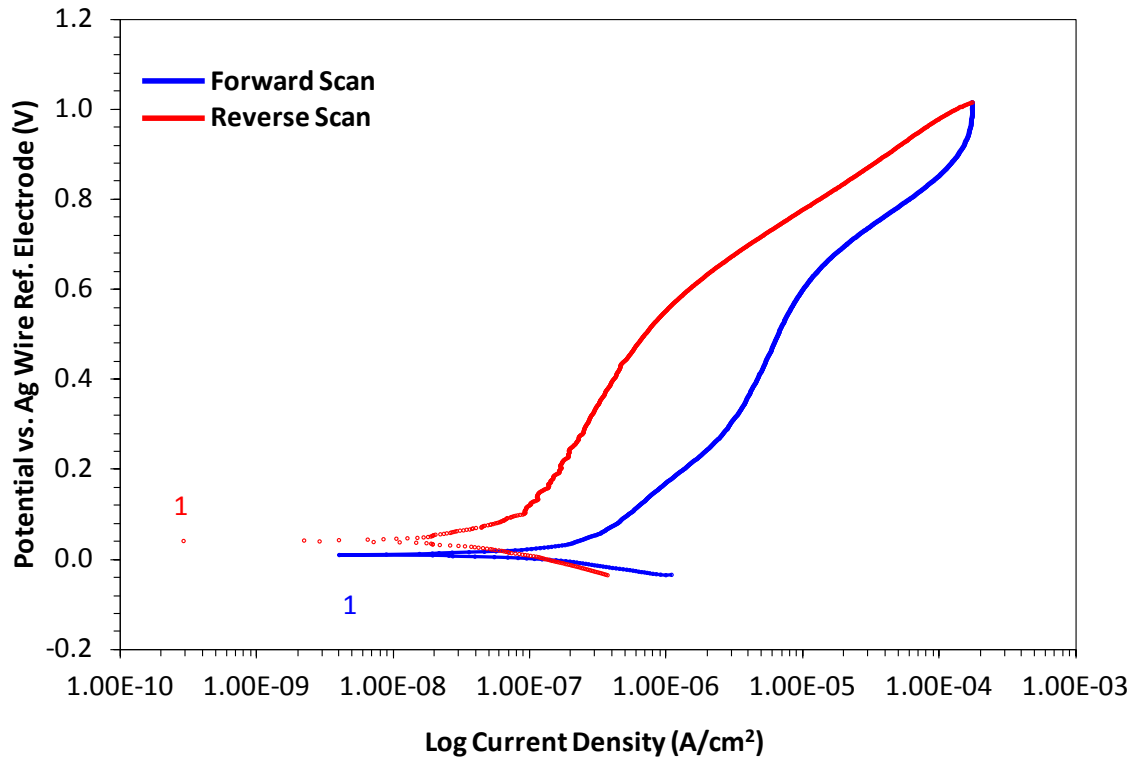


**Figure 8.15:  Stainless Steel 304L-SS in Neat IL NDIL0046 at 150$^o$C**
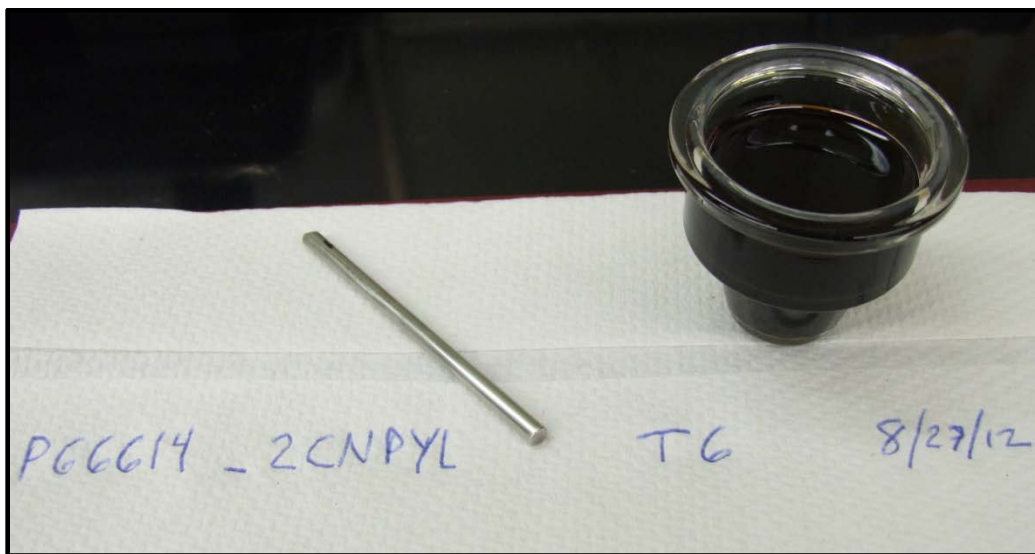


**Figure 8.16:  Post-Test 6 Neat IL NDIL0046 and 304L-SS Test Specimen**

Appendix IV – Report from Trimeric on Final Systems Analysis

# Subtask 19.2 Milestone Report:
# Final Systems Analysis

**Date:** 30 September 2012

**To:** Dr. Edward Maginn, University of Notre Dame

**From:** Trimeric Corporation

**Prepared by:** Andrew J. Sexton, Duane B. Myers, Kevin S. Fisher, Katherine Searcy, Anne I. Ryan, and Carrie M. Beitler

**RE:** DOE Project #43091 (Ionic Liquids: Breakthrough Absorption Technology for Post-Combustion $CO_2$ Capture)

## DISCLAIMER

# 1    INTRODUCTION

This document presents the results of Subtask 19.2 "Complete Rigorous Systems Analysis" as described in the revised (July 2009) Statement of Project Objectives document. The activities in Subtask 19.2 represent an update of the previous process modeling for a hypothetical ionic liquid (IL) $CO_2$ capture system conducted under Subtask 16.0 in Phase 3 as reported by Trimeric in the August 4, 2010 milestone report, "Systems and Economic Analyses Update".

The systems analysis update included: 1) incorporating experimentally and theoretically determined key ionic liquid (IL) properties ($CO_2$ absorption capacity, density, viscosity, heat capacity, thermal stability) that govern the parasitic power requirements for an actual IL and 2) a preliminary economic evaluation to estimate the cost of electricity from a coal-fired power plant with post-combustion $CO_2$ capture using the actual and theoretical properties for NDIL0157.

The complete systems analysis includes an economic evaluation of purchased equipment costs, electric energy penalties and steam derating, capital costs, operating and maintenance costs, and cost of electricity from a greenfield supercritical pulverized coal (PC) power plant with 90% $CO_2$ capture that produces 550 MW of net electric power.

The process economics for the selected IL-based $CO_2$ capture system was then compared to Case 12 from the 2010 DOE Cost and Performance Baseline.[1] Case 12 details the economics of a supercritical PC power plant with $CO_2$ capture using Fluor's Econamine FG Plus[TM] process.

## 2   EXECUTIVE SUMMARY

The results of the ionic liquid $CO_2$ capture system analysis and cost of electricity estimates are summarized in this section.  More detailed information on the technical approach and results is provided in the sections to follow.

Process modeling and economic analysis were conducted for a $CO_2$ capture process using NDIL0157.  Process simulations with mass and energy balances were prepared.  Equipment in the process was then sized and selected, and purchased equipment costs were estimated from vendor information or costing software.  Finally, capital costs, operating costs and cost of electricity were estimated.  Costs for NDIL0157 were compared to a baseline case using monoethanolamine (MEA) absorbent taken from the 2010 Cost and Performance Baseline[1] and compared to costs for NDIL0046 evaluated in the previous milestone report for this project.[2]

The standard design basis for this evaluation is a 550 MW net supercritical coal-fired power plant using Illinois #6 subbituminous coal.  The location for this greenfield plant is a generic plant site in midwestern USA.  A wet flue gas desulfurization (FGD) unit was assumed to be located upstream of the $CO_2$ capture unit.  The target $CO_2$ removal was 90%.  Any captured $CO_2$ was assumed to be delivered at pipeline pressure (15.2 MPa; 2215 psia), transported 80 kilometers (50 miles) and sequestered in a saline formation at a depth of 1,239 m (4,055 ft).  The entire $CO_2$ capture system consisted of a single inlet gas conditioning train, multiple parallel capture units, and a single, common $CO_2$ compressor train.

Trimeric estimated that $CO_2$ capture increased the base cost of electricity from 5.89 ¢/kWh (Case 11 from the 2010 Cost and Performance Baseline) to 10.59 ¢/kWh for NDIL0157, assuming ionic liquid unit costs of $5,000/tonne and stainless steel materials of construction.  In comparison, the cost of electricity for DOE Case 12 ($CO_2$ capture using Fluor's Econamine FG Plus$^{TM}$ process) was estimated by WorleyParsons to be 10.70 ¢/kWh.

Overall, the economics of using NDIL0157 were estimated to be comparable to the Fluor Econamine FG Plus$^{TM}$ process (DOE Case 12).  Lower reboiler energy consumption for NDIL0157 was offset by higher compression energy requirements and higher capture and compression purchased equipment costs.  The higher purchased equipment costs for NDIL0157 can be attributed primarily to the lean/rich cross-exchanger (due to the higher viscosity of NDIL0157) and compression equipment (due to the lower regeneration pressure for NDIL0157).

In addition to showing comparable cost performance to DOE Case 12, NDIL0157 exhibited superior performance to NDIL0046, which was studied in the prior systems analysis.  Energy requirements were approximately 30% lower for NDIL0157 when compared to NDIL0046, and purchased equipment costs were approximately 36% lower.

Important parameters that influence the overall cost of electricity for the NDIL0157 $CO_2$ capture process include materials of construction, the viscosity of the IL, and the cost of the IL.  Preliminary corrosion studies performed by Babcock and Wilcox indicate that at temperatures below 100°C, corrosion rates for ILs are less than corrosion rates for MEA.  This suggests that

carbon steel is an acceptable material of construction for equipment operated at lower temperatures within the process. For example, if the IL absorber columns and packing were constructed of carbon steel instead of 316 stainless steel, the purchased equipment costs at 593 MW gross output would decrease by $11.2 MM, and the overall cost of electricity at 550 MW net output would decrease from 10.59 ¢/kWh to 10.35 ¢/kWh.

In addition to the absorber, another large contribution to the overall capture purchased equipment costs was the rich/lean cross-exchanger. A 50% reduction in IL viscosity (when compared to the current values) would decrease cross-exchanger purchased equipment costs by approximately $4.3 MM at 593 MW gross output, which results in a decrease in the cost of electricity from 10.59 ¢/kWh to 10.49 ¢/kWh. If the effects of reduced viscosity were combined with the effects of a carbon steel absorber, then overall cost of electricity at 550 MW net output would decrease from 10.59 ¢/kWh to 10.25 ¢/kWh.

The unit cost of ionic liquids has a direct impact on the annual variable operations costs of the $CO_2$ capture system. Assuming a degradation rate of 0.23 kg IL/MT $CO_2$ and a unit cost of $5/kg (or $5,000/tonne), the annual cost of IL solvent replacement is approximately $4.43 MM. If these unit costs were $10/kg or $15/kg, the annual cost of IL solvent replacement would increase to $8.86 MM and $13.29 MM, respectively. Assuming these unit costs, the overall cost of electricity at 550 MW net output would increase from 10.59 ¢/kWh to 10.77 ¢/kWh and 10.94 ¢/kWh, respectively.

## 3 DESIGN BASIS AND PROCESS DESCRIPTION

The basis for this study is a pulverized-coal-fired supercritical boiler with a wet FGD system. The unit fires Illinois #6 subbituminous coal, and the resulting flue gas composition from the 2010 Cost and Performance Baseline[1] is shown in Table 1. Sulfur dioxide is not included in this composition since any residual sulfur dioxide from the flue gas desulfurization system is removed prior to entering the $CO_2$ capture unit. A capacity factor of 85% was assumed for the economic analysis, and the $CO_2$ capture units were designed to remove 90% of the $CO_2$ from the flue gas stream.

**Table 1. Inlet Flue Gas Temperature, Pressure and Composition**

| Property | Value |
|---|---|
| Temperature | 58°C (136°F) |
| Pressure | 100 kPa (14.5 psia) |
| **Composition** | **Mole %** |
| $N_2$ | 67.93 |
| $O_2$ | 2.38 |
| $CO_2$ | 13.50 |
| $H_2O$ | 15.37 |
| Ar | 0.81 |

A generic process flow diagram for an IL-based $CO_2$ capture system is shown in Figure 1. The inlet flue gas passes through a blower to increase the pressure to 110.3 kPa (16.0 psia) and a direct contact cooler to lower the temperature to 40°C (104°F). The gas then enters the bottom of the absorber. Cooled, lean IL solution enters the top of the absorber, and rich solution exits the bottom of the absorber. Flue gas exits from the top of the absorber and flows to the stack. Rich solution exchanges heat with hot lean solution. The preheated rich solution flows to the stripper where $CO_2$ desorbs from solution. A steam-heated reboiler provides heat to the stripper column for $CO_2$ desorption and sensible heating of the liquid. Hot lean solution exits from the bottom of the stripper and is cooled through cross exchange with the rich solution. Warm stripper overheads flows to a condenser where the vapor is cooled and water is condensed. The remaining $CO_2$ vapor then flows to compression.

The captured $CO_2$ is compressed to pipeline pressure of 15.27 MPa (2215 psia). The compressor train has multiple stages of centrifugal compression with interstage coolers and separators. Compression increases the pressure to about 8.4 MPa (1215 psia). A multistage centrifugal pump then takes the $CO_2$ to its final pipeline conditions. A dehydration unit is included between the final compression stage and the multistage centrifugal pump to dry the $CO_2$.

Tanks and pumps for makeup solution and water are required in addition to a cooling water system for the entire $CO_2$ capture unit (water is needed for the coolers in the process). Finally, a

reclaimer system will be needed to remove degradation products as they accumulate in the solution over time.

Some minor differences in the equipment required by the conventional amine and ionic liquid processes are:

1) The lean solution pump may not be required in the ionic liquid process if the stripper is operated at elevated pressure (>586 kPa or 85 psia, provided by the upstream rich solution pump);
2) An absorber intercooler is used with the ionic liquid process because there is no excess water in the IL system to absorb the heat of reaction as there is in an amine system; and
3) Fewer compression stages may be used with the ionic liquids process if the stripper operates at higher pressure (MEA strippers typically operate in the 35-69 kPa or 5-10 psig range).
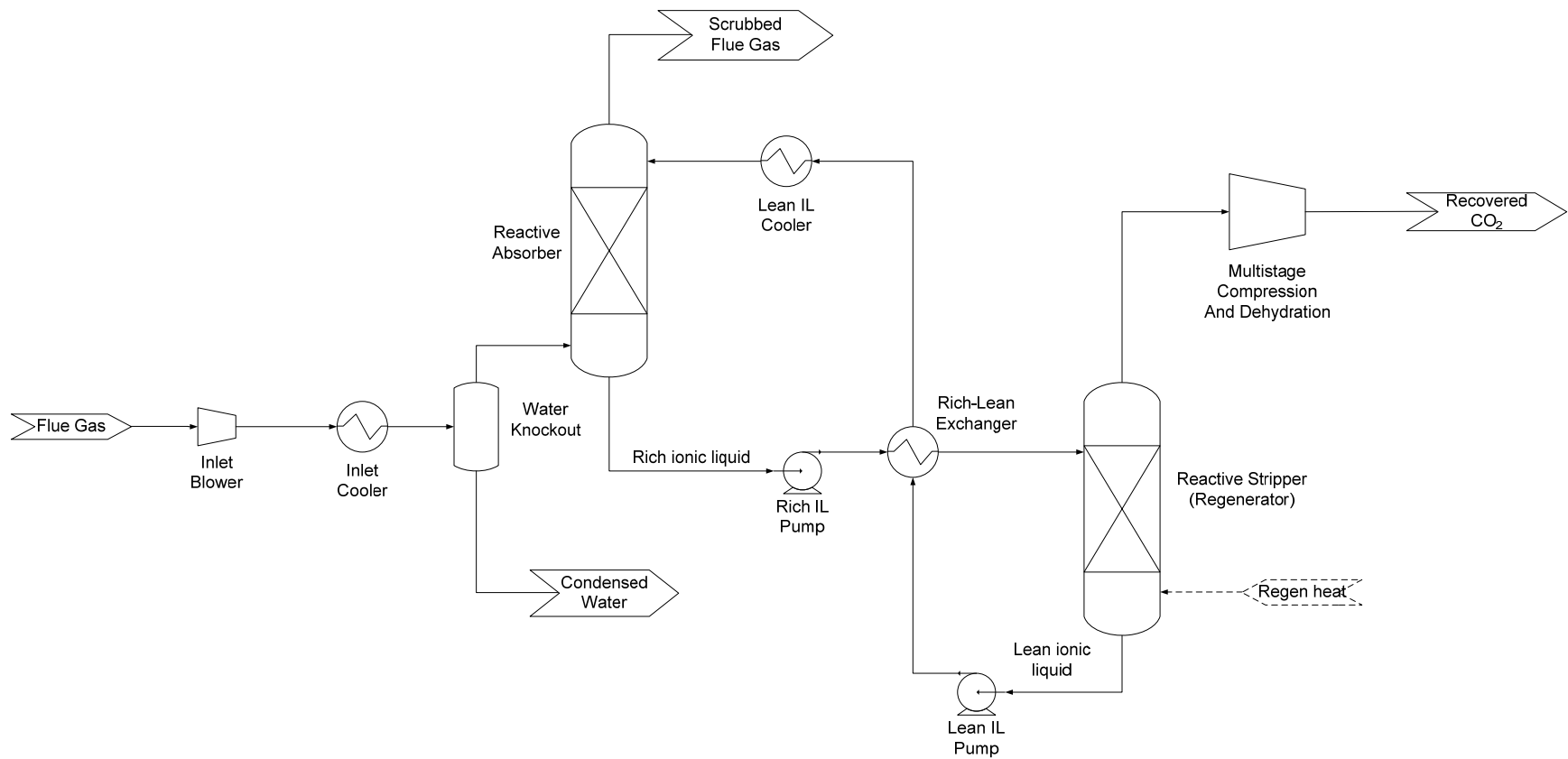
**Figure 1. Simplified Ionic Liquid (IL) CO$_2$ Capture Process Flow Diagram.**

# 4 IONIC LIQUID PROPERTIES AND MODELING

## 4.1 IL Properties

The $CO_2$ capture process modeling was conducted using an IL compound (NDIL0157) with properties measured and/or modeled by Notre Dame. NDIL0157 was assumed to have a 1:1 stoichiometry with $CO_2$, and the combined IL-$CO_2$ complex is abbreviated as IL*.

Improvements in IL chemistry and properties for $CO_2$ capture have occurred as IL development has progressed to the current generation of ILs. NDIL0157 viscosity does not increase when the IL* complex is formed, and at expected absorber operating temperatures the IL* viscosity is below 126 cP. The molar heat capacity of NDIL0157 is approximately half of the molar heat capacity of NDIL0046. We assumed that the thermal stability of NDIL0157 is the same as NDIL0046 thermal stability, which has been measured over a range of temperatures from 100 to 180 °C, and an Arrhenius expression has been developed to predict IL thermal degradation rates in the $CO_2$ capture process.

Theoretical data for $CO_2$ absorption was calculated as a function of total pressure and liquid mole fractions ($x$) of $CO_2$ and IL over a range of temperatures, assuming enthalpy ($\Delta H_{rxn}$) and entropy ($\Delta S_{rxn}$) values for the reaction of IL with $CO_2$ specified by Notre Dame. Additionally, the Henry's Law constant was calculated as a function of temperature using specified enthalpy ($\Delta H_{abs}$) and entropy ($\Delta S_{abs}$) values for the physical absorption of $CO_2$ into NDIL0157 at specified temperatures. The equations below were used to generate the $CO_2$ solubility isotherms explained above:

$$H(T) = e^{\Delta H/RT} e^{-\Delta S/R}$$

$$K_{eq}(T) = e^{-\Delta H/RT} e^{\Delta S/R}$$

All of this generated data was utilized to calculate an equilibrium constant value, K, at each temperature for each data set in terms of mole fraction (x).

$$K = \frac{x_{IL}^{*}}{x_{IL} x_{CO_2}}$$

The van't Hoff expression, which relates the change in temperature to the change in equilibrium constant (K), given the standard enthalpy change ($\Delta H°$) for the process, was used to calculate the overall heat of reaction (physical absorption and chemical reaction) between NDIL0157 and $CO_2$. The key IL properties used in the HYSYS model are listed in Table 2. Figure 2 shows the K and Henry's Law constant values versus temperature, and Figure 3 shows the fit of the equilibrium expression to the experimental data for the $CO_2$ capacity of NDIL0157.

**Table 2. Ionic Liquid Properties Assumed for Process Modeling.**

| | Value | | Units |
|---|---|---|---|
| | IL | IL* | |
| Molecular Weight | 322 | 366 | g/gmole |
| Liquid density | 3.9970 - 0.002(T) | 3.6065 − 0.002(T) | Density [=] kmol/m$^3$; T [=] K |
| Viscosity | $0.1728e^{(814/T-189.7)}$ | $0.1728e^{(814/T-189.7)}$ | Viscosity [=] cP; T [=] K |
| Heat capacity | 66.5 + 1.8828(T) | 75.5 + 2.1401(T) | Heat Capacity [=] J/gmole-K; T [=] K |
| Enthalpy of Reaction | 60 | | kJ/gmole ($CO_2$ basis) |
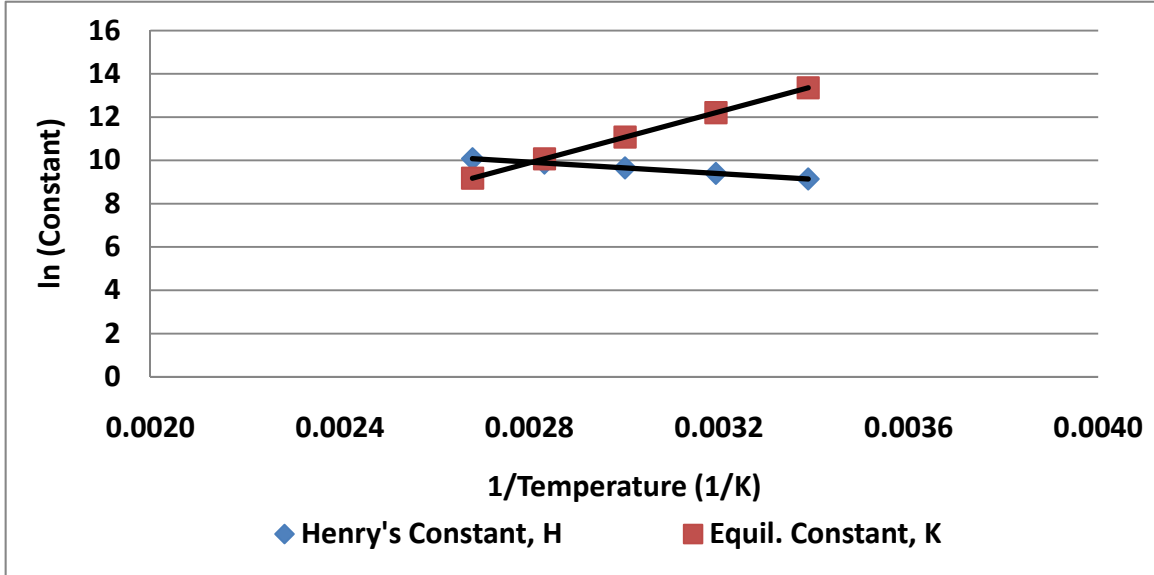


**Figure 2. Equilibrium and Henry's Law Constants as a Function of Temperature**
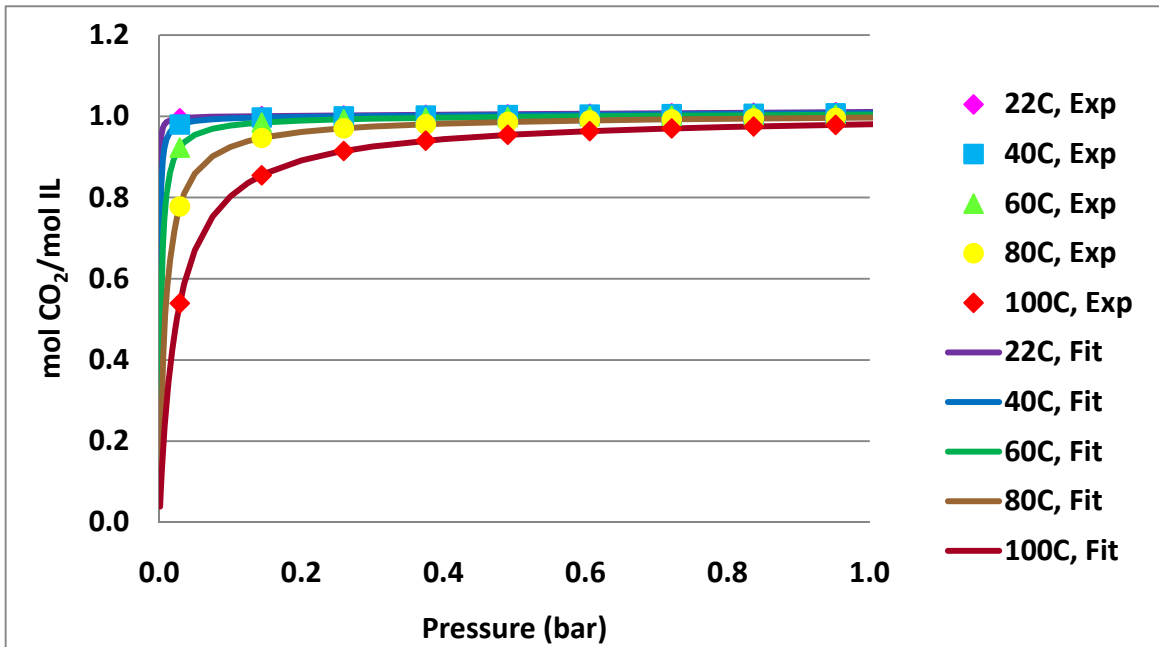
**Figure 3. Model Equilibrium Expression Versus Experimental Data**

The IL compounds developed by Notre Dame are not included in the standard HYSYS component database, so the pure IL and IL* were added to the database as "Hypothetical Components." The minimum information required to specify a hypothetical component in HYSYS is:

- Molecular weight,
- Critical temperature,
- Critical pressure,
- Critical molar volume,
- Acentric factor ($\omega$),
- Normal boiling point, and
- Ideal liquid density.

A number of other thermodynamic properties that may be entered for hypothetical components, but in many cases the information is not available for compounds under development (including standard enthalpy of formation, vapor pressure, vapor enthalpy, and Gibbs free energy). The HYSYS default is to estimate all other missing physical and thermodynamic properties from this minimum information using correlations, typically based on critical properties.

The critical property correlation approach was determined to be unacceptable for the IL process modeling, because the critical properties and acentric factor are not known definitively for the hypothetical IL compounds of interest, and the correlation methods are known to be crude approximations. The following estimated properties for the hypothetical IL and IL* compounds

were entered in the HYSYS "Point" and "Temperature Dependent" tabs for the individual components:

- Standard enthalpy of formation – The $\Delta H^{\circ}_f$ for IL generated by HYSYS using the critical property correlation was accepted for lack of a better number. The $\Delta H^{\circ}_f$ for IL* then was adjusted so that the resulting $\Delta H^{\circ}_{rxn}$ for the $CO_2$ – IL reaction matched the desired value of 60 kJ/mol.
- Vapor pressure – Per Notre Dame's direction, the Antoine constants were set to result in essentially zero vapor pressure over the expected range of process temperatures in the $CO_2$ capture process (i.e. no vaporization losses of the IL species in the absorber or regenerator).

The properties from Table 2 that were entered in the "Tabular Package" section of the Simulation Basis Property Package tab were:

- Liquid density – Correlations for the IL and IL* liquid densities as a function of temperature were entered.
- Heat capacity – Experimental and modeling data were available from Notre Dame for a representative IL liquid-phase heat capacity. Correlations for the IL and IL* vapor heat capacities as a function of temperature were entered in HYSYS to match the experimental liquid-phase heat capacity data.
- Liquid viscosity – The viscosity value from the Subtask 9.1 report (100 cP) was entered because the form of the viscosity equation shown in Table 2 is not available in HYSYS. This value is not utilized for any critical calculations in HYSYS and was input for reference only.

The NRTL activity coefficient model with Henry's Law for non-condensable components was the property package selected for the main process simulation. The NRTL activity coefficient model was selected because binary interaction parameters can be estimated in a straightforward way from experimental solubility data. The NRTL model was used to estimate the activity coefficients for IL, IL*, and $H_2O$, and binary interaction parameters for IL-$H_2O$ were assumed to be the same as NDIL0046. The IL*-$H_2O$ binary parameters were assumed to be the same as the IL-$H_2O$ parameters. However, the interaction between all IL species with one another was assumed to be ideal, so those binary interaction parameters were set to zero. The Henry's Law correlation for $CO_2$ in NDIL0157 was determined using desired hypothetical properties, while the Henry's Law correlations for $N_2$ and $O_2$ were assumed to be the same as NDIL0046.

The NRTL activity coefficient property package was not appropriate for the compression part of the $CO_2$ capture process; therefore, the compression and dehydration operations were created in a subflowsheet using the Peng-Robinson equation of state. All equation of state models for $CO_2$ are unreliable near the critical point, so there likely is some error in the absolute values of the compression work for any particular case. However, the relative differences in the compression power calculated for cases at different regeneration pressures (i.e. compressor suction pressures) should be consistent.

**4.2    Process Modeling Approach**

Aspen HYSYS software (version 7.3) was used to model the $CO_2$ capture process at a scale corresponding to 593 MW gross boiler electric capacity (prior to any parasitic load associated with the $CO_2$ capture unit). The reason for selecting a scale of 593 MW gross boiler electrical capacity will be explained in Section 5, which describes the costing methodology.

A standard absorption / stripping process configuration was used to model the IL $CO_2$ capture process. The HYSYS flowsheet is shown in Figure 4.  The absorber and stripper were assumed to have two equilibrium stages.  Increasing the number of stages may reduce the total equivalent work but likely would lead to increased equipment cost for taller columns.  The economics of the absorber and regenerator designs can be evaluated at a later time, if necessary, when rate and transport property data are available for a particular ionic liquid.

The $CO_2$ compression process was modeled in HYSYS as a multi-stage compressor up to 8377 kPa (1200 psig), followed by a multistage centrifugal pump to increase the pressure of the supercritical $CO_2$ to 15.27 MPa (2200 psig). The compressor consists of five stages, and the outlet pressure from each stage matches the outlet pressure specified in Stages 1 through 5 in Exhibit 4-2 of the 2010 DOE Cost and Performance Baseline. A dehydration step was included between the centrifugal compressor and the multistage centrifugal pump to meet typical pipeline requirements for water content.

WinSim Design II was used to determine cooling water requirements for flue gas cooling, steam condensate requirements for IP/LP steam desuperheating, and equivalent derating for IP/LP steam used for steam heater/reboiler heating.  Figure 5 illustrates a simplified process flow diagram for the steam system modeled in WinSim.

Other key process configuration choices were:

- The rich/lean heat exchanger temperature approach ΔT was specified to be 5°C (9°F); and
- The height of the rich IL inlet to the regenerator was specified to result in a pressure drop of 414 kPa (60 psi) from the rich/lean heat exchanger.
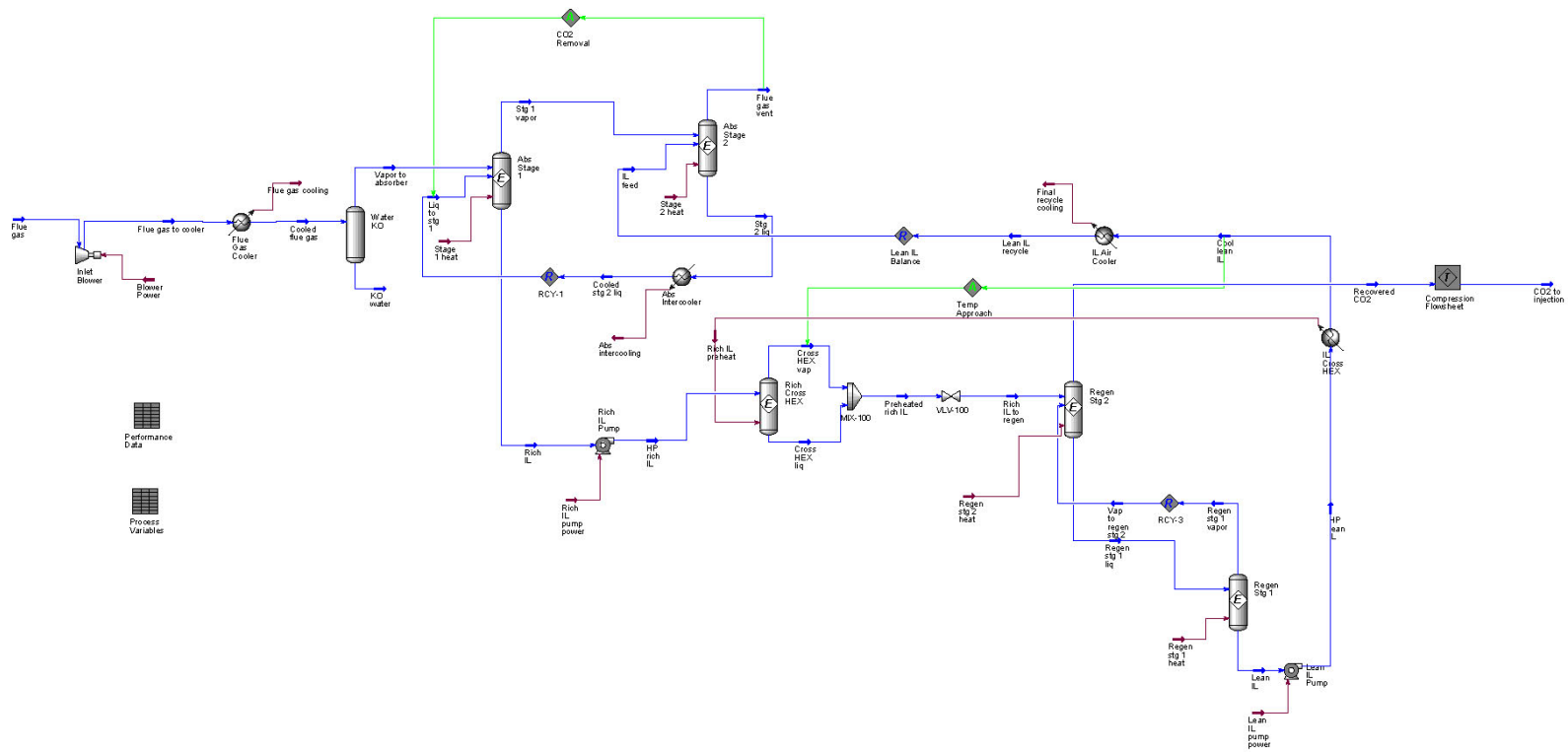
**Figure 4. HYSYS Flow Diagram for Ionic Liquid CO₂ Capture Process Modeling.**
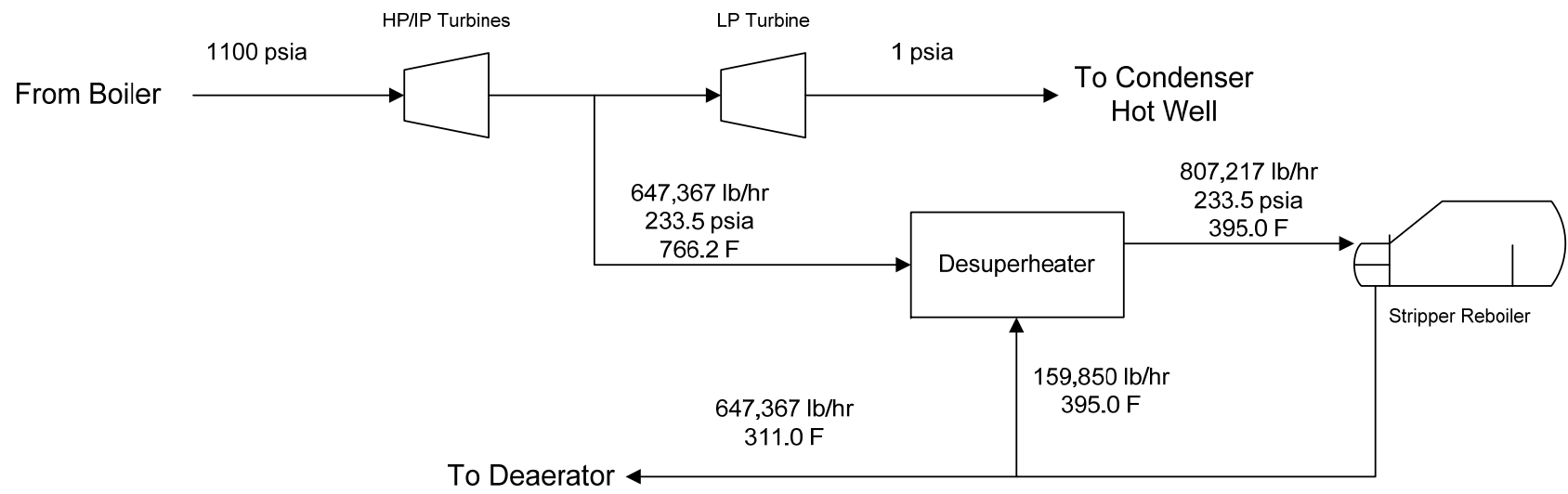
**Figure 5. IL CO$_2$ Capture Steam System PFD – 593 MW Gross Scale**

## 4.3 Sensitivity Analysis

A sensitivity study was conducted using the HYSYS model to select the regeneration conditions that would result in the lowest equivalent work for the IL system. The regeneration pressure and temperature were fixed, and then the circulation rate of the IL was adjusted until the $CO_2$ removal from the flue gas reached the 90% target. The range of regeneration conditions was varied until a point of minimum equivalent work was identified.

While the total equivalent work impacts the energy requirements of the capture system and subsequently the size (and cost) of the non-capture equipment, the IL circulation rate directly impacts the size (and cost) of the capture equipment. For a given regeneration temperature, a higher regeneration pressure resulted in a higher circulation rate. The results of the sensitivity study as a function of equivalent work are provided in Figure 6; the solid lines represent the equivalent work, while the dashed lines represent IL circulation rate.

A high-level economic analysis revealed that the additional capital costs associated with a higher IL circulation rate outweighed the energy savings from a reduction in total equivalent work. Therefore, it is desired to regenerate the IL solvent at low pressure and high temperature. In order to stay consistent with the NDIL0046 study, we have chosen 188°C (370°F) as the maximum regeneration temperature.

Based upon the results of the high-level economic analysis, the case with regeneration conditions at 188°C (370°F) and 101.3 kPa (0 psig) was selected as the optimum economic case; the material balance for this case is provided in Table 3.
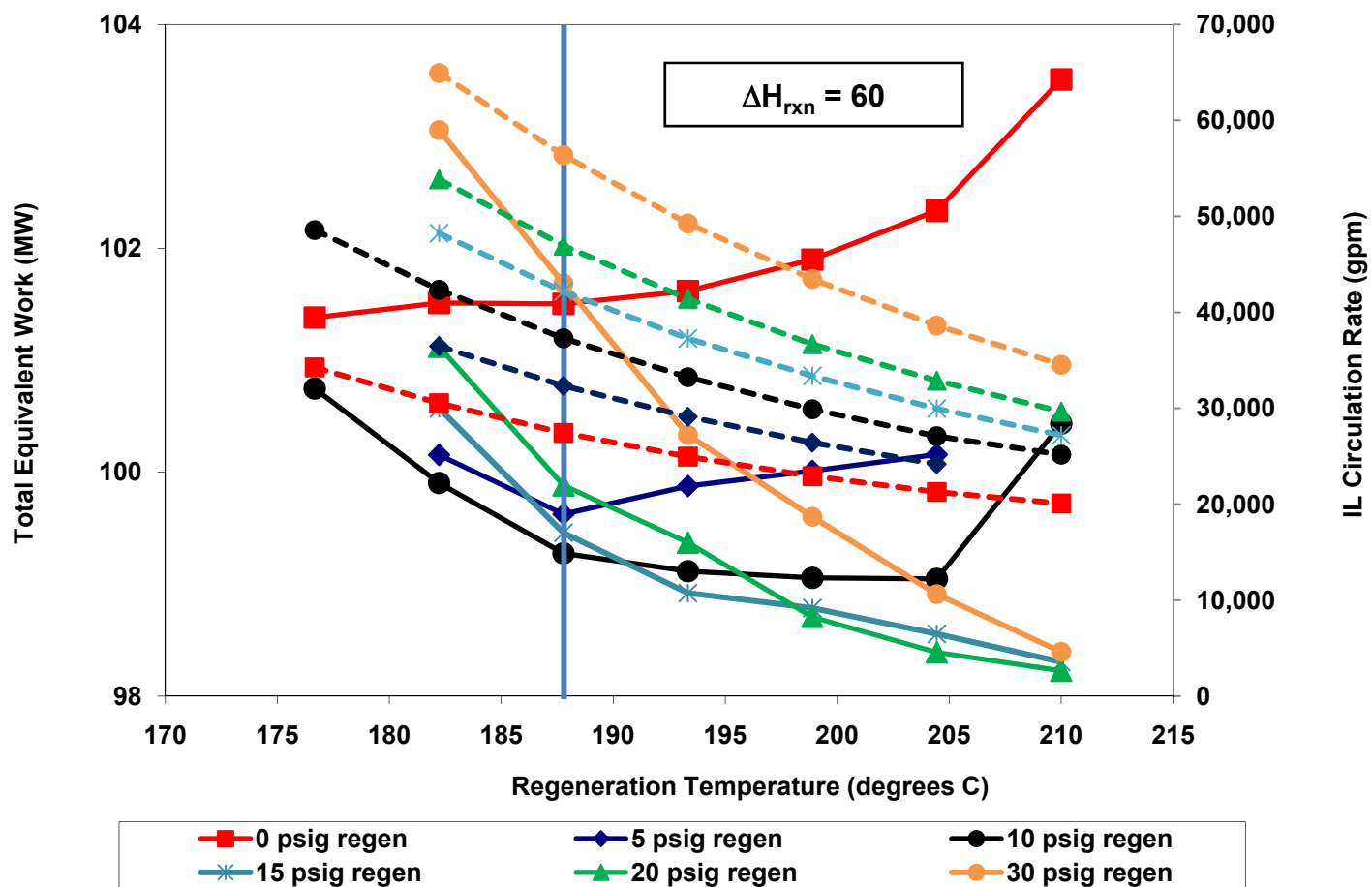
**Figure 6. Total Equivalent Work Sensitivity Study for NDIL0157 (solid lines = equivalent work, dashed lines = IL circulation rate).**

# Table 3. Material Balance for NDIL0157 HYSYS Model

| | Vapor to absorber | Stage 1 vapor | Flue gas vent | IL Feed | Stage 2 liquid | Rich IL | Preheated rich IL | Regen stg 1 liquid | Lean IL | Cool lean IL | Regen stg 1 vapor | Recovered $CO_2$ | Stg 1 Liq (abs) | HP rich IL |
|---|---|---|---|---|---|---|---|---|---|---|---|---|---|---|
| Temperature (°F) | 104.0 | 125.5 | 150.7 | 104.0 | 150.7 | 125.5 | 345.9 | 325.1 | 370.0 | 135.2 | 370.0 | 325.1 | 104.0 | 126.1 |
| Pressure (psia) | 15.9 | 15.0 | 15.0 | 20.7 | 15.0 | 15.0 | 85.0 | 14.7 | 14.7 | 49.7 | 14.7 | 14.7 | 15.0 | 85.0 |
| Molar flowrate (lbmole/hr) | 154,663 | 147,152 | 132,199 | 43,180 | 43,994 | 44,922 | 49,451 | 43,281 | 43,220 | 43,220 | 8,382 | 22,471 | 44,035 | 44,922 |
| Mass flowrate (lb/hr) | 4,612,678 | 4,304,424 | 3,669,193 | 14,836,450 | 15,471,735 | 15,794,362 | 15,794,345 | 15,217,762 | 14,850,183 | 14,850,183 | 367,547 | 943,792 | 15,486,082 | 15,794,362 |
| Density (lb/ft³) | 0.0784 | 0.0699 | 0.0636 | 67.44 | 66.70 | 67.51 | | 62.21 | 60.93 | 66.68 | 0.0724 | 0.0733 | 67.87 | 67.49 |
| Flow rate (gpm) | | | | 27,429 | 28,922 | 29,171 | | 30,501 | 30,387 | 27,768 | | | 28,449 | 29,178 |
| Flow rate (acfm) | 980,662 | 1,026,666 | 962,111 | | | | | | | | 84,617 | 214,565 | | |
| Mole fraction | | | | | | | | | | | | | | |
| $CO_2$ | 0.1488 | 0.1111 | 0.0174 | 0.0021 | 0.0001 | 0.0008 | 0.0923 | 0.0023 | 0.0021 | 0.0021 | 0.9938 | 0.9217 | 0.0001 | 0.0008 |
| IL | 0.0000 | 0.0000 | 0.0000 | 0.4931 | 0.1626 | 0.0119 | 0.1024 | 0.3002 | 0.4931 | 0.4931 | 0.0000 | 0.0000 | 0.1626 | 0.0119 |
| $IL-CO_2$ | 0.0000 | 0.0000 | 0.0000 | 0.5047 | 0.8167 | 0.9481 | 0.7696 | 0.6962 | 0.5047 | 0.5047 | 0.0000 | 0.0000 | 0.8167 | 0.9481 |
| $H_2O$ | 0.0674 | 0.0649 | 0.0659 | 0.0001 | 0.0193 | 0.0380 | 0.0346 | 0.0013 | 0.0001 | 0.0001 | 0.0062 | 0.0759 | 0.0193 | 0.0380 |
| $N_2$ | 0.7577 | 0.7964 | 0.8861 | 0.0000 | 0.0011 | 0.0010 | 0.0009 | 0.0000 | 0.0000 | 0.0000 | 0.0000 | 0.0020 | 0.0011 | 0.0010 |
| $O_2$ | 0.0262 | 0.0276 | 0.0306 | 0.0000 | 0.0002 | 0.0001 | 0.0001 | 0.0000 | 0.0000 | 0.0000 | 0.0000 | 0.0003 | 0.0002 | 0.0001 |
| Mass fraction | | | | | | | | | | | | | | |
| $CO_2$ | 0.2195 | 0.1672 | 0.0276 | 0.0003 | 0.0000 | 0.0001 | 0.0127 | 0.0003 | 0.0003 | 0.0003 | 0.9974 | 0.9659 | 0.0000 | 0.0001 |
| IL | 0.0000 | 0.0000 | 0.0000 | 0.4621 | 0.1489 | 0.0109 | 0.1033 | 0.2749 | 0.4621 | 0.4621 | 0.0000 | 0.0000 | 0.1489 | 0.0109 |
| $IL-CO_2$ | 0.0000 | 0.0000 | 0.0000 | 0.5376 | 0.8500 | 0.9869 | 0.8820 | 0.7248 | 0.5376 | 0.5376 | 0.0000 | 0.0000 | 0.8500 | 0.9869 |
| $H_2O$ | 0.0407 | 0.0400 | 0.0428 | 0.0000 | 0.0010 | 0.0019 | 0.0019 | 0.0001 | 0.0000 | 0.0000 | 0.0026 | 0.0326 | 0.0010 | 0.0019 |
| $N_2$ | 0.7116 | 0.7626 | 0.8943 | 0.0000 | 0.0001 | 0.0001 | 0.0001 | 0.0000 | 0.0000 | 0.0000 | 0.0000 | 0.0014 | 0.0001 | 0.0001 |
| $O_2$ | 0.0281 | 0.0302 | 0.0353 | 0.0000 | 0.0000 | 0.0000 | 0.0000 | 0.0000 | 0.0000 | 0.0000 | 0.0000 | 0.0002 | 0.0000 | 0.0000 |
| K value | | | | | | | | | | | | | | |
| $H_2O$ | | | | | 164.37 | 140.31 | 74.39 | 395.45 | 464.96 | 0.00 | | | | |
| $N_2$ | | | | | 3.42 | 1.71 | 12.15 | 59.97 | 98.02 | 0.00 | | | | |
| $O_2$ | | | | | 779.25 | 785.66 | 136.99 | 789.71 | 789.50 | 0.00 | | | | |
| $CO_2$/IL | | | | 0.5079 | 0.8340 | 0.9884 | 0.9884 | 0.7011 | 0.5079 | 0.5079 | | | 0.8341 | |
| Molarity | | | | 3.14 | 3.04 | 3.08 | | 1.02 | 2.83 | 2.84 | 3.11 | | 3.09 | |
| gmoles $CO_2$/liter | | | | 1.5931 | 2.4810 | 2.9177 | | 0.8809 | 1.9794 | 1.4394 | 1.5751 | | 2.5246 | |

# 5 PROCESS ECONOMICS EVALUATION

This section describes the approach used to estimate the capital and operating costs for the NDIL0157 $CO_2$ capture and compression process evaluated in this study. The stripper temperature and pressure for this case are 188$^o$C and 101.3 kPa (370°F and 14.7 psia), respectively. The process economics for NDIL0157 are then compared to Cases 11 (supercritical PC boiler without $CO_2$ capture) and 12 (supercritical PC boiler with $CO_2$ capture) from the 2010 DOE Cost and Performance Baseline.[1] The equipment sizing and cost methodology is discussed first, followed by a presentation of the results.

## 5.1 Capital and Operating Costs

This section describes the approach used to estimate the capital and operating costs for the NDIL0157 capture and compression case evaluated in this study. This includes a description of how the equipment was sized and costs were estimated, and a summary of the basis for the overall capital and operating cost estimates (including derating of the power plant).

In order to account for any differences between the sizing and costing methodologies used by Trimeric and the sizing and costing methodologies used by a different contractor that prepared the Case 12 estimates, it was necessary to adjust the Trimeric-estimated purchased equipment costs. The size of this adjustment was determined by comparing Trimeric's estimated costs for an MEA system to the costs reported in Case 12, which also includes an amine-based capture system. This same adjustment was then applied to Trimeric's estimated costs for the IL $CO_2$ capture systems to eliminate any differences arising from the costing/sizing methodologies.

This approach required the preparation of two purchased equipment cost estimates: one for MEA, and one for NDIL0157. Both capture cases were evaluated on the arbitrary basis of 593 MW electrical generating capacity as a matter of convenience since costing and sizing information were already available for the MEA case at that scale, which is equivalent to approximately 115 kg/s of $CO_2$ capture.[2,3] Furthermore, the selection of the 593 MW gross generating capacity for the IL case allowed a direct comparison of purchased equipment costs between the IL and MEA cases.

### 5.1.1 Equipment Sizing and Cost Sources

Tables 4 and 5 list the equipment in the MEA and NDIL0157 processes at 593 MW equivalent boiler electrical capacity, the key sizing criteria, and source of the purchased equipment costs (in English units). Design features for the main equipment in the process are discussed further below.

- Absorber Columns – The MEA and IL absorber columns were sized assuming an 80% approach to flood. Publicly available software from Koch-Glitsch (KGTower) was used to size the diameter of the towers assuming that a random packing such as cascade mini rings (CMR) or Flexipac structured packing would be used for the internals. A value of

126 cP was used in the program for NDIL0157 viscosity (per measured data) in the absorber to yield a conservative estimate of the tower diameters.

It was also assumed that the IL solution would have at least the same kinetic rate for $CO_2$ absorption as a MEA unit, until results from bench-scale absorption experiments are available. Thus, the NDIL0157 absorber tower would require the same height of packing as the vessels in the MEA base case. This assumption will need to be verified as more experimental data are available for the IL solution, although preliminary data from both Notre Dame and Babcock and Wilcox (B&W) suggest that this is a good assumption. It is assumed that both processes will require two parallel trains of field-fabricated square absorber towers.

- Stripper Columns – As with the absorber columns, the MEA and IL regeneration columns were sized assuming an 80% approach to flood. KGTower was used to size the diameter of the towers assuming that a random packing such as cascade mini rings (CMR) or Flexipac 1Y structured packing would be used for the internals.

  It was also assumed that the IL solution would have at least the same kinetic rate for $CO_2$ desorption as a MEA unit, until results from bench-scale absorption experiments are available. Thus, the NDIL0157 regeneration towers would require the same height of packing as the vessels in the MEA base case. This assumption will need to be verified as more experimental data are available for the IL solution. Four parallel trains of regeneration columns are assumed for MEA, while three parallel trains of regeneration columns are assumed for the IL case.

- Rich/Lean Exchanger – The rich/lean exchanger for the internal MEA case used a 10°C (18°F) approach on the cold side of the cross exchanger based on a heat and material balance from a previous study.[3]

  The rich/lean exchanger for the internal NDIL0157 case was sized assuming a 5°C (9°F) approach on the cold side of the cross exchanger. This is based on previous work[3] with amine systems that indicates that a low temperature approach in the cross exchanger results in less total equivalent work for stripping (at the expense of increased heat exchanger capacity). A plate and frame type exchanger was assumed for the cost analysis for both cases (cost estimates were vendor-supplied).

- Absorber Intercooling – The absorber column for the NDIL0157 case was sized assuming 40°C intercooling; solvent intercooling assists in improving mass transfer performance and reducing the required column height for $CO_2$ removal. The heat and material balance chosen for the Trimeric-internal MEA case from the 2005 SBIR report[3] does not include absorber intercooling.

- Compression and drivers – The $CO_2$ from the MEA and IL capture units are compressed (compression includes interstage cooling and water knockout) in a single train to 8.4 MPa (1200 psig). At this pressure the supercritical $CO_2$ forms a dense liquid-like phase that

can be pumped with multistage centrifugal pumps to pipeline pressure (15.3 MPa; 2200 psig).

Given the $CO_2$ capture flow rate, centrifugal compression would be applicable, and the number of compression stages was determined based on a maximum temperature limit of 149°C (300°F). The compressors for the NDIL0046 unit have electric drivers since there is not enough steam from the reboilers to provide all the power needed for compression and combinations of steam / electric drivers are not deemed practical by industry representatives.

- Exchangers – The water-cooled exchangers in these processes (i.e., absorber intercooler, lean cooler, compressor pre-, post-, and interstage-coolers) are all assumed to be cooled with power plant cooling tower water. Mechanical draft cooling towers are used with cooling water return and supply temperatures of 43 to 29°C (110°F to 85°F). Air-cooled exchangers were considered but are not the preferred choice due to the large heat requirements for this application and resulting size of the coolers.

  With regard to the regeneration columns, kettle reboilers were assumed for this study with a heat flux of 10,000 to 14,500 W/m$^2$ (4,500 to 6,500 Btu/hr-ft$^2$).

- Solution upkeep – It was assumed that the IL solution would require similar filters and a reclamation system as with an amine unit. Costs are based on typical sizing criteria for amine units until specific information on the IL solutions is available.

**Table 4. MEA CO$_2$ Capture Equipment Sizing Basis and Cost Source – 593 MW Equivalent Capacity (English Units)**

| Description | No. Trains | Type | Sizing Basis | MEA Process | Cost Source |
|---|---|---|---|---|---|
| *Inlet Gas Blower* | 1 | Centrifugal blower; SS or alloy process-wetter components | 1.5 psi increase | 4.9 MMlb/hr | Verbal quote from vendor for blower |
| *Absorber* | 2 | Packed tower (316SS CMR); Total packed height = 50 ft; 316SS vessel | Target of 80% approach to flood; Diameter sized using Aspen Plus; | 40 ft x 40 ft square tower; 300°F & 50 psia | Aspen Icarus |
| *Rich Pump* | 2 | Centrifugal, 316SS | Flow rate from simulations | 23,189 gpm; 242 ft | PDQ$ |
| *Rich Carbon Filter* | 2 | 316SS | Treats 15% of rich liquid flow (typical of amine unit) | 3,478 gpm | PDQ$ |
| *Particulate Filter* | 2 | 316SS | Treats 15% of rich liquid flow (typical of amine unit) | 3,478 gpm | PDQ$ |
| *Rich/Lean Exchanger* | 1 | Plate and frame; 316SS | 18F approach temperature | 1,741 MMBtu/hr; LMTD = 18; 300°F & 150 psia | Vendor Quote |
| *Stripper Column* | 4 | Packed tower; Total packed height = 5 ft; 316SS vessel | Target of 80% approach to flood; Diameter sized using Aspen Plus; | 18' diameter, 30' height; 300°F & 150 psia | PDQ$ |
| *Stripper Reboiler* | 4 | Kettle Reboiler; 316SS tubes and carbon steel shell | Typical steam/amine flux 4,500 to 6,500 Btu/hr-ft2; (from Figure 9-16, GPSA 10th) | 426 MMBtu/hr; 66,446 ft2; LMTD = 43; 400°F & 200 psia | PDQ$ |
| *Lean Solvent Cooler* | 2 | Plate and frame; 316SS | Cools process liquid to 104F | 490 MMBtu/h; LMTD = 19; 200°F & 150 psia | Vendor Quote |

**Table 4. MEA CO₂ Capture Equipment Sizing Basis and Cost Source – 593 MW Equivalent Capacity (English Units)**

| Description | No. Trains | Type | Sizing Basis | MEA Process | Cost Source |
|---|---|---|---|---|---|
| *Compressors* | 1 | Centrifugal; multistage (plus pump, separate line item); 316SS | 86% polytropic efficiency; Maximum temperature limit of 300F (sets compressor ratio) | 5 stages; 43,287 hp | Vendor Quote |
| *Compressor Driver - electric* | 1 | | Discharge pressure = 1,215 psia | 43,287 hp | Vendor Quote |
| *Multistage Centrifugal Pump* | 1 | Multistage centrifugal pump (ESP), 316SS | Discharge pressure = 2,215 psia | 2,992 hp | Scaled Vendor Quote |
| *Overhead Condenser* | 4 | Shell and tube; 316SS tubes and carbon steel shell; water cooled | Process cooling to 104F | 135 MMBtu/hr; 32,452 ft2; LMTD = 52; 300°F & 150 psia | PDQ$ |
| *Overhead Accumulator* | 4 | 316SS horizontal vessels | 5 minute residence time | 5 ft diameter; 15 ft length | PDQ$ |
| *Overhead Reflux Pump* | 4 | Centrifugal, 316SS | Flow rate from simulations | 243 gpm; 115 ft | PDQ$ |
| *Compressor Interstage Coolers* | 1 | Shell and tube; 316SS tubes and carbon steel shell; water cooled | Interstage cooling to 95F | 224 MMBtu/hr | Vendor Quote |
| *Compressor Interstage Separators* | 1 | 316SS horizontal vessels | 5 minute residence time | | Vendor Quote |
| *Makeup Tank* | 1 | Fixed roof tank | Estimated | 100,000 gal | PDQ$ |
| *Makeup Pumps* | 1 | Centrifugal | Estimated | 2 gpm at 74 ft | PDQ$ |
| *Water Tank* | 1 | Fixed roof tank | Estimated | 200,000 gal | PDQ$ |
| *Water Pump* | 1 | Centrifugal | Estimated | 116 gpm at 115ft | PDQ$ |
| *Surge Tank* | 2 | 316SS horizontal vessel | 15 minute residence time | 350,000 gal | PDQ$ |
| *Lean PZ Pump* | 2 | 316SS Centrifugal | Flow rate from simulation | 23,189 gpm at 34 ft | PDQ$ |
| *Reclaimer* | 1 | | % of solution sent and heated (0.5 to 3%) | 1,391 gpm | Scaled Vendor Quote |
| *Dehydration Unit* | 1 | TEG unit | To pipeline specifications; 7 lb/MMscf | 190 MMscfd | Scaled Vendor Quote |

**Table 5. NDIL0157 CO₂ Capture Equipment Sizing Basis and Cost Source – 593 MW Equivalent Capacity (English Units)**

| Description | No. Trains | Type | Sizing Basis | NDIL0157 | Cost Source |
|---|---|---|---|---|---|
| *Inlet Gas Blower* | 1 | Centrifugal blower; SS or alloy process-wetter components | 1.5 psi increase | 4.9 MMlb/hr | Vendor Quote |
| *Absorber* | 2 | Packed tower (316SS CMR #2); Total packed height = 50 ft; 316SS vessel | Target of 80% approach to flood; Diameter sized with KG Tower | 43' x 43' square tower; 300°F & 50 psia | Aspen Icarus |
| *Absorber Intercooler* | 2 | Plate and frame; 316SS | Cools to 104F | 358 MMBtu/h; 213,267 ft²; LMTD = 29; 300°F & 150 psia | Vendor Quote |
| *Absorber Intercooler Pump* | 2 | Centrifugal, 316SS | Flow rate from simulations | 28,922 gpm; 86 ft | PDQ$ |
| *Rich Solvent Pump* | 2 | Centrifugal, 316SS | Flow rate from simulations | 29,171 gpm; 149 ft | PDQ$ |
| *Rich Carbon Filter* | 2 | 316SS with teflon gasket | Treats 15% of rich liquid flow (typical of amine unit) | 4,376 gpm | PDQ$ |
| *Particulate Filter* | 2 | 316SS with teflon gasket | Treats 15% of rich liquid flow (typical of amine unit) | 4,376 gpm | PDQ$ |
| *Rich/Lean Exchanger* | 1 | Plate and frame; 316SS | 10 F approach temperature | 2,112 MMBtu/hr; 1,112,047 ft²; LMTD = 15; 400°F & 200 psia | Vendor Quote |
| *Stripper Column* | 3 | Packed tower (316SS CMR #2.5); Total packed height = 10 ft; 316SS vessel | Target of 80% approach to flood; Diameter sized using KG Tower | 19.5' diameter, 35' height; 400°F & 50 psia | PDQ$ |
| *Stripper Reboiler* | 3 | Kettle Reboiler; 316SS tubes and carbon steel shell | Typical steam/amine flux 4,500 to 6,500 Btu/hr-ft2; (from Figure 9-16, GPSA 10th) | 672 MMBtu/hr; 41,797 ft²; LMTD = 36; 400°F & 300 psia | PDQ$ |
| *Lean Solvent Cooler* | 2 | Plate and frame; 316SS | Cools process liquid to 104F | 232 MMBtu/h; 179,735 ft²; LMTD = 22; 400°F & 150 psia | Vendor Quote |

**Table 5. NDIL0157 CO₂ Capture Equipment Sizing Basis and Cost Source – 593 MW Equivalent Capacity (English Units)**

| Description | No. Trains | Type | Sizing Basis | NDIL0157 | Cost Source |
|---|---|---|---|---|---|
| *Compressors* | 1 | Centrifugal; multistage; 316SS | 86.63% polytropic efficiency; Maximum temperature limit of 300F (sets compressor ratio) | 5 stages; 52,591 hp | Vendor Quote |
| *Compressor Driver - electric* | 1 | | Discharge pressure = 1,215 psia | 52,591 hp | Vendor Quote |
| *Multistage Centrifugal Pump* | 1 | Electric submersible Pump (ESP), 316SS | Discharge pressure = 2,215 psia | 2,890 hp | Scaled Vendor Quote |
| *Overhead Condenser* | 3 | Shell and tube; 316SS tubes and carbon steel shell; water cooled | Process cooling to 104F | 47.5 MMBtu/hr; 2,961 ft²; LMTD = 67; 400°F & 150 psia | PDQ$ |
| *Overhead Accumulator* | 3 | 316SS horizontal vessels | 5 minute residence time | 2.5 ft diameter; 7 ft length | PDQ$ |
| *Overhead Reflux Pump* | 3 | Centrifugal, 316SS | Flow rate from simulations | 12.5 gpm; 115 ft | PDQ$ |
| *Compressor Interstage Coolers* | 1 | Shell and tube; 316SS tubes and carbon steel shell; water cooled | Interstage cooling to 95F | 248 MMBtu/hr | Vendor Quote |
| *Compressor Interstage Separators* | 1 | 316SS horizontal vessels | 5 minute residence time | | Vendor Quote |
| *Makeup Tank* | 1 | Fixed roof tank | Estimated | 25,000 gal | PDQ$ |
| *Makeup Pumps* | 1 | Centrifugal | Estimated | 0.4 gpm; 107 ft | PDQ$ |
| *Water Tank* | 1 | Fixed roof tank | Estimated | 50,000 gal | PDQ$ |
| *Water Pump* | 1 | Centrifugal | Estimated | 12.5 gpm; 115 ft | PDQ$ |
| *Lean Surge Tank* | 2 | 316SS horizontal vessel | 15 minute residence time | 400,000 gal | PDQ$ |
| *Lean Solvent Pump* | 2 | 316SS Centrifugal | Flow rate from simulation | 30,387 gpm; 165 ft | PDQ$ |
| *Reclaimer* | 1 | Similar reclamation system to MEA | % of solution sent and heated (0.5 to 3%) | 823 gpm | Scaled Vendor Quote |
| *Dehydration Unit* | 1 | TEG unit | To pipeline specifications; 7 lb/MMscf | 190 MMscfd | Scaled Vendor Quote |

316 stainless steel was assumed as the default material of construction. However, recent corrosion testing performed by B&W on NDIL0046 suggests that at absorber conditions carbon steel does not undergo significant corrosion with this class of ionic liquids. Therefore, the absorber columns were sized and costed as both stainless steel and carbon steel vessels.

No spares were included for major equipment such as absorbers and exchangers since the $CO_2$ capture unit would be analogous to $SO_2$ control on a flue gas desulfurization process in which no backup sparing is typically installed. A 50% spare capacity was assumed for pumps. All of these assumptions are identical to those used in the 2010 DOE Cost and Performance Baseline.[1]

As shown in Tables 4 and 5, the purchased equipment costs for the capture units and downstream compression trains were obtained from a combination of vendor quotes and costing software. The vendor quotes were adjusted as necessary using appropriate sizing parameters and scaling exponents for the different pieces of equipment. When vendor quotes were not available, PDQ$ (Preliminary Design and Quoting Service) was used to obtain equipment costs. PDQ$ is a software package that estimates current purchased equipment costs for chemical process equipment. Costs from PDQ$ are estimated in 2011 Q1 dollars. The software estimates pricing for fabricated equipment and catalog items that are based on vendor information. The costs of the field-fabricated and erected absorber columns were based on estimates developed using Aspen Icarus$^{TM}$ software for a previous project.

Table 6 shows a comparison of the purchased equipment costs for the MEA base case and NDIL0157. The inlet gas equipment (i.e., blower and direct contact cooler) are similar in cost since the gas is treated to the same inlet absorber conditions for all cases. The cost of NDIL0157 $CO_2$ capture equipment is about 13% higher than the MEA base case primarily because of the increased costs of the rich/lean cross-exchangers. NDIL0157 has a greater viscosity than MEA at exchanger operating conditions, which results in a lower overall heat transfer coefficient and larger required heat exchanger area. The purchased equipment costs for NDIL0157 $CO_2$ compression equipment is approximately 18% higher than MEA; this is because the MEA solvent is regenerated at a higher pressure than NDIL0157, which results in a higher first stage suction pressure and lower overall compression requirements. The cost for dehydration is relatively small and about the same for both options in the study so a detailed effort to size and select the dehydration equipment was not necessary. All of these differences result in NDIL0157 having a total purchased equipment cost about 14% higher than the MEA base case.

If the absorber columns are made of carbon steel as opposed to stainless steel, then purchased equipment costs for the NDIL0157 case are 0.5% less than the MEA base case; overall, total purchased equipment costs for NDIL0157 are approximately 3% higher than the MEA base case if the absorbers are made of carbon steel.

Additionally, while the results are not shown in Table 6, a high-level sensitivity analysis was performed on the lean/rich cross-exchanger to assess heat transfer performance as a function of viscosity. If the viscosity of NDIL0157 is reduced by approximately 50%, the required heat transfer area for the lean/rich cross-exchanger will decrease by an amount that equates to $4.3MM in savings in capture purchased equipment costs at 593 MW gross power.

It should be noted that the purchased equipment costs shown in Table 6 were scaled to June 2007 dollars using the *Chemical Engineering Plant Cost Index* to remain consistent with assumptions used in the 2010 Cost and Performance Baseline.[1]

**Table 6.  Comparison of Purchased Equipment Costs – 593 MW Electrical Equivalent**

| Description | MEA | NDIL0157 (SS Absorber) | NDIL0157 (CS Absorber) |
|---|---|---|---|
| Inlet Gas Blower | 2,841,000 | 2,839,000 | 2,839,000 |
| Absorber | 42,248,000 | 44,865,000 | 33,684,000 |
| Absorber Intercooler | | 3,216,000 | 3,216,000 |
| Absorber Intercooler Pump | | 498,000 | 498,000 |
| Rich Solution Pump | 472,000 | 544,000 | 544,000 |
| Rich Solution Carbon Filter | 147,000 | 355,000 | 355,000 |
| Particulate Filter | 205,000 | 107,000 | 107,000 |
| Rich/Lean Solution Exchanger | 6,435,000 | 21,976,000 | 21,976,000 |
| Lean Solution Cooler | 3,677,000 | 2,948,000 | 2,948,000 |
| Stripper | 3,184,000 | 3,525,000 | 3,525,000 |
| Reboiler | 15,769,000 | 10,938,000 | 10,938,000 |
| Overhead Condenser | 3,348,000 | 388,000 | 388,000 |
| Overhead Accumulator | 84,000 | 39,000 | 39,000 |
| Reflux Pump | 53,000 | 17,000 | 17,000 |
| Compressors[a] | 17,411,000 | 658,000 | 658,000 |
| Multistage Centrifugal Pump | 853,000 | 1,412,000 | 1,412,000 |
| Makeup Solution Tank | 227,000 | 21,142,000 | 21,142,000 |
| Makeup Solution Pump | 3,000 | 824,000 | 824,000 |
| Water Tank | 112,000 | 112,000 | 112,000 |
| Water Pump | 9,000 | 9,000 | 9,000 |
| Surge Tank | 1,256,000 | 69,000 | 69,000 |
| Lean Solution Pump | 547,000 | 12,000 | 12,000 |
| Reclaimer | 4,508,000 | 1,333,000 | 1,333,000 |
| Dehydration Unit | 1,966,000 | 1,965,000 | 1,965,000 |
| **Total** | **105,355,000** | **119,791,000** | **108,610,000** |
| **Capture** | **85,125,000** | **95,860,000** | **84,679,000** |
| **Compression** | **20,230,000** | **23,931,000** | **23,931,000** |

[a]The compressor skid package includes the electric motor, interstage coolers and interstage separators

### 5.1.2 Capital Costs

Because few equipment sizing details were provided for the capture and compression process of Case 12 in the 2010 DOE Cost and Performance Baseline, purchased equipment costs for MEA and the IL processes were determined using an internally consistent equipment sizing and costing methodology at 593 MW gross electric generating capacity. In order to compare the IL and MEA capture and compression processes on the same basis, a methodology was developed to scale up the internally-costed cases. Figure 7 illustrates the process used to scale these two cases from 593 MW boiler electrical capacity to 550 MW$_e$ net power.

After the purchased equipment costs were calculated at 593 MW boiler electrical capacity for both cases, a detailed energy analysis was conducted for the IL case to determine the gross boiler electrical capacity necessary to achieve 550 MW$_e$ net power. The derating for the 550 MW$_e$ net power MEA case was taken directly from Case 12 in the 2010 DOE Cost and Performance Baseline.[1]

Table 7 details the energy analyses for each case at 550 MW$_e$ net power. The IL case has a lower equivalent boiler electrical capacity (a smaller boiler and generator for the same net power output) compared to Case 12 because the IL case requires less steam consumption for solvent regeneration.

**Table 7.  Energy Analysis Summary – 550 MW Net Power**

| Description | Units | MEA (DOE Case 12) | Size/Methodology Adjusted NDIL0157 |
|---|---|---|---|
| Thermal Input | MW$_t$ | 1934.5 | 1814.6 |
| Equivalent Electrical Capacity of Boiler | MW$_e$ | 782.9 | 734.4 |
| Total Steam Turbine Power | MW$_e$ | 662.8 | 657.7 |
| Reboiler/Steam Heater Equivalent Power Lost | MW$_e$ | 120.1 | 76.7 |
| Compression | MW$_e$ | 44.9 | 51.2 |
| Capture Auxiliaries | MW$_e$ | 26.3 | 17.3 |
| Balance of Plant Auxiliaries | MW$_e$ | 41.7 | 39.1 |
| Net Power | MW$_e$ | 549.9 | 550.0 |
| Coal Feed Rate | kg/hr | 256,653 | 240,743 |

**Figure 7. Capital Cost Methodology**

For the two cases evaluated for purchased equipment costs at 593 MW boiler electrical capacity, a weighted costing exponent was determined using the following assumptions:

- An exponent of 0.6 was applied to the purchased equipment costs for a category of equipment where it was assumed a larger piece of equipment would be required to scale the capture process from 593 MW boiler electrical capacity to 550 $MW_e$ of net power (a larger absorber column for example).
- An exponent of 1.0 was applied to the purchased equipment costs for a category of equipment where it was assumed additional units would be required to scale the capture process from 593 MW boiler electrical capacity to 550 $MW_e$ of net power (additional pumps and heat exchangers for example).
- The weighted costing exponent for each case was calculated using the following equation:

$$\text{Average Cost Exponent} = \Sigma \, [(\text{Cost Exponent})_i * (\text{PEC})_i]/\text{Total PEC}$$

After each case was adjusted to 550 $MW_e$ of net power to match Case 12 using weighted costing exponents for each individual case, the internal estimate of $CO_2$ capture purchased equipment costs for MEA was 50.1% lower than Case 12 $CO_2$ capture purchased equipment costs, and 12.9% lower for compression purchased equipment costs. The offsets are attributable to differences in costing and sizing methodologies. For example, it is possible that there is a difference in the amine circulation rate from the Trimeric MEA analysis and the Fluor Econamine FG Plus$^{TM}$ process. In addition, there are differences in the process flowsheet; for instance, the Fluor process assumes that a packed tower is used for trim $SO_x$ removal upstream of the absorber, while a direct contact cooler was assumed for flue gas treating in the internal MEA case. In addition, the Fluor Econamine process assumes absorber intercooling. Capture and compression purchased equipment costs for each of the Trimeric cost estimates was multiplied by 2.01 and 1.15, respectively, to adjust for differences in costing and sizing methodologies for $CO_2$ capture and compression. Table 8 details purchased equipment costs at 550 MW net power for Case 12 and the IL case.

**Table 8. Capture and Compression Purchased Equipment Costs Summary – 550 MW Net Power.**

| Description | Units | MEA (DOE Case 12) | Size/Methodology Adjusted NDIL0157 |
|---|---|---|---|
| Equivalent Electrical Capacity of Boiler | $MW_e$ | 782.9 | 734.4 |
| Capture Purchased Equipment Costs | $MM | 207.8 | 225.1 |
| Compression Purchased Equipment Costs | $MM | 27.6 | 31.3 |

Purchased equipment costs for balance of plant (i.e. non-capture/non-compression) equipment for the IL case was determined by scaling Case 12 equipment costs based upon metrics such as equivalent electric capacity of the plant, gross power output of the plant, cooling water demand, etc. Cases 9 (subcritical PC boiler without $CO_2$ capture), 10 (subcritical PC boiler with $CO_2$

capture) and 12 (supercritical PC boiler) from the 2010 Cost and Performance Baseline were analyzed to determine cost exponents for each individual category of balance of plant equipment.

After purchased equipment costs were determined for capture, compression, and balance of plant equipment, costs associated with direct labor, engineering/home office, project contingency, and process contingency were then added to the purchased equipment costs to arrive at the total plant costs (TPC) for the entire power plant (including $CO_2$ capture and compression).

Per the 2010 Cost and Performance Baseline[1], the total overnight costs (TOC) for the power plant were determined from a combination of total plant costs and owner's costs, which comprise the following:

- Preproduction costs,
- Working capital,
- Inventory capital,
- Land,
- Financing costs, and
- Other owner's costs.

Total as-spent costs (TASC) are determined from total overnight costs by adding a multiplier to the TOC to account for interest and escalation during construction. Table 9 provides a summary of the total plant costs for Case 12 in comparison to the IL case, while Tables 10 and 11 detail the capital requirements for the IL case.

Total plant costs were approximately 0.6% lower for NDIL0157 versus DOE Case 12. Although NDIL0157 has of smaller balance of plant equipment due to lower energy requirements and steam derating, the majority of the energy savings are offset by higher purchased equipment costs for capture and compression for NDIL0157.

**Table 9. Total Plant Cost Comparison**

| Acct No. | Item/Description | Case 12[1] Total Plant Cost $M | Case 12[1] Total Plant Cost $/kW | NDIL0157 Total Plant Cost $M | NDIL0157 Total Plant Cost $/kW |
|---|---|---|---|---|---|
| 1 | Coal & Sorbent Handling | **$47,017** | $85 | **$45,158** | $82 |
| 2 | Coal & Sorbent Prep & Feed | **$22,444** | $41 | **$21,492** | $39 |
| 3 | Feedwater & Misc. BOP Systems | **$102,559** | $186 | **$96,231** | $175 |
| 4 | PC Boiler | | | | |
| 4.1 | PC Boiler & Accessories | **$369,145** | $671 | **$353,029** | $642 |
| 4.2 | SCR (w/4.1) | **$0** | $0 | **$0** | $0 |
| 4.3 | Open | **$0** | $0 | **$0** | $0 |
| 4.4-4.9 | Boiler BoP (w/ ID Fans) | **$0** | $0 | **$0** | $0 |
| | **Subtotal 4** | **$369,145** | **$671** | **$353,029** | **$642** |
| 5 | Flue Gas Cleanup | **$163,336** | $297 | **$155,708** | $283 |
| 5B | CO2 Removal & Compression | **$468,781** | $852 | **$510,342** | $928 |
| 6 | Combustion Turbine/Accessories | | | | |
| 6.1 | Combustion Turbine Generator | **$0** | $0 | **$0** | $0 |
| 6.2-6.9 | Combustion Turbine Other | **$0** | $0 | **$0** | $0 |
| | **Subtotal 6** | **$0** | **$0** | **$0** | **$0** |
| 7 | HRSG, Ducting & Stack | | | | |
| 7.1 | Heat Recovery Steam Generator | **$0** | $0 | **$0** | $0 |
| 7.2-7.9 | HRSG Accessories, Ductwork and Stack | **$37,527** | $68 | **$37,064** | $67 |
| | **Subtotal 7** | **$37,527** | **$68** | **$37,064** | **$67** |
| 8 | Steam Turbine Generator | | | | |
| 8.1 | Steam TG & Accessories | **$77,543** | $141 | **$77,122** | $140 |
| 8.2-8.9 | Turbine Plant Auxiliaries and Steam Piping | **$54,564** | $99 | **$52,365** | $95 |
| | **Subtotal 8** | **$132,107** | **$240** | **$129,486** | **$235** |
| 9 | Cooling Water System | **$60,962** | $111 | **$49,237** | $90 |
| 10 | Ash/Spent Sorbent Handling System | **$15,111** | $27 | **$14,585** | $27 |
| 11 | Accessory Electric Plant | **$80,933** | $147 | **$79,546** | $145 |
| 12 | Instrumentation & Control | **$25,837** | $47 | **$25,837** | $47 |
| 13 | Improvements to Site | **$15,723** | $29 | **$15,647** | $28 |
| 14 | Buildings & Structures | **$60,554** | $110 | **$58,641** | $107 |
| | **TOTAL COST** | **$1,602,037** | **$2,913** | **$1,592,004** | **$2,895** |

**Table 10. NDIL0157 Total Plant Cost Summary**

| Acct No. | Item/Description | Equipment Cost | Materials Cost | Labor Direct | Labor Indirect | Sales Tax | Bare Erected Cost $ | Engineering CM H.O. & Fee | Contingencies Process | Contingencies Project | Total Plant Cost $ | Total Plant Cost $/kW |
|---|---|---|---|---|---|---|---|---|---|---|---|---|
| 1 | Coal & Sorbent Handling | $19,299 | $5,189 | $11,547 | $0 | $0 | **$36,034** | $3,234 | $0 | $5,890 | **$45,158** | $82 |
| 2 | Coal & Sorbent Prep & Feed | $13,096 | $761 | $3,326 | $0 | $0 | **$17,182** | $1,506 | $0 | $2,804 | **$21,492** | $39 |
| 3 | Feedwater & Misc. BOP Systems | $51,490 | $0 | $24,279 | $0 | $0 | **$75,769** | $6,944 | $0 | $13,518 | **$96,231** | $175 |
| 4 | PC Boiler | | | | | | | | | | | |
| 4.1 | PC Boiler & Accessories | $187,350 | | $105,122 | $0 | $0 | **$292,472** | $28,464 | $0 | $32,094 | **$353,029** | $642 |
| 4.2 | SCR (w/4.1) | | | $0 | $0 | $0 | **$0** | $0 | $0 | $0 | **$0** | $0 |
| 4.3 | Open | | | $0 | $0 | $0 | **$0** | $0 | $0 | $0 | **$0** | $0 |
| 4.4- | Boiler BoP (w/ ID Fans) | | | $0 | $0 | $0 | **$0** | $0 | $0 | $0 | **$0** | $0 |
| | **Subtotal 4** | **$187,350** | **$0** | **$105,122** | **$0** | **$0** | **$292,472** | **$28,464** | **$0** | **$32,094** | **$353,029** | **$642** |
| 5 | Flue Gas Cleanup | $96,332 | $0 | $32,855 | $0 | $0 | **$129,187** | $12,366 | $0 | $14,155 | **$155,708** | $283 |
| 5B | CO2 Removal & Compression | $256,426 | $0 | $78,175 | $0 | $0 | **$334,601** | $31,992 | $58,692 | $85,057 | **$510,342** | $928 |
| 6 | Combustion Turbine/Accessories | | | | | | | | | | | |
| 6.1 | Combustion Turbine Generator | | | $0 | $0 | $0 | **$0** | $0 | $0 | $0 | **$0** | $0 |
| 6.2- | Combustion Turbine Other | | | $0 | $0 | $0 | **$0** | $0 | $0 | $0 | **$0** | $0 |
| | **Subtotal 6** | **$0** | **$0** | **$0** | **$0** | **$0** | **$0** | **$0** | **$0** | **$0** | **$0** | **$0** |
| 7 | HRSG, Ducting & Stack | | | | | | | | | | | |
| 7.1 | Heat Recovery Steam Generator | | | $0 | $0 | $0 | **$0** | $0 | $0 | $0 | **$0** | $0 |
| 7.2- | HRSG Accessories, Ductwork and Stack | $17,318 | $958 | $11,736 | $0 | $0 | **$30,012** | $2,751 | $0 | $4,301 | **$37,064** | $67 |
| | **Subtotal 7** | **$17,318** | **$958** | **$11,736** | **$0** | **$0** | **$30,012** | **$2,751** | **$0** | **$4,301** | **$37,064** | **$67** |
| 8 | Steam Turbine Generator | | | | | | | | | | | |
| 8.1 | Steam TG & Accessories | $56,485 | | $7,496 | $0 | $0 | **$63,981** | $6,130 | $0 | $7,011 | **$77,122** | $140 |
| 8.2- | Turbine Plant Auxiliaries and Steam | $26,172 | $1,190 | $14,754 | $0 | $0 | **$42,116** | $3,672 | $0 | $6,577 | **$52,365** | $95 |
| | **Subtotal 8** | **$82,657** | **$1,190** | **$22,250** | **$0** | **$0** | **$106,097** | **$9,802** | **$0** | **$13,587** | **$129,486** | **$235** |
| 9 | Cooling Water System | $16,498 | $8,144 | $14,999 | $0 | $0 | **$39,642** | $3,729 | $0 | $5,866 | **$49,237** | $90 |
| 10 | Ash/Spent Sorbent Handling System | $5,092 | $162 | $6,809 | $0 | $0 | **$12,063** | $1,160 | $0 | $1,361 | **$14,585** | $27 |
| 11 | Accessory Electric Plant | $24,842 | $10,454 | $29,635 | $0 | $0 | **$64,930** | $5,744 | $0 | $8,871 | **$79,546** | $145 |
| 12 | Instrumentation & Control | $10,017 | $0 | $10,156 | $0 | $0 | **$20,173** | $1,829 | $1,009 | $2,826 | **$25,837** | $47 |
| 13 | Improvements to Site | $3,303 | $1,899 | $6,666 | $0 | $0 | **$11,869** | $1,170 | $0 | $2,608 | **$15,647** | $28 |
| 14 | Buildings & Structures | $0 | $23,985 | $22,787 | $0 | $0 | **$46,772** | $4,220 | $0 | $7,649 | **$58,641** | $107 |
| | **TOTAL COST** | **$783,720** | **$52,742** | **$380,343** | | | **$1,216,804** | **$114,911** | **$59,701** | **$200,587** | **$1,592,004** | **$2,895** |

## Table 11. NDIL0157 Total Plant Cost Details

| Acct No. | Item/Description | NDIL0157 Equipment Cost | NDIL0157 Materials Cost | Direct Labor | Indirect Labor | Sales Tax | Bare Erected Cost $ | Eng'g CM H.O. & Fee | Process Contingency | Project Contingency | Total Plant Cost ($) | Total Plant Cost ($/kW) |
|---|---|---|---|---|---|---|---|---|---|---|---|---|
| 1 | Coal & Sorbent Handling | | | | | | | | | | | |
| 1.1 | Coal Receive & Unload | $3,955 | | $1,806 | $0 | $0 | $5,761 | $515 | $0 | $942 | $7,218 | $13 |
| 1.2 | Coal Stackout & Reclaim | $5,111 | | $1,158 | $0 | $0 | $6,269 | $549 | $0 | $1,023 | $7,841 | $14 |
| 1.3 | Coal Conveyors | $4,751 | | $1,145 | $0 | $0 | $5,897 | $516 | $0 | $962 | $7,375 | $13 |
| 1.4 | Other Coal Handling | $1,244 | | $265 | $0 | $0 | $1,509 | $132 | $0 | $246 | $1,887 | $3 |
| 1.5 | Sorbent Receive & Unload | $161 | | $48 | $0 | $0 | $209 | $19 | $0 | $34 | $262 | $0 |
| 1.6 | Sorbent Stackout & Reclaim | $2,592 | | $475 | $0 | $0 | $3,067 | $267 | $0 | $500 | $3,835 | $7 |
| 1.7 | Sorbent Conveyors | $925 | $200 | $227 | $0 | $0 | $1,353 | $117 | $0 | $220 | $1,690 | $3 |
| 1.8 | Other Sorbent Handling | $559 | $131 | $294 | $0 | $0 | $984 | $87 | $0 | $160 | $1,231 | $2 |
| 1.9 | Coal & Sorbent Hnd. Foundations | | $4,857 | $6,128 | $0 | $0 | $10,985 | $1,032 | $0 | $1,803 | $13,820 | $25 |
| | **Subtotal 1** | **$19,299** | **$5,189** | **$11,547** | **$0** | **$0** | **$36,034** | **$3,234** | **$0** | **$5,890** | **$45,158** | **$82** |
| 2 | Coal & Sorbent Prep & Feed | | | | | | | | | | | |
| 2.1 | Coal Crushing & Drying | $2,289 | | $447 | $0 | $0 | $2,736 | $239 | $0 | $447 | $3,421 | $6 |
| 2.2 | Coal Conveyor to Storage | $5,860 | | $1,279 | $0 | $0 | $7,139 | $624 | $0 | $1,164 | $8,927 | $16 |
| 2.3 | Coal Injection System | | | $0 | $0 | $0 | $0 | $0 | $0 | $0 | $0 | $0 |
| 2.4 | Misc. Coal Prep & Feed | | | $0 | $0 | $0 | $0 | $0 | $0 | $0 | $0 | $0 |
| 2.5 | Sorbent Prep Equipment | $4,415 | $190 | $917 | $0 | $0 | $5,522 | $481 | $0 | $901 | $6,904 | $13 |
| 2.6 | Sorbent Storage & Feed | $531 | | $203 | $0 | $0 | $735 | $65 | $0 | $120 | $920 | $2 |
| 2.7 | Sorbent Injection System | | | $0 | $0 | $0 | $0 | $0 | $0 | $0 | $0 | $0 |
| 2.8 | Booster Air Supply System | | | $0 | $0 | $0 | $0 | $0 | $0 | $0 | $0 | $0 |
| 2.9 | Coal & Sorbent Feed Foundation | | $571 | $479 | $0 | $0 | $1,050 | $97 | $0 | $172 | $1,319 | $2 |
| | **Subtotal 2** | **$13,096** | **$761** | **$3,326** | **$0** | **$0** | **$17,182** | **$1,506** | **$0** | **$2,804** | **$21,492** | **$39** |
| 3 | Feedwater & Misc. BOP Systems | | | | | | | | | | | |
| 3.1 | Feedwater System | $21,861 | | $7,061 | $0 | $0 | $28,923 | $2,533 | $0 | $4,718 | $36,173 | $66 |
| 3.2 | Water Makeup & Pretreating | $6,127 | | $1,972 | $0 | $0 | $8,099 | $766 | $0 | $1,773 | $10,638 | $19 |
| 3.3 | Other Feedwater Subsystems | $6,692 | | $2,829 | $0 | $0 | $9,521 | $853 | $0 | $1,557 | $11,931 | $22 |
| 3.4 | Service Water Systems | $1,201 | | $654 | $0 | $0 | $1,856 | $174 | $0 | $406 | $2,436 | $4 |
| 3.5 | Other Boiler Plant Systems | $8,269 | | $8,163 | $0 | $0 | $16,432 | $1,560 | $0 | $2,698 | $20,690 | $38 |
| 3.6 | FO Supply System & Nat Gas | $274 | | $343 | $0 | $0 | $618 | $58 | $0 | $101 | $777 | $1 |
| 3.7 | Waste Treatment Equipment | $4,154 | | $2,368 | $0 | $0 | $6,522 | $635 | $0 | $1,431 | $8,588 | $16 |
| 3.8 | Misc. Equip. (Cranes, Air Comp, Comm) | $2,911 | | $889 | $0 | $0 | $3,800 | $366 | $0 | $833 | $4,998 | $9 |
| | **Subtotal 3** | **$51,490** | **$0** | **$24,279** | **$0** | **$0** | **$75,769** | **$6,944** | **$0** | **$13,518** | **$96,231** | **$175** |

| Acct No. | Item/Description | NDIL0157 Equipment Cost | NDIL0157 Materials Cost | Direct Labor | Indirect Labor | Sales Tax | Bare Erected Cost $ | Eng'g CM H.O. & Fee | Process Contingency | Project Contingency | Total Plant Cost ($) | Total Plant Cost ($/kW) |
|---|---|---|---|---|---|---|---|---|---|---|---|---|
| 4 | PC Boiler | | | | | | | | | | | |
| 4.1 | PC Boiler & Accessories | $187,350 | | $105,122 | $0 | $0 | $292,472 | $28,464 | $0 | $32,094 | $353,029 | $642 |
| 4.2 | SCR (w/4.1) | | | $0 | $0 | $0 | $0 | $0 | $0 | $0 | $0 | $0 |
| 4.3 | Open | | | $0 | $0 | $0 | $0 | $0 | $0 | $0 | $0 | $0 |
| 4.4 | Boiler BoP (w/ ID Fans) | | | $0 | $0 | $0 | $0 | $0 | $0 | $0 | $0 | $0 |
| 4.5 | Primary Air System | | | $0 | $0 | $0 | $0 | $0 | $0 | $0 | $0 | $0 |
| 4.6 | Secondary Air System | | | $0 | $0 | $0 | $0 | $0 | $0 | $0 | $0 | $0 |
| 4.8 | Major Component Rigging | | | $0 | $0 | $0 | $0 | $0 | $0 | $0 | $0 | $0 |
| 4.9 | Boiler Foundations | | | $0 | $0 | $0 | $0 | $0 | $0 | $0 | $0 | $0 |
| | **Subtotal 4** | **$187,350** | **$0** | **$105,122** | **$0** | **$0** | **$292,472** | **$28,464** | **$0** | **$32,094** | **$353,029** | **$642** |
| 5 | Flue Gas Cleanup | | | | | | | | | | | |
| 5.1 | Absorber Vessels & Accessories | $66,950 | | $14,413 | $0 | $0 | $81,362 | $7,757 | $0 | $8,912 | $98,031 | $178 |
| 5.2 | Other FGD | $3,494 | | $3,959 | $0 | $0 | $7,453 | $724 | $0 | $818 | $8,995 | $16 |
| 5.3 | Bag House & Accessories | $19,189 | | $12,178 | $0 | $0 | $31,367 | $3,023 | $0 | $3,439 | $37,829 | $69 |
| 5.4 | Other Particulate Removal Materials | $1,298 | | $1,389 | $0 | $0 | $2,687 | $261 | $0 | $295 | $3,242 | $6 |
| 5.5 | Gypsum Dewatering System | $5,401 | | $917 | $0 | $0 | $6,318 | $602 | $0 | $692 | $7,612 | $14 |
| 5.6 | Mercury Removal System | | | $0 | $0 | $0 | $0 | $0 | $0 | $0 | $0 | $0 |
| 5.9 | Open | | | $0 | $0 | $0 | $0 | $0 | $0 | $0 | $0 | $0 |
| | **Subtotal 5** | **$96,332** | **$0** | **$32,855** | **$0** | **$0** | **$129,187** | **$12,366** | **$0** | **$14,155** | **$155,708** | **$283** |
| 5B | CO2 Removal & Compression | | | | | | | | | | | |
| 5B.1 | CO2 Removal System | $225,111 | | $68,350 | $0 | $0 | $293,461 | $28,058 | $58,692 | $76,042 | $456,253 | $830 |
| 5B.2 | CO2 Compression & Drying | $31,315 | | $9,824 | $0 | $0 | $41,139 | $3,935 | $0 | $9,015 | $54,089 | $98 |
| | **Subtotal 5B** | **$256,426** | **$0** | **$78,175** | **$0** | **$0** | **$334,601** | **$31,992** | **$58,692** | **$85,057** | **$510,342** | **$928** |
| 6 | Combustion Turbine/Accessories | | | | | | | | | | | |
| 6.1 | Combustion Turbine Generator | | | $0 | $0 | $0 | $0 | $0 | $0 | $0 | $0 | $0 |
| 6.2 | Open | | | $0 | $0 | $0 | $0 | $0 | $0 | $0 | $0 | $0 |
| 6.3 | Compressed Air Piping | | | $0 | $0 | $0 | $0 | $0 | $0 | $0 | $0 | $0 |
| 6.9 | Combustion Turbine Foundations | | | $0 | $0 | $0 | $0 | $0 | $0 | $0 | $0 | $0 |
| | **Subtotal 6** | **$0** | **$0** | **$0** | **$0** | **$0** | **$0** | **$0** | **$0** | **$0** | **$0** | **$0** |
| 7 | HRSG, Ducting & Stack | | | | | | | | | | | |
| 7.1 | Heat Recovery Steam Generator | | | $0 | $0 | $0 | $0 | $0 | $0 | $0 | $0 | $0 |
| 7.2 | HRSG Accessories | | | $0 | $0 | $0 | $0 | $0 | $0 | $0 | $0 | $0 |
| 7.3 | Ductwork | $8,971 | | $5,764 | $0 | $0 | $14,736 | $1,285 | $0 | $2,403 | $18,424 | $33 |
| 7.4 | Stack | $8,347 | | $4,884 | $0 | $0 | $13,231 | $1,274 | $0 | $1,451 | $15,956 | $29 |
| 7.9 | Duct & Stack Foundations | | $958 | $1,088 | $0 | $0 | $2,046 | $192 | $0 | $447 | $2,685 | $5 |
| | **Subtotal 7** | **$17,318** | **$958** | **$11,736** | **$0** | **$0** | **$30,012** | **$2,751** | **$0** | **$4,301** | **$37,064** | **$67** |

| Acct No. | Item/Description | NDIL0157 Equipment Cost | NDIL0157 Materials Cost | Direct Labor | Indirect Labor | Sales Tax | Bare Erected Cost $ | Eng'g CM H.O. & Fee | Process Contingency | Project Contingency | Total Plant Cost ($) | Total Plant Cost ($/kW) |
|---|---|---|---|---|---|---|---|---|---|---|---|---|
| 8 | Steam Turbine Generator | | | | | | | | | | | |
| 8.1 | Steam TG & Accessories | $56,485 | | $7,496 | $0 | $0 | $63,981 | $6,130 | $0 | $7,011 | $77,122 | $140 |
| 8.2 | Turbine Plant Auxiliaries | $378 | | $811 | $0 | $0 | $1,189 | $116 | $0 | $131 | $1,436 | $3 |
| 8.3 | Condenser & Auxiliaries | $5,262 | | $1,939 | $0 | $0 | $7,201 | $689 | $0 | $789 | $8,679 | $16 |
| 8.4 | Steam Piping | $20,532 | | $10,123 | $0 | $0 | $30,655 | $2,576 | $0 | $4,985 | $38,215 | $69 |
| 8.9 | TG Foundations | | $1,190 | $1,881 | $0 | $0 | $3,071 | $291 | $0 | $672 | $4,035 | $7 |
| | **Subtotal 8** | **$82,657** | **$1,190** | **$22,250** | **$0** | **$0** | **$106,097** | **$9,802** | **$0** | **$13,587** | **$129,486** | **$235** |
| 9 | Cooling Water System | | | | | | | | | | | |
| 9.1 | Cooling Towers | $12,250 | | $3,814 | $0 | $0 | $16,064 | $1,536 | $0 | $1,760 | $19,361 | $35 |
| 9.2 | Circulating Water Pumps | $2,551 | | $197 | $0 | $0 | $2,747 | $231 | $0 | $298 | $3,276 | $6 |
| 9.3 | Circulating Water System Auxiliaries | $645 | | $86 | $0 | $0 | $731 | $69 | $0 | $80 | $880 | $2 |
| 9.4 | Circulating Water Pump | | $5,114 | $4,956 | $0 | $0 | $10,070 | $943 | $0 | $1,652 | $12,664 | $23 |
| 9.5 | Make-up Water System | $542 | | $724 | $0 | $0 | $1,266 | $121 | $0 | $208 | $1,595 | $3 |
| 9.6 | Component Cooling Water System | $511 | | $407 | $0 | $0 | $918 | $87 | $0 | $151 | $1,156 | $2 |
| 9.9 | Circ Water System Foundations & Structures | | $3,031 | $4,815 | $0 | $0 | $7,846 | $742 | $0 | $1,718 | $10,305 | $19 |
| | **Subtotal 9** | **$16,498** | **$8,144** | **$14,999** | **$0** | **$0** | **$39,642** | **$3,729** | **$0** | **$5,866** | **$49,237** | **$90** |
| 10 | Ash/Spent Sorbent Handling System | | | | | | | | | | | |
| 10.1 | Ash Coolers | | | $0 | $0 | $0 | $0 | $0 | $0 | $0 | $0 | $0 |
| 10.2 | Cyclone Ash Letdown | | | $0 | $0 | $0 | $0 | $0 | $0 | $0 | $0 | $0 |
| 10.3 | HGCU Ash Letdown | | | $0 | $0 | $0 | $0 | $0 | $0 | $0 | $0 | $0 |
| 10.4 | High Temperature Ash Piping | | | $0 | $0 | $0 | $0 | $0 | $0 | $0 | $0 | $0 |
| 10.5 | Other Ash Recovery Equipment | | | $0 | $0 | $0 | $0 | $0 | $0 | $0 | $0 | $0 |
| 10.6 | Ash Storage Silos | $682 | | $2,099 | $0 | $0 | $2,781 | $273 | $0 | $305 | $3,359 | $6 |
| 10.7 | Ash Transport & Feed Equipment | $4,411 | | $4,519 | $0 | $0 | $8,929 | $854 | $0 | $978 | $10,762 | $20 |
| 10.8 | Misc. Ash Handling Equipment | | | $0 | $0 | $0 | $0 | $0 | $0 | $0 | $0 | $0 |
| 10.9 | Ash/Spent Sorbent Foundation | | $162 | $191 | $0 | $0 | $353 | $34 | $0 | $77 | $464 | $1 |
| | **Subtotal 10** | **$5,092** | **$162** | **$6,809** | **$0** | **$0** | **$12,063** | **$1,160** | **$0** | **$1,361** | **$14,585** | **$27** |
| 11 | Accessory Electric Plant | | | | | | | | | | | |
| 11.1 | Generator Equipment | $1,719 | | $279 | $0 | $0 | $1,998 | $186 | $0 | $164 | $2,348 | $4 |
| 11.2 | Station Service Equipment | $4,860 | | $1,596 | $0 | $0 | $6,456 | $604 | $0 | $530 | $7,590 | $14 |
| 11.3 | Switchgear & Motor Control | $5,587 | | $949 | $0 | $0 | $6,536 | $606 | $0 | $714 | $7,856 | $14 |
| 11.4 | Conduit & Cable Tray | | $3,503 | $12,115 | $0 | $0 | $15,618 | $1,511 | $0 | $2,569 | $19,699 | $36 |
| 11.5 | Wire & Cable | | $6,610 | $12,760 | $0 | $0 | $19,370 | $1,632 | $0 | $3,149 | $24,151 | $44 |
| 11.6 | Protective Equipment | $261 | | $887 | $0 | $0 | $1,148 | $112 | $0 | $126 | $1,387 | $3 |
| 11.7 | Standby Equipment | $1,355 | | $31 | $0 | $0 | $1,386 | $127 | $0 | $151 | $1,664 | $3 |
| 11.8 | Main Power Transformers | $11,059 | | $184 | $0 | $0 | $11,243 | $854 | $0 | $1,210 | $13,306 | $24 |
| 11.9 | Electrical Foundations | | $402 | $835 | $0 | $0 | $1,175 | $112 | $0 | $258 | $1,545 | $3 |
| | **Subtotal 11** | **$24,842** | **$10,454** | **$29,635** | **$0** | **$0** | **$64,930** | **$5,744** | **$0** | **$8,871** | **$79,546** | **$145** |

| Acct No. | Item/Description | NDIL0157 Equipment Cost | NDIL0157 Materials Cost | Direct Labor | Indirect Labor | Sales Tax | Bare Erected Cost $ | Eng'g CM H.O. & Fee | Process Contingency | Project Contingency | Total Plant Cost ($) | Total Plant Cost ($/kW) |
|---|---|---|---|---|---|---|---|---|---|---|---|---|
| 12 | Instrumentation & Control | | | | | | | | | | | |
| 12.1 | PC Control Equipment | | | $0 | $0 | $0 | $0 | $0 | $0 | $0 | $0 | $0 |
| 12.2 | Combustion Turbine Control | | | $0 | $0 | $0 | $0 | $0 | $0 | $0 | $0 | $0 |
| 12.3 | Steam Turbine Control | | | $0 | $0 | $0 | $0 | $0 | $0 | $0 | $0 | $0 |
| 12.4 | Other Major Component Control | | | $0 | $0 | $0 | $0 | $0 | $0 | $0 | $0 | $0 |
| 12.5 | Signal Processing Equipment | | | $0 | $0 | $0 | $0 | $0 | $0 | $0 | $0 | $0 |
| 12.6 | Control Boards, Panels & Racks | $516 | | $309 | $0 | $0 | $825 | $78 | $41 | $142 | $1,085 | $2 |
| 12.7 | Distributed Control System Equipment | $5,207 | | $910 | $0 | $0 | $6,117 | $568 | $306 | $699 | $7,690 | $14 |
| 12.8 | Instrument Wiring & Tubing | $2,823 | | $5,600 | $0 | $0 | $8,423 | $718 | $421 | $1,434 | $10,996 | $20 |
| 12.9 | Other I & C Equipment | $1,471 | | $3,337 | $0 | $0 | $4,808 | $466 | $240 | $551 | $6,066 | $11 |
| | **Subtotal 12** | **$10,017** | **$0** | **$10,156** | **$0** | **$0** | **$20,173** | **$1,829** | **$1,009** | **$2,826** | **$25,837** | **$47** |
| 13 | Improvements to Site | | | | | | | | | | | |
| 13.1 | Site Preparation | | $56 | $1,120 | $0 | $0 | $1,176 | $116 | $0 | $259 | $1,551 | $3 |
| 13.2 | Site Improvements | | $1,843 | $2,288 | $0 | $0 | $4,131 | $407 | $0 | $908 | $5,447 | $10 |
| 13.3 | Site Facilities | $3,303 | | $3,258 | $0 | $0 | $6,561 | $646 | $0 | $1,442 | $8,650 | $16 |
| | **Subtotal 13** | **$3,303** | **$1,899** | **$6,666** | **$0** | **$0** | **$11,869** | **$1,170** | **$0** | **$2,608** | **$15,647** | **$28** |
| 14 | Buildings & Structures | | | | | | | | | | | |
| 14.1 | Boiler Building | | $8,622 | $7,582 | $0 | $0 | $16,204 | $1,456 | $0 | $2,649 | $20,310 | $37 |
| 14.2 | Turbine Building | | $12,357 | $11,517 | $0 | $0 | $23,874 | $2,152 | $0 | $3,904 | $29,930 | $54 |
| 14.3 | Administration Building | | $641 | $678 | $0 | $0 | $1,319 | $120 | $0 | $216 | $1,654 | $3 |
| 14.4 | Circulation Water Pumphouse | | $176 | $140 | $0 | $0 | $316 | $28 | $0 | $52 | $397 | $1 |
| 14.5 | Water Treatment Buildings | | $778 | $708 | $0 | $0 | $1,486 | $134 | $0 | $243 | $1,862 | $3 |
| 14.6 | Machine Shop | | $428 | $288 | $0 | $0 | $716 | $63 | $0 | $117 | $896 | $2 |
| 14.7 | Warehouse | | $291 | $292 | $0 | $0 | $584 | $53 | $0 | $95 | $731 | $1 |
| 14.8 | Other Buildings & Structures | | $237 | $202 | $0 | $0 | $439 | $40 | $0 | $72 | $551 | $1 |
| 14.9 | Waste Trating Building & Structures | | $454 | $1,380 | $0 | $0 | $1,834 | $174 | $0 | $301 | $2,309 | $4 |
| | **Subtotal 14** | | **$23,985** | **$22,787** | **$0** | **$0** | **$46,772** | **$4,220** | **$0** | **$7,649** | **$58,641** | **$107** |
| | **TOTAL COST** | **$783,720** | **$52,742** | **$380,343** | | | **$1,216,804** | **$114,911** | **$59,701** | **$200,587** | **$1,592,004** | **$2,895** |

| | | | |
|---|---|---|---|
| **Owner's Costs** | | | |
| **Preproduction Costs** | | | |
| 6 Months All Labor | | $10,538 | $19 |
| 1 Month Maintenance Materials | | $1,532 | $3 |
| 1 Month Non-Fuel Consumables | | $1,833 | $3 |
| 1 Month Waste Disposal | | $305 | $1 |
| 25% of 1 Months Fuel Cost at 100% CF | | $1,849 | $3 |
| 2% of TPC | | $31,840 | $58 |
| **Total** | | **$47,897** | **$87** |

| Acct No. | Item/Description | NDIL0157 Equipment Cost | NDIL0157 Materials Cost | Direct Labor | Indirect Labor | Sales Tax | Bare Erected Cost $ | Eng'g CM H.O. & Fee | Process Contingency | Project Contingency | Total Plant Cost ($) | Total Plant Cost ($/kW) |
|---|---|---|---|---|---|---|---|---|---|---|---|---|
| | **Inventory Capital** | | | | | | | | | | | |
| | 60 day supply of fuel, consumables at 100% CF | | | | | | | | | | $17,997 | $33 |
| | 0.5% of TPC (spare parts) | | | | | | | | | | $7.960 | $14 |
| | **Total** | | | | | | | | | | **$25,957** | **$47** |
| | | | | | | | | | | | | |
| | **Initial Cost for Catalyst and Chemicals** | | | | | | | | | | $2,849 | $5 |
| | **Land** | | | | | | | | | | $900 | $2 |
| | **Other Owner's Costs** | | | | | | | | | | $238,801 | $434 |
| | **Financing Costs** | | | | | | | | | | $42,984 | $78 |
| | **Total Overnight Costs (TOC)** | | | | | | | | | | **$1,951,391** | **$3,548** |
| | TASC Multiplier | | | | | | | | | | 1.140 | |
| | **Total As-Spent Cost (TASC)** | | | | | | | | | | **$2,224,586** | **$4,045** |

### 5.1.3 **Operating costs**

The major operating and maintenance (O&M) costs for the $CO_2$ capture and compression processes are separated into two categories: fixed and variable operating costs. Fixed annual operating costs include labor (maintenance, operating and administrative/support) and property taxes/insurance. Variable operating costs include maintenance materials, consumables, waste disposal and fuel. Byproduct credits, if there are any, are not included. A capacity factor of 85% was used as stated in the 2010 Cost and Performance Baseline. Solvent losses are included in the O&M cost estimates for Case 12 (0.10 kg MEA/MT $CO_2$) and the IL case (0.23 kg IL/MT $CO_2$).[i]

The degradation rate for NDIL0157 was assumed to be the same as the degradation rate that was obtained from measured analytical data for NDIL0046 provided by Notre Dame. The degradation rate for NDIL0046 was calculated using the appropriate degradation rate for the temperature expected in a specific area of the process (i.e., absorber, surge tank, stripper), a rough estimate of the solution inventory for the equipment, and the mass of $CO_2$ removed from the flue gas.

Figure 8 illustrates the methodology used to calculate O&M costs for the IL process. Variable operating costs (all consumables with the exception of the IL solvent, makeup water, fuel, etc.) were scaled from Case 12 to the IL solvent based upon the equivalent electric capacity of the plant and raw water demand.

The total O&M costs for the IL case are shown in Table 12. Fixed operating costs were 0.5% lower for NDIL0157 versus DOE Case 12, and variable operating costs were 2.5% lower for the NDIL0157 versus DOE Case 12. NDIL0157 makeup costs were slightly higher than MEA makeup costs, but the higher makeup costs were offset by lower makeup water, consumables and fuel costs, as well as the absence of a corrosion inhibitor (DOE Case 12 specifies corrosion inhibitor for the Econamine FG Plus™ process, while currently we are assuming no corrosion inhibitor for NDIL0157 because stainless steel materials of construction were specified, and preliminary B&W corrosion tests suggest that carbon steel is acceptable at absorber conditions).

---

[i] The MEA solvent loss rate reported for Case 12 is lower than other values reported in prior literature (ABB *CO₂ Recovery from Flue Gas/Turbine Exhaust Gas: Kerr-McGee/Lummus Carbon Dioxide Recovery Technology.* ABB Lummus Global: 1998; 12).
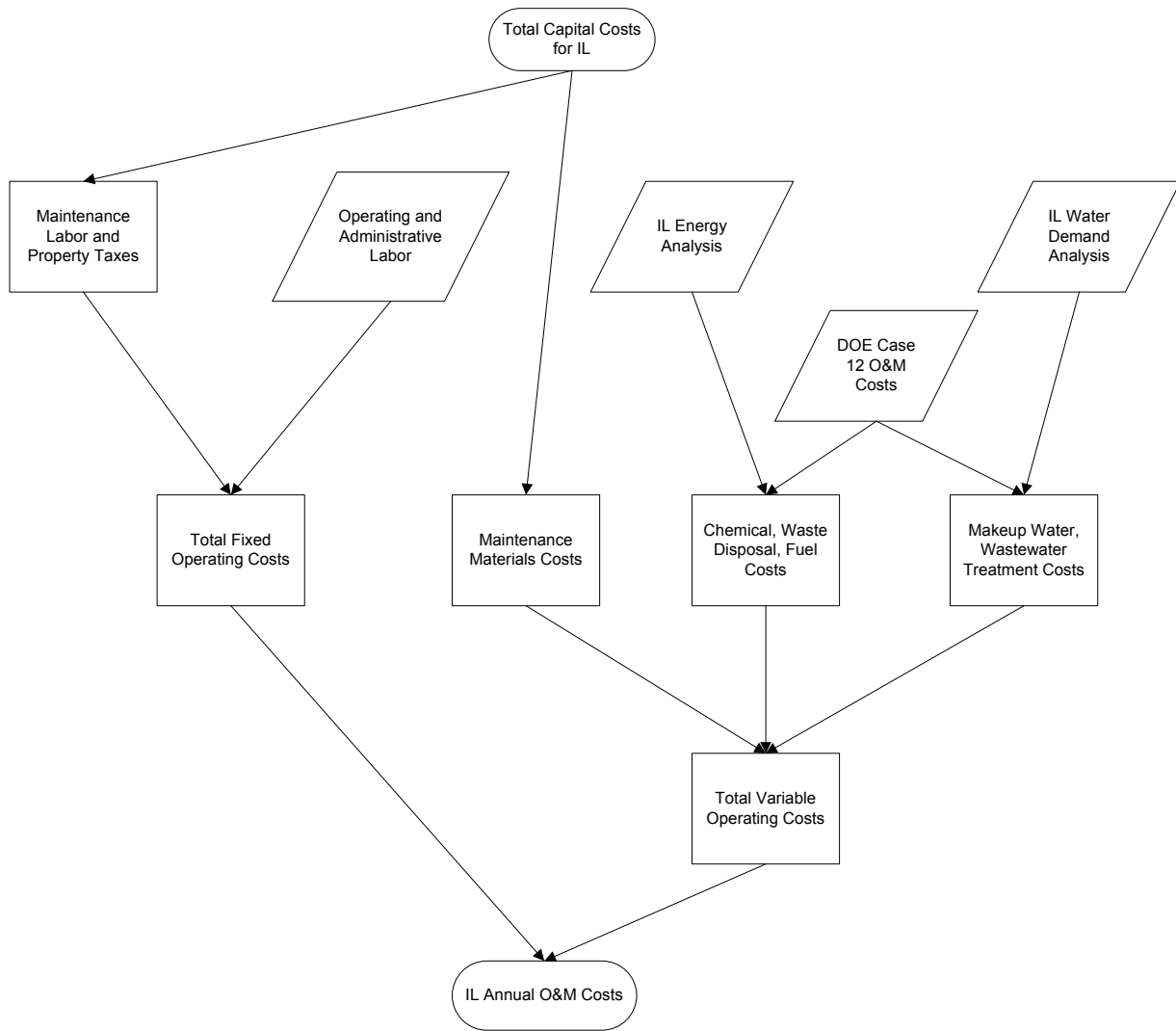
**Figure 8.  Operating & Maintenance Cost Methodology**

**Table 12. NDIL0157 Initial and Annual Operating and Maintenance Costs**

### Operating & Maintenance Labor

#### Operating Labor

| | | |
|---|---|---|
| Operating Labor Rate (Base) | 34.65 | $/hr |
| Operating Labor Burden | 30.00 | % of base |
| Labor O-H Charge Rate | 25.00 | % of labor |

Operation Labor Requirements (O. J.) Per Shift

| | 1 unit/mod | Total Plant |
|---|---|---|
| Skilled Operator | 2.0 | 2.0 |
| Operator | 11.3 | 11.3 |
| Foreman | 1.0 | 1.0 |
| Lab Tech's, etc. | 2.0 | 2.0 |
| TOTAL - O. J.'s | 16.3 | 16.3 |

| | Annual Cost ($) | Annual Unit Cost ($/kW-net) |
|---|---|---|
| Annual Operating Labor Cost | $6,444,907 | $11.718 |
| Maintenance Labor Cost | $10,415,464 | $18.937 |
| Administrative & Support Labor | $4,215,093 | $7.664 |
| Property Taxes and Insurance (2% of TPC) | $31,840,074 | $57.891 |
| **TOTAL FIXED OPERATING COSTS** | **$52,915,538** | **$96.210** |

| Variable Operating Costs | | $/kWh-net |
|---|---|---|
| **Maintanance Material Cost** | **$15,623,196** | |

| | Consumption | | | | | |
|---|---|---|---|---|---|---|
| Consumables | Initial Fill | /Day | Unit Cost | Initial Fill Cost | | |
| **Water (per 1000 gallons)** | 0 | 6,136 | 1.08 | **$0** | **$2,059,063** | **$0.00050** |
| | | | | | | |
| **Chemicals** | | | | | | |
| MU & WT Chem. (lbs) | 0 | 29,701 | 0.17 | $0 | $1,594,750 | $0.00039 |
| Limestone (ton) | 0 | 644 | 21.63 | $0 | $4,324,787 | $0.00106 |
| Carbon (for Mercury Removal) (lb) | 0 | 0 | 1.05 | $0 | $0 | $0.00000 |
| IL Solvent (ton) | 618 | 3.15 | 4,545.45 | $2,808,197 | $4,439,007 | $0.00108 |
| NaOH (tons) | 73 | 6.81 | 433.68 | $31,484 | $916,240 | $0.00022 |
| H2SO4 (tons) | 69 | 6.50 | 138.78 | $9,615 | $279,803 | $0.00007 |
| Corrosion Inhibitor | 0 | 0 | 0.00 | $0 | $0 | $0.00000 |
| Activated Carbon (lb) | 0 | 1,633 | 1.05 | $0 | $531,988 | $0.00013 |
| Ammonia (19% NH3) (tons) | 0 | 95 | 129.82 | $0 | $3,387,272 | $0.00094 |
| **Subtotal Chemicals** | | | | **$2,849,296** | **$15,923,847** | **$0.00389** |
| | | | | | | |
| **Other** | | | | | | |
| Supplemental Fuel (Mbtu) | 0 | 0 | 0.00 | $0 | $0 | $0.00000 |
| SCR Catalyst (m3) | 0 | 0.40 | 5,775.94 | $0 | $717,584 | $0.00018 |
| Emission Penalties | 0 | 0 | 0.00 | $0 | $0 | $0.00000 |
| **Subtotal Other** | | | | **$0** | **$717,584** | **$0.00018** |
| | | | | | | |
| **Waste Disposal** | | | | | | |
| Fly Ash (ton) | 0 | 494 | 16.23 | $0 | $2,487,063 | $0.00061 |
| Bottom Ash (ton) | 0 | 123 | 16.23 | $0 | $621,766 | $0.00015 |
| **Subtotal - Waste Disposal** | | | | **$0** | **$3,108,829** | **$0.00076** |
| | | | | | | |
| **By-products & Emissions** | | | | | | |
| Gypsum (tons) | 0 | 996 | 0 | $0 | $0 | $0.00000 |
| **Subtotal By-Products** | | | | **$0** | **$0** | **$0.00000** |
| | | | | | | |
| **TOTAL VARIABLE OPERATING COSTS** | | | | **$2,849,296** | **$37,432,519** | **$0.00914** |
| | | | | | | |
| **Fuel (ton)** | 0 | 6,369 | 38.18 | **$0** | **$75,448,653** | **$0.01842** |

### 5.1.4  Derating

The energy requirements to operate the main facility and the $CO_2$ capture unit are withdrawn from the main power facility output either through electricity or steam. This decreases the net electrical output of the plant. Power requirements of electric motors (i.e., inlet blower, pumps, and electric compressor drivers) translate directly to electrical derating (a decrease in $MW_e$). Energy requirements that are supplied using steam, such as the heat requirements for the reboilers and steam heaters, must be converted into electrical derating by calculating the amount of electrical generating capacity that the steam would have supplied to the main power facility had the steam not been diverted to the $CO_2$ capture system. The low-pressure steam in a power plant is typically discharged from the low-pressure turbine (72% isentropic efficiency) at a pressure of 1 psia.

The steam taken from the turbine will be de-superheated with steam condensate exiting the reboiler, so the superheated steam mass flow rate will be less than the saturated steam mass flow rate. This is taken into account in the reboiler derating calculations. Table 13 details the steam properties, flow rate and derating for each case at 550 MW of net power. Superheated steam was extracted at the IP/LP crossover at conditions optimized for the Fluor Econamine FG Plus$^{TM}$ process for Case 12 per the 2010 Cost and Performance Baseline.

It was assumed that the IL $CO_2$ capture process would uses the same power plant steam cycle as Case 12, and superheated steam was extracted at the IP/LP crossover at a pressure that corresponds to saturated steam temperature of 202°C. The amount of steam needed for the reboiler in the NDIL0157 case is 36% of that required in the MEA reboiler, but the derating factor is approximately 42% higher per unit of steam because higher temperature steam is required for IL solvent regeneration. Overall, the reboiler derating is approximately 36% lower for the IL case compared to Case 12.

**Table 13. Steam and Derating Summary – 550 MW Net Power**

| Description | Units | Case 12 | NDIL0157 |
|---|---|---|---|
| Net Boiler Electrical Capacity | $MW_e$ | 783 | 734 |
| Superheated Steam Flow Rate | lb/hr | 1,784,000 | 647,000 |
| Desuperheat Water Flow Rate | lb/hr | 252,000 | 160,000 |
| Saturated Steam Flow Rate | lb/hr | 2,036,000 | 807,000 |
| Steam Pressure | psia | 73.5 | 233.5 |
| Superheated Steam Temperature | °F | 556.3 | 766.2 |
| Saturated Steam Temperature | °F | 306.3 | 395.0 |
| Derating Factor | hp-hr/lb steam | 0.0903 | 0.1284 |
| Reboiler Derating | $MW_e$ | 120.1 | 76.7 |

Table 14 provides a detailed breakdown of power plant energy performance for the NDIL0157 case, while Table 15 summarizes the energy performance of the IL process in comparison to Case 12. Case 12 plant performance detailed in the 2010 Cost and Performance Baseline

included the $CO_2$-capture portion of cooling water pumps and cooling tower fans; however, in Tables 14 and 15, energy requirements for cooling water pumps and cooling tower fans dedicated to $CO_2$ capture are included with capture auxiliaries.

**Table 14. NDIL0157 Plant Performance Summary**

| POWER SUMMARY (Gross Power at Generator Terminals, kWe) | |
| --- | --- |
| Steam Turbine Power | 657,666 |
| **TOTAL (STEAM TURBINE) POWER, kWe** | 657,666 |
| **AUXILIARY LOAD SUMMARY, kWe** | |
| Coal Handling & Conveying | 478 |
| Pulverizers | 3,611 |
| Sorbent Handling & Reagent Preparation | 1,173 |
| Ash Handling | 694 |
| Primary Air Fans | 1,688 |
| Forced Draft Fans | 2,157 |
| Induced Draft Fans | 10,431 |
| SCR | 66 |
| Baghouse | 94 |
| Wet FGD | 3,855 |
| Capture Auxiliaries | 17,323 |
| $CO_2$ Compression | 51,227 |
| Miscellaneous Balance of Plant | 1,876 |
| Steam Turbine Auxiliaries | 375 |
| Condensate Pumps | 525 |
| Circulating Water Pumps | 5,989 |
| Ground Water Pumps | 854 |
| Cooling Tower Fans | 3,086 |
| Transformer Losses | 2,148 |
| **TOTAL AUXILIARIES, kWe** | 107,652 |
| **NET POWER, kWe** | 550,013 |
| Net Plant Efficiency (HHV) | 30.3% |
| Net Plant Heat Rate, kJ/kWh (Btu/kWh) | 11,877 (11,234) |
| **CONDENSER COOLING DUTY, $10^6$ kJ/hr ($10^6$ Btu/hr)** | |
| **CONSUMABLES** | |
| As-received Coal Feed, kg/hr (lb/hr) | 240,743 (529,634) |
| Limestone Sorbent Feed, kg/hr (lb/hr) | |
| Thermal Input, kWt | 1,814,600 |
| Raw Water Withdrawal, $m^3$/min (gpm) | |
| Raw Water Consumption, $m^3$/min (gpm) | 24.5 (6,478) |

**Table 15.  Energy Analysis Summary – 550 MW Net Power.**

| Description | Units | MEA (DOE Case 12) | Size/Methodology Adjusted NDIL0157 |
|---|---|---|---|
| Thermal Input | MW$_t$ | 1934.5 | 1814.6 |
| Equivalent Electrical Capacity of Boiler | MW$_e$ | 782.9 | 734.4 |
| Total Steam Turbine Power | MW$_e$ | 662.8 | 657.7 |
| Reboiler/Steam Heater Equivalent Power Lost | MW$_e$ | 120.1 | 76.7 |
| Compression | MW$_e$ | 44.9 | 51.2 |
| Capture Auxiliaries | MW$_e$ | 26.3 | 17.3 |
| Balance of Plant Auxiliaries | MW$_e$ | 41.7 | 39.1 |
| Net Power | MW$_e$ | 549.9 | 550.0 |
| Coal Feed Rate | kg/hr | 256,653 | 240,743 |

Plant thermal input is approximately 6% lower for the IL case versus Case 12 (48.5 MW equivalent boiler electrical capacity).  This reduced the size and cost of balance of plant equipment for the IL case versus MEA for a fixed net power output.  This difference is primarily due to the lower reboiler energy requirements for NDIL0157 as compared to MEA.

## 5.2    Economic Analysis and Results

This section uses the annualized cost summary to compare the cost of electricity (COE) for the NDIL0157 case to Case 12 from the 2010 DOE Cost and Performance Baseline.  The cost of electricity for the IL case was calculated based upon an equation provided on page 62 of the 2010 DOE Cost and Performance Baseline and compared to the cost of electricity for Cases 11 and 12.  All cases include 0.57 cents/kWh for TS&M (transportation, storage & monitoring of $CO_2$).  Figure 9 provides a flowsheet that details all the inputs into the COE equation.

Table 16 summarizes the COE results. The COE values for NDIL0157 and DOE Case 12 were very similar, indicating a slight economic advantage to NDIL0157.  The base plant cost of electricity was 5.89 ¢/kWh, per DOE Case 11.

As shown in Table 16, the cost of electricity for the MEA base case is 10.70 ¢/kWh; this represents an increase in cost of electricity of 82%.  The cost of electricity for NDIL0157 is 10.59 ¢/kWh, which represents an increase in cost of electricity of 80%.

**Table 16. COE Summary – 550 MW Net Power**

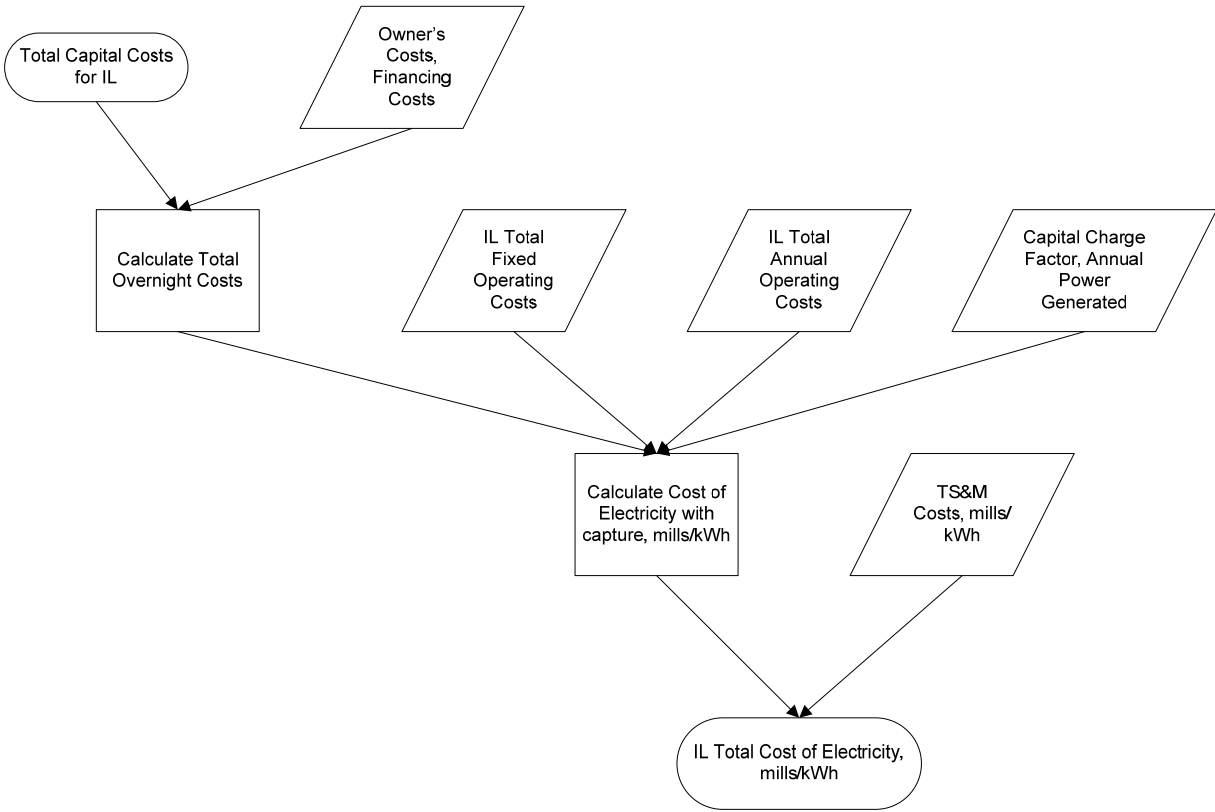| Description | Case 12 | NDIL0157 |
|---|---|---|
| Cost of Electricity, ¢/kWh | 10.13 | 10.02 |
| TS&M, ¢/kWh | 0.57 | 0.57 |
| Total COE, ¢/kWh | 10.70 | 10.59 |
| COE w/o Capture, ¢/kWh (Case 11) | 5.89 | |
| Percent Increase in COE | 81.7% | 79.7% |

**Figure 9.  Cost of Electricity Methodology**

## 5.3    Comparison to NDIL0046

Although the systems analysis for NDIL0157 was performed assuming a grassroots plant with a net electrical generating capacity of 550 MW, past studies were performed assuming a retrofit $CO_2$ capture unit placed on an existing power plant with a gross generating capacity of 500 MW. However, a 500 MW gross generating capacity from the prior IL systems analysis now corresponds to 593 MW gross generating capacity for a fixed $CO_2$ production rate, based upon updated guidance from DOE for boiler operation and $CO_2$ emitted per MW of electricity produced in the 2010 DOE Cost and Performance Baseline.

Table 17 summarizes the energy performance and required purchased equipment costs for NDIL0157 versus NDIL0046 and DOE Case 12. Energy requirements were approximately 30% lower and purchased equipment costs were approximately 36% lower for NDIL0157 when compared to NDIL0046, and purchased equipment costs were approximately 36% lower. Overall, NDIL0157 exhibits superior cost performance compared to NDIL0046.

**Table 17. Summary Comparison at 500 MW Gross Capacity**

| Description | Units | DOE Case 12 | NDIL0046 | NDIL0157 |
|---|---|---|---|---|
| Regeneration Temperature | | 110°C (230°F) | 188°C (370°F) | 188°C (370°F) |
| Regeneration Pressure | | 170 kPa (10 psig) | 136kPa (5 psig) | 101kPa (0 psig) |
| Energy Derating at 500 MW Gross Capacity | MW$_e$ | 132 | 167 | 117 |
| Purchased Equipment Costs | $MM | 105.4 | 188.6 | 119.8 |

A comparison of the properties for NDIL0046 and NDIL0157 is shown in Table 18.  The economics for NDIL0157 are favorable when compared to NDIL0046 because the net loading of NDIL0157 is much greater, which results in a much lower solvent circulation rate.  This is due to the fact that NDIL0157 was designed to have a stronger binding energy with $CO_2$, which results in the higher capacity. Figures 10 and 11 demonstrate the operating capacities of NDIL0157 and NDIL0046 and their respective optimum economic conditions.

**Table 18. Comparison of NDIL0046 and NDIL0157 Properties**

| Metric/Parameter | NDIL0046 | NDIL0157 |
|---|---|---|
| Ionic Liquid MW | 575 | 322 |
| Liquid Density, kmol/m$^3$ (T in Kelvin) | 1.8662 – 0.001(T) | 3.9970 – 0.002(T) |
| Liquid Viscosity, cP (T in Kelvin) | 0.2347*e$^{(875/T – 178.5)}$ | 0.1728*e$^{(814/T – 189.7)}$ |
| Heat Capacity, J/gmole-K (T in Kelvin) | 623.6 + 1.9125(T) | 66.45 + 1.8828(T) |
| Enthalpy of Reaction [Reference state: 25°C, 1 atm; $CO_{2(g)}$ + $IL_{(l)}$ = $IL-CO_{2(l)}$], kJ/gmole $CO_2$ | 43.07 | 60 |
| Inert Fraction of Ionic Liquid | 0.0682 | 0.0000 |
| Direct Contact Cooler Outlet Temperature, °C | 40 | 40 |
| Regenerator Bottom Temperature, °C | 187.8 | 187.8 |
| Regeneration Top Pressure, kPa (absolute) | 135.8 | 101.4 |
| Absorbent Net $CO_2$ Loading [rich loading – lean loading], mole $CO_2$ /mole ionic liquid (for minimized equivalent work case) | 0.139 | 0.480 |
| Absorbent Net $H_2O$ Loading [rich loading – lean loading], mole $H_2O$/mole ionic liquid (for minimized equivalent work case) | 0.0505 | 0.0379 |
| Fraction of $CO_2$ Recovered from Flue Gas | 0.90 | 0.90 |
| Rich/Lean Exchanger Approach Temperature, °C | 5 | 5 |
| Ionic Liquid Losses, kg/hour | 574.2 | 574.2 |
| Ionic Liquid Makeup Costs, $/metric ton | 5,000 – 15,000 | 5,000 – 15,000 |
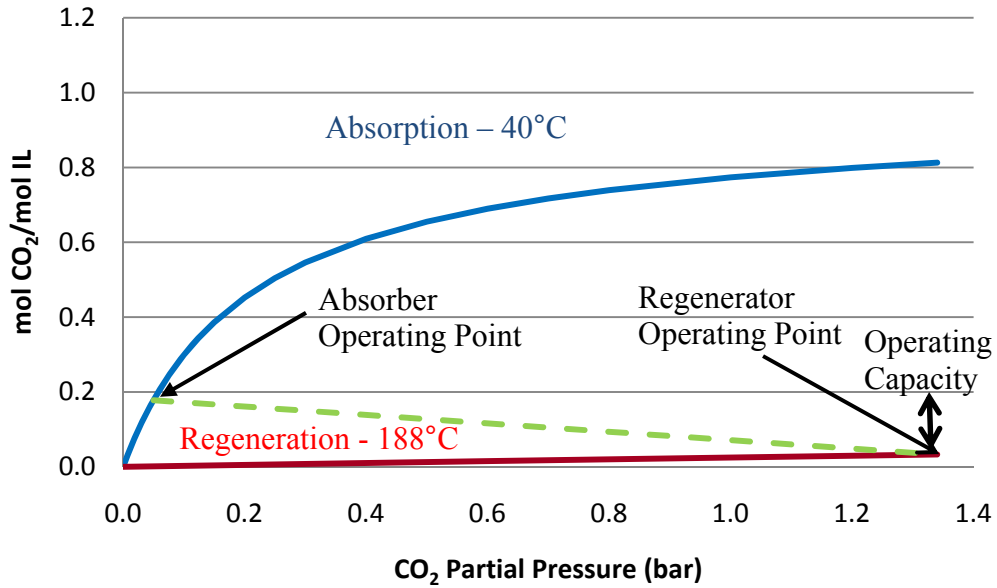
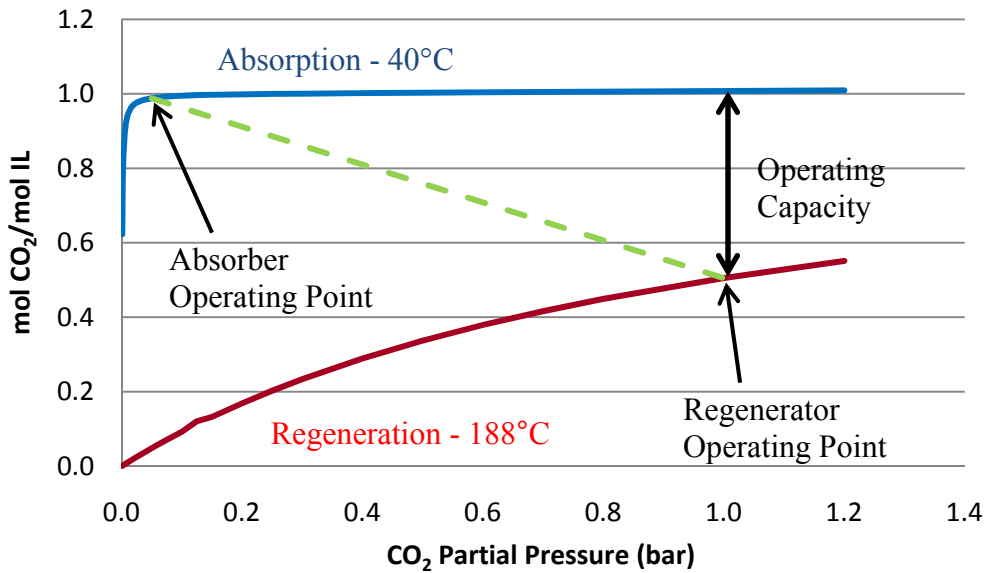**Figure 10. Operating Capacity of NDIL0046**



**Figure 11. Operating Capacity of NDIL0157**

# 6 CONCLUSIONS AND IMPORTANT FACTORS AFFECTING ECONOMIC ANALYSIS

The economic comparison shows that NDIL0157 provides comparable performance to the standard MEA technology for $CO_2$ capture (DOE Case 12). The major conclusions of this work are:

- Estimates for increases in the cost of electricity associated with $CO_2$ capture were 82% for DOE Case 12 (from 5.89 to 10.70 ¢/kWh) and 80% (10.59 ¢/kWh) for NDIL0157.

- On the basis of 550 MW net power production, the energy penalty for electrical power requirements and steam derating for NDIL0157 is 49 MW lower than DOE Case 12. This lower energy penalty results in a smaller-sized power plant, and lower capital costs for non-capture/compression equipment.

- Estimated steam heater/reboiler steam mass flow rate requirements for NDIL0157 were approximately 36% of the steam requirements of DOE Case 12.

- Compression power requirements for NDIL0157 were approximately 14% higher than the compression power requirements for DOE Case 12, due to the $CO_2$ overhead entering the first stage of compression at a lower pressure.

- $CO_2$ capture purchased equipment costs for NDIL0157 were approximately 13% higher than the purchased equipment costs for DOE Case 12.

- Preliminary corrosion tests from B&W suggest that carbon steel is acceptable material of construction for the absorber columns. Constructing the absorber columns from carbon steel as opposed to stainless steel would reduce the overall cost of electricity by 0.24 ¢/kWh at 550 MW net power.

- If the heat transfer performance of NDIL0157 can be improved, then the capture purchased equipment costs can potentially be decreased. A high-level sensitivity study shows that a 50% reduction in viscosity can improve heat transfer in the lean/rich cross-exchanger and reduce the cost of electricity by approximately 0.10 ¢/kWh at 550 MW net power.

- Compression purchased equipment costs for NDIL0157 were approximately 18% higher than the compression purchased equipment costs for DOE Case 12, due to the lower first stage suction pressure.

- NDIL0157 has better energy performance and lower purchased equipment cost requirements when compared to NDIL0046.

- NDIL0157 exhibits similar economic performance to the established technology described in DOE Case 12 for post-combustion $CO_2$ capture.

# 7 REFERENCES

[1] Department of Energy (DOE) National Energy Technology Laboratory (NETL). "Cost and Performance Baseline for Fossil Energy Plants Volume 1: Bituminous Coal and Natural Gas to Electricity", Revision 2, November 2010, DOE/NETL 2010/1397.

[2] Fisher, K.S., *et al. Advanced Amine Solvent Formulations and Process Integration for Near-Term CO2 Capture Success*. Final Report to U.S. Department of Energy, National Energy Technology Laboratory (NETL). Grant No. DE-FG02-06ER84625, June 2007.

[3] Fisher, K.S., *et al. Integrating MEA Regeneration with Compression and Peaking to Reduce $CO_2$ Capture Costs*. Final Report to U.S. Department of Energy, National Energy Technology Laboratory (NETL). Grant No. DE-FG02-04ER84111, June 2005.

[4] Department of Energy (DOE) National Energy Technology Laboratory (NETL). "Carbon Capture and Sequestration Systems Analysis Guidelines", April 2005.